NASA CR- 132699
N75-25090
N75-25090 CR-142938
N75-25091 CR-142937

REACTING FLUIDS LABORATORY

FINAL REPORT
ON
NASA GRANT NGR 19-001-016 Langley

EVALUATION OF THE ENERGY TRANSFER IN THE CHAR ZONE DURING ABLATION

Part II: In-Depth Response of Ablative Composites

by
Ralph W. Pike, Professor
Principal Investigator
Eduardo G. del Valle, Research Associate
Gary C. April, Research Associate
Department of Chemical Engineering

December 15, 1974

Volume I

LOUISIANA STATE UNIVERSITY

IN DEPTH RESPONSE OF

ABLATIVE COMPOSITES

VOLUME I

A Dissertation

Submitted to the Graduate Faculty of the
Louisiana State University and Agricultural
and Mechanical College in partial fulfillment
of the requirements for the degree of
Doctor of Philosophy

in

The Department of Chemical Engineering

---

by

Eduardo Gonzalez del Valle
B.S., Louisiana State University, 1965
M.S., Louisiana State University, 1969

May 1975

To Margarita for her love,
patience, understanding
and hard work

ACKNOWLEDGEMENT

The author wishes to express his gratitude to Dr. Ralph W. Pike for his guidance and encouragement throughout this research. His close attention and time given to the latter stages of this research and to the completion of this dissertation are more than gratefully acknowledged.

Appreciation is also expressed to the National Aeronautics and Space Administration's Langley Research Center which sponsored the research and, especially to Robert T. Swann, Grant Monitor, whose interest and consultation gave an added sense of achievement to the research.

The author is very grateful to John Balhoff for his very conscientious and time-consuming effort he performed in executing many of the computer runs while the author was away from the campus and for his valuable assistance in bringing to my attention a number of numerical bugs.

The author is also grateful to Dr. Frank Groves, Dr. Richard Farmer and Dr. Albert Wehe for their valuable suggestions and comments.

Finally, the author wishes to especially thank his wife, Margarita, for her many long hours and tireless effort of typing and proofreading this dissertation, and

for the encouragement, cheerful support and love she provided to help finalize the writing of the dissertation.

TABLE OF CONTENTS

VOLUME I

VOLUME II

LIST OF TABLES

LIST OF FIGURES

ABSTRACT

This research has dealt with the analysis of the in-depth response of phenolic-nylon and silicone elastomer ablative composites. The calculations of the total energy absorbed were performed by the coupling of the virgin plastic zone with the decomposition and the char zone. This was achieved by taking into account the energy absorbed by the reacting gases that flow into the char zone as a result of the depolymerization of the virgin plastic ablator and, in addition, by taking into account the energy absorbed associated with this depolymerization process. The bulk of the research was concentrated on phenolic-nylon ablative composite since it has shown the superior performance in comparison with other ablators in high heating rate environments. Frozen, equilibrium and non-equilibrium analyses were developed for this composite. A non-equilibrium or kinetic analysis was not developed for silicone elastomers, because of insufficient data on the complex solid-state reactions that are known to occur in the silicone-carbon system. However, for the silicone elastomers the in-depth response was modeled by using equilibrium analysis which demonstrated the flexibility and generality of the computer analyses developed.

In this research we were able to identify the important energy absorbing mechanisms in an ablator. In the plastic

zone the predominant energy absorbing mechanism is due to the decomposition of the plastic itself. In the char the predominant mechanisms are transpiration cooling, endothermic chemical reactions, and sublimation of carbon. In conjunction with the equilibrium and frozen flow analyses it was established that chemical reactions become important energy absorbing mechanisms above 2000°F, while sublimation does not become an important contributing factor unless the temperature is above about 4700°F.

For the phenolic-nylon ablator it was determined that a non-equilibrium flow analysis, employing detailed kinetic equations of the pyrolysis gases and a detailed analysis of the depolymerization of the virgin plastic composite, was necessary to accurately describe the in-depth response of the ablative composite.

In the non-equilibrium flow analysis the important chemical reactions and kinetic data for a temperature range of 500°F to approximately 6000°F were determined by screening over one hundred chemical reactions. For each of the fifteen reactions finally selected to model the chemical behavior of the pyrolysis gases an equilibrium constant was computed to provide a means of calculating the reverse reaction rate constant and therefore, make the reactions reversible and thermodynamically consistent.

The decomposition/char zone temperature interface for

all the cases analyzed was always higher than 2000°F in the non-equilibrium flow analysis, and the pyrolysis gases that transpired into the char zone reacted very quickly. As a consequence of the very rapid reaction rate in the non-equilibrium analysis it was necessary to use very small step-sizes in the Runge-Kutta numerical solution in order to maintain the stability of the solution. This resulted in excessive amounts of computer time which limited the number of cases analyzed. The numerical difficulties experienced with the non-equilibrium analysis were due to a phenomenon called stiffness. Because of this the minimum total mass flux analyzed for the non-equilibrium flow analysis was 0.35 lb/ft^2-sec. However, no such restrictions were necessary for equilibrium or frozen flow.

Parameter studies with pressure and char surface recession velocities were conducted to determine the effect that these variables had on the total energy absorbed by the ablator. It was found that pressure had very little effect on the energy absorption below 4000°F, both for equilibrium and non-equilibrium analyses. Surface recession velocity had an effect on the decomposition/char zone temperature interface, with the interface temperature increasing with increasing recession velocity.

Although frozen flow analysis proved to be a very poor approximation to the total amount of energy absorbed,

equilibrium analysis, using free energy minimization, proved to be a reasonable approximation to non-equilibrium. Although it suffers from its inherent simplifying assumption that the gases are always in chemical equilibrium.

It was found that the silicone elastomer ablator showed the same trends observed for the phenolic-nylon ablator for the several parameter studies considered. However, it was found that the phenolic-nylon ablator is the more efficient of the two because it absorbs more energy per pound of material.

CHAPTER I

INTRODUCTION

This research describes the decomposition in-depth of ablative composites along with the transport phenomena of pyrolysis gases which result from the decomposition of these plastics as they flow through the porous char of char-forming ablators. In particular, the pyrolysis products are those formed by the thermal degradation of nylon-phenolic resin and silicone elastomer composites. The nature and extent of chemical reactions among the pyrolysis products and the char, along with the energy absorbed by the combined pyrolysis and char zone, are given major emphasis in this research. Likewise, the determination of the important chemical reactions with thermodynamically consistent kinetic data are necessary in developing a realistic analysis for predicting the thermal performance of ablative heat shields, and they have been obtained in this research.

The Design of Thermal Protection Systems

It is a well known fact that vehicles reentering planetary atmospheres need to dissipate enormous amounts of energy. This energy dissipation is achieved by reducing the speed of the vehicle by either the use of rockets or by taking advantage of the frictional drag of the atmosphere to decelerate the vehicle. The former solution is not an

acceptable design practice since it increases the fuel requirements for a mission. This presents, however, some severe thermal and structural requirements for reentry vehicles (1, 2) since all of the energy the vehicle possesses at reentry, kinetic as well as potential, must be converted into heat. To illustrate that this energy can indeed be great, Figure 1-1 compares the energy per unit mass as a function of entry speed V_E, in kilometers per second, for several heat shield materials (3). To dissipate this great amount of energy several methods of solutions are possible (4, 7, 8). These are: (1) Heat Sink, (2) Radiation Cooling, (3) Transpiration Cooling and (4) Ablative Cooling.

Heat Sink: This method consists of providing enough mass with high enough heat capacity to safely absorb the heat input to the vehicle (12).

Radiation Cooling: This method of cooling is achieved by using highly reflective surfaces such that most of the heat incident to the body, by either convection and/or radiation, is reflected back rather than absorbed by the vehicle (13).

Transpiration Cooling: This technique injects fluid into the boundary layer through openings in the body. This injection of mass produces a substantial heat blockage that reduces the net heat transfer to the body by virtue of the thickening of the boundary layer.

Ablative Cooling: This form of thermal protection is

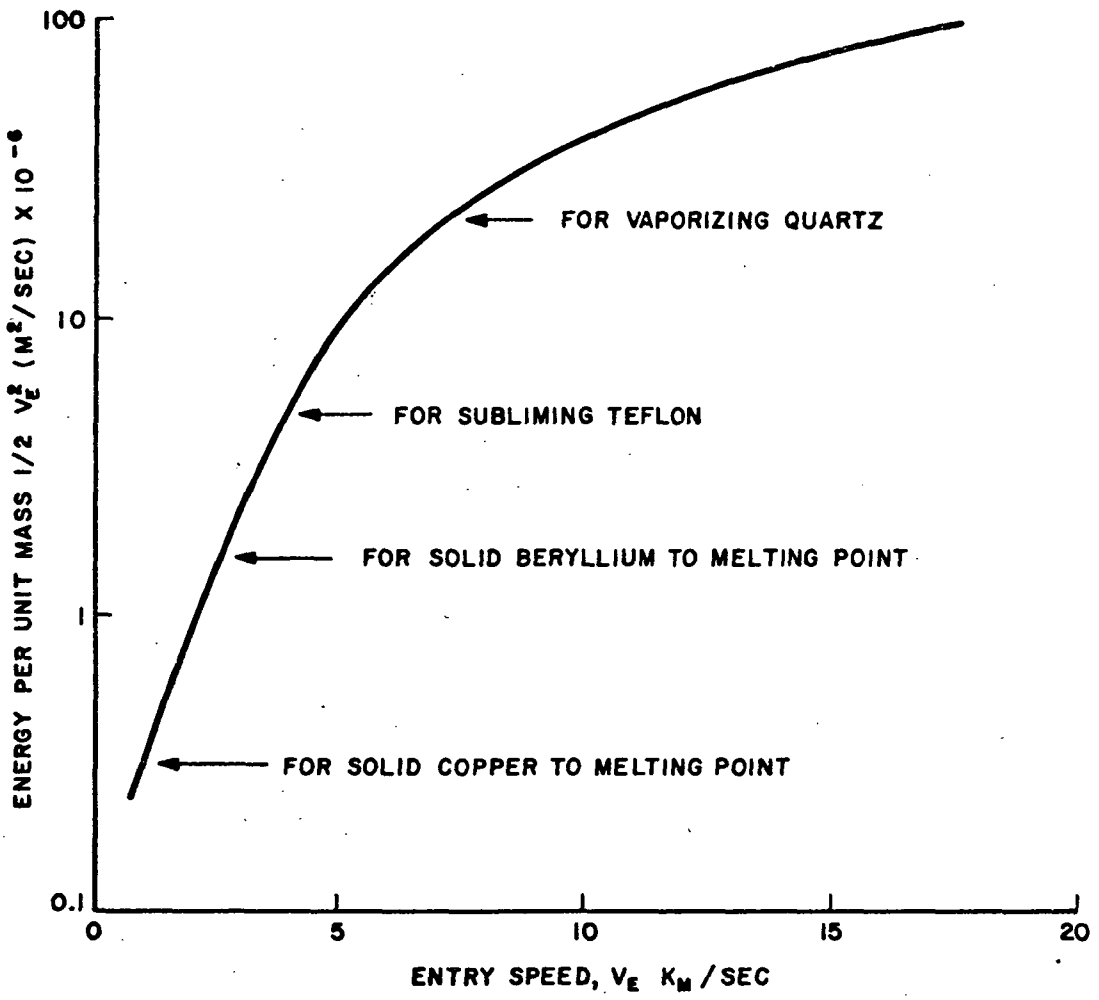

FIGURE I-1 COMPARISON OF THE ENERGY PER UNIT MASS AS OF FUNCTION OF ENTRY SPEED, (3).

achieved by the sacrificial loss of the material covering the body. The energy absorption is achieved by a change of phase. This phase change can be melting, vaporizing, and/or subliming.

Of the four techniques, the first three suffer from excessive weight penalties to the vehicle. The feasibility of ablation heat shields for satellite reentry was established in the late 50's and early 60's (2). Although absorption of heat by phase change is the distinguishing feature of ablation, energy dissipation by radiation, conduction, convection, transpiration, cooling and chemical reactions is likewise achieved (8, 9). Georgiev, et. al. (5) has a discussion of the various factors affecting the choice of a heat sink, ablation, or radiation shield to use for thermal protection systems.

In addition, Lees (11), presents an example which illustrates, that for a good thermal conductor such as copper, the peak heat transfer rate should be limited to about 1,000 BTU/ft^2-sec, for 30 seconds for a maximum allowable temperature of 1500^{o}F. This clearly shows the limitations which are imposed on vehicles made of non-melting solids. Scala (14) compares the effectiveness of transpiration cooling with ablating cooling and concludes that ablation is more effective than transpiration cooling on a coolant mass consumption basis. Later, Beusman and Weisman (15) showed that transpiration cooling would be more effective if water were to be used as the coolant.

Aerodynamic Heating of Blunt Bodies vs. Slender Bodies

It was said that for a body entering the atmosphere, which is braked by aerodynamic drag, all of the energy possessed by the vehicle is converted into heat. Fortunately however, only a fraction of the total kinetic energy need be transferred to the vehicle as heat. The approximate amount can be determined from the following analysis presented by Allen(3). He simplified the motion equation to consider only the most important term, the drag term. Then,

$$\frac{mdV}{dt} = -\frac{1}{2} C_D \rho V_E^3 A \qquad (1\text{-}1)$$

where m is the vehicle's mass, V_E the entry speed, t the time, ρ the air density, A the reference area and C_D the drag coefficient based on A.

The rate of heat transfer to the vehicle was shown to be:

$$\frac{dq}{dt} = \frac{1}{2} C_H \rho V_E^3 A \qquad (1\text{-}2)$$

where q is the heat input and C_H is the heat transfer coefficient.

By combining these two equations it was shown that the heat input for the entire braking process was given by the following expression:

$$q = \frac{C_H}{C_D} \frac{1}{2} mV_E^2 \qquad (1\text{-}3)$$

That is, the amount of heat given to the body is determined

by the ratio, which he called, the "energy ratio", of the heat transfer coefficient, C_H, to the drag coefficient, C_D. Using Reynolds analogy and assuming that only convective heating occurs, it was shown that:

$$\eta = \frac{C_H}{C_D} = \frac{C_F}{2\ (C_{D_P} + C_F)} \qquad (1\text{-}4)$$

where C_F is the skin friction coefficient and C_{D_P} is the pressure drag coefficient. It should be noted that blunt bodies have much greater pressure drag coefficient than slender bodies. Hence the fraction of heat transferred to the body is less than for slender bodies. This interesting relation formed the basis for using blunt bodies as reentry vehicles under high heating load conditions and for long time reentry (6). "Depending on the relative amount of laminar and turbulent flow a slender vehicle designed with a length to diameter ratio of 3.0, for example, would have between about 6 to 16 times as severe a heating problem as a blunt vehicle designed to produce no lift", (6).

Thermal Protection System for Manned Reentry

It was previously stated that heating for a reentry vehicle is produced by conversion of the kinetic energy of the moving body into thermal energy when it decelerates. For an efficient thermal protection system most of the incident heat must be disposed at the outer surface. Any of the four possible methods previously mentioned can be used effectively. However, it has been demonstrated that abla-

tion cooling is best suitable for manned reentry missions (3,8).

Ablative Materials: Ablative materials are generally made of a ceramic, a plastic, or reinforced system formed by a combination of plastic and an inorganic fiber. In general plastics and related composites have been widely used (16). Ideally, these ablative materials must possess low thermal conductivity, high heat capacity and large heats of degradation (8). This is needed to effectively protect the vehicle from the high heating environment encountered during reentry.

Success has been achieved by employing composites of nylon, phenolic resin, silicon elastomers and others. A partial list of some of these composites is presented in Table 1-1. These composites fall into broad categories, non-charring(thermoplastic) and charring (thermosetting). A non-charring ablator is one which vaporizes and decomposes into gases with little or no residue remaining on the ablative surface (17). Teflon is one such non-charring compound. The charring ablator vaporizes, but it decomposes into low molecular weight pyrolysis gases and a carbonaceous residue. The gases are heated as they travel through the char layer with chemical reactions occurring. These gases when injected into the boundary layer effectively block part of the heat input to the vehicle surface by thickening the boundary layer. Phenolic-nylon is an example of a charring

Table 1-1. List of Materials Tested for Heat Protection of Reentry Vehicles (14)

Plastics:	Ceramics:	Reinforced Systems:
Polytetrafluoroethylene (Teflon)	Fused Silica	Glass Fiber-reinforced Phenolics
Polyethylene	Zirconia	Metal Fiber-reinforced Ceramics
Polyamides	Magnesia	Organic Resin-filled Porous Ceramics
Phenolics	Foamed Ceramics	Ceramic-filled Metal Honeycombs
Modified Epoxies		Inorganic Particle-filled Refractory
Foamed Resins		
Carbonized Resins		

ablator. "In general charring ablators, subliming ablators and melting ablators provide the most effective thermal tection system" (18). Of these, the charring ablator normally provides the most efficient thermal protection shield for a wide variety of applications including manned reentry vehicles (18,19). For this reason charring ablators have been studied.

Ablation: " Ablation is an orderly heat and mass transfer process in which large amounts of thermal energy are expended by sacrificial loss of surface region material" (19). To date certain physical and chemical aspects of the process are well known and understood. A description of those physical and chemical processes for a charring ablator follows.

Charring Ablator; Physical Process: On high speed planetary reentry, the high temperature generated by viscous forces causes the plastic ablator to undergo a number of physical and chemical changes with the formation of a carbonaceous residue. A cross section of the ablative composite with the accompanied flow field is illustrated in Figure 1-2.

The heat input from the surrounding flow field is absorbed, dissipated, blocked, and conducted into the plastic material substrate (19). Initially, the heat flow in penetrates at a low rate because of the low thermal

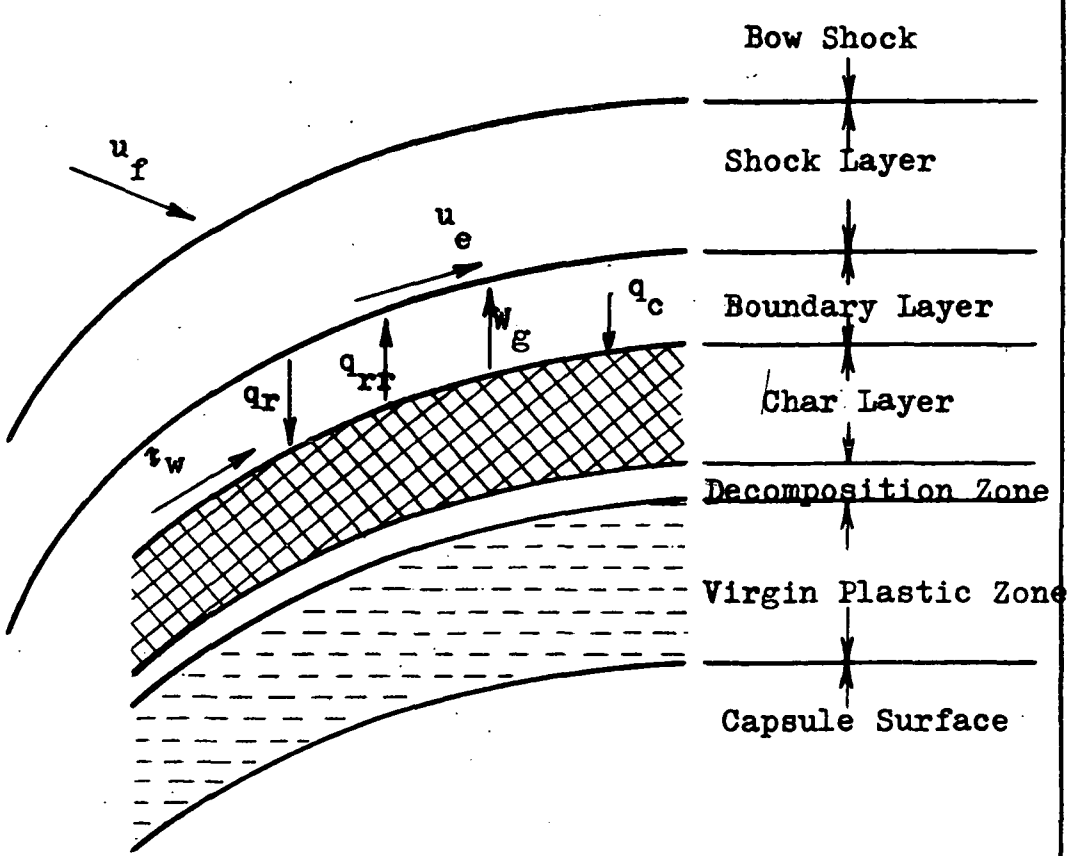

u_f - velocity of the flow field
u_e - velocity at the boundary layer edge
τ_w - shear force at the char surface
q_r - radiative heat transfer to the char surface
q_{rr} - reradiative heat transfer from the char surface
W_g - mass flux of pyrolysis gases leaving char surface
q_c - convective heat transfer to the char surface

Figure 1-2. Schematic Diagram of the Various Zones Developed During Reentry of a Capsule Protected by a Char Forming Ablative Heat Shield.

conductivity of the ablator. This causes a rapid temperature rise on the surface with subsequent phase change and thermal degradation of the material into pyrolysis gases and a porous carbon char. During this phase change of the virgin plastic composite into bases and char an enormous amount of heat is absorbed. This prevents the interior of the vehicle from getting excessively hot. The pyrolyzed gases flow through the char to the surface and in the process absorb heat due to their own heat capacity (transpiration cooling) and in addition, undergo, mostly endothermic chemical reactions. The pyrolyzed gases are injected into the boundary layer producing a blowing effect and thus, reducing the net heat transfer to the surface of the vehicle. The char produced from the decomposition of the plastic material and the further cracking of the pyrolysis gases, has a double protective effect. It acts as an insulator for the virgin material by effectively reducing the rate of heat conducted to it. It also acts as a radiation shield by radiating back part of the heat incident to the surface. Thus the char serves to control the surface temperature and greatly restrict the flow of heat into the substrate interior (19).

Summary

This chapter has illustrated the severe heating problems encountered by vehicles entering planetary

atmospheres. It was shown that for high heating rates and long reentry time blunt body vehicles would absorb less heat than slender body vehicles. Of the several methods proposed to overcome the thermal barrier, ablation cooling was shown to be superior to the others for manned vehicle applications. In addition, it was shown that char forming ablators would normally provide better thermal protection for a wide variety of applications including manned reentry vehicles. Finally, it was illustrated that most of the heat transferred into the vehicle was absorbed at the decomposition zone and by the gases flowing through the char zone. For this reason, it is important that any theoretical analysis designed to predict the thermal response of ablative composites have an accurate description of the decomposition zone and char zone since they are the important heat absorbing regions. In the subsequent chapter several analyses proposed to describe the decomposition zone and char zone are reviewed in the light of present knowledge of the ablation process.

REFERENCES

1. Achard, R. T., "Fundamental Relationship for Ablation and Hyperthermal Heat Transfer," Air Force System Command, Technical Report AFFDL-TR-66-25, AH-633-677, (April 1966).

2. Hurcwicz, H. and R. Mascola, "Thermal Protection System Application, Research of Materials Properties and Structural Concepts," AVCO Technical Report No. ML-TDR-64-32, AD-611-772, (January 1965).

3. Allen, H. J., "Some Problems of Planetary Atmosphere Entry," Journal of the Royal Aeronautics Society, 71, 813-820, (December 1967).

4. Penner, S. S. and O. P. Sharma, "Ablation With Radiant Heating," Zeitschrift fur Flugwissenschaften, 14, 169-179 (1966).

5. Georgiev, S., H. Hidalgo and M. C. Adams, "On Ablation for the Recovery of Satellites," AVCO Research Laboratory, Research Report 47 (1959).

6. Allen, H. J. and J. A. Eggers, Jr., "A Study of the Motion and Aerodynamic Heating of Ballistic Missiles Entering Earth's Atmosphere at High Supersonic Speeds," NACA TR-1381, (1958).

7. Kelley, J. B. and M. R. L'Ecuyer, "Transpiration Cooling-Its Theory and Application," Report No. TM-66-5, Jet Propulsion Center, Purdue University, Contract NsG-592, N66-30856, (June 1966).

8. Steverdine, B. and V. A. Nieberlein, "Ablation for Heat Shielding," Chemical Engineering, 72, 163-168, (July 19, 1965).

9. Fein, M. M., S. J. Tunkel and M. S. Cohen, "New Developments in Ablative Cooling," CEP Symposium Series, 60, 99-1, (1964).

10. Chapman, D. R., "On the Corridor and Associated Trajectory Accuracy for Entry of Manned Spacecraft into Planetary Atmospheres," Proceedings of the Tenth International Astronautical Congress, Springer-Verlay Publishing Co., Vienna, Austria, (1960).

11. Lees, L., "Ablation in Hypersonic Flows," Reported from Seventh Anglo-American Aeronautical Conference, Institute of the Aeronautical Science, Inc., New York, (1960).

12. Libby, P. A., "Preliminary Analysis of the Capabilities of a Composite Slab for an Advance Heat Sink Design, ARS Journal, 31, 658-659, (May 1961).

13. Rosner, D. E., "Surface Temperature of High Speed Radiation Cooled Bodies in Dissociating Atmospheres," ARS Journal, 31, 1013-1016, (July 1961).

14. Scala, S. M., "Thermal Protection of a Reentry Satellite," ARS Journal, 29, Sept. 1959, pp. 670-672.

15. Beusman, C. C. and J. Weisman, "Comparison of Transpiration and Ablation Cooling," ARS Journal, 30, June 1960, pp. 573-575.

16. Schimidt, D. L., Engineering Design for Plastics, Chapter 13, Reinhold Publishing Co., Inc., New York (1962).

17. Matting, F. W. and D. R. Chapman, "Analysis of Surface Ablation of Non-charring Materials with Description of Associated Computing Program," NASA TN-D-3758, (December 1966).

18. Brewer, W. D., C. W. Stround and R. K. Clark, "Effect of the Chemical State of Pyrolysis Gases on Heat Shield Mass," NASA TN-D-4975 (December 1968).

19. Schimidt, D. L., "Research Trends in Ablative Plastics and Composites," AIAA 6th Structures and Materials Conference, Palm Springs, Calif. (April 5-7, 1965).

20. April, G. C., "Evaluation of the Energy Transfer in the Char Zone During Ablation," Ph.D. Dissertation, Louisiana State University, Baton Rouge, Louisiana. (1969).

CHAPTER II

A REVIEW OF ANALYSES DESCRIBING DECOMPOSITION IN-DEPTH FOR THE ABLATIVE PROCESS OF CHAR FORMING ABLATORS

Research and development of ablative heat shield composites for space vehicles can be grouped into two broad categories. The first involves the detailed investigation of the physical and chemical processes which occur during ablation. In these studies particular attention has been given to the experimental investigation of plastic decomposition chemistry (1-4), valid analytical descriptions of the pyrolysis zone (5-10), and the flow of pyrolysis gases through porous media (11-22). In addition, studies have been made of the effects that char oxidation (23-32), thermal property variations (33-39), porosity and permeability of the char (34-37, 17), composition of the pyrolysis gases entering the char zone (40-43), environmental conditions (43-47), char spallation (48-50), boundary layer interaction (51-58), radiation (59-69) and others (70-92), have on the accurate prediction of the thermal performance of ablative composites. The second category covers the analysis of the transient response of the combined heat and mass transfer mechanism which occurs between the heat shield and the flow field (7, 51, 53, 58, 84, 111). Research in

both areas is essential in developing more effective thermal protective system for reentry vehicles. The former category improves the accuracy of the transient response computation by supplying better experimental and theoretical understanding of individual physico-chemical processes which occur during ablation. The latter allows for a more economic and effective thermal design of the ablative heat shield.

As mentioned in Chapter I, this research describes the decomposition in-depth of ablative composites along with the transport phenomena of pyrolysis gases which result from the decomposition of these plastics as they flow through the porous char of char-forming ablators. In particular, the pyrolysis products are those formed by the thermal degradation of nylon-phenolic resin and silicone elastomer composites. The nature and extent of chemical reactions among the pyrolysis products and the char, along with the energy absorbed by the combined pyrolysis and char zone, are given major emphasis in this research. Likewise, the determination of the important chemical reactions with thermodynamically consistent kinetic data are necessary in developing a realistic analysis for predicting the thermal performance of ablative heat shields, and they have been obtained in this research.

In one phase of this research April (19) made a state of the art study of the flow of pyrolysis gases in the char zone and reviewed the important works related to this area.

In this chapter the emphasis is placed on the quasi-steady analysis for describing decomposition in-depth of virgin material composites. In addition, some of the typical transient response analyses are briefly discussed. In particular, the transient analyses of Swann, et. al. (58), Clark (111), Kendall, et. al. (51,53), and Kratch, et. al. (83), will be reviewed. Finally, a summary of previous research on flow in the char zone are presented. The discussion of analyses used for the description of the decomposition process in virgin plastic ablative composites follows below.

Decomposition In-Depth of Virgin Plastic Composites

Several methods are available for the treatment of the thermal decomposition process of plastic composites. They differ primarily in whether the chemical decomposition of the plastic is assumed to occur in a single reaction plane (5, 6) at a fixed temperature, or whether a spacially continuous decomposition in-depth is used (7, 8, 9). The analysis in this research assumes the decomposition of the plastic ablator to occur spacially, and the temperature limits within the reaction zone is determined by the kinetics of the decomposition of the virgin material. The frequency factor, activation energy and the order of equations can be obtained from thermogravimetric analysis for particular materials of interest (1-4). In Figure 2-1 a typical thermogravimetric curve is shown for a low density

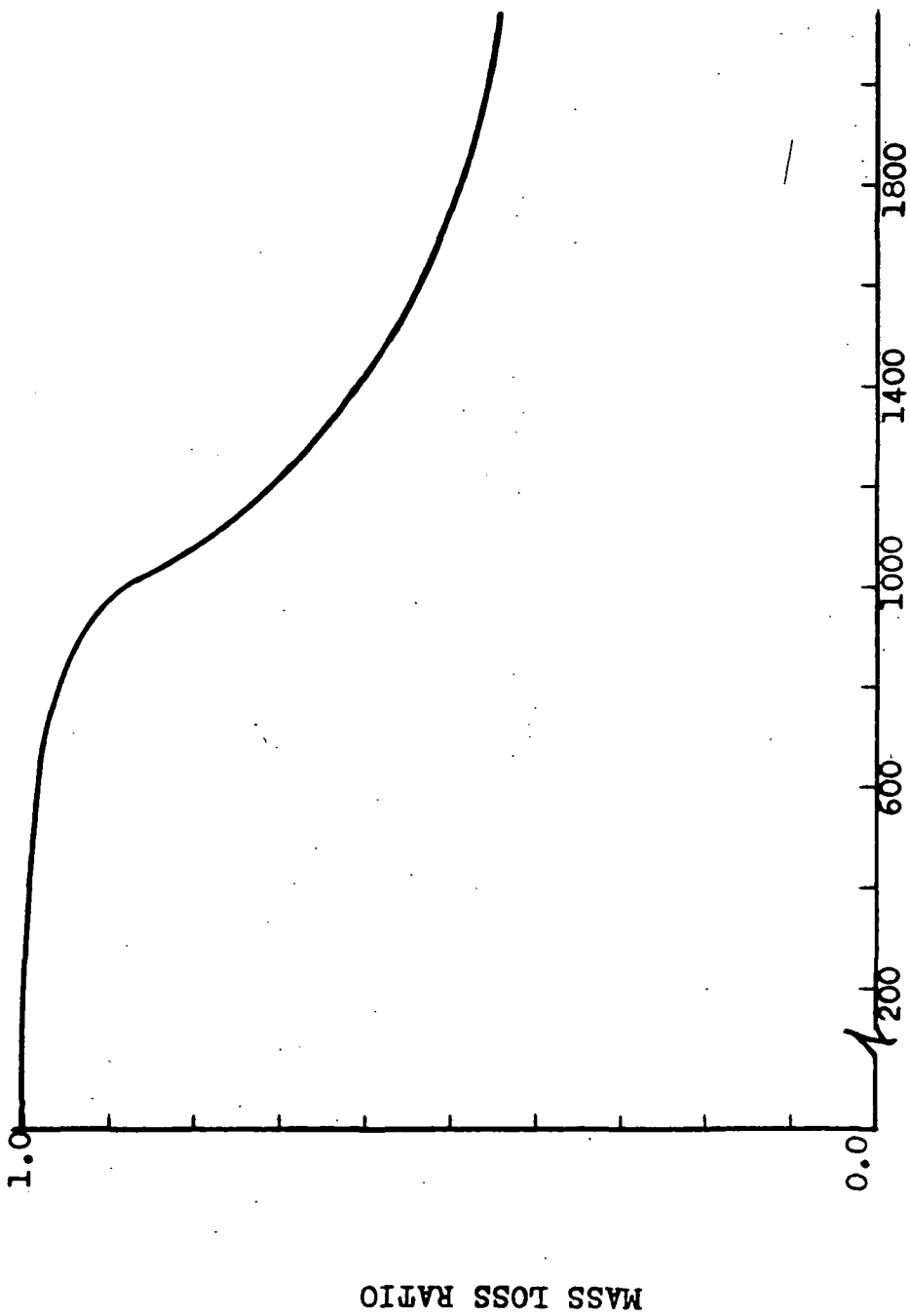

Figure 2-1. Typical Thermogravimetric Curve Relating the Mass Loss as a Function of Temperature for a Phenolic-Nylon Resin (2).

nylon-phenolic resin composite (2).

It is possible to calculate from this data the rate of pyrolysis gas generation W_g. The rate of mass loss of a material is affected by the rate at which the temperature is increased (deg/sec); that is, the heating rate. The inaccuracies resulting from the effect that the heating rate has on the pyrolysis gas generation rate, W_g, can be eliminated by the use of a kinetic expression of the form of Equation (2-1) below (1). This equation describes the rate of change of density, with time and is independent of the heating rate.

$$\frac{-1}{\rho_{i,o}} \frac{d\rho_i}{dt} = (\rho_i - \rho_s)/\rho_{i,o})^{n_i} \; Ae^{-(E_i/RT)} \qquad (2\text{-}1)$$

One approach to modeling the decomposition of plastic composites has been presented by Kondo and co-workers (3). Their analysis assumes decomposition to occur spacially rather than on a single plane. The authors state that this method of analysis should be used when the plastic material is made of different composites. They compare their analytical solutions with experimental data and report good correlation.

Another study of the decomposition process for plastic composites has been presented by Stroud (5, 6). In this investigation, the effects that kinetics, heat of pyrolysis, and surface recession velocity has on the reaction zone thickness, and the temperature range at which decomposition

of plastic occurs is examined. Kondo and co-workers (8), as mentioned, noticed also that the reaction zone thickness is affected by different parameters. In an attempt to simplify a very complex process Stroud (5, 6) studies, in addition, the assumption that the decomposition of plastic composites could occur at a single plane. His analysis shows that this simplification is usually valid for one reacting species and is considered to be a good engineering approximation.

Another analysis which considers decomposition reactions to occur over a finite region is that of Scala and Gilbert (9). Their analysis differs from that of Kondo et. al. (8) and Stroud (5, 6) in that the reaction zone thickness is assumed to be a constant. This is a drawback since this does not allow for the investigation of the effects of kinetics and heating rate on reaction zone thickness. Scala and Gilbert (9) discuss, in addition, some of the difficulties encountered by earlier investigators in describing the decomposition process accurately. They attributed the chief difficulty to an experimentally observed phenomena which showed that the mass generation rate, W_g, varied widely at high heating rates. Better experimental techniques and better correlation of experimental data (1, 2) seemed to have diminished some of the difficulties encountered by earlier investigators. An equation of the form of (2-1) was suggested by Friedman (9) to eliminate the uncertainties of the mass generation term caused by high heating rates.

Since decomposition in-depth is an important ingredient in the analysis of the ablation process, the work of Stroud (5, 6) and Kondo and co-workers (8) are reviewed in this chapter in detail. The work of Stroud (5, 6) is important because it determines and examines the important parameters which affect decomposition and reaction zone thickness. It is significant, in addition, because it attempts to simplify a very complex process, that of the decomposition of plastic composites, with the assumption that decomposition occurs at a single plane, and shows under which conditions this simplification holds.

The work of Kondo and co-workers (8) is also important in that they establish the necessity of considering decomposition to occur over a finite region and they examine, as in the case of Stroud (5, 6), the important variables that affect reaction zone thickness. The work of Stroud (5, 6) is presented in the following section.

Study of the Chemical Reaction Zone in Charring Ablators and the Reaction Plane Approximation During Thermal Degradation by Stroud

The work (5, 6) was a systematic approach of studying and establishing the important variables that affect the theoretical treatment of the thermal decomposition of plastic ablative composites. In addition, the validity of the approximation of describing decomposition of the plastic as taking place in a single reaction plane was studied. This was found to be a good engineering approximation for

one reacting species. The analysis with its assumptions is presented, and the results are summarized below.

The energy flow in the ablative heat shield on a large body entering the atmosphere is approximately one-dimensional, and therefore the energy equation for a chemically reacting solid was approximated by Stroud (5, 6) as:

$$\sum_{i=1}^{c} \frac{\partial \rho_i}{\partial t} H_{i,s} + \rho_i C_{p_{i,s}} \frac{\partial T}{\partial t} - \frac{\partial W_i}{\partial y} H_{i,g} - W_i C_{p_{i,g}} \frac{\partial T}{\partial y} = \frac{\partial}{\partial y} \left(k_s \frac{\partial T}{\partial y}\right) \qquad (2\text{-}2)$$

The above equation carries the assumption that the kinetic energy term can be neglected since it is three orders of magnitude smaller than the combined effects of the chemical and thermal energy terms. In addition the pressure was assumed to remain constant throughout the material because of the high permeability of chars. The author reasoned that "in practice, materials which form chars of low permeability and low strength would not be used due to the danger of internal pressure blowing off periodically and thus reducing the efficiency of the material" (5).

From the continuity equation

$$\bar{\nabla} \cdot \rho \bar{u} = - \frac{\partial \rho}{\partial t} \qquad (2\text{-}3)$$

where $\bar{u}$ is the velocity vector for the pyrolysis gases, and, therefore, for one-dimensional flow it becomes:

$$\frac{\partial \rho}{\partial t} = - \frac{\partial W}{\partial y} \tag{2-4}$$

Substitution of Equation (2-4) into (2-2) results in:

$$\sum_{i=1}^{c} \rho_i \, C_{p_{i,s}} \frac{\partial T}{\partial t} = \frac{\partial}{\partial y}\left(k_s \frac{\partial T}{\partial y}\right) + \sum_{i=1}^{c}\left[\frac{\partial \rho_i}{\partial t}(H_{i,g} - H_{i,s}) + W_i \, C_{p_{i,g}} \frac{\partial T}{\partial t}\right] \tag{2-5}$$

Notice that the number of gas components is numerically equal to the number of solid components in the ablator. This stems from the assumption made (5, 6) that each solid component degrades to a single gas species.

By assuming a quasi-steady state, that is, one in which the total mass flux of the system is constant, Stroud was able to eliminate the time dependence of the equation by using the following transformation:

$$\hat{y} = y - vt$$

where v is the surface recession velocity. Therefore, after the transformation is performed Equation (2-5) becomes:

$$k_s \frac{d^2T}{d\hat{y}^2} + \sum_{i=1}^{c}\left(C_{p_{i,g}} W_i \frac{dT}{d\hat{y}} - v \frac{d\rho_i}{d\hat{y}} \Delta H_i + v\rho_i \, C_{p_{i,s}} \frac{dT}{d\hat{y}}\right) = 0 \tag{2-6}$$

It should be noted that the assumption of constant thermal conductivity is valid only over a short temperature range, since the term dk/dT can become appreciable at higher temperatures. In our research the restriction of constant thermal conductivity was not made.

Stroud (5, 6) further simplified the energy equation by assuming that the specific heats of all constituents were the same, and from the quasi-steady assumption:

$$W = v\rho_o - v\sum_{i=1}^{c} \rho_i \qquad (2\text{-}7)$$

where ρ_o is the density of the virgin composite before degradation, Equation (2-6) was put into the form:

$$\frac{k_s d^2T}{dy^2} \sum_{l=z}^{c} \left(-vd\rho_i \frac{}{d\hat{y}} \Delta H_i + \rho_o v C_{p_{i,s}} \frac{dT}{d\hat{y}}\right) = 0 \qquad (2\text{-}8)$$

By integrating Equation (2-8) once, evaluating the constant of integration and letting $\eta=\hat{y} C_{p_{i,s}} \rho_o/k_s$, Equation (2-8) was transformed to:

$$\frac{dT}{d\eta} + \sum_{i=1}^{c} \left[\frac{\Delta H_i \rho_{i,o}}{C_{p_{i,s}} \rho_o} \left(1- \frac{\rho_i}{\rho_{i,o}}\right)\right] + T-T_o = 0 \qquad (2\text{-}9)$$

To obtain ρ_i as a function of the temperature T, and the dimensionless distance, η, an Arrhenius type relation of the form shown below was used:

$$\frac{d\bar{\rho}_i}{dt} = - \bar{\rho}_i \eta A_i e^{- E_i/RT} \qquad (2\text{-}10)$$

where ρ_i is a dimensionless density of the form:

$$\bar{\rho}_i = \frac{\rho_i}{\rho_{i,o}} \tag{2-11}$$

which expresses the ratio of the density of the composite i at an instant of time with respect to the original density $\rho_{i,o}$, of the virgin material. A_i is the frequency factor of the reaction and n, the order of the reaction.

It is worthwhile to note at this point, that Stroud (5, 6) assumed that the degradation of each composite i can be described by a single kinetic expression. However, it should be noted that this is not true in most cases. For phenolic-nylon and for other composites as well, more than one Arrhenius expression is necessary to describe the decomposition kinetics (1, 2).

From the continuity equation we have:

$$\frac{d\bar{\rho}_i}{dt} = - v \frac{d\bar{\rho}_i}{d\hat{y}} \tag{2-12}$$

and using the previous definition of η we have that Equation (2-12) becomes:

$$\frac{d\bar{\rho}_i}{dt} = - \frac{C_{p_{i,s}} \rho_o}{k_s} v^2 \frac{d\rho_i}{d\eta} \tag{2-13}$$

which when substituted into Equation (2-10) gives:

$$\frac{d\bar{\rho}_i}{d\eta} = \frac{k_s}{C_{p_{i,s}} \rho_o v^2} \bar{\rho}_i^{\,n} A_i e^{-E_i/RT} \tag{2-14}$$

which expresses the change of the dimensionless density ρ_i , with the dimensionless distance, η.

Two expressions were obtained by integrating Equation (2-14). One for $n \neq 1$ and was shown to be:

$$\bar{\rho}_i = \left[(n-1) \frac{k_s}{C_{p_{i,s}} \rho_o v^2} A_i \int_{\eta=o}^{\infty} e^{-(E_i/RT)} \cdot d\eta + 1 \right]^{\frac{-1}{1-n_i}} \qquad (2\text{-}15)$$

The other was for a reaction of order one; i.e., n=1, and was shown to be:

$$\bar{\rho}_i = \exp\left[- \frac{k_s}{C_{p_{i,s}} \rho_o v^2} A_i \int_{\eta=o}^{\infty} e^{-E_i/RT} \cdot d\eta \right] \qquad (2\text{-}16)$$

At this point in his development Stroud (6) simplified his analysis by considering only that one degradation reaction was taking place. For this case, the following transformation was found to be convenient.

$$\theta = \frac{RT}{E} \qquad (2\text{-}17)$$

Applying this transformation to Equation (2-9) a dimensionless form of the energy equation was obtained.

$$\frac{d\theta}{d\eta} + \frac{R\Delta H \rho_{1,0}}{E\, C_p\, \rho_0} (1-\bar{\rho}) + \theta \frac{RT_o}{E} = 0 \qquad (2\text{-}18)$$

where $\rho_{1,0}$, is the initial density of the only reactable species present.

Equations (2-15), or (2-16) and Equation (2-18) were

solved simultaneously by numerical techniques to determine the value of temperature as function of distance in the ablation material. The numerical scheme used, as reported by Stroud (6), consisted of first holding the value of the temperature constant in the density equation and integrating the equation over a small increment of distance. Then, the density was held constant at its calculated value in Equation (2-18) while this differential equation was solved over a small spacial increment.

Stroud (6) solved the energy equation for a number of different conditions by varying such parameters as the frequency factor, the activation energy, the heat of pyrolysis, the surface recession rate and the order of the reaction, and studied the effect that these parameters had on such things as the temperature profile reaction zone thickness and the reaction plane approximation. In Figure (2-2) the local density through the reaction zone is shown as a function of distance for two different values of the frequency factor. The curves shown were obtained for first order reactions. These curves were arbitrarily translated so that they would coincide when 50% of the degradable plastic had decomposed.

The reaction plane approximation is also shown. The char thickness was determined by considering that the char recession rate and the linear velocity of the reaction zone were the same. The thickness of the reaction zone was arbitrarily defined as the distance between the point at

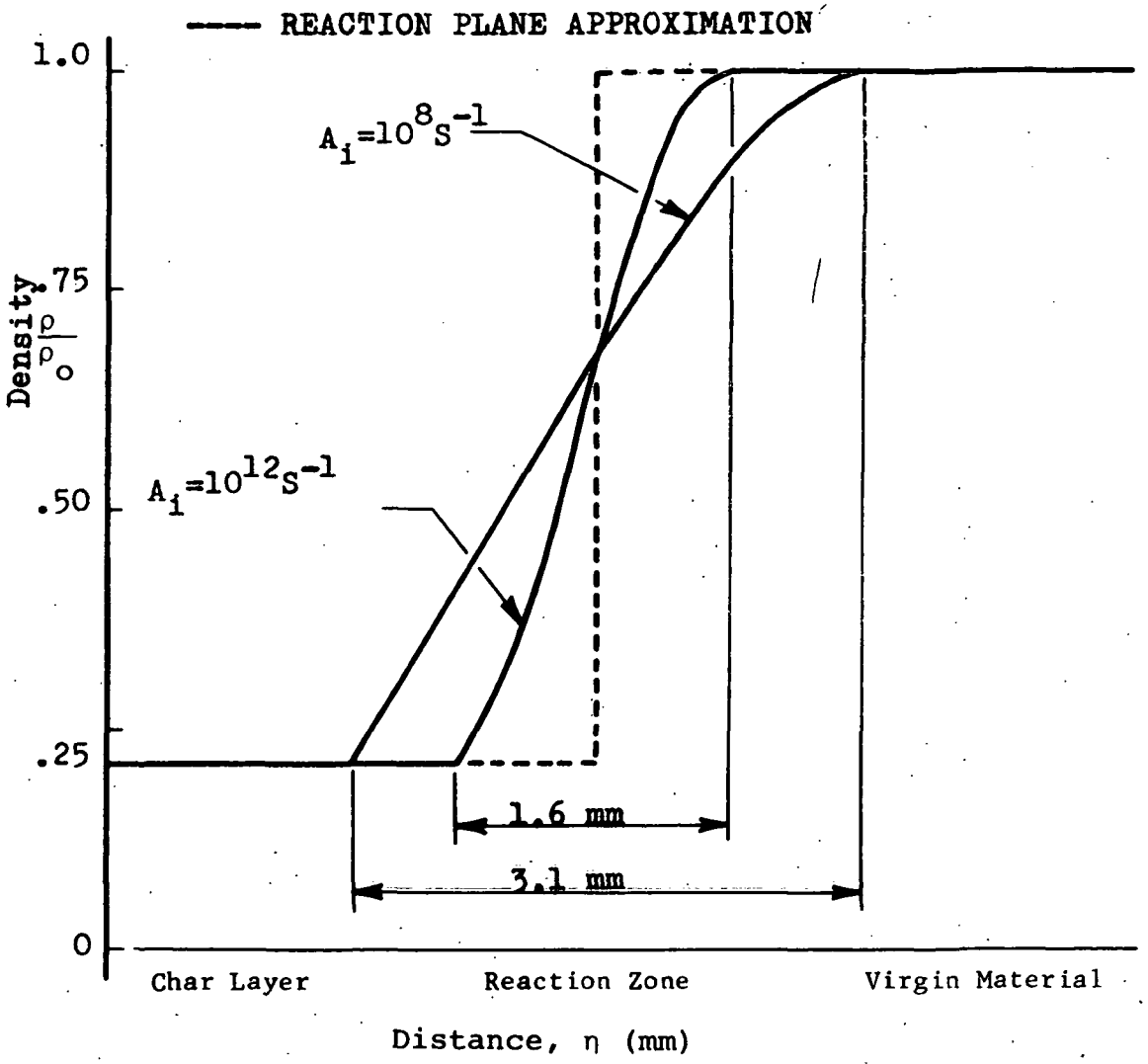

Figure 2-2. Variation of the Density Profile of the Virgin Plastic Through the Polymer Reaction Zone with Frequency Factor, as Reported by Stroud (6).

which the local density reached a value of 98 percent and the point at which it reached 2 percent of the original density of the reactable species. In the example shown by Stroud (6) 80 percent of the material was reactable. The two values of the frequency factor used in Figure 2-2 were said to be typical of a number of ablation materials. An increase in the frequency factor from 10^8 sec^{-1} to 10^{12} sec^{-1} produces a decrease in the reaction zone thickness of about 50 percent, from 2.1 mm to 1.6 mm. This seems reasonable to expect since a higher frequency factor implies a greater degradation rate and, therefore, a shorter time for degradation with a corresponding smaller reaction zone thickness. The two values of the frequency factor shown are said to be typical of a number of ablative materials.

Figure 2-3 exhibits the effects of surface recession velocity on reaction zone thickness for two values of the heat of pyrolysis. The curves were calculated for first order reactions and a frequency factor of 10^{12} sec^{-1}. A recession velocity of 25 micrometers per second (μm/s) was said to be representative of those obtained for charring ablators presently known. The curves of Figure 2-3 show that surface recession velocity has a greater impact than heat of pyrolysis on reaction zone thickness. The reason why the reaction zone thickness decreases with increasing surface recession velocity is that the greater the surface recession velocity, the greater the temperature gradient across the reaction zone. This steep temperature gradient

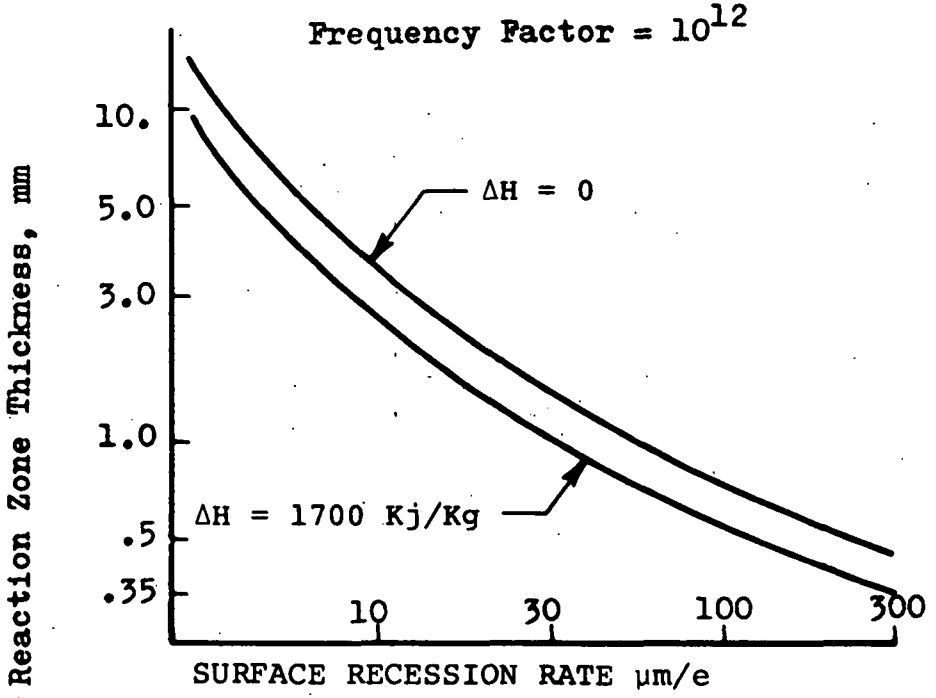

Figure 2-3. Effect of Surface Recession Velocity and Heat of Pyrolysis on Reacting Zone Thickness (5, 6).

causes the plastic to degrade rapidly thus reducing the time of reaction and hence, the thickness of the reaction zone. It appears that if the reaction zone thickness decreases with increasing surface recession velocity, the reaction plane approximation is asymptotically approached as the surface recession velocity increases. And therefore, the reaction plane approximation becomes more accurate the higher the surface recession velocity. An increase in the heat of pyrolysis produces a decrease in the thickness of the reaction zone. However, the size of the change of the reaction zone thickness is not as great as with the surface recession velocity.

Figure 2-4 illustrates the effect of activation energy. It demonstrates that the reaction zone thickness is practically independent of activation energy. "These results lead to an important conclusion regarding the effects of the frequency factor on ablative performance. The thickness of the reaction zone is controlled almost entirely by the frequency factor, whereas the pyrolysis temperature is strongly influenced by activation energy" (6). Activation energy and frequency factors have been shown to affect pyrolysis in different ways, hence a unique value of each must be found if accurate results are required.

Stroud (6) proceeded to define, what he called, the "median temperature of reaction" as that temperature at which 50 percent of the reactable material has been degraded. By using the median temperature definition, to get

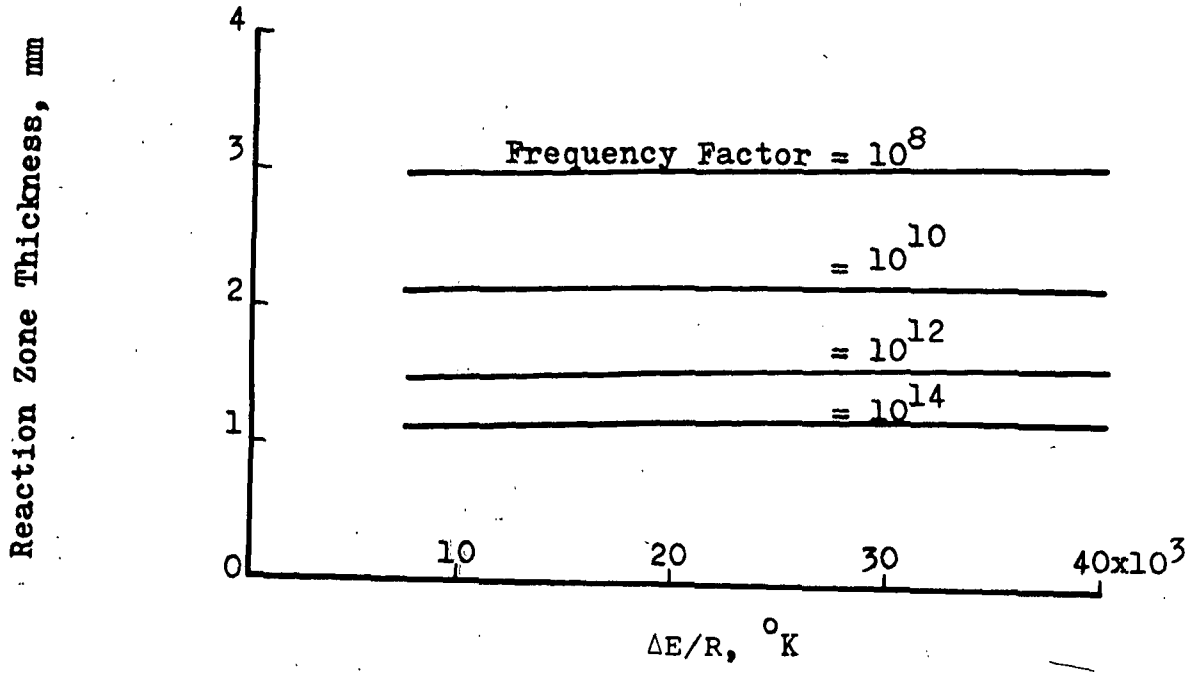

Figure 2-4. Effect of Activation Energy on Reaction Zone Thickness (5,6).

that point in space where the degradation reactions were supposed to take place in a plane, he was able to obtain correlations for the mass generation rate for reactions of order one-half, one and two. These are shown below:

$$w_{1/2} = (\rho_o - \rho_c)\sqrt{\frac{k_s A}{\rho_o C_{p_{i,s}}}}\, e^{-\left\{\frac{0.7+2.2\Delta\bar{H}}{2(0.955)} - \frac{1}{2(0.955\ \theta m)}\right\}} \qquad (2\text{-}19)$$

for first order reaction:

$$w_1 = (\rho_o - \rho_c)\sqrt{\frac{k_s A}{\rho_o C_{p_{i,s}}}}\, e^{-\left\{\frac{1.5+3.6\Delta\bar{H}}{2(0.955)} - \frac{1}{2(0.955\ \theta m)}\right\}} \qquad (2\text{-}20)$$

for second order reaction:

$$w_2 = (\rho_o - \rho_c)\sqrt{\frac{k_s A}{\rho_o C_{p_{i,s}}}}\, e^{-\left\{\frac{1.7+1.8\Delta\bar{H}}{2(0.945)} - \frac{1}{2(0.945\ \theta m)}\right\}} \qquad (2\text{-}21)$$

where the dimensionless median temperature $1/\Theta$ is obtained by using the equations shown below. These equations were developed by Stroud (6) and are: for a half order reaction:

$$\frac{1}{\Theta_m} = -0.7 + 0.955 \ln \bar{A} - 2.2\ \Delta\bar{H} \qquad (2\text{-}22A)$$

for a first-order reaction:

$$\frac{1}{\Theta_m} = -1.50 + 0.955 \ln \bar{A} - 3.6\ \Delta\bar{H} \qquad (2\text{-}22B)$$

and for a second order reaction:

$$\frac{1}{\Theta_m} = -1.70 + 0.945 \ln \bar{A} - 1.8\ \Delta\bar{H} \qquad (2\text{-}22C)$$

Equations (2-19), (2-20) and (2-21) hold when

$$0 \leq \Delta H \leq 0.5$$

$$10^6 \leq \bar{A} \leq 10^{15}$$

Equation (2-19), (2-20) and (2-21) give the mass flow rates of pyrolysis gases for the reaction plane approximation for one reactable species. These flow rates locate the reaction plane at the median point in the reaction zone as was shown in Figure 2-2. Thus, it was shown that the rate of pyrolysis is a function of thermophysical data which can be readily obtained from thermogravimetric analysis. The correlations derived by Stroud (6) are only valid for one reactable species, and of course for high surface recession velocities. The author did not present a study, nor did he speculate on what possible effects more than one reactable species would have in his analysis of the reaction plane approximation. However, he did show a comparison between the reaction plane approximation and the more complicated in-depth analysis for the case of one reactable species. This is illustrated in Figure 2-5. For each frequency factor shown, the temperature distribution obtained with the reaction plane approximation is close to that obtained with the more complicated in-depth analysis. This agreement, as stated by the author, illustrates the accuracy that is possible to achieve using the reaction plane approximation when quasi-steady conditions exist.

Several conclusions were drawn by Stroud (6) from studying and solving the equations for a wide range of

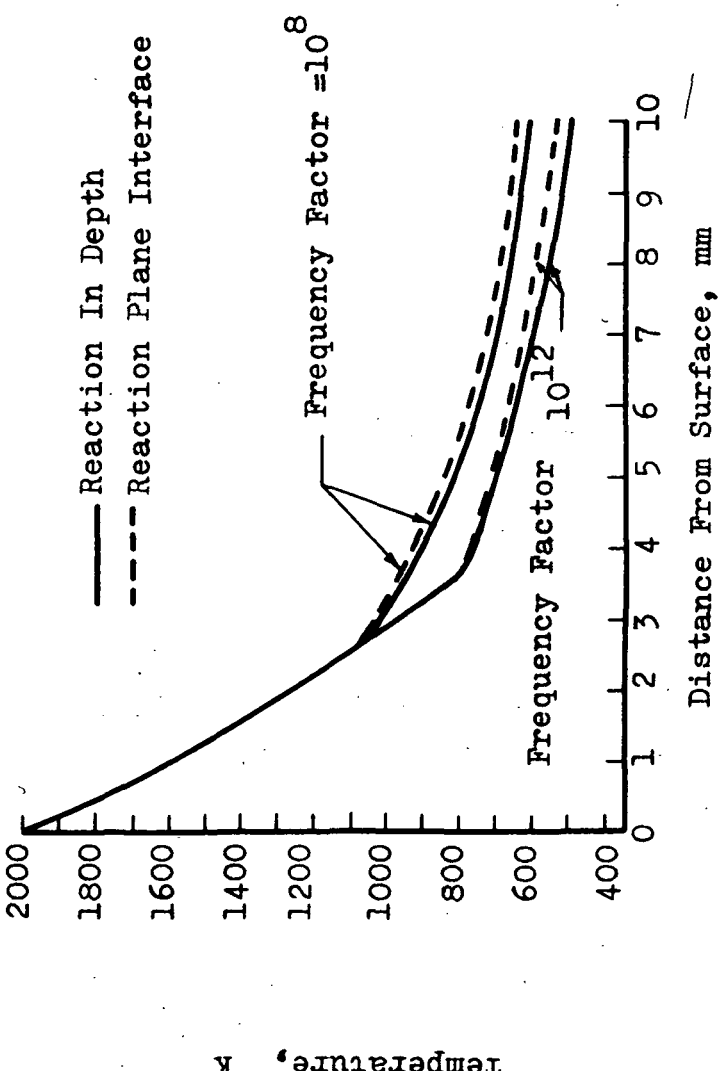

Figure 2-5. Comparison of Temperature Profiles Calculated by Reaction In Depth Analysis and Reaction Plane Approximation (5, 6).

quasi-steady state conditions. These were: 1) The temperature distribution in the ablation material is strongly dependent on the heat of pyrolysis; 2) Since activation energy and frequency factors have different effects of pyrolysis, it is necessary to obtain unique and accurate values for each of these parameters; 3) The total mass flow of pyrolysis and the median temperature can be correlated on the basis of the Arrhenius formula; 4) The reaction plane approximation, which incorporates the Arrhenius pyrolysis temperature, gave satisfactory agreement with reaction in-depth analyses and with experiments for one reactable species.

The contributions of Stroud's studies (5, 6) have been to define those conditions under which the reaction plane approximation can be used for one degrading species without loss of accuracy. In addition, his studies have shown the critical effect that decomposition kinetics have on the accurate description of the ablation process. This indicates the necessity of obtaining unique and accurate values for the frequency factor and activation energy of the degradation process. In the following section the work of Kondo and co-workers (8) is discussed.

An Analysis of Steady State Ablation of Charring Materials by Kondo, Fujiwara and Matsomuto

Physical Model: The work of Kondo, et. al. (8) is a one-dimensional, steady-state, ablation analysis where the thermal decomposition reaction in the charring material is

treated separately from the aerothermochemistry of the flow adjacent to the surface and the gas injection from the surface of the solid material. The study "is restricted to the analysis of the pyrolysis reaction in the charring material". (8). The material is considered to consist of three chemically different zones, namely, virgin material (solid), pyrolysis zone (solid and gas) and the char layer (solid and gas). In Figure 2-6 these three zones are illustrated. The pyrolysis zone regression velocity is assumed to be equal to the surface recession of the char. The recession of the char layer is assumed to be caused by three mechanisms: (1) Char layer being compressed by stagnation high pressure, (2) Char being consumed by the reaction of the pyrolysis gases with the carbonaceous char, and (3) by heterogenous reactions with the gas on the surface.

Basic Assumptions of Kondo's et. al. Analysis: Before introducing the basic equations of the analysis we shall summarize some of their basic important assumptions:

1) One -dimensional analysis. That is, the heat flow and gas flow were assumed normal to the ablating surface.

2) Quasi-steady analysis. Thus the recession velocity, v, is constant.

3) The pyrolysis reaction is a simple chemical reaction which changed the plastic material into gases plus

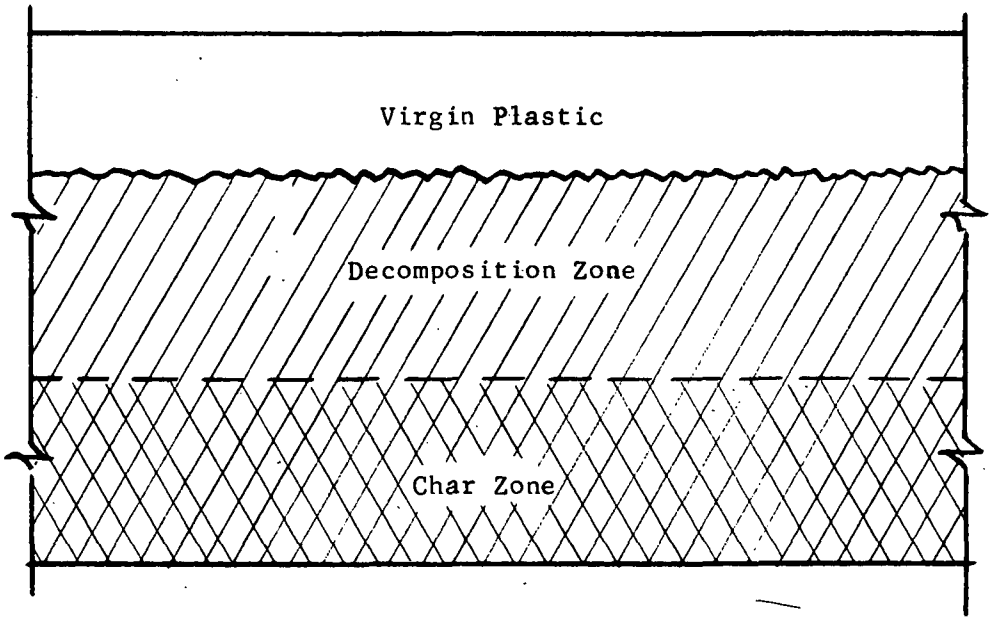

Figure 2-6. A Schematic Diagram of the Three Chemically Distinct Zones Used by Kondo et. al. (8) in Their Analysis of Steady State Ablation of Charring Materials.

char.

4) Thermal equilibrium between the gas and solid was assumed.

5) The assumption of constant physical properties across the reaction zone was used.

6) The viscocity of the gas was neglected in the energy equation.

7) The thickness of the ablating material was considered to be large in comparison with the width of the char layer or pyrolysis layer. Therefore, the virgin material was assumed to be located at the infinite distance.

It is pertinent to comment at this point on some of the above assumptions since they relate directly to the analysis proposed in our research. The assumption of thermal equilibrium is acceptable. Clark (16) found in his experimental studies with simulated chars that this was a fair approximation of what actually occurs during the ablation process. April (19) in his experimental work found in addition, that there was less than 200° F between simulated pyrolysis gases entering a char and the carbonaceous matrix. This temperature difference was measured approximately 1/4" away from the back surface of the char before the gases entered it. The assumption of thermal equilibrium allows in addition a simplification of the model by not having to consider the energy transfer between the gas and the solid matrix. The decomposition of the virgin material is assumed to be described by a simple Arrhenius

formula. As was mentioned before, this approach tends to make the kinetics independent of the heating rate at which they were obtained. This approach has been used also by Stroud (5, 6), Scala and Gilbert (9) and others (10, 84, 85). In this research the Arrhenius expression is also used. However, a more complicated model of seven kinetic reactions is used. Kondo and co-workers (8) neglect the viscosity of the gases and, therefore, assumed that viscuous effects on the energy equation are negligible. In Chapter III this assumption is shown to be realistic for this type of analysis. On the other hand, their assumption of constant physical properties is not accurate. The temperature difference that typical char forming ablators could experience during reentry is of the order of 4000°F to 5000°F. Over this temperature range change in physical and thermodynamic properties is significant.

Fundamental Equations: The coordinates used by Kondo et. al. (8) are shown in Figure 2-7. The y axis is coincident with the reverse direction of reaction which extends from zero to $-\infty$. The origin is taken at the initial position of the solid surface at y=0. The equation of continuity for the solid material was shown to be:

$$\frac{\partial}{\partial t}(\rho_s a) = -\rho_s a A (e^{-E/RT} - \alpha) \qquad (2\text{-}23)$$

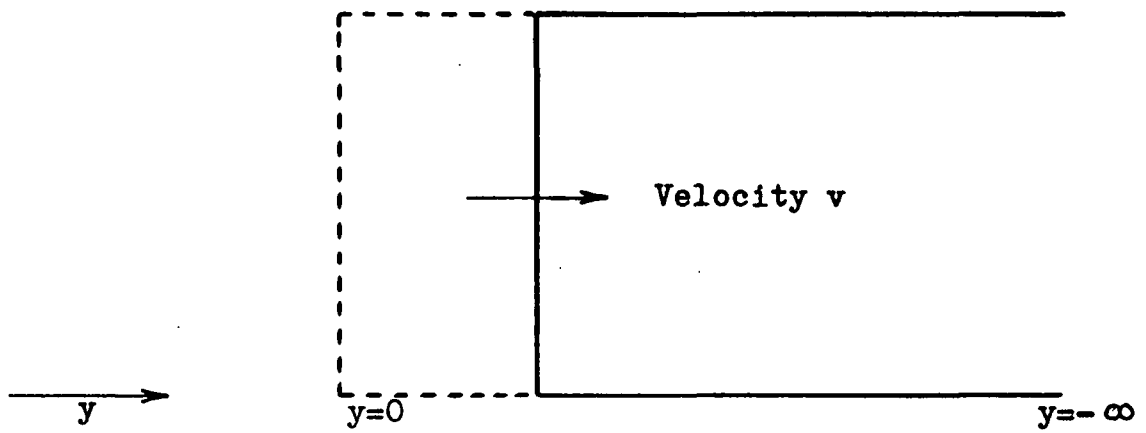

Figure 2-7. Illustration of the Coordinate Used by Kondo et. al. (8), Where the y Axis is Coincident With the Reverse Direction of Reaction, Whick extends From 0 to - Infinity and Where the Origin is Taken at the Initial Position of the Solid Surface at y=0.

where

$$\alpha = e^{-E/RT}\Big|_{-\infty} \tag{2-24}$$

The equation of continuity for the pyrolysis gases is:

$$\frac{\partial}{\partial t}\{\rho_g\ (1-a)\} + \frac{\partial}{\partial y}\{\rho_g\ u_g\ (1-a)\} = \rho_s\ a\ A\ (e^{-E/RT} - \alpha) \tag{2-25}$$

where "a" is an effective cross sectional area of the solid material in the pyrolysis zone. It is defined as "the ratio between the density of char at the surface and that of the virgin material, since the density of char crushed into powders equals to that of virgin material according to the experimental results. 'a' changes to 1 on the boundary of the virgin material". (8).

The equation of motion is:

$$\rho_g \frac{\partial u_g}{\partial t} + \rho_g\ u_g \frac{\partial u_g}{\partial y} = -\frac{\partial P}{\partial y} \tag{2-26}$$

and the energy equation is:

$$\frac{\partial}{\partial y}\left[k_g\ a \frac{\partial T}{\partial y} + k_s\ (1-a)\ \frac{\partial T}{\partial y}\right] - \frac{\partial}{\partial y}\left[\rho_g u_g\ C_{p,g}\ (1-a)\right] =$$

$$-\rho_s\ A\ Q\ (e^{-E/RT} - \alpha) + \frac{\partial}{\partial t}\left[\rho_s\ C_{p,s}\ T\ \alpha\right] + \frac{\partial}{\partial t}\left[\rho_g C_{p,g}(1-a)\ T\right] \tag{2-27}$$

The first bracketed term on the left hand side expresses the increase in thermal energy by heat conduction. The second term on the left hand side represents the thermal energy absorbed by the pyrolysis gases due to convection.

The right hand side of the equation represents the energy change by pyrolysis reaction (first term) and by non-steady effect (last two terms).

Finally:

$$P = \frac{1}{M_W} \rho_g RT \qquad (2\text{-}28)$$

which is the ideal gas equation of state. Equations (2-23) and (2-25) to (2-28) are the fundamental relationships used to solve for the system of five unknowns. P, ρ_g, T, a and u_g.

Coordinate Transformation: Kondo, et. al. (8) took advantage of their quasi-steady assumption and performed a coordinate transformation. v, the regression velocity was assumed constant and therefore, the coordinate transformation is:

$$\hat{x} = y + v\ t \qquad (2\text{-}29)$$

which means that the coordinate system moves with the regression velocity of the pyrolysis zone.

Performing this transformation the equation of continuity for the solid becomes:

$$\frac{d}{d\hat{x}} (a\ v) = -\ a\ A\ (e^{-E/RT} - \alpha) \qquad (-30)$$

and that for the gas:

$$\frac{d}{d\hat{x}} \{\rho_g\ (1-a)\ (v+u_g)\} = \rho_s\ a\ A\ (e^{-E/RT} - \alpha) \qquad (2\text{-}31)$$

The equation of motion becomes:

$$\rho_g \ (u_g + v) \ \frac{du_g}{d\hat{x}} = - \frac{dP}{d\hat{x}} \qquad (2\text{-}32)$$

and finally the energy equation is transformed to:

$$\{k_s \ a + k_g \ (1-a)\} \ \frac{d^2T}{d\hat{x}^2} + \{k_s \ \frac{da}{d\hat{x}} - k_g \ \frac{da}{d\hat{x}} - \rho_g \ u_g \ C_{p,g}$$

$$(1-a) \ - \rho_s \ v \ C_{p,s} \ a\} \ \frac{dT}{d\hat{x}} \ + \{\rho_g \ u_g \ C_{p,g} \ \frac{da}{d\hat{x}} - \rho_s \ v \ C_{p,s} \ \frac{da}{d\hat{x}}\} T$$

$$= \ - \rho_s \ a \ A \ (e-1) \qquad (2\text{-}33)$$

Combining Equations (2-30) and (2-31), integrating and evaluating the constant of integration, Kondo, et. al. (8) obtained the following equation:

$$\rho_g \ u_g = v(\rho_s - \rho_g) \qquad (2\text{-}34)$$

Since $\rho_s >> \rho_g$ Equation (2-34) becomes:

$$\rho_g \ u_g = \rho_s \ v \qquad (2\text{-}35)$$

The authors assumed that since u_g and v are small in comparison with the sound velocity, the pressure P can be considered constant. Moreover, the authors assumed that $k_g << k_s$, which is generally the case. By neglecting k_g and substituting Equation (2-35) into (2-33), the energy equation was shown to be:

$$k_s \ a \ \frac{d^2T}{d\hat{x}^2} + \{k_s \ \frac{da}{d\hat{x}} - \rho_s \ v \ C_{p,g} \ (1-a) - \rho_s \ v \ C_{p,s} \ a\} \ \frac{dT}{d\hat{x}} +$$

$$\rho_s \ v \ \frac{da}{d\hat{x}} \ (C_{p,g} - C_{p,s}) \ T = -Q \ \rho_s \ a \ A \ (e^{-E/RT} - \alpha)$$

$$(2\text{-}36)$$

Equations (2-30) and (2-36) with boundary conditions:

$$T = T_o \text{ or} \left(\frac{dT}{d\hat{x}}\right)_o = \text{given at } \hat{x} = 0$$

$$a = a_o = \frac{\rho_{char}}{\rho_s} \quad \text{at } \hat{x} = 0 \tag{2-37}$$

and

$$T = T_{-\infty} \quad \text{and} \quad a = 1 \quad \text{at } \hat{x} = -\infty \tag{2-38}$$

There are four boundary conditions for the first and second order differential Equations (2-30) and (2-36) involving two unknowns T(x) and a(x). Therefore, the regression velocity v was determined as an eigen-value of the equations (8)

Non-Dimensional Equations: Kondo and co-workers (8) found it convenient to non-dimensionalize Equations (2-30) and (2-36) by defining the following non-dimensional groups:

$$\gamma = C_{p,s}/C_{p,g} \tag{2-39}$$

$$Q^* = Q/C_{p,g}\, T_{-\infty} \tag{2-40}$$

$$\theta = T/T_{-\infty} \tag{2-41}$$

$$\theta_o = T_o/T_{-\infty} \tag{2-42}$$

$$E^* = E/RT_{-\infty} \tag{2-43}$$

$$\hat{x}/L = \xi \tag{2-44}$$

$$\beta = AL/ve^{-E^*/\theta} \tag{2-45}$$

In addition the author chose to define a characteris-

tic area $L^2 = k_s/(a\ C_{p,g}\ \rho_s\ e^{E^*/\theta_o})$.

Substitution of the above terms in Equation (2-30) results in

$$\frac{da}{d\xi} = -\beta\ a\ e^{E^*/\theta_o}\ (e^{-E^*/\theta_o} - \alpha) \qquad (2\text{-}46)$$

and into (2-37) results in a dimensional form of the energy equation which is:

$$\frac{d^2\theta}{d\xi^2} = \{\frac{1}{\beta} \cdot \frac{1-a}{a} + \beta\ e^{E^*/\theta_o}\ (e^{-E^*/\theta_o} - \alpha)\}\ \frac{d\theta}{d\xi} +$$

$$(\gamma-1)\ e^{E^*/\theta_o}\ (e^{-E^*/\theta_o} - \alpha)\ \theta + Q^*\ e^{E^*/\theta_o}(e^{-E^*/\theta} - \alpha) = 0 \qquad (2\text{-}47)$$

while the new boundary conditions are:

$$a = a_o,\ \theta = \theta_o \text{ or } \frac{d\theta}{d\xi_o} = \text{given at } \xi = o$$

and

$$a = 1,\ Q^* = 1 \text{ at } \xi = -\infty$$

Equations (2-46) and (2-47) were solved numerically for the above boundary conditions. The value of the parameters γ=1.0, E^*=3.0, a_o=23, and $T_{-\infty}$=300°K were used in the numerical solution and were said to be typical of phenolic resin composites (8).

Numerical Solution: Equation (2-46) and (2-47) have a family of solutions depending on the value of β and $(d\theta/d\xi)_o$ respectively. However, there is a unique value

of β that satisfies the condition that at $\xi = -\infty$, a=1. The solid line in Figure 2-8 shows this solution, which the authors choose to call a:OK. The dotted line represents a solution for which the value of β does not satisfy the final of a=1. Similarly, there is a unique value of $(d\theta/d\xi)$ which satisfies the condition that at $\xi = -\infty$, θ=1. Figure 2-9 illustrates the correct solution, line θ:OK. The dotted line is a solution which does not satisfy the final value of θ=1. This type of final value problem is usually solved by trial and error. However, Kondo, et. al. (8) choose to solve graphically for these values of β and $(d\theta/d\xi)_o$. This graphical solution is illustrated in Figure 2-10. The curve a:OK is the locus of the points corresponding to the values $(d\theta/d\xi)_o$ and β to get the solution a (ξ), which satisfies the boundary conditions for a. The curve θ:OK indicates the combination of $(d\theta/d\mu)_o$ and β which gives the solution $\theta(\xi)$ which satisfies the boundary conditions for θ. Therefore, the intersection of these two curves determine the appropriate values of $(d\theta/d\xi)_o$ and β which satisfy simultaneously both equations.

In Figure 2-11 it is shown that the thermal decomposition process takes place over a finite region. Note that $da/d\xi$ given by Equation (2-46) is the non-dimensional expression of the decomposition process. As stated by Kondo, et. al. (8) many researchers have assumed that the pyrolysis reactions occur at the surface of the "heat conducting region" (which is the virgin material) and have

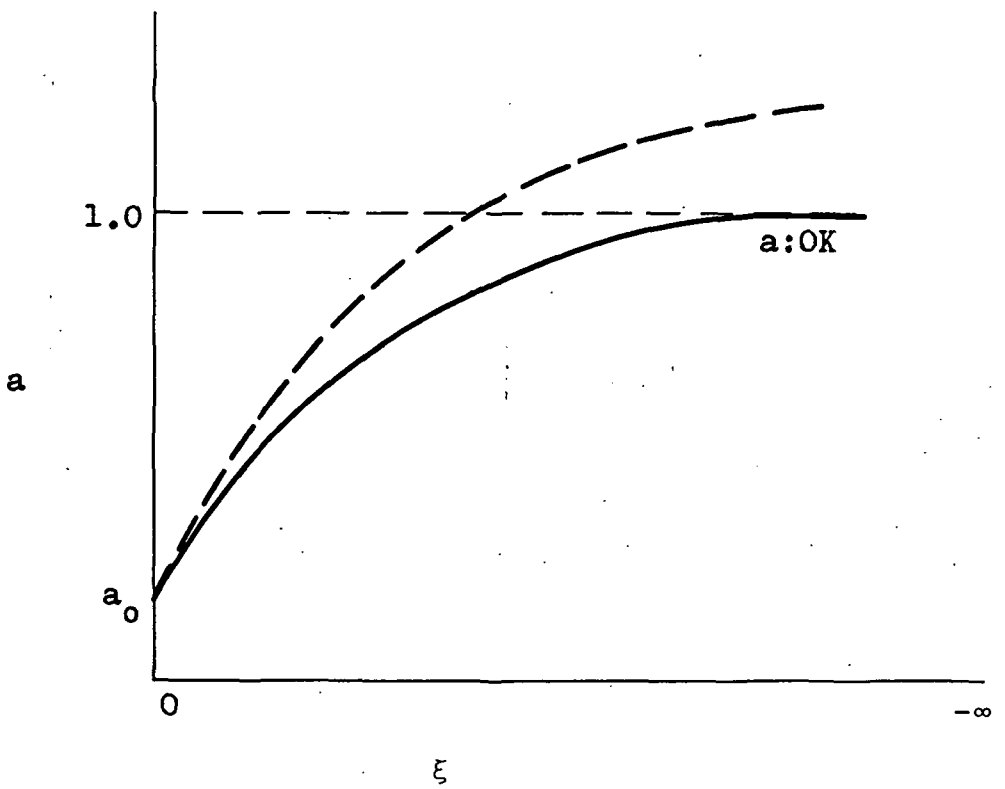

Figure 2-8. Kondo's (8) Technique for Searching for a Unique Value of a.

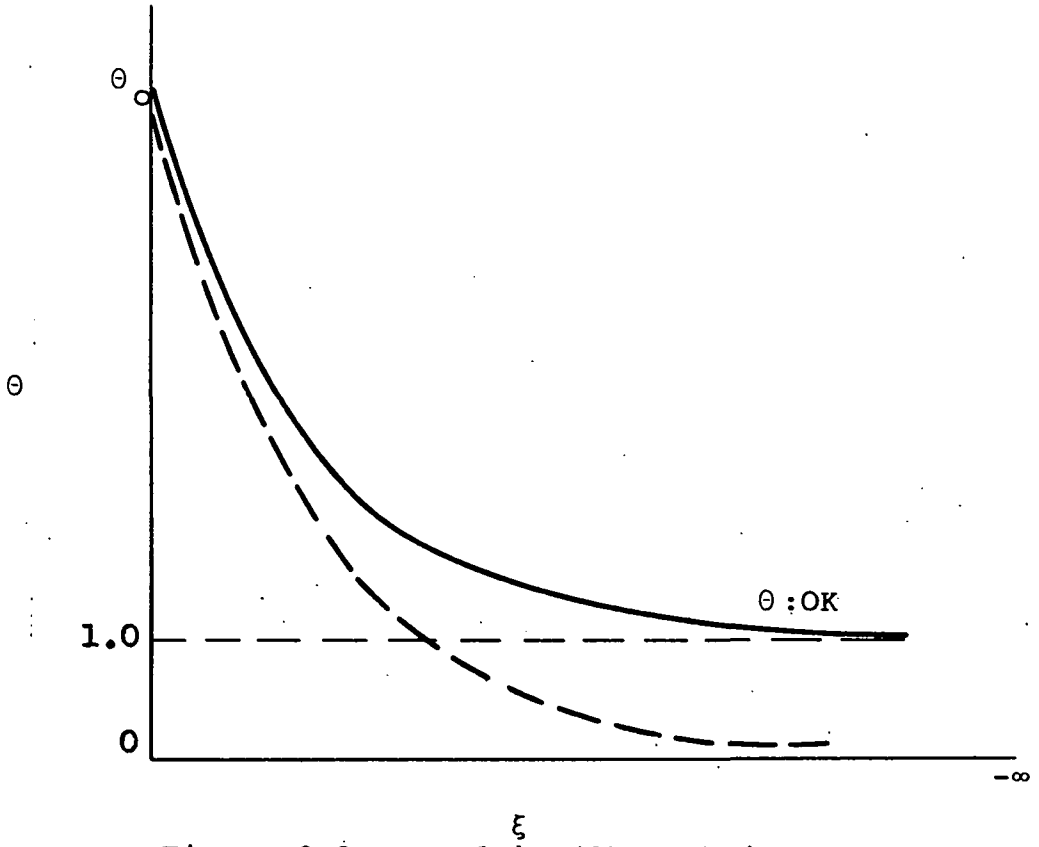

Figure 2-9. Kondo's (8) Technique for Searching for a Unique Value of Θ.

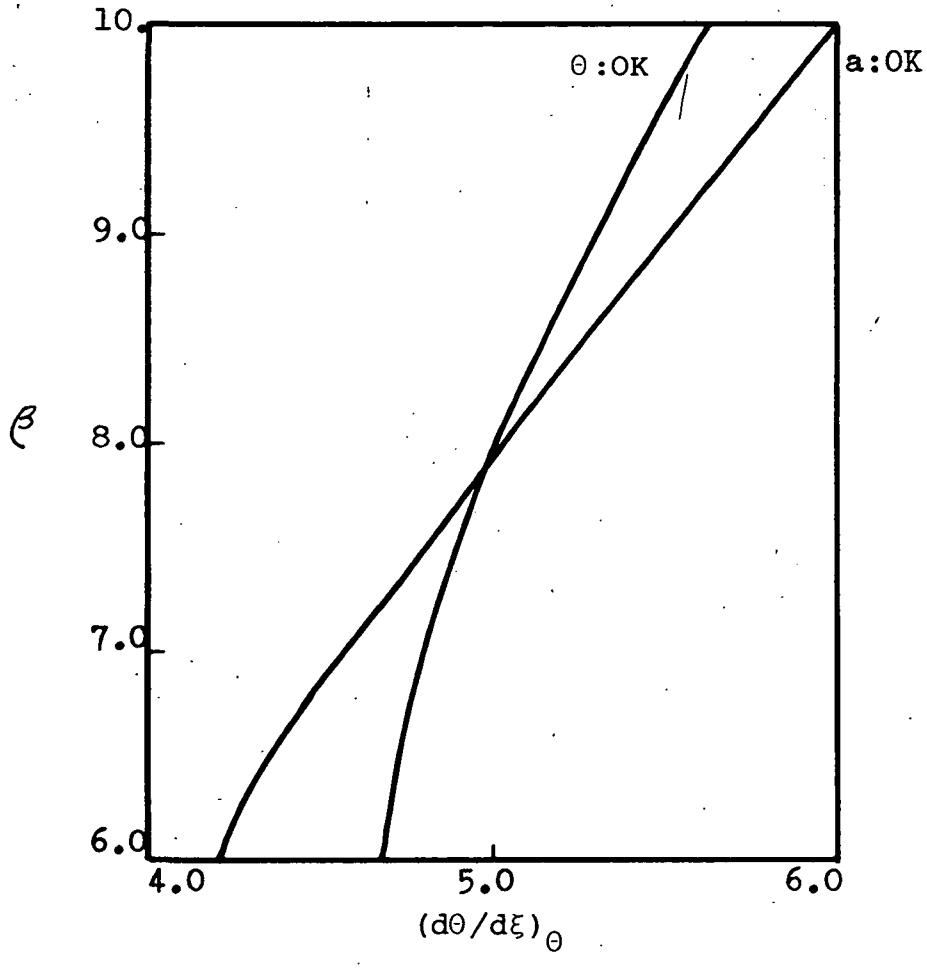

Figure 2-10. Illustration of Kondo's (8) Technique for Determining the Eigenvalues for the Equation Describing the In Depth Response of Ablative Composites.

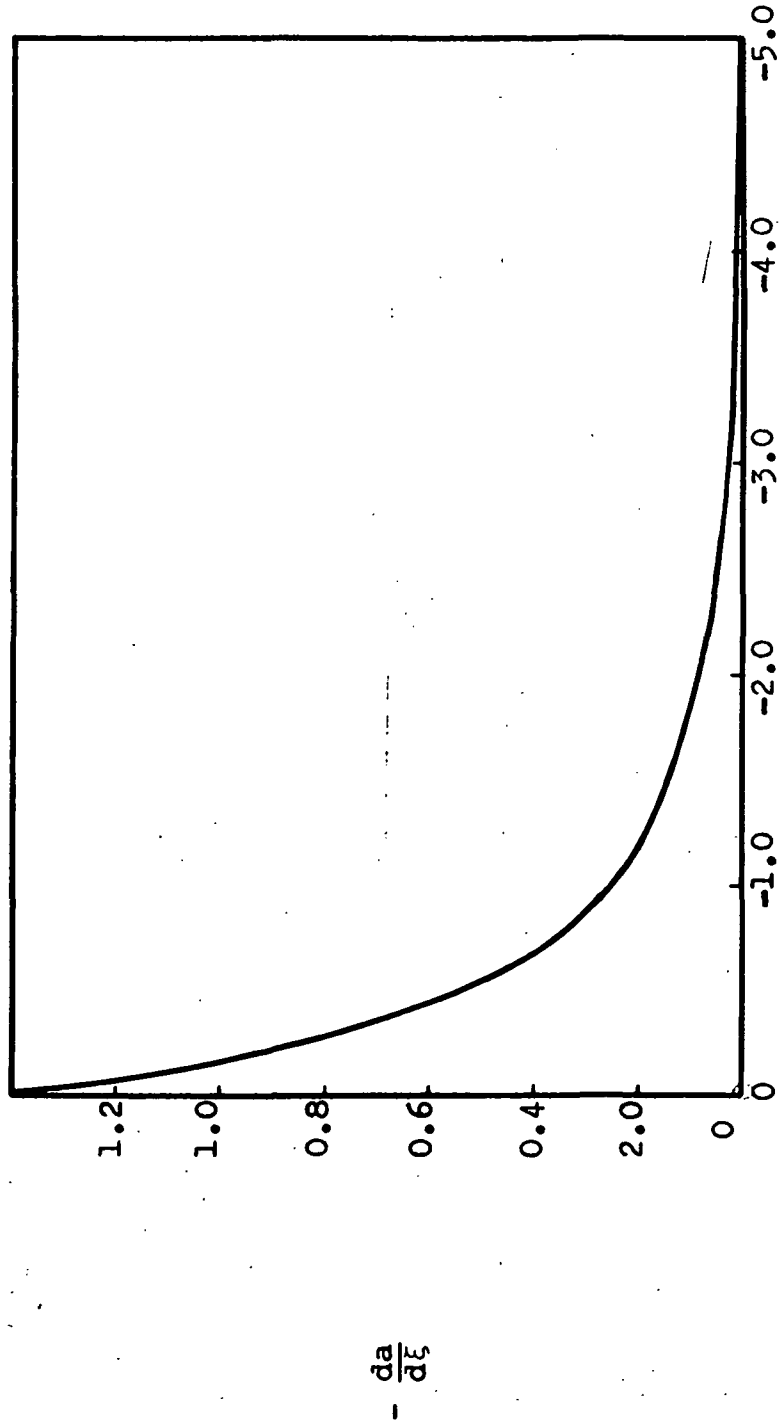

Figure 2-11. Illustration of the Dimensionless Decomposition Rate Behavior at a Value of Θ =0.6 as calculated by Kondo (8) for a dimensionless distance ξ.

neglected the depth of the pyrolysis reaction as is shown in Figure 2-11. This, the authors claimed, is inadequate.

The effect of the change in the non-dimensional temperature, θ_o, on the temperature profile θ, is illustrated in Figure 2-12.

In summary, the ablation analysis of Kondo and coworkers (8) is for a one-dimensional ablation model. The most significant contribution of their analysis is to have indicated the importance of considering decomposition in depth to take place in a final region of space. However, their assumption of constant physical properties is considered to be a serious limitation in the analysis. In addition, the assumption that phenolic resin decomposition is described by a single Arrhenius expression is inadequate. As has been indicated before, several pseudo-order kinetic expressions of the Arrhenius type are required to adequately describe decomposition of phenolic nylon resin composites (1, 2).

In the following sections typical transient response analyses along with a summary of related work of flow in the char zone are discussed. This summary is given to support our mathematical analysis and to justify some of the assumptions made. We refer to the work of April (19) for a more detailed discussion of the subject of transpiration cooling, carbon deposition and related areas.

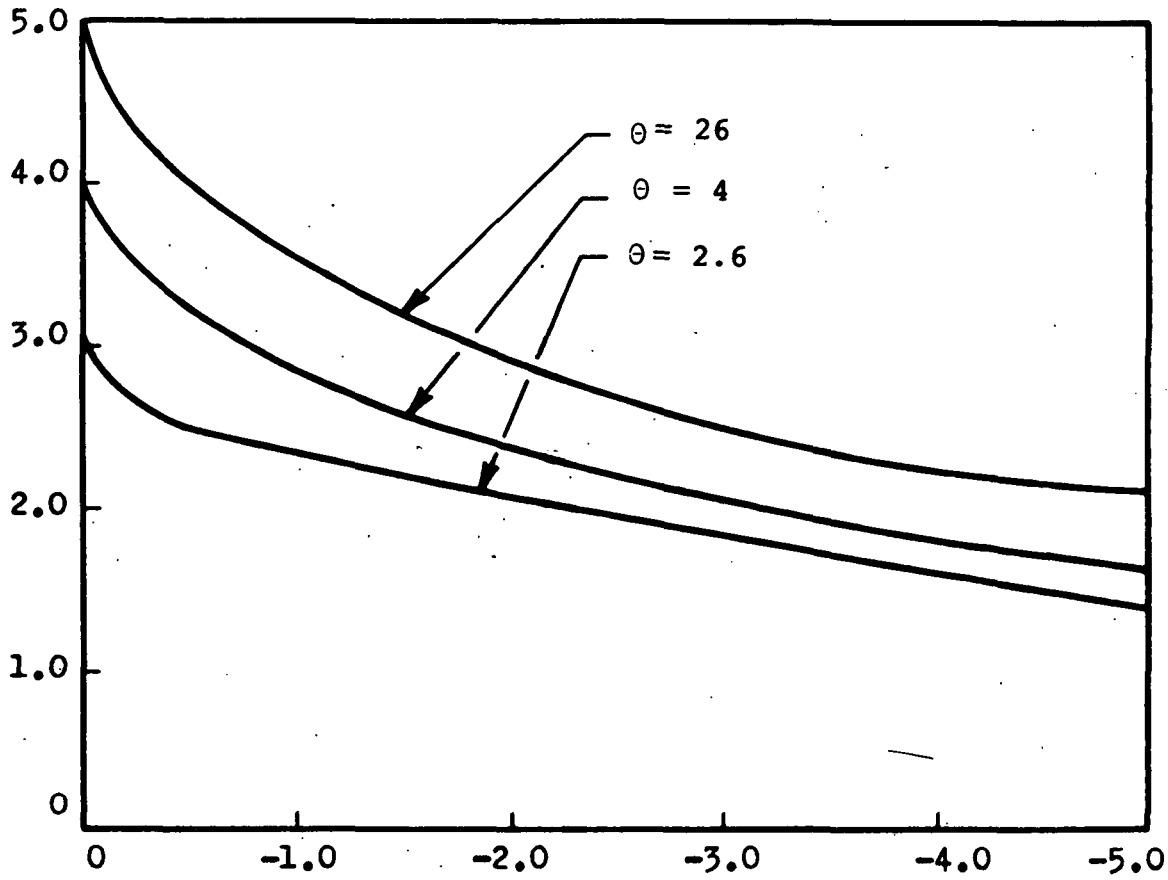

Figure 2-12. Behavior of Dimensionless Temperature Profile of Kondo (8) for Different Dimensionless Surface Temperatures θ.

Transient Analyses to Describe the Response of Thermal Protection Systems

The need for the accurate description of the thermal response of ablative composites is required to insure a safe design for thermal protection of reentering space vehicles. The necessity is also dictated by the desirability of reducing expensive ground testing to a minimum. Although these facilities have improved over the years, all the complex interactions of the shock heated gas and the ablative heat shield are not easy to simulate in these ground test facilities (55, 93-99). Therefore, accurate and realistic mathematical analyses are needed to effectively predict the thermal response of ablative composites under a wide variety of external flow field conditions.

Almost all major aerospace companies and governmental agencies interested in ablative heating have analyses of the transient response of thermal protective systems. The literature on this subject is abundant. Lapple and co-workers (106) have compiled over 525 references on the area of ablation of related topics. More recently Penner and Olfe (87) in their chapter on ablation, have more than thirty references on major aspects of the ablation process, for both charring and non-charring materials. To try to cover just a small percentage of these references would be a difficult and time consuming task without contributing much insight into the analysis proposed in this research.

Moreover, April (19) has written a detailed review on some of the most important work in transpiration cooling and has an extensive list of references on the more important aspects of the ablative process. In addition to the three previously mentioned references, there are some important review articles on the topic of ablation which have extensive bibliographies on the subject (100-106). For these reasons, it would be considered repetitious to go over this material which has been thoroughly covered in other places. Rather it is best to devote a brief discussion to what we consider to be four important and typical transient ablation analyses. These are those of: Swann, et. al. (58), Kendall, et. al. (51, 53) and Kratch, et. al. (83), and Clark (111). In addition we will summarize in a later section some of the research done on flow of pyrolysis gases through porous chars and related areas.

The ablative analysis of Swann, et. al. (58) is a one-dimensional analysis of the transient response of plastic composites. The thermal response of materials was described with as many as three different layers, and the first two could have moving boundaries. The coupling of the flow field to the ablative surface was done by means of an energy balance. This energy balance was performed at the char surface, where the convective heating rate was computed using either a linear or quadratic approximation to the blocking effectiveness for a laminar boundary layer.

The cold-wall convective heating rate and the radiant heating rate incident on the surface were specified functions of time. These values were used as inputs in their numerical solution. The surface removal mechanisms were considered to be vaporization at the sublimation temperature, and diffusion and/or reaction controlled oxidation of the carbon at the surface.

The energy equation for the one-dimensional, non-steady flow of pyrolysis gases in the char zone was given as:

$$- \frac{\partial}{\partial x} \{k_g \frac{\partial T}{\partial x}\} + \{\frac{W}{W_o} C_{p,g} + \frac{\sum_{j=1}^{n} H_j R_j}{W_o \frac{\partial T}{\partial x}} W_o\} \frac{\partial T}{\partial x}$$

$$= - \rho_g C_{p,g} \frac{\partial T}{\partial t} \qquad (2\text{-}48)$$

The term in brackets has been labeled the reacting gas heat capacity. In this bracketed term, $\sum_{j=1}^{n} H_j R_j$ accounts for the heat effects of chemical reactions. When the flow is frozen, that is, no chemical reactions take place, the term $\sum_{j=1}^{n} H_j R_j$ equals zero. However, when there are chemical reactions, this term is non-zero. This type of analysis is used to predict the transient one-dimensional thermal performance of charring ablator heat protection system when exposed to a hyperthermal environment.

The analysis of Kendall, et. al. (51-53) is a transient one-dimensional analysis of the coupled, laminar, chemically reacting, boundary layer to the ablative surface.

The boundary layer solution was related to the shock layer by specifying edge boundary conditions. Similarly, the boundary layer solution was related to the transient response of the ablative composite by surface conditions. Four options were available to couple the laminar, chemically-reacting, boundary layer to the char surface. These included specifying 1) wall enthalpy, 2) mass flux of each gas species as they entered the char zone, 3) equilibrium mass flux at the surface or 4) coupled mass and energy balance at the wall as provided by a transient charring conduction solution.

The one-dimensional in-depth analysis considered that the decomposition of the virgin material could be described by means of an equilibrium analysis; that is, the decomposition reactions were in chemical equilibriu. The assumption of chemical equilibrium between the pyrolysis gases and the char, results in an overprediction of carbon deposition. To avoid this problem Kendall and co-workers (51-53) assumed that no carbon deposition occurred, and that only gas phase reactions took place. A modified form of Darcy's Law was used to calculate the pressure drop across the char layer.

The analysis of Kratsch, et. al. (83) was a one-dimensional, transient analysis of the coupled mass and energy balance in char forming ablative composites. Depolymerization of the plastic ablative composite was modeled by an Arrhenius type kinetic expression obtained

from thermogravimetric data. The receding surface boundary conditions and the convective and radiative heating were specified input functions to the numerical calculations. In addition, chemical errosion of the surface was specified. The in-depth analysis of the char layer considered the pyrolysis gas products to be in thermo-chemical equilibrium. However, the assumption of chemical equilibrium between the pyrolysis gas and the char, as previously mentioned, results in an over prediction of carbon deposition. To avoid this problem only gas phase reactions are considered and the amount of carbon was empirically adjusted to that found by experiments.

This work was one of the first attempts to describe a rather complex system with an analysis that was not restricted to simplifications of frozen flow, constant physical properties, or omitted heat absorption terms.

Another work that treats the complex physico-chemical phenomena of a charring ablator is that of Clark (111). Clark's work parallels that of the already mentioned work of Swann (58), but Clark expands the mathematical treatment by taking into account, in more detail, various thermal, chemical and mass transfer processes present in ablation. Clark's work is distinctive from that of Swann mainly in three respects. One is a detailed chemical kinetic treatment of the pyrolysis gases in the char. The other is a method of describing mass deposition in the char. Finally, and most important, is the complexity of

taking into account thermal non-equilibrium effects between the pyrolysis gases and the char. One interesting observation is that Clark uses Stroud's (5, 6) reaction plane approximation to take into account the thermal decomposition process of plastic composites. His stated reason is that such an assumption was necessary to provide a second boundary condition for the gas-momentum conservation equation. What Clark surprisingly fails to mention is that the reaction plane approximation to describe the decomposition of the virgin plastic is valid only when it can be described by one reactable species. This point is stressed because Clark's numerical examples concern phenolic-nylon which we know can be described by at least seven degradation reactions. We know from the work of Stroud that the higher the surface recession velocity, the better is the reaction plane approximation. However, as we mentioned before, Stroud did not quantify this velocity, neither did he speculate as to how good his reaction plane approximation would be for those materials such as phenolic-nylon, where more than one reactable species is present. Clark is not clear either in this respect. Nowhere in the text of his work was he explicit about the limitations of the reaction plane approximation, although we have to assume that he was aware of them.

In summary, Clark's analysis has the following salient features:

1) One-dimensional transient.
2) Multilayer system (char layer, uncharred layer and insulation layer.
3) Intereaction of the external surface with the boundary layer by taking into account surface oxidation, sublimation and mechanical erosion.
4) Homogenous and heterogenous chemical reactions within the char layer which account for mass deposition.
5) Thermal non-equilibrium between the char layer and the pyrolysis gases.
6) Reaction plane approximation to account for decomposition of uncharred layer.

Clark's work was very thorough and extensive. He studied in detail the various thermal, chemical and mass transfer phenomena in the ablative process. His analysis predicts that the overall performance for a low density phenolic-nylon is 16 percent greater than the performance calculated by the analysis of Swann (58). Clark attributes this difference in predicted performance to the consideration of char layer deposition in his analysis.

Although Clark does not state the actual CPU time required to solve his model, he does state that the computer solutions are time consuming. The objective of his program was to develop the capability of analyzing ablation systems will all the complicating factors already mentioned to provide guidance in selecting the most

important effects. In this way, he provided means of calibrating less complex analyses to account for those effects which are found to be significant.

The next section presents a summary of previous research of flow in the char zone.

Summary of Previous Research of Flow in the Char Zone

One of the most recent studies of flow in the char zone was done by April (19). His mathematical analysis consisted in a non-equilibrium, one-dimensional, steady flow model which accurately predicted the energy transfer in the char zone of a nylon-phenolic resin composite, for front surface temperatures of up to 3000^{o}F. The important chemical reactions and kinetic data for a temperature range of 500^{o}F to 3000^{o}F, with experimental simulation to 2300^{o}F, were determined and incorporated into the mathematical analysis. His analysis, in conjunction with experimental results obtained in a Char Zone Thermal Environment Simulator were used to show the shortcomings of the limiting cases of frozen and equilibrium flow analysis in predicting the true behavior within the char layer. Comparisons of the experimental data for low density phenolic-nylon chars were made with the results obtained using graphite as a simulated char. The non-equilibrium flow analysis was used to accurately predict the energy transport in the graphite medium using the same important reactions and kinetic data developed for flow

through chars. April (19) conducted studies to determine carbon deposition and decomposition product distribution for methane and phenol using carbon-14 tracers. Carbon deposition measurements within the char layers were used to locate the temperature where chemical reactions among the pyrolysis product became significant. In addition, oxidation of nylon-phenolic resin chars were studied to determine the rate of oxidation of the char with distance from the front surface. It was found that oxidation was taking place at all depths within the char; that is, reaction rate limited. This, however, is not surprising because it confirms results published by Scala (109). A graphical illustration is given in Figure 2-13. April's experimental data did not exceed 2300°F which falls outside the diffusion controlled regime as shown in Figure 2-13, and this is consistent with the results presented by Scala (109).

A considerable amount of information pertaining to the problem associated with the formulation of an accurate ablative analysis was discussed by April (19) or Scala (109). Others that have contributed to the understanding of the flow of gases through porous matrices have been Koh and del Casal (11, 12), Clark (16), and Weger and coworkers (17, 18). These studies have been especially useful in evaluating the magnitude of the terms in the equation of change in the development of more accurate and realistic ablative analyses. For this reason the

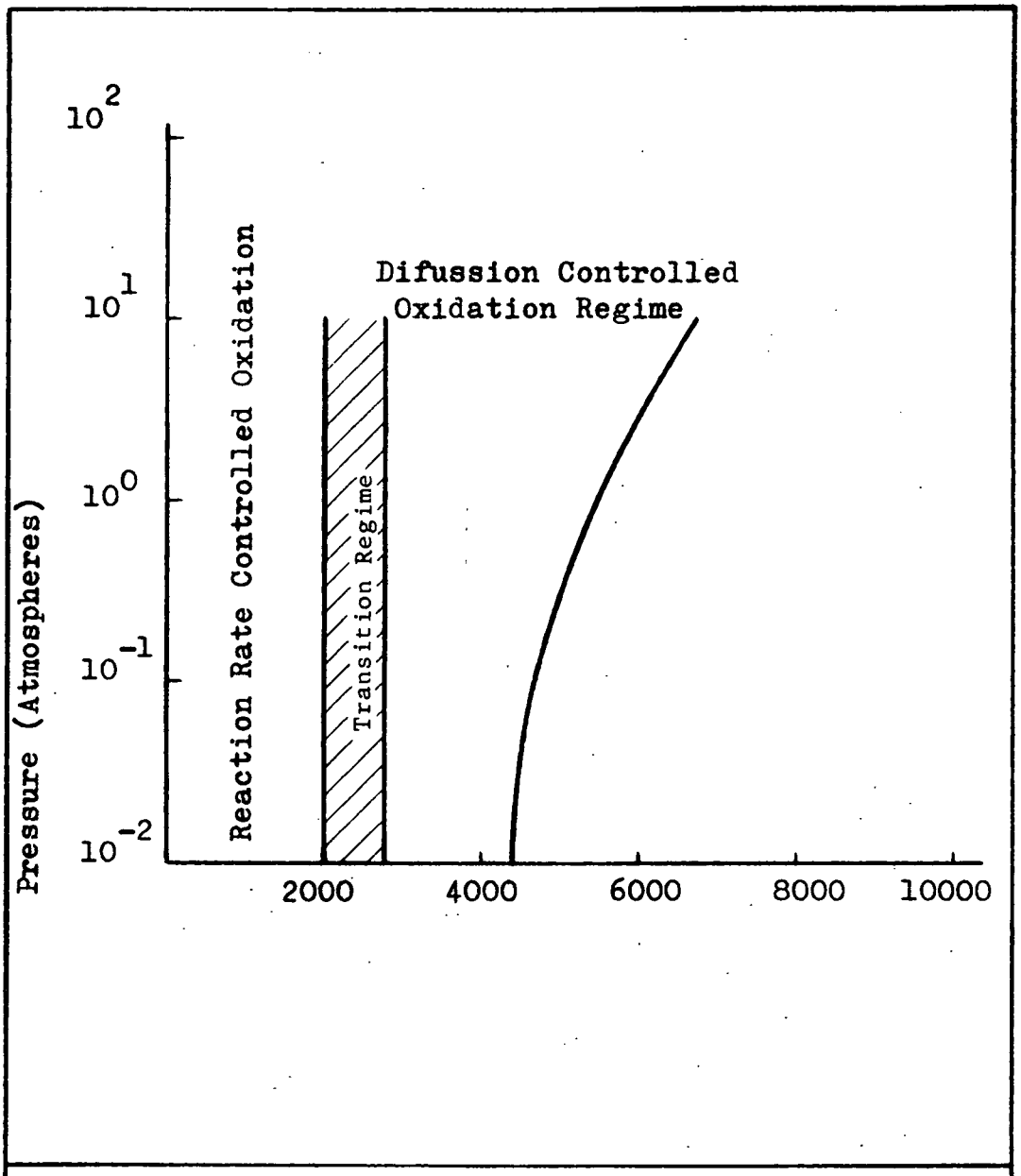

Figure 2-13. Mass Transfer Regimes for Ablating Graphite After Scala (109).

important conclusions and recommendations drawn from these authors will be summarized below.

Thermal Equilibrium Between the Gas and Char: It is important to determine the existence of thermal equilibrium since this can greatly reduce the complexity of the equations of change (11). If a small temperature difference exists between the gas and the solid matrix, it is likely that the effect on the energy transfer will be negligible. April (19) measured the temperature of the pyrolysis gases 1/4 inch away from the back surface of the experimental char, and found the difference to be approximately 200^{o}F. He reasoned, that by the time these pyrolysis gases would arrive at the back surface of the char the thermal gradient should be further reduced. Clark (16) reported differences of 200^{o} R to 800^{o}R at the midpoint of 0.021-0.33 feet thick graphite and carbon matrices over a wide range of mass flux values, 0.018 to 0.07 lb/ft^{2}-sec. These large differences were the result of the initial gradient (2000^{o}R-3000^{o}R) between the gas and solid at the matrix back surface. This abnormally large gradient was produced by the resistance heating apparatus used to simulate high temperature reentry (4000^{o}R). This however, is not representative of the conditions encountered on the back surface of the char during reentry. Instead, the pyrolysis gas and char back surface temperatures are approximately equal to the plastic decomposition temperature (1500^{o}R). Since no large

initial gradient between the gas and solid phases exists this assumption should be valid.

Variable Physical Properties: The assumption of constant physical properties is only valid over a relatively small temperature range. In ablative cooling where the temperature can exceed 3000°F changes in physical properties must be expected.

Koh and del Casal (11) noted significant differences in the results obtained between the constant and variable fluid physical properties model. Their findings were for solid matrices for porosities greater than 0.5. This was apparently attributed to the increasing importance of gas convective heat transfer effects in the high porous matrix. The only modes of energy transfer accounted for were gas convection and solid conduction. In ablative cooling using nylon-phenolic resin chars with porosities between 0.7 and 0.8, the gas convective term will be significant and hence, properties must be considered variables over the large temperature range.

With regard to the solid, or char properties, Weger, et. al. (17, 18) measured the change of char porosity and permiability when carbon deposition, or depletion occurred. They found these properties to have measurable changes. These results, however, were obtained for materials with porosities of 0.21 to 0.35. The effects of these changes on the pressure drop and energy transfer for

high porosity (0.7-0.8) materials were not determined. Until more pertinent data is obtained for high porous materials, the permiability and porosity have to be taken as constant in the analysis. This is a good approximation in any porous material where excessive carbon deposition or depletion does not occur.

Modified Form of Darcy's Law: This equation is used to describe the momentum transfer for flow through porous media. Darcy's empirical equation relates the fluid velocity to the pressure drop within the porous media. Weger, et. al. (17, 18) found that a modified form of Darcy's Law gave a better prediction of the pressure drop across porous materials. This modified form of the law had an additional term which accounted for the inertial effects. These effects become significant for mass fluxes exceeding (0.01 lb/ft^2-sec). For ablative cooling mass fluxes can be as high as 0.05 lb/ft^2-sec. Hence, the modified form of Darcy's Law should be used.

Various Modes of Energy Absorption: In all the work reviewed in this chapter which dealt with the temperature distribution in porous media, gas convection and solid conduction were considered to be major modes of energy transfer within the char. Recently, the Southern Research Institute has investigated the effect of internal radiation as a mechanism of heat transfer (37). While admitting that this mechanism can be important it was difficult,

experimentally, to separate this effect from others. Therefore, they incorporated the radiation effect in the thermal conductivity they reported.

Gas conduction in most cases was ignored. Koh and del Casal (12) presented results which clearly defined when gas conduction could be neglected. This occurred for either high mass flow rates, or small temperature differences across the porous material. At low flow rates (0.01 lb/ft^2-sec), or large temperature differences ($3000^{\circ}F$), energy absorption by gas conduction becomes important. Since these conditions are present in ablative cooling, gas conduction must be taken into account in any realistic analysis. The effects of chemical reactions on the energy absorption and the physical properties of the material are discussed below.

Effects of Chemical Reactions: The various effects that chemical reactions have on flow through porous media have been discussed by a number of authors (13, 16, 17, 18). Koh and del Casal (13) and Clark (16) considered chemical reactions as important modes of absorption, while Weger, et. al. (17, 18) used them to explain the changes in the physical properties of the porous specimen due to carbon deposition or depletion. In any realistic analysis involving high temperature flows, chemical reactions must be considered. Clark (16) found in his studies of methane flow through porous carbon and graphite that there were

three distinct chemically reacting zones. At low temperatures, a frozen flow region where no significant chemical reactions occurred was observed. As the temperature increased an intermediate region where chemical reactions were kinetically controlled was noted. Finally, the third distinct region was that in which reactions were in chemical equilibrium. It is likely that for more complex chemical systems, such as the pyrolysis products produced from the degradation of plastic composites, the gases would undergo a similar transition from frozen through non-equilibrium to equilibrium. Therefore, a non-equilibrium flow analysis would be required to accurately predict the energy absorption within the char layer. Weger et. al. (18) also observed a non-equilibrium region where the reactions were kinetically controlled.

We have established the importance of a non-equilibrium flow analysis as a pre-requisite to an accurate description of the energy transfer for ablative composites. Two important problems, however, remain to be discussed. One is the accurate description of the composition of the pyrolysis gases entering the char zone. The other is finding the important chemical reactions with thermodynamically consistent kinetic data, that occur in the temperature range of interest. These will be discussed in the two remaining sections of this chapter.

Pyrolysis Gas Composition: In order to realistically

describe the flow of pyrolysis gases through the char zone, and consequently, obtain an accurate prediction of the energy transfer, the pyrolysis gas composition must be accurately known. The current state of the knowledge precludes prediction of the products for decomposition reactions for even relatively simple polymers. Prediction of the pyrolysis products from a mixture of polymer, such as those contemplated for use in heat shields, is especially difficult and therefore must be determined experimentally. Reactions of the pyrolysis product among themselves and with the pyrolyzing resin further complicates the analysis.

In all previous research to date, simplified gases (helium, methane, etc.) or gas mixtures (methane, carbon monoxide, hydrogen, etc.) were used. While these are part of the decomposition products, they do not constitute the entire product composition expected from the decomposition of phenolic-nylon plastic composites. Nelson (1) and Sykes (2) addressed themselves to the problem of identifying the products of pyrolysis. April (19) used these studies concurrently with his own studies, and that of others to achieve an accurate description of the pyrolysis product stream composition entering the back surface of the char. A summary of April's (19) results along with additional findings of the product distribution is presented in Appendix F.

Determination of the Important Chemical Reactions and Associated Reaction Kinetic Data: To describe the flow of pyrolysis gases, and hence, to correctly predict the energy absorbed by chemical reactions it is essential that the important chemical reactions be established and the accurate kinetic data be determined for these reactions. This is important, as previously mentioned, because chemical reactions do have a profound effect on the energy absorption. To achieve this goal, out of the chaotic state of the reaction kinetic data in the literature (107), it was necessary to devise orderly and systematic procedures to select, and properly screen the reactions and their corresponding kinetic data. A continuous search and screening technique has been used during this study to update the reactions included in the analysis. Each reaction chosen must be based on the pyrolysis products composition initially present, plus the products produced by the further cracking of the pyrolysis gases.

More difficult than establishing the important chemical reactions is the task of locating accurate sources of kinetic data for the chosen reactions. Many times there is a total absence of kinetic data in the literature. Other times several sources of data appear, often, conflicting (108). In this research the kinetic data has been analyzed for consistency with thermodynamic principles. In addition the reverse reaction rate constants have been obtained by using the chemical equilibrium constant. The technique

used to decide which reaction to include in the analysis and which data to use is discussed in Chapter V.

Summary

In this chapter a detailed presentation of two analyses describing the decomposition in-depth of plastic composites has been given. These analyses were those of Stroud (5, 6) and Kondo and co-workers (8). Stroud's analysis was mainly concerned with determining whether the assumption of a decomposition reaction taking place in a plane, could be considered a valid engineering approximation. He found that his reaction plane approximation would hold for a quasi-steady, one-dimensional flow of gases, where one species was considered reacting and where the surface recession velocity was high. Kondo and co-workers (8), on the other hand showed the importance of considering the decomposition reactions to take place in a finite region. As in the case with Stroud they considered only one degrading reaction to describe the decomposition of the plastic. Both analyses used an Arrhenius type expression to describe the kinetics of the decomposition process of the plastic. It was established that Arrhenius type expressions were independent of the heating rate and thus suitable for these analyses where the heating rates could vary.

The transient analyses of Swann, et. al. (58), Kendall et. al. (51,53), Kratch, et. al. (83) and Clark (111), were

briefly discussed. In addition, a brief summary of previous research of flow in the char zone was presented. These were the works of Koh and del Casal (11-13), Weger, et. al. (17, 18), and Clark (16), which showed the importance of considering chemical reactions as significant modes of energy transfer and as mechanisms which affect the physical properties of the flowing gases and the solid matrix. These and other considerations have been taken into account in the analysis for describing both decomposition in-depth and the flow of gases in the char zone, in this research. This will be shown in the next chapter.

REFERENCES

1. Nelson, J. B., "Determination of Kinetic Parameters of Six Ablation Polymers by Thermogravimetric Analysis," NASA TN D-3919 (April 1967).

2. Sykes, G. F., Jr., "Decomposition Characteristics of a Char-Forming Phenolic Polymer Used for Ablative Composites," NASA TN D-3810 (February 1967).

3. Ladacki, Michael, J. V. Hamilton and S. N. Cohn, "Heat of Pyrolysis of Resin in Silica-Phenolic Ablator," AIAA Journal, 4, 1798-1801 (October 1966).

4. Freidman, H. L., "Pyrolysis of Plastics in a High Vacuum Arc Image Furnace-2," Journal of Applied Polymer Science, 9, 1005-1009 (1965).

5. Stroud, C. W., "A Study of the Chemical Reaction Zone in Charring Ablators During Thermal Degradation," Paper 33b, National Meeting of the A.I.Ch.E., Dallas, Texas (February 6-9, 1966).

6. Stroud, C. W., "A Study of the Reaction-Plane Approximation in Albation Analysis," NASA TN D-4817 (October 1968).

7. Curry, M. D., "An Analysis of a Charring Ablator Thermal Protection System," NASA TN D-3150 (December 1965).

8. Kondo, Jiro, Roshitak Fujiwara, Takenori Matsumoto, "Steady State Ablation," In Proceedings, International Symposium on Space Technology and Science, 7th, Tokyo, Japan. Ed. Yasuhiro Kuroda, Tokyo, Agne Publishing Company, Inc. (1968).

9. Scala, S. M. and L. M. Gilbert, "Thermal Degradationof a Char-Forming Plastic During Hypersonic Flight," ARS Journal, 32, 917-923 (1962).

10. Newman, R. L., "A Kinetic Treatment of Ablation," J. Spacecraft Rockets, 3, 449-452 (1965).

11. Koh, J. C. Y. and E. P. del Casal, "Heat and Mass Flow Through Porous Matrices for Transpiration Cooling," Paper 16, Proceedings of the 1965 Heat Transfer and Fluid Mechanics Institute, Stanford University Press, Los Angeles, California, 263-81 (June 21-23, 1965).

12. Koh, J. C. Y., E. P. del Casal, R. W. Evans, and V. Deriugin, "Fluid Flow and Heat Transfer in High Temperature Porous Matrices for Transpiration Cooling," Technical Report AFFDL-TR-66-70, The Boeing Company, 207 pages (May 1966).

13. Koh, J. C. Y. and E. P. del Casal, "Heat and Mass Transfer with Chemical Reactions for Fluid Flow Through a Porous Matrix in Re-Entry Thermal Protection," A.I.A.A. Fourth Aerospace Sciences Meeting, Los Angeles, California (June 27-29, 1966).

14. Kelley, J. B. and M. R. L'Ecuyer, "Transpiration Cooling - Its Theory and Application," JPC 422, Report Number TM-66-5, Jet Propulsion Center, Purdue University, Lafayette, Indiana, 153 Pages (June 1966). N66-30856.

15. Green, D. W. and R. H. Perry, "Heat Transfer with a Flowing Fluid Through a Porous Media," Heat Transfer, ed. by J. W. Westwater, Gas Chemical Engineering Symposium Series, 57, (32) (1961).

16. Clark, Ronald K., "Flow of Hydrocarbon Gases in Porous Media at Elevated Temperatures," M.S. Thesis, University of Virginia, 108 Pages (August 1968).

17. Weger, Eric, Jere Brew and Roger Schwind, "An Investigation of Carbon Deposition in Chars," Report BSD-TR-66-385, Washington University, St. Louis, Missouri, 84 Pages (1966).

18. Weger, Eric, Jere Brew and Ronald Servais, "An Investigation of Carbon Deposition in Chars - II," Report SAMSo-TR-68-123, Washington University, St. Louis, Missouri, 96 Pages (January 1968).

19. April, Gary C., "Energy Transfer in the Char Zone of a Charring Ablator," Ph.D. Dissertation, Louisiana State University, Baton Rouge, La., 568 Pages (May 1969).

20. Pike, R. W., G. C. April and E. G. del Valle, "Non-Equilibrium Flow and the Kinetics of Chemical Reactions in the Char Zone," NASA CR-66455 (July 15, 1967).

21. April, G. C., R. W. Pike and E. G. Del Valle, "Transport Phenomena in the Char Zone During Ablation. I: Evaluation of the Energy Transfer for Frozen and Equilibrium Flow," Paper 13d, 63rd National Meeting of the A.I.Ch.E., Salt Lake City, Utah (May 1967).

22. del Valle, E. G., R. W. Pike and G. C. April, "Transport Phenomena in the Char Zone During Ablation. II: Equilibrium Composition of Degradation Products of Ablation," Paper 13e, 63rd National Meeting of the A.I.Ch.E., Salt Lake City, Utah (May 1967).

23. Dow, M. B. and R. T. Swann, "Determination of the Effects of Oxidation on Performance of Charring Ablators," NASA TR R-196 (June 1964).

24. Waldberg, D. G., "Analytical Study of Diffusion Controlled Char Oxidation and Its Effect on Steady State Ablation of Plastic Materials," NASA TR R-242 (July 1966).

25. Wakefield, R. M., and J. H. Lundell, R. R. Dickey, "The Effects of Oxygen Depletion in Gas Phase Chemical Reactions on the Surface Recession of Charring Ablators," AIAA Paper Number 68-302, Presented at AIAA-ASME Ninth Structures, Structural Dynamics and Materials Conference, Palm Springs, California, April 1-3, 1968.

26. Leont'yev, A. I., E. P. Volchkov, Ye. G. Zaulichnyg, Ye. I. Sinayko, "Experimental Determination of Graphite Ablation Rates Under Conditions of Substantial Nonisothermality," NASA TTF-11, 738, (1968). N68-28211.

27. Nolan, J. E. and S. M. Scala, "Aerothermodynamic Behavior of Pyrolytic Graphite During Sustained Hypersonic Flight," ARS Journal, 32, 26-35 (1962).

28. Bro, P. and S. Steinberg, "Study of Chemical Surface Reactions in a High Temperature Flow System with Arc Heated Gases," ARS Journal, 32, 528-532 (1962).

29. Moore, J. A. and M. Zlotnick, "Combustion of Carbon in an Air Stream," ARS Journal, 31, 1388-1397 (1961).

30. Bishop, W. M. and V. DiCristina, "The Combustion and Sublimation of Carbon at Elevated Temperatures," A.I.A.A. Paper 68-789, Presented at A.I.A.A. Third Thermophysics Conference, Los Angeles, California, June 24-26, 1968.

31. Dolton, T. A., H. E. Goldstein, and R. E. Maurer, "Thermodynamic Performance of Carbon in Hyperthermal Environment," AIAA. Paper 68-754, Presented at AIAA. Third Thermophysics Conference, Los Angeles, California, June 24-26, 1968.

32. Lundell, J. H., R. R. Dickey and J. W. Jones, "Performance of Charring Ablative Materials in the Diffusion Controlled Surface Combustion Regime," A.I.A.A. Paper 67-328, Presented at A.I.A.A. Thermophysics Specialist Conference, New Orleans, Louisiana, April 17-20, 1967.

33. Pittman, C. M. and W. D. Brewer, "Analytical Determination of the Effect of Thermal Property Variations on the Performance of a Charring Ablator," NASA TN D-3486 (July 1966).

34. Wilson, R. G. (Compiler), "Thermophysical Properties of Six Charring Ablators From 140°K to 700°K and Two Chars From 800°K to 3000°K," NASA TN D-2991 (October 1965).

35. Engelke, W. T., C. M. Pyron, and C. D. Pears, "Thermal and Mechanical Properties of Non-Degraded and Thermally Degraded Phenalic-Carbon Composite," NASA CR-896 (October 1967).

36. Sanders, H. G., E. D. Smyly and C. D. Pears, "An Investigation of Some Thermal and Mechanical Properties of a Low Density Phenolic-Nylon Ablation Material," NASA CR-66731 (February 1969).

37. Engelke, W. T., C. M. Pyron, Jr. and C. D. Pears, "Thermophysical Properties of Low Density Phenolic-Nylon Ablation Material," NASA Cr-809 (July 1967).

38. Smyly, E. D., C. M. Pyron, Jr. and C. D. Pears, "An Investigation of the Mechanisms of Heat Transfer in Low Density Phenolic-Nylon Chars," NASA CR-966 (December 1967).

39. Shaw, T. E., D. C. Garner and D. E. Florence, "Effects of Uncertainties in Thermophysical Properties on Ablation Efficiency," A.I.A.A. Paper 65-639, Presented at A.I.A.A. Thermophysics Specialist Conference, Monterey, California, September 13-15, 1965.

40. Vojvodich, N. S., and R. B. Pope, "Effects of Gas Composition on the Ablation Behavior of a Charring Material," AIAA Journal, J., 2, 536-542 (1964).

41. Brewer, D. W., C. W. Stroud, and R. K. Clark, "Effect of the Chemical State of Pyrolysis Gases on Heat Shield Mass," NASA Tn D-4975 (December 1968).

42. Pope, R. B. and J. A. Parker, "Analysis of Ablation Products and Boundary-Layer Chemistry of Ablating Materials with a Mass Spectrometer," NASA TMX-60482 (1968).

43. Swann, T. R., W. D. Brewer and R. K. Clark, "Effects of Composition, Density, and Environment on the Ablative Performance of Phenolic-Nylon," NASA Tn D-3908 (April 1967).

44. Hearne, L. F., W. D. Coleman, J. M. Lefferdo, L. W. Gallagher and J. H. Chin, "A Study of the Effects of Environmental and Ablator Performance Uncertainty on Heat Shielding Requirements for Hyperbolic Entry Vehicles." Vol. -1, NASA Cr-73224 (1968).

45. Ibid., Vol.-II, Summary of Calculations, NASA CR-73225 (1968).

46. Swann, R. T., M. B. Dow, and S. S. Tompkins, "Analysis of the Effect of Environmental Conditions on the Performance of Charring Ablators," J. Spacecraft Rockets, 3, 61-67 (1966).

47. Coleman, W. D., L. F. Hearne, J. M. Lefferdo, N. S. Vojvodich, "A Study of the Effects of Environmental and Ablator Performance Uncertainties on Heat Shielding Requirements for Blunt and Slender Hyperbolic-Entry Vehicles," A.I.A.A. Paper 68-154, Presented at A.I.A.A. Sixty Aerospace Sciences Meeting, New York, New York, January 22-24, 1968.

48. Allen, H. J., "Some Problems of Planetary Atmospheric Entry," J. Roy. Aero. Soc., 71, 813-820 (1967).

49. Syverston, C. A., "Research Problems in Atmosphere Entry and Landing for Manned Planetary Mission," NASA TN D-4977 (January 1969).

50. Mathieu, R. D., "Mechanical Spallation of Charring Ablators on Hyperthermal Environments," AIAA Journal, 2, 1621-1627 (1964).

51. Kendall, R. M., E. P. Bartlett, R. A. Rindal and C. B. Moyer, "An Analysis of the Coupled Chemically Reacting BoundaryLayer and Charring Ablator," Part I, Summary Report, NASA Cr-1060 (June 1968).

52. Bartlett, E. P., R. M. Kendall, R. A. Rindal, "An Analysis of the Coupled Chemically Reacting Boundary Layer and Charring Ablator": Part IV, A Unified Approximation for Mixture Transport Properties for Multicomponent Boundary-Layer Applications, NASA Cr-1063 (June 1968).

53. Kendall, R. M., R. A. Rindal, and E. P. Bartlett, "A Multicomponent Boundary Layer Chemically Coupled to an Ablating Surface," AIAA Journal, 5, 1063-1071 (1967).

54. Marvin, J. G. and C. M. Akin, "Combined Effects of Mass Addition and Nose Bluntness on Boundary Layer Transition," A.I.A.A. Paper 69-706, Presented at A.I.A.A. Fluid and Plasma Dynamics Conference, San Francisco, California, June 16-18 (1969).

55. Bushnell, D. M. and I. E. Beckwith, "Calculation of Non-Equilibrium Hypersonic Turbulent Boundary Layers and Comparison with Experimental Data," A.I.A.A. Paper 69-684, Presented at A.I.A.A. Fluid and Plasma Dynamics Conference, San Francisco, California, June 16-18, 1969.

56. Hoshizaki, H., "Heat Transfer in Planetary Atmospheres at Super-Satellite Speeds," ARS Journal, 32, 1544-1551 (1962).

57. Martin, E. D., "Inviscid Hypersonic Flow Over a Blunt Body with High Rates of Mass and Heat Transfer," NASA TN D-4252 (March 1968).

58. Swann, R. T., C. M. Pittman and J. C. Smith, "One Dimensional Numerical Analysis of the Transient Response of Thermal Protection Systems," NASA TN D-2976 (September 1965).

59. Sheehan, P. J., R. E. Gannon and T. S. Laszlo, "Ablation Test of Heat Shield Materials Under Radient Heating," A.I.A.A. Paper 66-44, Presented at A.I.A.A. Third Science Meeting, New York, New York (January 24-26, 1966).

60. Studerus, C. J., C. L. Kyriss, H. Rie and C. V. Dohner, "Theoretical Evaluation of the Simulation of Radiative Heating of Planetary Entry Vehicles," A.I.A.A. Paper 69-634, Presented at A.I.A.A. Fourth Thermophysics Conference, San Francisco, California (June 16-18, 1969).

61. Hoshizaki, H., and L. E. Lasher, "Convective and Radiative Heat Transfer to an Ablating Body," A.I.A.A. Paper 67-327, Presented at the A.I.A.A. Thermophysics Specialist Conference, New Orleans, Louisiana, April 17-20, 1967.

62. Hoshizaki, H., and K. H. Wilson, "Viscous, Radiating Shock Layer about a Blunt Body," A.I.A.A. Journal, 3, 1614-1622 (1965).

63. Hoshizaki, H., and K. H. Wilson, "Convective and Radiative Heat Transfer During Superorbital Entry," A.I.A.A. Journal, 5, 25-35 (1967).

64. Georgiev, S., J. D. Teare and R. A. Allen, "Hypervelocity Radiative Heat Transfer," AVCO RESEARCH NOTE 264, AFBSD-TN-61-33, AFCRL-62-39, AVCO Research Laboratories, Everett, Massachusetts, August 1961.

65. Davy, C. W., R. A. Craig, G. T. Chapman, and D. L. Compton, "Ablation-Products Radiation from Cones," AIAA Journal, 2, 1583-1589 (1964).

66. Penner, S. S., O. P. Sharma, "Ablation with Radiant Heating," Zeitschrift für Flugwissenschaften, 14, 170-179 (1966).

67. Brunner, M. J., "Aerodynamic and Radiant Heat Input to Space Vehicles Which Re-Enter at Satellite and Escape Velocity," ARS Journal, 31, 1102-1111 (1961).

68. Bloor, M. I. G., "Effect of Radiative Heat Loss on Steady Hypersonic Flow Past a Blunt Body," J. Fluid Mech., 29, 485-494 (1967).

69. Studerus, C., H. Rie, C. Kryiss and C. Dohner, "Flow Fluid Computations for Blunt Bodies in Planetary Environment (Equilibrium," NASA Cr-94239 (August 1967).

70. del Casal, E. P., "The Effects of Multi-dimensional Flow Through Porous Matrices in Mass Transfer Cooling," A.I.A.A. Paper No. 69-149, Presented at A.I.A.A. Seventh Aerospace Sciences Meeting, New York, New York, January 20-22, 1969.

71. Bush, G. H., and M. B. Dow, "Multidimensional Gas Flow Through Permeable Char Layers and Its Effects on Ablation," NASA TR R-296 (January 1969).

72. Ungar, E. W., "Particle Impacts on the Melt Layer of an Ablating Body," ARS Journal, 30, 799-805 (September 1960).

73. Schmidt, G. A., D. G. Flom, T. F. Geib, J. C. Fries and F. A. Luay, "Impact Studies on Ablation-Resistant Composites," G. E. Space Science Laboratory Report R65SD3, General Electric, Philadelphia, Pennsylvania (February 1965).

74. Ostrach, S., "Heat Transfer With Receding Boundaries and Other Complications," N67-13160.

75. Beusman, C. C. and J. Weisman, "Comparison of Transpiration and Ablation Cooling," ARS Journal, 30, 573-574 (1960).

76. Nagler, R. G., "The Mars Transit and Entry Environment: A New Problem for Heat Shields," Jet Propulsion Laboratory Technical Report 32-1145 (1967).

77. Parker, J. A., E. L. Winkler, "The Effect of Molecular Structure on the Thermochemical Properties of Phenolics and Related Polymers," NASA TR R-276 (November 1967).

78. Waldberg, G. D. and R. K. Crouch, "Exploratory Investigation of the Effect of Nylon Grain Size on Ablation of Phenolic Nylon," NASA TN D-3465 (August 1966).

79. Cochran, T. H. and S. Ostrach, "Body Rotation Effects on Melting Ablation," NASA TN D-4614 (June 1968).

80. Moss, N. J. and W. E. Howell, "A Study of the Performance of Low-Density Phenolic-Nylon Ablators," NASA Tn D-5257 (June 1967).

81. Scala, S. M., "A Study of Hypersonic Ablation," General Electric Company, Missile and Space Vehicle Department, Report R59SD438 (September 1959).

82. Myers, H. and D. B. Harmon, Jr., "Energy Transfer Process in Decomposing Polymeric Systems," Douglas Aircraft Company, Missile and Space Systems Division, Report 1020 (September 1960).

83. Kratsch, K. M., L. F. Hearne and H. R. McChesney, "Thermal Performance of Heat Shield Composites During Planetary Entry," NASA-A.I.A.A. National Meeting, Palo Alto, California (September 30-October 1, 1963).

84. Swann, R. T., "Approximate Analysis of the Performance of Char-Forming Ablators," NASA TR R-195 (June 1964).

85. Beecher, N. and R. E. Rosenweig, "Ablation Mechanism in Plastics With Inorganic Reinforcement," ARS Journal, 31, 532-539 (1961).

86. Rosenweig, R. E. and Beecher, N., "Theory for the Ablation of Fiberglas-Reinforced Phenolic Resin," AIAA Journal, 1, 1802-1809 (1963).

87. Penner, S. S., and D. B. Olfe, Radiation and Reentry, Academic Press, New York, 1968.

88. Hidalgo, H., "Ablation of Glassy Material Around Blunt Bodies of Revolution," ARS Journal, 30, 806-814 (1960).

89. Chen, H. N., "Simplified Solution for Ablation in a Finite Slab," AIAA Journal, 3, 1148-1149 (1965).

90. Adarkar, D. B., "Comment on Simplified Solutions for Ablation in a Finite Slab," AIAA Journal, 4, 1495-1497 (1966).

91. Adarkar, D. B. and L. B. Hartsook, "An Integral Approach to Transient Charring Ablator Problems," AIAA Journal, 4, 2246-2248 (1966).

92. Barker, D. H., J. W. Kordig, R. D. Belnap and A. F. Hall, "A Simplified Method of Predicting Char Formation in Ablating Rocket Exit Cones," Chemical Engineering Progress Symposium Series, 61, (59), 108-114 (1965).

93. Thickstum, W. R., "Reacting Heating Simulation," NAVORD REPORT 6791, (December 1960).

94. Sheehan, P. J., R. E. Gannon and T. S. Laszlo, "Ablation Test of Heat Shield Materials Under Radiant Heating," AIAA Paper No. 66-44, Presented at Third Aerospace Science Meeting, New York, New York (January 24-26, 1966).

95. Vojvodich, S. N., "Hypervelocity Heat Protection--A Review of Laboratory Experiments," N68-23395.

96. Chapman, J. A. and M. B. Dow, "Arc Tunnel Evaluation of Some Ablative Heat Shield Materials for the X-15-2," NASA Tn D-3753 (February 1967).

97. Krusos, J. N., "Study of Ceramic Heat Shields for Lifting Reentry Vehicles," NASA Cr-861 (August 1967).

98. Economos, C., "Ablation Test on Plastic Models in a Hypersonic Wind Tunnel," ARS Journal, 32, 1074-1081 (1962).

99. Kubota, Toshi, "Ablation With Ice at M=5.8," ARS Journal, 30, 1164-1169 (1960).

100. Martin, J. J., Atmospheric Reentry, Prentice-Hall, Inc., Englewood Cliffs, New Jersey (1966).

101. Steverding, B. and V. A. Nieberlein, "Ablation for Heat Shielding," Chemical Engineering, 72, 163-169 (1965).

102. Schmidt, D. L., Engineering Design for Plastic, Chapter 13, Reinhold Publishing Company, Inc. New York (1962).

103. Diaconis, N. S., W. R. Warren, Jr. and T. E. Shaw, "The Hypervelocity Heat Protection System," Propulsion and Reentry, XVIth International Astronautical Congress, Athens (1965).

104. Freedman, S. I., Developments in Heat Transfer, Chapter 5, M.I.T. Press, Cambridge, Massachusetts (1962).

105. Scala, S. M., Development in Heat Transfer, Chapter 17, M.I.T. Press, Cambridge, Massachusetts (1962).

106. Lapple, C. E., A. P. Brady, and D. L. Chamberlain, Jr., "Mechanism of Ablation of Char-Forming Ablative Plastics," Stanford Research Institute, California, ASD-TR61-204 (September 1961).

107. Bahn, S. G., "Status Report of Efforts on Engineering Selection of Reaction Rate Constants for Gaseous Chemical Species at High Temperature with a Review of $H+CO_2 = OH + CO$ and $CO_2 + M = O + CO + M$," The Combustion Institute (Western State Section), Spring Meeting, WSS/CI Paper 67-11, La Jolla, California (April 24-25, 1967).

108. del Valle, E. G., R. W. Pike and G. C. April, "Modeling for a Set of Complex Chemical Reactions at High Temperatures," Project 20F, Presented at the Symposium of Recent Advances in Kinetics, Sixty-First Annual Meeting, Los Angeles, California (December 1-5, 1968).

109. Scala, S. M., "Thermal Protection of a Reentry Satellite," ARS Journal, 29, 670-672 (September 1969).

110. del Valle, E. G. and R. W. Pike, : "Computation of the Equilibrium Composition of Reacting Gas-Solid Mixture with Material and Energy Balance Constraints", NGR, 19-001-059, RFL-10, March 1, 1970.

111. Clark, R. K., "An Analysis of a Charring Ablator with Thermal Non-equilibrium, Chemical Kinetics, and Mass Transfer", NASA TN D-7180, June 1973.

CHAPTER III

DEVELOPMENT OF THE MATHEMATICAL ANALYSIS FOR THE EVALUATION OF THE ENERGY TRANSFER IN THE DECOMPOSITION ZONE AND CHAR ZONE OF A CHARRING ABLATOR

Introduction

The previous mathematical analyses (1, 2) to predict the energy transfer in the char zone are handicapped by the limitation that the char zone depth has to be specified a priori. At the point selected as the interface between the char and pyrolysis zones, it is necessary to specify the interface temperature, heat of pyrolysis, pyrolysis gas mass flux, and pyrolysis gas composition. However, physically there is not a sharp interface between the two regions since polymer degradation, pyrolysis gas generation and char formation occur over a rather wide temperature range. In fact, polymer degradation begins at about 200°C, and about 80 percent is pyrolysed at 475°C (3). At this temperature heat absorption by the pyrolysis gases is becoming significant as a result of changes in sensible enthalpy and chemical reactions. Consequently, the combined energy absorption must be predicted from considering both the polymer degradation and the gas-char interaction simultaneously.

The pyrolysis products, formed by the thermal degradation of the plastic composite enter the char layer and transpire through the front surface of the char, at Z=L. A schematic diagram illustrates this in Figure 3-1. These gases entering from the decomposition zone experience a temperature increase as they flow through the porous char, and absorb heat by virtue of their own heat capacity and due to mostly endothermic chemical reactions. These endothermic reactions are due to the further cracking of the pyrolysis gases into lower molecular weight species. These species react with each other and with the carbonaceous char layer producing further endothermic reactions.

The description of the momentum, energy, and mass transfer equations for the combined decomposition-char zone analysis is obtained by simplification of the general equations of change (continuity, momentum and energy) to forms applicable to a chemically reacting flow (equilibrium and non-equilibrium), through the decomposition zone and char layer of a char forming ablator. Finally, typical boundary conditions are specified, followed by a discussion of the numerical solution of the equations.

Statement of the Problem

To predict the energy transferred in the combined decomposition-char zone the equations of change are written to apply to any point in the flow field. Using a quasi-steady analysis, or steady state approximation, the point

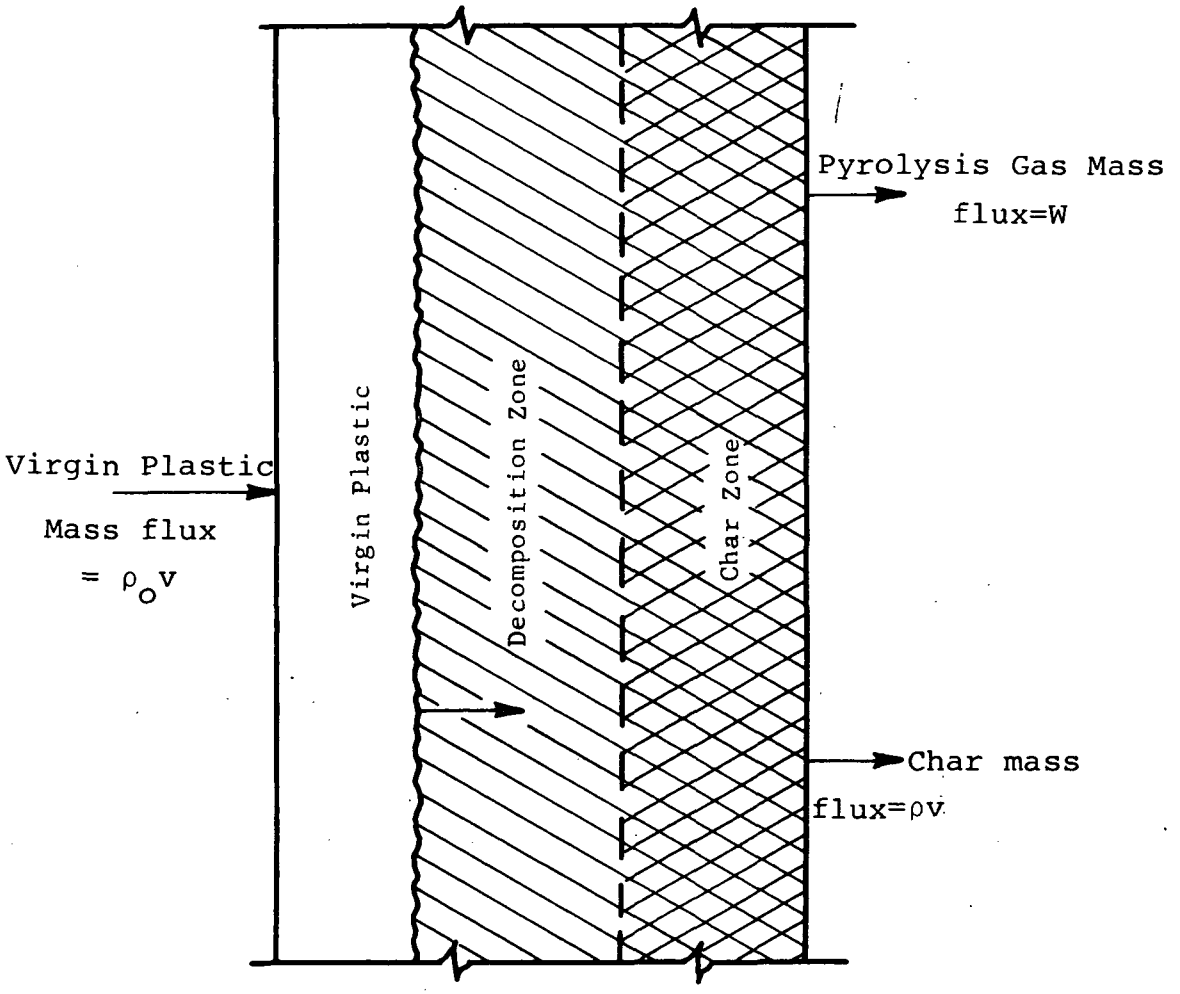

Figure 3-1. A Sketch of the Virgin Plastic, Decomposition and Char Zone.

of view is taken of an observer moving with the negative surface recession velocity, v. This is illustrated in Figure 3-1 which shows schematically the mass fluxes of virgin plastic, pyrolysis gases and solid. The point at which thermal degradation of the plastic is initiated is taken to be that of Z=0.

The material balance relating the virgin plastic flow with the flow of pyrolysis gases and degrading solid in the combined decomposition-char zone as written by Stroud (4) is:

$$\rho_o v = W + \rho v \qquad (3\text{-}1)$$

where W is the total mass flux, v is the surface recession velocity, and ρ_o and ρ are the virgin and degrading solid densities respectively. This assumes that the bulk volume of the char is the same as that of the virgin plastic, which is generally the case.

Referring to Equation (3-1) for a known surface recession velocity and densities of the virgin and degrading composite, the gas mass flux can be computed. In addition, the composition of the gases generated by the decomposition of the virgin plastic composites must be known to be able to accurately predict the energy absorbed due to chemical reactions in the char zone. As illustrated in Figure 3-1,

these pyrolysis products enter the char zone and exit through the front surface of the char, at Z=L. Changes in the mass flux of the various species within the char occur as a result of chemical reactions at finite reaction rates, R_j.

The particular restrictions and assumptions made in the formation of the combined zone analysis are presented and justified subsequently. The simplifications of the general equations of change resulting from these restrictions follow. Finally, the solutions of the resulting equations for frozen (no chemical reactions), equilibrium (calculated from thermodynamics), and non-equilibrium (calculated from reaction kinetics) flow are given.

Restrictions to the General Equations of Change for Flow in the Combined Decomposition-Char Zone

Several restrictions and assumptions are applied to simplify the general equations of change to reduce their complexities. In the subsequent discussion, these assumptions and restrictions are analyzed and justified.

Quasi-Steady and One Dimensional Flow of Pyrolysis Gases: The assumption of steady flow of the pyrolysis gases is based on the fact that after a brief initial period of time the thickness of the char has been shown to remain constant. The data of Peters and Waddin (5) in Figure 3-2 for a 50 : 50 weight ratio of nylon-phenolic

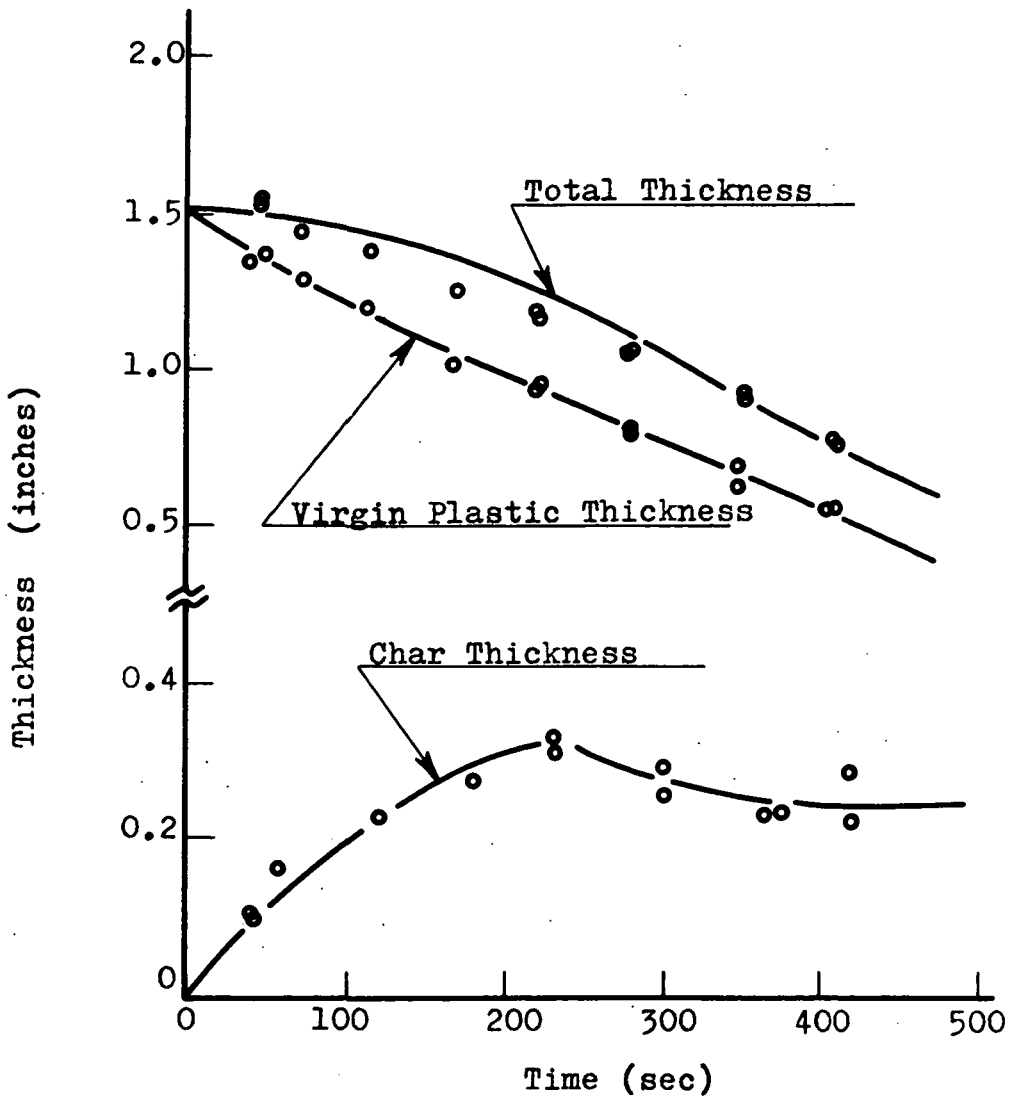

Figure 3-2. Thickness of the Char and Virgin Plastic as a Function of Time (5).

ablative composite, formed in a subsonic electric arc jet shows this graphically. This implies that the rate of formation of char, formed from the degradation products of the virgin material equals the rate of consumption of the char by air oxidation and/or mechanical erosion by the flow in the boundary layer. In addition, to this, the quasi-steady analysis is justifiable because the residence time of a fluid particle of pyrolysis gas is small (less than 0.01 seconds) when compared to the rate of change of the char surface.

The one dimensional assumption is easily justified since the radii of curvature of reentering spacecrafts (e.g., Mercury, Gemini, and Apollo) are large (about 5 to 8 feet) in comparison with the char thickness ($\sim$1/4 of an inch) and as such, the flow is one dimensional and normal to the front surface.

Pyrolysis Products Behave as a Perfect Gas Mixture: The assumption that the pyrolysis products behave as a perfect gas mixture implies that the equations of state for ideal gases are applicable. This is a realistic assumption considering the high temperatures (1500-6000^{o}F), and low pressures ($\sim$1 atm) encountered in planetary reentry by blunt body vehicles. However, it also implies that the heat capacity is that of a real gas and hence, a function of temperature. In Table 3-1 the values of the compressibility factor, Z, are presented for some of the

TABLE 3-1: Compressibility factors for some of the important constituents of the pyrolysis gases at 450°K.

Species	T_c °K	P_c (atm)	T_r	P_r	Z
CH_4	190.7	45.8	1.84	0.022	0.995
C_2H_4	283.1	50.5	1.23	0.020	0.995
C_2H_6	305.4	48.2	1.14	0.021	0.995
C_6H_6	562.1	43.6	0.62	0.021	0.995
C_7H_8	594.0	41.6	0.58	0.024	0.995
H_2O	647.3	218.6	0.54	0.0045	1.0
NH_3	405.5	111.3	0.863	0.009	1.0
CO	133.0	34.5	2.63	0.029	1.0
CO_2	304.2	72.9	1.15	0.014	0.995

most important constituents of the pyrolysis gases. The temperature at which Z has been calculated is 450°K. This temperature is the lowest at which the pyrolysis gases are formed. It is also the temperature at which degradation of the plastic is initiated. T_c and P_c are the critical temperature and pressure, and T_r and P_r are the reduced temperature and pressure for the respective gases. As is shown in Table 3-1 all of the compressibility factors are greater than 0.995; which justifies the assumption of ideality.

Virgin Material, Char and Gas Physical Properties: Because of the existence of a large temperature gradient from the front surface of the char layer to the virgin material, physical property variations with temperature must be considered. Variations with temperature of the virgin material's thermal conductivity is accounted for. Thermal conductivity variations with temperature have been reported by Wilson (5), Engelke (6) and Nagler (7). For the char, the porosity change with temperature is not accounted for due to a lack of experimental data on the subject. The value of the porosity is thus kept constant throughout the analysis. The thermal conductivity variations with temperature of the virgin material, the pyrolysis gases and the char are taken into consideration in the analysis. The data used is that reported by the Southern Research Institute (6) and the Jet Propulsion

Laboratory (7) of the California Institute of Technology. These data were fitted empirically and are presented in Appendix C.

Thermal Equilibrium Between the Pyrolysis Gas Products and the Char: The temperature gradient between the pyrolysis gas products and the porous carbon matrix is assumed to be small. This is supported by data presented by Koh and del Casal (8) in which they showed a maximum temperature difference of 300°F for the flow of air and helium through packed beds of spheres. The maximum temperature of the matrix was 2700°F.

Clark (9) also addressed himself to the problem of quantitatively determining the existence of a thermal gradient. He reported differences of 200 to 800°R between the gas and the porous matrix over a wide range of mass fluxes, 0.018 to 0.07 lbs/ft^2 sec. In this particular investigation thermal non-equilibrium between the gas and solid is primarily caused by the resistance heating method for achieving temperatures between 3000°R and 4000°R. In ablative heat protection applications the gas flowing from the pyrolysis zone into the char layer is at the local char temperature, and the abnormally large temperature difference characteristic of the resistence heating apparatus is non-existent. Therefore, the assumption of thermal equilibrium between the gas and char in ablative

cooling should be a very good approximation to the real behavior.

Momentum Transfer in the Char Zone: The modified form of Darcy's Law was used to determine the pressuee drop across the char layer. This was based on the work of Weger et al. (10). It was shown in this work that the inclusion of an inertial term gave a more accurate prediction of the experimental pressure drop for values of the mass flux of the order of 0.05 lb/ft^2-sec.

PV Work and Viscous Dissipation: The pressure drop across one quarter inch thick, low density nylon-phenolic resin char was experiementally determined by April (2) which showed it to be approximately 15 lbs/ft^2 for a pyrolysis gas mass flux of 0.05 lb/ft^2-sec and a front surface termpature of 2000°F. In addition, he computed the PV work contribution to the energy transport equation and showed it to be 1.2 BTU/ft^3sec. This was compared to the convective energy term, evaluated at the back surface where the temperature was small, and was shown to be 1000 BTU/ft^3-sec for a gradient of approximately 40,000°F/ft and an average heat capacity of 0.5 BTU/lb-°F. This clearly demonstrated that the PV work term in the energy equation was negligible. Since the velocity ($\sim$ 5 ft/sec) and the viscocity ($\sim$ 0.05 cp) of the gas mixture is small, the energy generated by

viscous dissipation can be neglected also and the term omitted from the energy equation. This allows for the uncoupling of the momentum and energy equation. Thus simplifying considerably the numerical solution of the problem.

Diffusional Transport: Energy, or mass transport by diffusion, is negligibly small in comparison with the bulk fluid transport. The average residence time of a gas particle in a one-quarter inch thick char layer is 0.01 seconds for a mass flux of 0.05 lb/ft^2-sec.

Derivation of the Equations of Change for Flow in the Combined Decomposition-Char Zones

The application of the above restriction to the general equations for flow of the pyrolysis gases in the combined decomposition-char zone is now discussed.

Specie Continuity Equation: Referring to Figure 3-1 the specie's continuity equation for the ith component of a gas mixture for flow through a porous medium is (11):

$$\frac{D\rho_i}{Dt} = -\rho_i\,(\bar{\nabla}\cdot\bar{u}) - (\bar{\nabla}\cdot\bar{J}_i) + R_i \qquad (3\text{-}2)$$

where ρ_i is the concentration, J_i, the mass flux by diffusion, R_i, the rate of generation of chemical specie i and $\bar{u}$ is the velocity of the pyrolysis products within the pores.

For a steady, one dimensional flow of gases, neglecting mass transport by diffusion, Equation (3-2) reduces to:

$$\frac{d}{dz}(\rho_i u) = R_i \qquad (3\text{-}3)$$

Assuming that the pyrolysis gases do not lose or gain any mass by reaction, Equation (3-3) becomes, summing over all the gas species:

$$\sum_{i=1}^{n} \frac{d}{dz}(\rho_i\ u) = 0 \qquad (3\text{-}4)$$

However, if the pyrolysis gases lose weight due to carbon deposition, Equation (3-4) becomes:

$$\sum_{i=1}^{n} \frac{d}{dz}(\rho_i\ u) = -R_c \qquad (3\text{-}5)$$

where R_c is the amount of carbon deposition. If we define W_p as the mass flux of pyrolysis gases based on the cross-sectional area of voids in the char (units of lbs/ft^2_{voids}-sec) we can say that:

$$\frac{dW_p}{dz} = \sum_{i=1}^{n} \frac{d}{dz}(\rho_i\ u) = -R_c \qquad (3\text{-}6)$$

Equation (3-6) says that any change of the mass flux of pyrolysis gases is due to the loss of carbon.

Momentum Equation: The momentum equation for flow through porous media was formulated by H. P. G. Darcy in 1856 (8). Darcy observed during experiments with a one dimensional packed bed that gas velocity at any point in the bed was directly proportional and in the same direction to the pressure gradient at that point. In vector notation, including the effect of body forces when considering a vertical flow direction, Darcy's Law is:

$$\overline{u} = - \frac{\gamma}{\varepsilon\mu} \cdot (\overline{\nabla}P - \rho g) \qquad (3\text{-}7)$$

Applying this equation to a one-dimensional, horizontal flow through a porous char layer and solving for the pressure gradient gives:

$$- \frac{dP}{dz} = \frac{\mu}{\gamma} \quad (u\varepsilon) \qquad (3\text{-}8)$$

This equation is valid at low gas flow velocities within the porous medium. However, at high gas velocities it is necessary to add a term to account for the inertial effects. This additional term leads to a modified form of Darcy's Law:

$$- \frac{dP}{dz} = \frac{\mu}{\gamma} (u\varepsilon) + \beta\rho \quad (u\varepsilon)^2 \qquad (3\text{-}9)$$

Multiplying both sides of Equation (3-9) by the gas density, ρ, followed by substitution of the ideal gas equation of state ($\rho = PM_w/RT$) on the left hand side of the Equation (3-9), results in Equation (3-10):

$$-\frac{M_w P}{RT}\cdot\frac{dP}{dz} = \rho\,(\mu/\gamma)\,(u\varepsilon) + \beta\rho^2\,(u\varepsilon)^2 \qquad (3\text{-}10)$$

If we define W as the total mass flux of pyrolysis gases based on the total area, we have that:

$$W = \varepsilon W_p = \varepsilon\rho u \qquad (3\text{-}11)$$

therefore substitution of Equation (3-11) into Equation (3-10) results after rearrangement:

$$-PdP = \frac{RT}{M_w}\left[(\mu/\gamma)\,W + \beta\,(W)^2\right] \qquad (3\text{-}12)$$

Integration of Equation (3-12) between the front surface pressure ($P = P_L$ at $Z = L$) and any point within the char layer, (P at Z), results in an integral equation for the pressure distribution over the char.

$$P = \left\{P_L^2 + 2R\left[\int_z^L (\mu/\gamma)\,W\,(T/M_w)\,dz + \int_z^L \beta\,(T/M_w)\,(W)^2\,dz\right]\right\}^{1/2} \qquad (3\text{-}13)$$

In this equation all parameters that vary with temperature (hence, char distance) are left under the

integral signs. These variations are calculated by polynomials in temperature and from the solution of the energy equation.

Energy Equation. To formulate the equation that describes the energy transfer in the combined decomposition-char zone, the energy equations for the gas and for the solid are written separately. They are later combined considering that the gas and solid are at the same temperature at any cross section in the flow; that is in thermal equilibrium.

The general form of the energy equation for a gas mixture containing n species is (11):

$$\rho \bar{C}_p \frac{DT}{Dt} = - (\bar{\nabla} \cdot \bar{q}) - (\bar{\bar{T}} : \bar{\nabla} \bar{u}) + \sum_{i+1}^{n} (\bar{J}_i \cdot \bar{g}_i) +$$

$$\left(\frac{\partial \ln \bar{V}}{\partial \ln T} \right)_{P, x_i} \frac{DP}{Dt} + \sum_{i=1}^{n} H_i \left[(\bar{\nabla} \cdot \bar{J}_i) - R_i \right] \qquad (3\text{-}14)$$

For a one dimensional steady flow of gases in the combined zones, neglecting viscous dissipation, work against gravity and diffusional effects, compared to the heat transferred by conduction, convection and chemical reactions, Equation (3-14) becomes:

$$\rho \bar{C}_p \frac{u dT}{dz} = - \frac{d}{dz} (q_z) + \frac{\partial \ln \bar{V}}{\partial \ln T} \cdot \frac{u dP}{dz} - \sum_{i=1}^{n} H_i R_i \qquad (3\text{-}15)$$

For an ideal gas $\frac{\partial \ln \bar{V}}{\partial \ln T}$ is one (11). Furthermore, the work by pressure forces across a high porous char can be neglected as has been shown in the previous section and Equation (3-15) simplifies to:

$$\rho \bar{C}_p \; u \frac{dT}{dz} = - \frac{d}{dz} (q_z) - \sum_{i=1}^{n} H_i \, R_i \qquad (3\text{-}16)$$

where q_z is, from Fourier's Law of heat conduction:

$$q_z = - k_g \frac{dT}{dz} \qquad (3\text{-}17)$$

The energy equation for a reacting gas flow through a porous media follows directly from multiplying Equation (3-16) by the porosity ε and by substituting the definition of Equation (3-11) and Equation (3-17) into Equation (3-16) and is:

$$\varepsilon \cdot \frac{w}{\varepsilon} \cdot \bar{C}_p \frac{dT}{dz} = \varepsilon \frac{d}{dz} \left(k_g \frac{dT}{dz} \right) - \varepsilon \sum_{i=1}^{n} H_i \, R_i \qquad (3\text{-}18)$$

where $\varepsilon \cdot \frac{w}{\varepsilon} \cdot \bar{C}_p \frac{dT}{dz}$ is the convective term

$\varepsilon \frac{d}{dz} \left(k_g \frac{dT}{dz} \right)$ is the conduction term

$\varepsilon \sum_{i=1}^{n} H_i \, R_i$ accounts for the thermal effects of the gaseous chemical reactions.

Similarly, the energy equation for the solid in the combined decomposition-char zone simplified for the same restrictions to the following form:

$$(1-\varepsilon)C_{p_s}\rho_s \, v \frac{dT}{dz} = (1-\varepsilon) \frac{d}{dz}\left(k_s \frac{dT}{dz}\right) + (1-\varepsilon) \sum_{i=n+1}^{1} H_i R_i + q(T) \qquad (3\text{-}19)$$

where

$(1-\varepsilon) C_{p_s}\rho_s \, v \frac{dT}{dz}$ is the convective term

$(1-\varepsilon) \frac{d}{dz}\left(k_s \frac{dT}{dz}\right)$ is the conductive term

$(1-\varepsilon) \sum_{i=n+1}^{1} H_i R_i$ accounts for the thermal effects due to chemical reactions of the char.

$q(T)$ accounts for the thermal effects due to degradation of polymer.

The q(T) function for this research has been obtained from data reported by Sykes (12) for important phenolic-nylon and silicone elastomers heat shield components. Typical curves reported by Sykes for phenolic micro-balloons, phenolic resin and nylon are shown in Figure 3-3.

The total energy transferred in the combined decomposition-char zone is formed by adding Equations (3-18) and (3-19) and by using the definition of W of Equation (3-11):

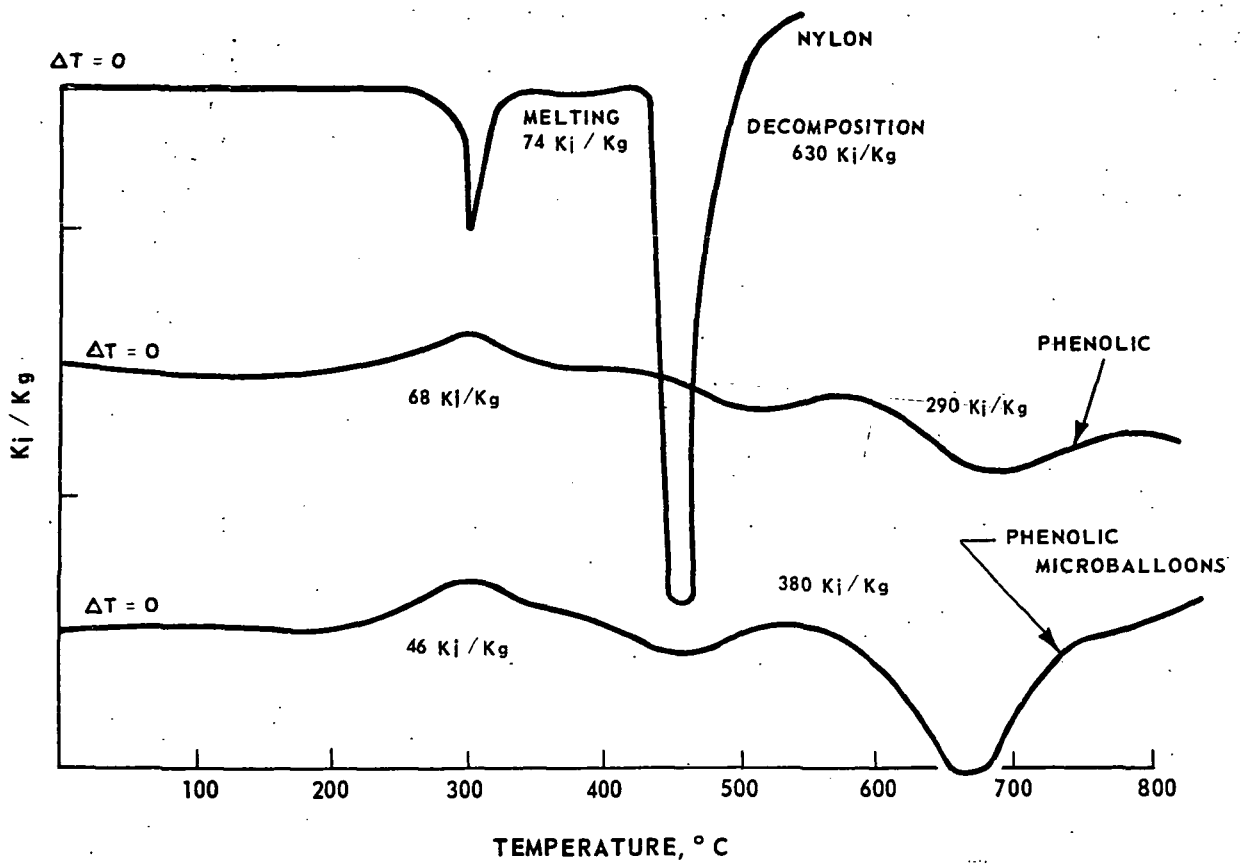

Figure 3-3. Differential Thermal Analysis Thermogram of Nylon, Phenolic and Phenolic Microballoons as Reported by Sykes and Nelson, (3).

$$[\varepsilon\, C_p\, W_p + (1-\varepsilon)\, C_{p_s}\, \rho_s v]\, \frac{dT}{dz} = \frac{d}{dz}\left(k_e \frac{dT}{dz}\right) - \sum_{i=1}^{1} H_i\, \bar{R}_i + q(T) \qquad (3\text{-}20)$$

where k_e represents an effective thermal conductivity defined as:

$$k_e = \varepsilon\, \bar{k}_g + (1-\varepsilon)\, k_c \qquad (3\text{-}21)$$

$\bar{k}_g$ is the thermal conductivity of the flowing pyrolysis gases and k_c that of the solid matrix.

In addition the term $\sum_{i=1}^{1} H_i\, \bar{R}_i$ is defined as:

$$\sum_{i=1}^{1} H_i\, \bar{R}_i = \sum_{i=1}^{n} H_i\, R_i + (1-\varepsilon) \sum_{i=n+1}^{1} H_i\, R_i \qquad (3\text{-}22)$$

The above represents the energy absorbed by the chemical reactions on a "total volume" basis. The solution of the energy equation, Equation (3-20), gives the temperature distribution in the combined decomposition char zone.

In addition to the equations of change just developed, one additional equation is considered. This is the equation for the net heat absorption within the combined zones.

Heat Flux Equation. The heat flux equation is used to determine the net heat transfer to the char layer and decomposition zone in the charring ablator. It is defined as the difference in the heat flux values at Z=0 located in the virgin material, and that of the front surface of the char, at Z=L, and is:

$$q_{net} = q_L - q_0 = k_e \left.\frac{dT}{dz}\right|_{z=L} - k_e \left.\frac{dT}{dz}\right|_{z=0} \qquad (3\text{-}23)$$

Solving for $k_e \cdot \frac{dT}{dZ}$ term of the energy equation, Equation (3-20), substituting it into Equation (3-23) and integrating gives the equation needed to evaluate the net heat flux within the combined zones; which is:

$$q_{net} = \int_{T_0}^{T_L} \sum_{i=1}^{n} \varepsilon \, C_{p_i} W_p \, x_i \, dT + (1-\varepsilon) \int_{T_0}^{T_L} C_{p_s} \, \rho_s \, v \, dT$$

$$+ \int_{T_0}^{T_L} \sum_{i=1}^{1} \frac{H_i \, \bar{R}_i}{dT/dz} \, dT + \int_{T_0}^{T_D} \frac{q(T)}{dT/dz} \cdot dT \qquad (3\text{-}24)$$

T_o is the temperature at Z=0, T_D is the maximum temperature of the decomposition zone, and T_L is the temperature at Z=L.

If we define Q as:

$$Q = \int_{T_o}^{T_D} \frac{q(T)}{dT/dz} \cdot dT + \int_{T_o}^{T_D} (1-\varepsilon)\ C_{p_s}\ \rho_s\ v\ dT \qquad (3\text{-}25)$$

we have:

$$q_{NET} = \int_{T_o}^{T_L} \sum_{i=1}^{n} \varepsilon\ C_{p_i} W_p\ x_i\ dT + (1-\varepsilon) \int_{T_D}^{T_L} C_{p_s}\ \rho_s\ v\ dT$$

$$+ \int_{T_o}^{T_L} \sum_{i=1}^{1} \frac{H_i\ \bar{R}_i}{dT/dz} \cdot dT + Q \qquad (3\text{-}26)$$

where the first term of Equation (3-26) represents the heat absorbed due to the sensible enthalpy change of the gases. The second term accounts for the sensible enthalpy change of the solids. The subsequent term accounts for the heat absorbed by the chemical reactions. This term is calculated under three chemically distinct flow conditions. One is frozen in which case the term is zero. A second is equilibrium, in which the rate of heat absorption is calculated by considering the species to be in chemical equilibrium, and, the third is

non-equilibrium in which this rate is calculated considering the species to be reacting at a finite rate. The finite rate or non-equilibrium analysis is the most difficult to implement for several reasons. One is the problem of selecting the important chemical reactions with which to model the chemically reacting flow system. A second difficulty is the evaluation of the wealth of kinetic data for the important chemical reaction, and the selection of that data which will most typically represent a chosen reaction.

Of the two reacting flow analyses, the non-equilibrium flow is more complex than the chemical equilibrium analysis. The latter involves the solution of a set of algebraic equations with the energy equation, while the former requires the solution of the energy equation with coupled, ordinary non-linear differential equations which are the species continuity equations. There is sometimes associated with the solution of ordinary differential equations, with widely separated eigen values, a phenomena called stiffness. This phenomena is present in chemically reacting flow systems where very fast reactions occur. A more thorough discussion of this problem is presented in Chapter V, and it will be shown how this phenomena can cause numerical instabilities and require the integration step

size to be very small. Finally, Q, the last term in Equation (3-26) is the rate of heat absorbed in the pyrolysis of decomposition zone, and was defined by Equation (3-25).

A summary of the important differential equations for describing the energy transferred in the decomposition zone and char zone is given in Table 3-2. In the following sections the boundary conditions and the numerical solution of these equations are discussed which will complete the theoretical discussion of the combined zone analysis.

Boundary Conditions for the Solution of the Energy and Species Continuity Equations in the Combined Decomposition Zone and Char Layer

The energy equation describing the one dimensional flow of heat in the decomposition zone and the char layer of a charring ablator is a second order, non-linear differential equation with variable coefficients. The energy equation is coupled to the species continuity equations which are first order differential equations. The momentum equation, as previously mentioned, was uncoupled from the energy equation because PV work was negligible.

April (2), who solved the energy equation for the char layer only, considered two sets of boundary conditions. The first set specified the temperature

TABLE 3-2 Summary of the important equations related to the flow of pyrolysis products in the char zone.

Species Continuity Equation: (3-3)

$$\frac{d}{dz}(\rho_i u) = R_i$$

Momentum Equation Darcy's Law: (3-13)

$$P = \{P_L^2 + 2R \cdot \left[\int_Z^L \mu/\gamma \; W(T/M_W)dz + \int_Z^L \beta(T/M_W)\,(W)^2\,dz\right]\}^{1/2}$$

Energy Equation: (3-20)

$$\{\varepsilon \bar{C}_p W_p + (1-\varepsilon)C_{p_s}\rho_s v\}\frac{dt}{dz} = \frac{d}{dz}\left(k_e \frac{dT}{dz}\right) - \sum_{i=1}^{1} H_i \bar{R}_i = q(T)$$

Heat Flux: (3-24)

$$q_{net} = \sum_{i=1}^{n} \int_{T_o}^{T_L} (\varepsilon C_{p_i} W_p X_i dt + (1-\varepsilon) \int_{T_o}^{T_L} C_{p_s}\rho_s v\, dT \sum_{i=1}^{1} \int_{T_o}^{T_L} \frac{H_i R_i}{dt/dz} \cdot dt + \int_{T_o}^{T_D} \frac{q(T)}{dt/dz} \cdot dt$$

at the front surface, and, the temperature and pyrolysis gas composition at the back surface of the char. These conditions made the solution of the energy equation a two point boundary value problem which required an iterative procedure. A second set of boundary conditions specified the temperature, composition and back surface heat flux and made this an initial value problem. For both the initial and final value problems the thickness of the char was considered to be 1/4 inch. The pyrolysis gas mass flux, W, in addition, was considered a parameter and was varied between 0.01 and 0.05 (lbm/ft^2 - sec).

In the present analysis the two point boundary value problem was not considered. Rather than specifying, in addition to the back surface boundary conditions, the char thickness and the front surface temperature, the thickness of the char was allowed to be determined by the front surface temperature. The front surface temperature was a parameter in the solution and thus eliminated the necessity for an iterative solution. Not only does this simplify the problem but it eliminates, in addition, some of the artificiality associated with fixing the thickness of the char.

In this analysis the back surface temperature, the back surface heat flux and the composition of the plastic composite were specified. Unfortunately, the current state of the art precludes prediction of the composition of the pyrolysis product from a known combination of plastic composites. Therefore, it was necessary to specify, in addition, the pyrolysis gas composition. How this composition was arrived at is discussed in Appendix G. The boundary conditions selected were therefore:

$$T = T_o \text{ with } T_L \text{ as a parameter}$$

$$\left.\frac{dT}{dz}\right|_o = - \frac{q_p}{k_e} \qquad (3\text{-}27)$$

$$x_i = x_{i\,o},\ i = 1 \ldots n$$

Once the energy equation is solved, the momentum equation is solved by specifying the front surface pressure. Because the pressure drop is small (~15 lbs/ft^2), the assumption of constant pressure in the solution of the energy equation can be considered valid.

The computer program implementation for the combined char layer and decomposition in depth is presented in detail in Appendix A together with a complete listing of the program.

As mentioned in the Introduction, this research deals with the development of a mathematical analysis to predict the energy transfer for the combined decomposition zone and char layer. In addition, it deals with developing the analysis for the char zone to 5500°F. Decomposition in depth is now analyzed, and this is followed by a brief description of the application of the transport equations to frozen, equilibrium and non-equilibrium flow in the combined zones.

Analysis of Decomposition in Depth. It was previously stated that the previous mathematical analysis (2, 12) to predict the energy transfer in the char zone is handicapped by the arbitrary separation of the decomposition zone and char layer. This analysis was useful in bounding the energy absorption in the char zone. However, the energy transferred in the two zones can be predicted accurately by a combined analysis of both the decomposition zone and char zone.

A schematic diagram was shown in Figure 3-1 for the quasi-steady model with the combined zones. The point of view was taken of an observer moving with the negative surface recession velocity, v. It was shown by a simple material balance (Equation (3-1)) that by knowing the density of the virgin and degrading materials,

the mass flux W of the gases could be calculated. This differs from the previous analysis (2, 12) where the mass flux of pyrolysis gases, W, was a specified parameter at the back surface of the char. The present analysis also differs in that the thickness of the char is treated as a variable rather than a specified parameter.

The analysis of decomposition in depth requires that the rate of mass loss, or rate of density change with temperature be known accurately. Data for the densities of virgin and degrading composites as a function of temperature have been reported by Sykes and Nelson (3) and Madorski (14). The data of Sykes and Nelson (3) is particularly useful since it is for phenolic-nylon resins; this data was obtained using thermogravimetric analyses techniques. In Chapter II, the importance of using a kinetic equation of the Arrhenius type to correlate the experimental mass loss rate data for polymers, was discussed. It was indicated in this chapter that the mass loss of a material was affected by the heating rate, and that this effect was a source of difficulties for earlier researchers modeling the decomposition process. Sykes and Nelson (3) used a pseudo-order kinetic expression of the Arrhenius type to eliminate this influence. The equation is:

$$\frac{-d\rho_i}{dt} = \rho_{i,o}\left[(\rho_i - \rho_{c,i})/\rho_{i,o}\right]^{n_i} A_i \exp\left[-E_i/RT\right] \tag{3-28}$$

Equation (3-28) expresses the rate of change of density of a polymer with temperature. $\rho_{i,o}$ is the initial or virgin density. ρ_i is the density of the material at temp-rature T, ρ_c the residual or char density, and A_i and E_i are the well known frequency factor and activation energy parameters.

In the present mathematical analysis it has been assumed that when an ablative composite degrades, it degrades independently of the other components; that is, no interaction is assumed to occur among the composites. There is no known experimental data, at least to the author, that takes into account these interactive effects. Therefore, of necessity, this simplifying assumption has been made. This is expressed mathematically:

$$\frac{d\rho}{dt} = \sum_{i=1}^{k} \frac{d\rho_i}{dt} \tag{3-29}$$

and for a quasi-steady flow the time dependent term can be modified by:

$$\frac{d\rho}{dt} = v\,\frac{d\rho}{dz} \tag{3-30}$$

Thus, knowing the kinetic parameters for the various components in a blend of virgin material, specifying the surface recession velocity, and the temperature history from the energy equation, the variation in density of the virgin material can be predicted by the use of Equations (3-28), (3-29) and (3-30). The pyrolysis gas mass flux is then calculated by Equation (3-1).

Application of the Transport Equations to Frozen, Equilibrium, and Non-Equilibrium Flow of Gases in the Combined Decomposition Char Zone

There are two limiting cases currently used to simplify the analysis of the flow of pyrolysis gases. These are frozen and equilibrium flow. Frozen flow considers that there are no chemical reactions among the pyrolysis gases and thus, gives a lower bound of the energy absorbed by these gases in the combined decomposition-char zone. Equilibrium flow, on the other hand, assumes that there are chemical reactions which are in chemical equilibrium. This case gives the upper limit on the energy absorbed by the pyrolysis gases.

The correct answer, however, lies between these two limiting cases. A major portion of this research has dealt with the development of a third analysis, a non-equilibrium flow analysis which predicts more

accurately the actual behavior within the decomposition-char zone. In this section the equations of continuity, momentum, energy and surface heat transfer are applied to develop each of the three flow analyses. In the two subsequent chapters the solution of the particular equations for each analysis is shown and compared with each other.

Frozen Flow. In the frozen flow analysis the pyrolysis products entering the char layer are assumed not to undergo chemical reactions. Therefore, the composition of these gases remain constant throughout. The only energy absorbed by the gases is convective energy. This energy is absorbed as the gases transpire through the char. This analysis gives the lower limit on the amount of energy absorbed in the combined zones since it does not account for the heat absorbed by endothermic chemical reactions. Of all three cases, this is the simplest to solve because the heat absorption term due to chemical reaction is zero. This is:

$$\sum_{i=1}^{1} H_i \, \bar{R}_i = 0 \qquad (3\text{-}31)$$

which simplifies the energy and heat flux equations. Applying this to the equations of change previously developed results in the following simplifications:

Continuity Equation:

$$W = W_p \, \varepsilon = \varepsilon \rho u = \text{constant} \tag{3-11}$$

Momentum Equation:

$$P = \left\{ P_L^2 + 2R \cdot \left[\int_Z^L (u/\gamma) \, W \, (T/M_w) \, dz \right. \right.$$

$$\left. \left. + \int_Z^L \beta \, (T/M_w) \, W^2 \, dz \right] \right\}^{1/2} \tag{3-13}$$

Energy Equation:

$$[\varepsilon \, \bar{C}_p \, W_p + (1-\varepsilon) \, C_p \, \rho \, v] \, \frac{dT}{dz} = \frac{d}{dz} \left(k_e \, \frac{dT}{dz} \right) - q(T)$$

(3-32)

Heat Flux Equation:

$$q_{NET} = \sum_{i=1}^{n} \int_{T_o}^{T_L} \varepsilon \, W_p \, C_{p_i} \, x_i \, dT + q \, (T) \tag{3-33}$$

The numerical solution of these equations is discussed in a later section.

Equilibrium Flow. The equilibrium flow analysis assumes that the chemical species are in thermochemical equilibrium. This analysis gives the upper limit on the amount of heat absorbed in the combined zones. The reason is that reactions occurring both in the decomposition and char zone are predominantly endothermic. The set of equations which are applicable to this analysis is the same as the equations previously developed: Continuity (3-11), momentum (3-13), energy (3-20) and heat flux (3-24). But in this case:

$$\sum_{i=1}^{1} H_i \bar{R}_i \neq 0 \qquad (3\text{-}34)$$

The species continuity equation, (3-2), can be rewritten in terms of the molal flux of the species, and is:

$$R_i = \frac{d}{dz}(\rho u) = \frac{d}{dT}(W x_i)\frac{dT}{dz} \qquad (3\text{-}35)$$

Therefore, in order to evaluate the term $\sum_{i=1}^{1} H_i \bar{R}_i$ which accounts for the heat absorbed by the reactions, the mass flux W, and the mass fraction x_i of the species must be known as a function of temperature. The species composition and molal ratio of gases to carbon are a function of temperature, pressure and elemental composition

of the virgin plastic and can be calculated by one of many approaches (see Chapter IV). In this study free energy minimization is used.

Non-Equilibrium Flow. This analysis is the most complex of the three. It involves the solution of a second-order, non-linear differential equation with variable coefficient (the energy equation), coupled to n (where n is the number of species) ordinary, non-linear, differential equations (species continuity equations. For the chemical equilibrium case, on the other hand, a set of non-linear algebraic equations were solved coupled to the energy equation. Numerically, this is a much simpler problem.

For the non-equilibrium analysis the rate of reaction R_i is calculated using finite rate chemistry. This requires knowledge of the specific reactions taking place, and also requires evaluation of the kinetic data for particular reactions chosen. The topic of kinetic data evaluation is covered in Appendix D. Once the rate of reaction, R_i, of each specie is calculated, the heat absorbed by the chemical reaction is treated in the same manner as was in the chemical equilibrium analysis case. The numerical solution of the energy equation, which is the subject of the next section, is essentially the same for both analyses.

Numerical Solution of the Equations of Change

It was shown earlier in the chapter that to formulate the differential equations to describe the energy transfer in the combined zones, the continuity and energy equations, for the gas and solids, were written separately. Then these equations were combined by considering that there were no thermal gradients between them; the result was Equation (3-20):

$$[\varepsilon \bar{C}_p W_p + (1-\varepsilon) C_{p_s} \rho_s v] \frac{dT}{dz} = \frac{d}{dz}\left(k_e \frac{dT}{dz}\right) - \sum_{i=1}^{1} H_i \bar{R}_i + q(T) \qquad (3\text{-}20)$$

This equation is an ordinary, second order, non-linear (since the terms within the brackets are functions of temperature) differential equation with variable coefficient. This type of equation requires a numerical integration scheme because there are no known analytical solutions for this type of non-linear equation. A fourth order Runge-Kutta formulae was used because of the accuracy and straight forward nature of the self starting method.

Numerical Solution of the Differential Energy Equation

To solve Equation (3-20) it is necessary to transform the equation to a form suitable for numerical integration. This is done by expanding Equation (3-20) and solving for the second order term. The result is:

$$\frac{d^2T}{dz^2} = \frac{1}{k_e}\left[\varepsilon\,\bar{C}_p\,W + (1-\varepsilon)\,C_p\,\rho\,v - \frac{dk_e}{dT}\right]\cdot\frac{dT}{dZ}$$

$$+\sum_{i=1}^{1} H_i\,\bar{R}_i/(dT/dZ) + q/(dT/dZ)\Big]\cdot\frac{dT}{dZ} \qquad (3\text{-}36)$$

Equation (3-36) has the form:

$$\frac{d^2T}{dZ^2} = f\ (T,\ \dot{T})\ \frac{dT}{dZ} \qquad (3\text{-}37)$$

Where A represents the terms within the bracket of Equation (3-36) divided by the effective thermal conductivity, k_e. Notice that A is a function of both temperature T and the gradient $\dot{T}$ $(= \frac{dT}{dZ})$.

A commonly employed procedure for the Runge-Kutta is to convert the second order Equation (3-37) into two first order equations to be solved simultaneously (16). The procedure is as follows:

Let

$$\dot{T} = \frac{dT}{dZ} \tag{3-38}$$

Substituting the above in Equation (3-37) gives:

$$\frac{d\dot{T}}{dZ} = f(\dot{T}) \tag{3-39}$$

Solving Equations 3-38 and 3-39 simultaneously gives the wanted solution. A summary of these equations is given in Table 3-3.

The general formulae, as they apply to the solution of the differential energy equation is given in Table 3-4. The truncation error of this technique is of the order $O(h^5)$ where h is the step size (16).

Note that the term $f(T,\dot{T})$ of Equation (3-36) has an implicit dependence on the mole flux of each specie i. This implicit dependence is in the term $\sum_{i=1}^{l} H_i \bar{R}_i$. Therefore, the species continuity equation must be solved simultaneously with the energy equation when reactions occur in the flow field.

Check Procedure. The Runge-Kutta computer implemented solution was checked by numerically solving Equation (3-37) with f, constant, and comparing it to the analytically exact solution of the equation.

TABLE 3-3. Conversion of a Second Order Differential Equation to the Equivalent set of Two First Order Differential Equations.

$$\frac{d^2T}{dZ^2} = f(T,\dot{T})\ \frac{dT}{dZ} \qquad (3\text{-}37)$$

which decomposes into two first order equations shown below:

$$\frac{dT}{dZ} = \dot{T} = G(\dot{T}) \qquad (3\text{-}38)$$

$$\frac{d\dot{T}}{dZ} = f(\dot{T}) = F(T,\dot{T}) \qquad (3\text{-}39)$$

TABLE 3-4. General Formulation for the Evaluation of the Runge-Kutta Parameters for the Simultaneous Solution of Two First Order Differential Equations (16).

$$T_{N+\bar{T}} = T_N + (B_1 + 2\,(B_2 + B_3) + B_4)/6 \qquad (3\text{-}40)$$

$$\dot{T}_{N+1} = \dot{T}_N + M\,(C_1 + 2\,(C_2 + C_3) + C_4)/6 \qquad (3\text{-}41)$$

$$\begin{aligned}
B_1 &= h \cdot G(\dot{T}) \\
C_1 &= h \cdot F(T, \dot{T}) \\
B_2 &= h\ G(\dot{T} + \tfrac{1}{2} C_1) \\
C_2 &= h\ F(T + \tfrac{1}{2} B_1,\ \dot{T} + \tfrac{1}{2} C_1) \\
B_3 &= h\ G(\dot{T} + \tfrac{1}{2} C_2) \\
C_3 &= h\ F(T + \tfrac{1}{2} B_2,\ \dot{T} + \tfrac{1}{2} C_2) \\
B_4 &= h\ G\ (\dot{T} + C_3) \\
C_4 &= h\ F(T + B_3,\ \dot{T} + C_3)
\end{aligned} \qquad (3\text{-}42)$$

This comparison is shown in Table 3-5 for different step sizes.

Numerical Solutions of the Heat Flux and Momentum Equations

The solution of the heat flux and momentum equations are obtained after the temperature profile has been established, i.e., the energy equation has been solved. The momentum equation was uncoupled from the energy equation, as previously explained, because the energy dissipated by PV work was considered small when compared to the energies by convection and chemical reactions. The equations for the heat flux and pressure are first order, integral equations with variable coefficient.

The heat flux equation is:

$$q_{NET} = \sum_{i=1}^{n} \int_{T_o}^{T_L} \varepsilon \, W_p \, C_{p_i} \, X_i \, dT + \int_{T_o}^{T_D} q(T) \, dT$$

$$+ \sum_{i=1}^{1} \frac{H_i \bar{R}_i}{dT/dZ} \cdot dT \qquad (3\text{-}43)$$

The first term in the equation is the heat absorbed by convection in the combined decomposition-char zone. The second term is that absorbed by the polymer degradation in the decomposition zone. Note

TABLE 3-5. Comparison of the Fourth Order Runge-Kutta Solution With the Analytical Solution of $\frac{d^2T}{dZ^2} = A \frac{dT}{dZ}$ for 100 Integration Steps.

Numerical	Analytical	Distance
T of	T of	Z
500.0	500.0	0
920.7	920.7	0.1
1385.6	1385.6	0.2
1845.7	1845.7	0.3
1899.4	1899.4	0.4
3094.8	3094.9	0.5
3788.4	3788.5	0.6
4554.9	4556.0	0.7
5402.0	5402.1	0.8
6338.2	6338.4	0.9
7372.9	7373.1	1.0

$T_{initial} = 500^{o}F$

$\left.\frac{dT}{dZ}\right|_{Z=0} = 1000$

that the integration limits are from T_o to T_D. Where T_D is the temperature at which all of the virgin material has been degraded to gases and char. The last term accounts for the heat absorbed by chemical reactions.

The pressure equation is:

$$P = \left\{ P_L^2 + 2R \left[\int_Z^L (u/\gamma)\, W\, (T/M_W)\, dZ + \int_Z^L \beta\, (T/M_W)\, W^2\, dZ \right] \right\}^{1/2} \qquad (3\text{-}44)$$

Equation (3-44) was integrated using Simpson's Rule. The general formula for the Simpson's Rule analysis is (23):

$$fdZ = \frac{h}{3} \left[f_o + 4\,(f_i + f_3 + \ldots + f_{2n-1}) + 2\,(f_2 + f_4 \ldots + f_{2n-2} + f_{2n}) \right] - \frac{nh^5}{90}\, f^4 \qquad (3\text{-}45)$$

where $\frac{nh^5}{90}\, f^4$ is the truncation error.

In terms of the pressure distribution equation, the Simpson's Rule functions are:

$$\int f_{P_1}\, dZ = \int (u/\gamma)\, W\, (T/M_W)\, dZ \qquad (3\text{-}46)$$

$$\int f_{P_2}\, dZ = \int \beta\, (T/M_W)\, dZ \qquad (3\text{-}47)$$

A study on the value of the step size h that would minimize the truncation error and maximize the accuracy of the approximate solution was done by April (2). A comparison of his results for various step sizes is given in Table 3-6.

Summary of the Theoretical Development of the Equations of Change for Flow in the Combined Decomposition Char Zone

The importance of considering both the decomposition zone and char layer as important heat absorbing regions was presented. The Equations of change (continuity momentum and energy) were developed to describe the flow of gases and to predict the energy transfer in the combined regions. These equations were developed for three flow conditions. Namely frozen, equilibrium, and non-equilibrium flow. The method of determining the effects of the latter two flow conditions was presented. In addition, the equations to describe the degradation kinetics of the virgin material were discussed. Finally, the numerical procedure was discussed, along with the comparison to verify the accuracy of the computer implemented solution.

The following two chapters, Chapter IV and V will discuss the methods used to calculate chemical equilibrium and non-equilibrium chemistry, respectively.

TABLE 3-6 Comparison of various Simpson's rule increment sizes for the frozen flow, variable properties model. (2).

Dimensionless char distance	Pressure (lb/ft^2) Simpson's Rule Increment Sizes			
(z/L)	20	50	100	200
0.00	2175.5921	2175.5918	2175.5913	2175.5912
0.33	2173.4147	2173.4144	2173.4139	2173.4138
0.67	2168.7373	2168.7368	2168.7364	2173.7364
1.00	2160.0000	2160.0000	2160.0000	2160.0000

Conditions: $W = 0.05\ lb/ft^2\text{-sec}$ $L = 0.0208$ ft $\varepsilon = 0.8$

Gas Composition: (Mole/Mole Gas)

$CO = 0.245$, $CO_2 = 0.046$, $CH_4 = 0.570$, $N_2 = 0.073$, $C_6H_6 = 0.068$

Although the development of the chemical equilibrium analysis (Chapter IV) will appear to be more difficult than for non-equilibrium analysis (Chapter V), the computer implemented solution of the latter has given severe numerical difficulties which will be thoroughly discussed.

REFERENCES

1. Pike, R. W., G. C. April and E. G. del Valle, "Non-Equilibrium Flow and the Kinetics of Chemical Reactions in the Char Zone," NASA CR-66455, July 15, 1967.

2. April, G. C., "Evaluation of the Energy Transfer in the Char Zone During Ablation; Part 1: Theoretical and Experimental Results for Heat Shield Surface Temperatures up to 3000°F." Ph.D. Dissertation, Chemical Engineering Department, Louisiana State University, Baton Rouge, Louisiana, May 1969.

3. Sykes, G. F. and J. B. Nelson, "Thermoanalysis of Ablation Materials," Preprint TV, 61st National Meeting A.I.Ch.E., Houston, Texas (February 19-23, 1967).

4. Stroud, C. W., "A Study of the Chemical Reaction Zone in Charring Ablators During Thermal Degradation," Preprint No. 33b, National Meeting A.I.Ch.E., Dallas, Texas (February 6-9, 1966).

5. Wilson, R. Gale, "Thermophysical Properties of Six Charring Ablators from 140° to 700°K and Two Chars from 800° to 3000°K," NASA TN D-2991 (October 1965).

6. Engelke, W. T., C. M. Pyron, Jr., and C. D. Pears, "Thermophysical Properties of a Low Density Phenolic-Nylon Ablation Material," NASA CR-809 (July 1967).

7. Nagler, R. G., "The Thermal Conduction Process in Carbonaceous Chars," JPL Technical Report 32-1010, Jet Propulsion Laboratory, California Institute of Technology, Pasadena, California (February 1967).

8. Koh, J. C. and E. P. del Casal, "Heat and Mass Flow Through Porous Matrices for Transpiration Cooling," Paper 16, Proceedings of the 1965 Heat Transfer and Fluid Mechanics Institute, Stanford University Press, Los Angeles, California, 263-81 (June 21-23, 1965).

9. Clark, Ronald K., "Flow of Hydrocarbon Gases in Porous Media at Elevated Temperatures," M.S. Thesis, University of Virginia, 108 pages (May 1968).

10. Weger, Eric, Jere Brew and Ronald Servais, "An Investigation of Carbon Deposition in Chars-II," Report SAMSO-TR-68-123, Washington University, St. Louis, Missour, 96 pages (January 1968).

11. Bird, R. B., W. E. Stewart, and E. N. Lightfoot, Transport Phenomena, John Wiley and Sons, Inc., New York, 828-30 (1960).

12. Sykes, G. F., "Decomposition Characteristics of a Char-Forming Phenolic Polymer Used for Ablative Composites," NASA-TN D-3810 (February 1967).

13. Pike, R. W., G. C. April and E. G. del Valle, "Evaluation of the Energy Transfer in the Char Zone During Ablation"; Part 1: Theoretical and Experimental Results for Heat Shield Surface Temperatures up to 3000°F--Final Report, Louisiana State University, NGR-19-001-016 (May 1, 1969).

14. Madorski, S. L., Thermal Degradation of Polymers, Interscience Publisher, New York (1964).

15. Nelson, J. B., "Determination of Kinetic Parameter of Six Ablation Polymers by Thermogravimetric Analysis," NASA-TN D-3919 (April 1967).

16. McGormic, J. M. and M. G. Salvadori, Numerical Methods in Fortran, Prentice-Hall, Inc., Englewood Cliffs, New Jersey (1966).

CHAPTER IV

CHEMICAL EQUILIBRIUM ANALYSIS

Introduction

A general method for computing complex chemical equilibrium in a multicomponent, polyphase system is presented in detail (1, 2). This method, called the Chemical Equilibrium Analysis, is a modified version of the RAND method, which is also known as free energy minimization. It was originally presented by White, Johnson and Dantzig (3) for computing complex chemical equilibrium for an ideal gas system. It was subsequently extended to multiphase systems by Kubert and Stephanou (4) and others (5-7). In addition to this discussion of the method, brief comparisons with some other well known methods (8, 9, 10) for computing chemical equilibrium are presented. These comparisons will justify the choice of free energy minimization as a more flexible and easier method to implement on a machine for highly complex chemical systems.

The literature on the computation of complex chemical equilibrium is so extensive that it would detract from the main purpose of this chapter to review

all of it especially since a very extensive and well documented review on the historical development of chemical equilibrium was published recently by Zeleznik and Gordon (11, 12). A more modest undertaking was presented by del Valle et al. (13). At the end of the chapter, comments will be made on some of the other publications (16-66) which are available for solving the nonlinear chemical equilibrium equation. It will be realized that all these techniques are but minor variations of the most general methods (3, 8, 9, 10). It should be noted that the solution of the chemical equilibrium problems can be categorized either as the solution of a system of non-linear equation by the functional iteration method, i.e., equilibrium constant formulation (8, 9) or, as the direct minimization of the Gibbs free energy by descent method (3, 10). In this chapter the latter method is developed.

Condition for Chemical Equilibrium

The condition for chemical equilibrium in any reacting system at constant temperature and pressure is that the change in free energy of the reactions must be zero (14). Stated another way, the sum of the free energies of the individual components, i.e. the total free energy of the system, shall be a

minimum. A negative free energy may be considered as a driving force which causes a reaction to approach equilibrium. It can also be considered to be a measure of the departure of the reacting system from an equilibrium state. Thus, it is through this departure and hence, through its minimization that chemical equilibrium is calculated.

Stochiometric Balance

The law of the conservation of mass requires that for a chemically reacting system with no nuclear reactions that the chemical elements be conserved regardless of the number of phases being present at equilibrium. The stochiometric relation can be expressed as:

$$\sum_{i=1}^{n} a_{ij}\, x_i + \sum_{i=n+1}^{l} a_{ij}\, x_i = b_j \qquad j = 1....m \qquad (4\text{-}1)$$

where a_{ij} is the formula number giving the amount of gram-atoms of the j^{th} chemical element in the i^{th} species. The moles of each specie present in the system is denoted by x_i. The gram-atoms of each element j is denoted by b_j. The number of gaseous chemical species is n, and the number of condensed species is denoted by n+1 to j.

Conservation of Charge

When ionization is present in a system, the conservation of charge can be expressed in a form similar to Equation (4-1). Thus:

$$\sum_{i=1}^{l} a_{i,m+1} x_i = b_{m+1} \qquad (4\text{-}2)$$

where $a_{i,m+1}$ is the charge on the i^{th} specie, x_i is the number of moles of each specie, and b_{m+1} is zero, if the system is electrically neutral. Thus if we consider a charge as the m + 1 element we can use an equation of the form of Equation (4-1).

The Equation of Free Energy

It was previously stated that one of the conditions for chemical equilibrium was that the total free energy of the system be a minimum. To minimize the free energy an appropriate expression of this function is necessary. At equilibrium, the free energy of each specie in a mixture at any temperature T can be obtained by integrating the definition of fugacity (14) in terms of the free energy ($d\bar{F}_T = RTd\ln\bar{f}_i$). This integration gives:

$$(\bar{F}_T)_i - (\bar{F}_T^0)_i = RT \ln \bar{f}_i/\bar{f}_i^0 \quad i = 1...n \qquad (4\text{-}3)$$

but

$$\alpha_i = \frac{\bar{f}_i}{\bar{f}_i^{\,0}} \qquad i = 1...n \qquad (4\text{-}4)$$

Equation (4-4) is the definition of activity. Thus, Equation (4-3) becomes:

$$(\bar{F}_T)_i - (\bar{F}_T^{\,0})_i = RT \ln \alpha_i$$

or

$$(\bar{F}_T)_i = (\bar{F}_T^{\,0})_i + RT \ln \alpha_i \qquad i = 1,...n \qquad (4\text{-}5)$$

Up to this point there have been no restrictions posed on a chemically reacting system. At this juncture the two restrictions are introduced. One is the restriction that the chemically reacting gases are ideal. This in itself is not too severe if the analysis is constrained to high temperatures and low pressures, which is precisely the area of investigation in this research.* The second restriction is to assume that there is no mixing among the condensed or solid species, i.e., they remain in their pure state. Hence the activity of the solid can be taken to be one.

---

*In references 6, 45 and 46, non-idealities are considered.

Free Energy Minimization

Ideal Gas. For an ideal gas α_i the activity of the specie i can be taken to be equal to its partial pressure, p_i. Thus Equation (4-5) becomes:

$$(\bar{F}_T)_i = (\bar{F}_T^0)_i + RT \ln p_i \qquad i = 1,...n \qquad (4\text{-}6)$$

Solid Phase. In the event of solid carbon or any other condensed specie present in the system, Equation (4-5) can be simplified by recalling the fact that the activity of a solid or pure condensed specie is one. Therefore:

$$(\bar{F}_T)_i = (\bar{F}_T^0)_i \qquad i = n+1,...1 \qquad (4\text{-}7)$$

Equations for Free Energy of a Complex Gas-Solid Mixture. Consider a mixture containing 1 chemical species (n gaseous and n + 1 to 1 condensed) from chemical elements. Let

$$\bar{x} = \sum_{i=1}^{n} x_{i,gas} \qquad (4\text{-}8)$$

where x_i is the moles of specie i of the gas and $\bar{x}$ is the total moles of the reacting mixture. The definition of partial pressure is:

$$p_i = P \cdot \frac{x_i}{\bar{x}} \qquad i = 1...n \qquad (4\text{-}9)$$

where P is the total pressure of the reacting system. Substituting Equation (4-9) in (4-6) and multiplying by x_i/RT results in:

$$\frac{x_i(\bar{F}_T)_i}{RT} = \frac{x_i(\bar{F}_T^0)_i}{RT} + x_i \left[\ln P + \ln x_i/\bar{x}\right] \qquad i = 1...n \qquad (4\text{-}10)$$

It is convenient to define

$$f_i = \frac{x_i(\bar{F}_T)i}{RT} \qquad i = 1,...1 \qquad (4\text{-}11)$$

and

$$c_i = \frac{(\bar{F}_T^0)_i}{RT} + \ln P \qquad i = 1,...n \qquad (4\text{-}12)$$

Combining Equations (4-11) and (4-12) with (4-10) gives the free energy function for the gases and is shown below:

$$f_{i,gas} = x_i \left(c_i + \ln \frac{x_i}{\bar{x}}\right) \qquad i = 1,...n \qquad (4\text{-}13)$$

It can be observed that c_i will be constant at constant T and P, and x_i will be the only variable to be determined from thermodynamic equilibrium. A similar expression for the solid or, condensed phase is obtained by multiplying both sides of Equation (4-7) by x_i/RT. Making use of the definition of Equation (4-11)

results in the free energy function for the solid, which is

$$f_{i,solid} = x_i \, (\bar{F}_T^0/RT)_i \qquad i = n+1,\ldots 1 \qquad (4\text{-}14)$$

The total free energy of the mixture is obtained by summing Equations (4-13) and (4-14), and this gives:

$$F(X) = \sum_{i=1}^{n} f_{i,gas} + \sum_{i=n+1}^{1} f_{i,solid} \qquad (4\text{-}15)$$

or

$$F(X) = \sum_{i=1}^{n} x_i \, [c_i + \ln x_i/\bar{x}] + \sum_{i=n+1}^{1} x_i (\bar{F}_T^0/RT)_i \qquad (4\text{-}16)$$

where $X = (x_1, x_2, \ldots, x_1)$

A set of equations is now developed to enable the computation of the set of x_i's that satisfy Equation (4-1) (material balance) and makes the free energy function, of Equation (4-16) a minimum.

Rationale for the Iterative Procedure. At a given temperature and pressure it is necessary to determine the amount of each chemical specie, x_i, present that minimizes the free energy. However, problems arise when standard minimization techniques

are applied directly to F(X) and the associated material balance constraint. This is because the equations resulting from setting the first partial derivation with respect to x_i equal to zero cannot be solved explicitly for the independent variables, x_i. Therefore, it is convenient to make a quadratic approximation to the free energy function which permits the independent variables to be expressed explicitly. Then an iteration scheme is developed such that this quadratic approximation approaches the actual value of the free energy function at the point of minimum free energy. To develop these equations for the quadratic approximation and the iterative scheme, select any positive set of mole values of $Y = (y_1, y_2, \ldots y_l)$ which satisfy the material balance equations, Equation (4-1), as the initial estimate of the composition. There, the value of the total free energy function of the mixture is:

$$F(Y) = \sum_{i=1}^{n} y_i \left(c_i + \ln \frac{y_i}{\bar{y}}\right) + \sum_{i=n+1}^{l} y_i \, (\bar{F}_T^{\,0})_i/RT \qquad (4\text{-}17)$$

However, it is not necessarily true that the assumed mole numbers are the ones for the components in thermodynamic equilibrium. For this to be true the free energy must be a minimum and the

material balance equations satisfied. Therefore the objective of the iteration scheme to be developed is to locate the point of minimum free energy by using the quadratic approximation to the free energy function and have the material balance constraints satisfied. The approach will be to form the quadratic approximation of the free energy function at X expanded about Y. Then the adjoint equation employing Lagrange multipliers will be formed with this approximation and the m material balance constrait equations. At this point, the usual procedure would be to set partial derivatives with respect to the independent variables, $(x_1, x_2, \ldots x_l)$ and the Lagrange multipliers $(\pi_1, \pi_2, \ldots \pi_m)$ equal to zero, and solve simultaneously the resulting set of m + l equations for the minimum of the constrained quadratic approximation. Then the procedure would be repeated employing some convergence criteria to approach the point of minimum free energy.

It is more convenient, however, to use a variation of this procedure which requires that only m + 1 + s equations be solved simultaneously, where s is the number of solid or condensed species, rather than m + 1 + n + s equations. Since a quadratic approximation is used, the linear equations resulting

from taking the partial derivatives with respect to the x_i's can be solved directly for the $x_{i,gas}$'s in terms of the Lagrange Multipliers, π_j's and $\bar{x}$, the total moles of gases. This permits eliminating $x_{i,gas}$ in the material balance equations and results in the m + 1 + s equations to be solved simultaneously for the π_j's $\bar{x}$, and x_i, solid. There are m equations with the π_j's as the independent variables which result from the elimination of x_i in the material balance equations on the individual elements, Equation (4-1). The other equations are Equation (4-8) and the ones from setting the partial derivative with respect to $x_{i,solid}$ of the adjoint equation equal to zero. These equations will be developed and placed into a matrix form. Then a convergence procedure will be discussed to insure that the point of minimum free energy is obtained.

Quadratic Approximation to the Free Energy Function. The problem is to expand F(X) in the neighborhood of Y in terms of the difference $\Delta_i = (x_i - y_i)$. To do this a Taylor series expansion for the free energy function at X, F(X), expanded about Y, the estimated values, results in the quadratic approximation to F(X), which follows:

$$Q(X)=F(Y) + \sum_{i=1}^{1} \frac{\partial F(Y)}{\partial y_i} \cdot \Delta_i + \frac{1}{2} \sum_{i=1}^{1} \sum_{k=1}^{1} \left(\Delta_i \frac{\partial}{\partial y_i} + \Delta_k \frac{\partial}{\partial y_k}\right)^2 \cdot$$

$$F(Y)+.... \qquad (4\text{-}18)$$

where

$$\left(\Delta_i \frac{\partial}{\partial y_i} + \Delta_k \frac{\partial}{\partial y_k}\right)^2 \equiv \Delta_i{}^2 \frac{\partial^2}{\partial y_i{}^2} + 2\,\Delta_i\,\Delta_k \frac{\partial^2}{\partial y_i \partial y_k} +$$

$$\Delta_k{}^2 \frac{\partial^2}{\partial y_k{}^2} \qquad (4\text{-}19)$$

Neglecting any terms higher than second order, Equation (4-18) becomes:

$$Q(X) = F(Y) + \sum_{i=1}^{1} \frac{\partial F(Y)}{\partial y_i} \Delta_i + \frac{1}{2} \sum_{i=1}^{1} \sum_{k=1}^{1} \frac{\partial^2 F(Y)}{\partial y_i \partial y_k} \Delta_i \Delta_k \qquad (4\text{-}20)$$

Taking the appropriate partial derivative gives:

$$\frac{\partial F(Y)}{\partial y_i} = c_i + \ln y_i/\bar{y} \qquad 1 \leq i \leq n \qquad (4\text{-}21)$$

$$\frac{\partial F(Y)}{\partial y_i} = \frac{(\bar{F}_T{}^0)_i}{RT} \qquad n+1 \leq i \leq 1 \qquad (4\text{-}22)$$

$$\frac{\partial^2 F(Y)}{\partial y_i\, y_k} = \frac{\delta_{ik}}{y_i} - \frac{1}{\bar{y}} \qquad 1 \leq i \leq n \qquad (4\text{-}23)$$

where δ_{ik} is the Kronecker delta ($\delta_{ik} = 0$ for $i=j$ and $\delta_{ik} = 1$ for $i \neq j$) and not that the second partials in the case of condensed species are zero.

Substituting Equation (4-21), (4-22) and (4-23) in (4-20) results in the quadratic approximation to the free energy function at X expanded about Y, and is:

$$Q(X) = F(Y) + \sum_{i=1}^{n} \left(c_i + \ln \left(\frac{y_i}{\bar{y}}\right)\right) \Delta_i + \sum_{i=n+1}^{l} \frac{(\bar{F}^0_T)_i \Delta_i}{RT}$$

$$+ \frac{1}{2} \sum_{i=1}^{n} \sum_{k=1}^{n} \left(\frac{\delta_{ik}}{y_i} - \frac{1}{\bar{y}}\right) \Delta_i \Delta_k \qquad (4\text{-}24)$$

where Q(X) is the quadratic approximation to the free energy function. It has been shown that both F(X) and Q(X) are positive definite and hence, both functions are convex (3, 4, 11, 53). Thus, each has a unique minimum.

Lagrange Multiplier Formulation and Minimization. The problem is now one of obtaining the minimum of the function Q(X) subject to the material balance constraints of Equations (4-1). The adjoint equation, or constrained equation, is formed using the method of Lagrange's undetermined multipliers. The result is:

$$G(X) = Q(X) + \sum_{j=1}^{m} \pi_j \left(b_j - \sum_{i=1}^{n} a_{ij} x_i - \sum_{i=n+1}^{l} a_{ij} x_i\right) \qquad (4\text{-}25)$$

where π_j is the Lagrange multiplier.

At this point the usual procedure would be to set partial derivatives with respect to the independent variable (x_1, x_2, $x_3 \ldots x_l$) the Lagrange multipliers (π_1, $\pi_2, \ldots \pi_m$) equal to zero. That is, to minimize G(X) it is required that the following conditions be satisfied:

$$\frac{\partial G}{\partial x_i} = 0 \quad \text{and} \quad \frac{\partial G}{\partial \pi_j} = 0 \tag{4-26}$$

Then the procedure would be to solve simultaneously the resulting set of m+1 equations where l = n + s, s being the total number of solid or condensed species. This would be repeated employing some convergence criteria to approach the point minimum free energy. However, as has been said before, it is more convenient to use a different procedure which requires that only m + 1 + s equations be solved simultaneously rather than m + n + s equations. Since a quadratic approximation is used, the linear equations resulting from taking the partial derivatives with respect to the x_i's can be solved directly. Performing the partial differentiation of Equation (4-25); the constrained quadratic approximation, results in the following expression:

$$\frac{\partial G(X)}{\partial x_i} = \frac{\partial Q(X)}{\partial x_i} - \sum_{j=1}^{m} \sum_{j=1}^{m} a_{ij} \pi_j = 0 \quad 1 \leq i \leq 1 \qquad (4\text{-}27)$$

It is necessary to develop the expression for $\frac{\partial Q(X)}{\partial x_i}$. Thus, taking the derivative of Equation (4-24) results in:

$$\frac{\partial Q(X)}{\partial x_i} = \left(c_i + \ln y_i/\bar{y} \right) + \left(\frac{x_i}{y_i} \quad \frac{\bar{x}}{\bar{y}} \right)$$

$$1 \leq i \leq n \qquad (4\text{-}28)$$

and

$$\frac{\partial Q(X)}{\partial x_i} = \frac{\bar{F}_T{}^0}{RT}_i \qquad i = n + 1....1 \qquad (4\text{-}29)$$

Substituting Equations (4-28) and (4-29) in (4-27) results in the following expressions:

$$\frac{\partial G}{\partial x_i} = [c_i + \ln y_i/\bar{y}] + [x_i/y_i - \bar{x}/\bar{y}] -$$

$$\sum_{j=1}^{m} \pi_j a_{ij} = 0 \qquad i = 1....n \qquad (4\text{-}30)$$

and

$$\frac{\partial G}{\partial x_i} = \frac{(\bar{F}^0 T)_i}{RT} - \sum_{j=1}^{m} \pi_j a_{ij} = 0 \quad i = n + 1..1 \quad (4\text{-}31)$$

Since $y_i > 0$ we may solve for x_i in (4-30) and obtain:

$$x_{i,gas} = f_i(y) + (y_i/y)\,\bar{x} + \sum_{j=1}^{m} (\pi_j\, a_{ij})\, y_i$$

$$i = 1,\ldots n \qquad (4\text{-}32)$$

This gives n explicit equations for the moles of the gases in terms of the m + 1 unknowns, and $\bar{x}$. Equation (4-23) permits the elimination of $x_{i,gas}$ from the material balance equations. Substitution of Equation (4-32) into (4-1) results in m equations of the form given below:

$$\sum_{i=1}^{n} \frac{a_{ik}\, y_i}{\bar{y}} \cdot \bar{x} + \sum_{j=1}^{m} \sum_{i=1}^{n} [(a_{ij})\,(a_{ik})\, y_i]\, \pi_j +$$

$$\sum_{i=n+1}^{l} a_{ik}\, x_i = b_k + \sum_{i=1}^{n} a_{ik}\, f_i\,(Y) \qquad k = 1,\ldots m$$

(4-33)

For the purpose of simplifying the above, it is convenient to define:

$$\sum_{i=1}^{n} a_{ik}\, y_i = b_k' \qquad k = 1,\ldots m \qquad (4\text{-}34)$$

and

$$\frac{\bar{x}}{\bar{y}} = \bar{u} \qquad (4\text{-}35)$$

In addition

$$r_{jk} = r_{kj} = \sum_{i=1}^{n} (a_{ij})\ (a_{ik})\ y_i \quad (j, k = 1, 2, \ldots m) \tag{4-36}$$

Equation (4-33) on re-arranging becomes:

$$\sum_{j=1}^{m} r_{jk}\ \pi_j + b'_k \bar{u} + \sum_{i=n+1}^{l} a_{ik}\ x_i = b_k + \sum_{i=1}^{n} a_{ik}\ f_i\ (Y) \qquad (k = 1, \ldots m) \tag{4-37}$$

This represents m equations in m + 1 + s unknowns π'_js, u and $x_{i,\text{solids}}$. An additional independent equation is obtained by noting that $\sum x_i = \bar{x}$ and by summing Equation (4-32) from i = 1 to n the following equation is obtained.

$$\sum_{j=1}^{m} b'_j\ \pi_j = \sum_{i=1}^{n} f_i\ (Y) \tag{4-38}$$

The additional s equations needed to compute the amount of condensed (or solid) phases present are obtained from Equation (4-31). This results in:

$$(\bar{F}_T^{\,0}/RT)_i = \sum_{j=1}^{m} a_{ij}\ \pi_j \qquad i = n + 1 \ldots 1 \tag{4-39}$$

These equations, which are to be solved simultaneously, are summarized and given in general form in Table 4-1. When the equations are solved, values for the moles of condensed species are obtained directly. Also, the values of the Lagrange multipliers π_j and that of u are obtained. These two latter values are substituted in Equation (4-32) to calculate the moles of the gas species. A more detailed exposition of the procedure to follow is given below.

Computation Procedure. The iterative procedure is initiated by assuming any positive solution $Y = (y_1, y_2, \ldots y_l)$ which satisfies the material balance equations, Equation (4-1). Then, the value of $f_i(y)$ are determined by Equations (4-13) and (4-14) as are the values of r_{jk} by Equation (4-36). Next the system of equations in Table 4-1 are solved simultaneously. Note that the solution to these equations give m values of the Lagrange multipliers. π_j, the value of $\bar{u} = (\bar{x}/\bar{y})$ and values of x_i's solid. In addition, it should be noted that the values of $x_{i,solids}$ are the only ones directly obtained from the simultaneous solution of these equations. The values of $x_{i,gas}$ are not obtained directly from this solution, but must be computed using Equation (4-32) which is in terms of the known values π_j and $\bar{u}$. The

TABLE 4-1. General Equations for the Solution of the Equilibrium Composition of Gas-Condensed Mixture by the Free Energy Minimization Technique."

$$r_{11}\pi_1 + r_{12}\pi_2 + \ldots r_{1m}\pi_m + b_1'\bar{u} + a_{K+1,1}x_{K+1} + \ldots + a_{q,1}x_q = b_1 + \sum_{i=1}^{K} a_{i1}f_i(Y)$$

$$r_{21}\pi_1 + r_{22}\pi_2 + \ldots r_{2m} + b_2'\bar{u} + a_{K+1,2}x_{K+1} + \ldots a_{q,2}x_q = b_2 + \sum_{i=1}^{K} a_{i2}f_i(Y)$$

$$r_{31}\pi_1 + r_{32}\pi_2 + \ldots r_{3m}\pi_m + b_3'\bar{u} + a_{K+1,3}x_{K+1} + \ldots + a_{q,3}x_q = b_3 + \sum_{i=1}^{K} a_{i3}f_i(Y)$$

$$r_{41}\pi_1 + r_{42}\pi_2 + \ldots r_{4m}\pi_m + b_4'\bar{u} + a_{K+1}x_{K+1} + \ldots + a_{q,4}x_q = b_4 + \sum_{i=1}^{K} a_{i4}f_i(Y)$$

$$\vdots$$

$$r_{m'1}\pi_1 + r_{m2}\pi_2 + \ldots r_{mm}\pi_m + b_m'\bar{u} + a_{K+1}x_{K+1} + \ldots + a_{q,m}x_q = b_m + \sum_{i=1}^{K} a_{im}f_i(Y)$$

$$b_1\pi_1 + b_2\pi_2 + \ldots + b_m\pi_m = \sum_{i=1}^{K} f_i(Y)$$

$$a_{n+1,1}\pi_i + \ldots + a_{n+q,m}\pi_m = (F^o/RT)_{K+1}$$

TABLE 4-1 (continued)

$a_{n+2mk}\pi_k + \ldots + a_{n+2mn}\pi_n$	$= (F^o/RT)_{K+2}$
$a_{q1}\pi_1 + a_{q,2}\pi_2 + \ldots + a_{q,m}\pi_m$	$= (F^o/RT)_q$

*Note that equations have been written for more than a condensed phase.

new and improved values of x_i can be used, if they are all positive, as a starting point for the next iteration. However, negative x_i's can occur and steps should be taken to avoid this possibility and thus, insure convergence. This is discussed below in the context of common numerical problems encountered when using iterative schemes.

Numerical Problems in Convergence Procedure

Convergence in an iterative calculation, involves, usually, three numerical problems: (1) How to insure numerical convergence. (2) How to determine the step size for a given iteration. (3) How to determine when to stop in the computation cycle.

How to Insure Numerical Convergence. Normally in the iterative procedure, the amount of each specie x_i which is calculated at the minimum of the constrained quadratic approximation, is used as the new estimate for the following iteration. To insure that oscilations and over-corrections will not occur, the following convergence scheme similar to that of White et al. (3) was used.

To prevent oscillations, the gradient of the free energy function can be examined, and the values of the x_i's determined that insure the free energy

will always decrease. To do this, a parametric representation of the free function is formulated. This is done by taking the values of the moles of each specie x_i calculated at a given iteration to estimate the values of the moles of the chemical species $y_{i(new)}$ for the next iteration. Thus,

$$y_{i(new)} = y_{i(old)} + \lambda\Delta_i \qquad 1 \leq i \leq 1 \qquad (4\text{-}38)$$

and

$$\Delta_i = x_i - y_{i(old)} \qquad 1 \leq i \leq 1 \qquad (4\text{-}39)$$

where λ is the parameter of the line through x_i, and $y_{i,old}$, and it can vary from zero to one. The value for λ that was used to insure convergence is discussed in a later part of this section.

The free energy function can be expressed in terms of the convergence parameter λ by substituting $y_{i(new)}$ of Equation (4-38) in Equation (4-16). The result is:

$$F(\lambda) = \sum_{i=1}^{n} [y_i + \lambda\Delta_i]\,[c_i + \ln y_i + \lambda\Delta_i/\bar{y} + \lambda\bar{\Delta}\,] + \sum_{i=n+1}^{1} [y_i + \lambda\Delta_i] \cdot \left(\frac{\bar{F}^o}{RT}\right)_i \qquad (4\text{-}40)$$

where in the above expression y_i is equivalent to $y_{i(old)}$ of Equation (4-39) and $\bar{\Delta} = \bar{x} - \bar{y}$.

To determine the direction (increase or decrease) of the free energy function, the derivative with respect to λ is examined after every iteration. The derivative is easily computed and is:

$$\frac{dF(\lambda)}{d\lambda} = \sum_{i=1}^{n} \Delta_i \left[c_i + \ln y_i + \lambda \Delta i / y + \lambda \bar{\Delta}\right] + \sum_{i=n+1}^{l} \Delta_i \left(\frac{\bar{F}^o}{\bar{R}\bar{T}}\right)_i \tag{4-41}$$

If the directional directive $dF/d\lambda$ is negative a descent path is followed. That is the value of the free energy function in the r+1 iteration will be less than in the r^{th} iteration. When this procedure is continued the minimum is eventually reached. However, when a non-negative value of the directional derivative is obtained, the value of λ (step size) should be reduced until a negative value of this derivative is obtained. A more thorough discussion on the proper value of λ is given below.

How to Determine the Step Size for a Given Iteration. The original paper of White, Johnson and Dantzig (3) on which the technique developed in this chapter is based, does not shed much light on the size of the iteration step, or convergence parameter λ that is required for converences. However, recently Zeleznik

and Gordon (11, 12) showed that for a function of λ $F(\lambda) \equiv [F\ (\bar{y} + \lambda\ \bar{\Delta})]$* the optimum value of the step size can be found. This is possible since the condition for equilibrium is that the free energy be a minimum. This is equivalent to determining λ by solving the equation:

$$\Delta_i^T \frac{\partial F}{\partial \bar{y}} \Bigg|_{\bar{y}_{new} = \bar{y}_{old} + \lambda\ \bar{\Delta}_i} = 0 \qquad (4\text{-}42)$$

where Δ_i^T denotes the transposer of the matrix.

This optimum value of λ allows for a better control of the path of descent with the corresponding decrease in the number of iteration necessary to reach the minimum.

Practical consideration, however, dictate that a minimum amount of time be spent in this phase of the iterative procedure. Consequently, it is best to sacrifice a few extra iterations and obtain in return a faster estimate of the value of λ. This was done by Oliver et al. (15). Their technique consisted in choosing the specie with the largest negative value of Δ_i and computing a value of λ' such that $y_{i(new)}$ be zero; therefore

---

* The bar ($\bar{\ }$) denotes a vector.

$$\lambda' = - \frac{y_{i(old)}}{\Delta_i} \qquad (4\text{-}43)$$

Then λ was set to some fraction of λ'. They proposed $0.99\ \lambda'$. We have found from experience that 0.9λ works better.

However, this procedure alone, does not insure convergence. It is possible to fine a value of λ which meets the above requirement but yet makes $dF/d\lambda$ positive. This has the effect of increasing the free energy rather than decreasing it and can cause the solution to diverge. Therefore, one must check if λ' calculated by Equation (4-43) makes the gradient $dF/d\lambda$ negative. If it does not, the value of λ' must be further reduced until this condition is satisfied.

It is possible to encounter situations where the value of λ becomes practically zero. This will most likely occur when trace species are present, that is, when the value of y_i, the moles of a specie is very small. A criteria has been developed to automatically eliminate trace species from the computation in the chemical equilibrium analysis program. These procedures are further discussed in the section on trace species. It should be stated that one should never allow the correction $\lambda\Delta_i$ to be less than 6 or 7 orders of

magnitude smaller than y_i since this would make the convergence scheme very time consuming. More will also be said about this in the section dealing with trace species.

It has been observed that as the minimum is approached large changes in λ occur, which cause the value of $dF/d\lambda$ to become smaller. This allows for a control path of descent, and convergence to the minimum is obtained.

How to determine where to stop. It was established in the above paragraph that as long as $dF/d\lambda$ remains negative, the iterative cycle will continue to calculate new and improved values of the y's. In principle the iteration should be stopped when:

$$\sum_{i=1}^{n} | \Delta_i | = 0 \qquad (4\text{-}44)$$

However, this criteria is impractical to achieve in a digital machine because of round-off error. Rather, the criteria should be determined by these four basic questions: 1) How accurate should the answer be? 2) How many significant figures are available in the digital machine? 3) Can a little accuracy be sacrificed for time? 4) How accurate is the input data?

In most cases the data is the constraining factor. There is no point in getting successive checks in the six or seven significant figure when the thermodynamic data is only good to three at most four significant digits. We have found from experience that when

$$0.001 \leq \sum_{i}^{1} | \Delta_i | \leq 0.01 \qquad (4\text{-}45)$$

rapid convergence and accurate values result.

There are other criterias that can be used to test for convergence. One would be to take successive values of the free energies and compare them. When the difference is less than a pre-requisite number of significant figures stop the iteration. Similarly, the value of the gradient $dF/d\lambda$ can be examined. When its value is close to zero we are assured of having reached the minimum, i.e., equilibrium. Although these last two criterias seem to be logical choices, we have found that when using Equation (4-45) better convergence control is achieved.

Gaseous Trace Species

When very little is known about a particular chemical system, one is forced to consider as many chemical species as thermodynamic data is available

for them. In the case, for example, where carbon and hydrogen react there are many possible products of reaction. At high temperature it would be expected that lower molecular weight hydrocarbons would exist while at lower temperatures, higher molecular weight species would be expected. This is probably the most one can safely infer from basic chemistry knowledge. But little else can be said. Hence, when it is desired to know the equilibrium composition of a hydrocarbon mixture at different temperature and pressure, one, of necessity, needs to consider all probable hydrocarbon species. Under these conditions, it is very possible that many of the chemical species assumed to be present will only be in trace quantities. However, it will be illustrated how species which are trace at a particular temperature and pressure can become important at other temperatures. This will show that trace species cannot arbitrarily be eliminated from the computation, especially, for those systems where varying temperatures and pressure can be encountered. Thus, it becomes important to devise an automatic procedure to eliminate trace species momentarily from the computations so as to speed up the convergence, to the minimum free energy, and later reintroduce them at the end of the iteration.

To show that the elimination of trace species has no effect on the equilibrium composition of major components. Table 4-2 illustrates this with the example of the equilibrium composition of a 40 percent nylon and 60 percent phenolic resin composite. The temperature is 800°C and the pressure one atmosphere. Run 1 shows the equilibrium composition for twenty one assumed species. Run 2 was performed with C_2H, C_3H, C_4H, and C_3 taken as zero composition. Since the equilibrium composition of Run 1 predicts that these four species have negligible mass fractions, their elimination produced no effect on the equilibrium composition of the seventeen remaining species.

In Table 4-3, however, the results are strikingly different between Run 1 and Run 2 for a temperature of 3100°C. In this case the elimination of the species C_2H, C_3H, C_4H and C_3 does have a profound effect on the composition. Although these four species were trace species at 800°C this is now not true at 3100°C, and thus illustrates the importance of considering as many species as thermodynamic data is available. This is especially true when the chemical system under consideration is studied under a diverse range of temperature conditions.

TABLE 4-2. Equilibrium Composition of the Pyrolysis Gases of a 40 Percent by Weight of Nylon and 60 Percent Phenolic Resin at P = 1 atm and T = 800°C.

	Mass Fraction	
Species	Run 1	Run 2
H	0.5483×10^{-9}	0.5483×10^{-9}
H_2	0.6788×10^{-1}	0.6788×10^{-1}
CH_3	0.1148×10^{-7}	0.1148×10^{-7}
CH_4	0.1893×10^{-1}	0.1893×10^{-1}
C_2H_2	0.7475×10^{-8}	0.7475×10^{-8}
C_2H_4	0.5910×10^{-6}	0.5910×10^{-6}
C_2H_6	0.4606×10^{-6}	0.4606×10^{-6}
C_6H_6	0.8471×10^{-13}	0.8471×10^{-13}
N_2	0.3875×10^{-1}	0.3875×10^{-1}
NH_3	0.3275×10^{-4}	0.3275×10^{-4}
HCN	0.4101×10^{-5}	0.4101×10^{-5}
H_2O	0.1409×10^{-1}	0.1409×10^{-1}
OH	0.8392×10^{-12}	0.8392×10^{-12}
CO2	0.8776×10^{-2}	0.8776×10^{-2}
CO	0.2220	0.2220
CN	0.1006×10^{-14}	0.1006×10^{-4}
C_2H	0.1347×10^{-16}	0.
C_3H	0.6904×10^{-18}	0.
C_4H	0.5722×10^{-22}	0.
C_3	0.7290×10^{-28}	0.
C	0.6295	0.6295

TABLE 4-3. Equilibrium Composition of the Pyrolysis Gases of a 40 Percent by Weight of Nylon and 60 Percent Phenolic Resin at P = 1 atm and T = 3100°C.

Species	Mass Fraction Run 1	Mass Fraction Run 2
H	0.2510	0.2859
H_2	0.3318	0.4304
CH_3	0.9268×10^{-4}	0.1369×10^{-3}
CH_4	0.5311×10^{-5}	0.8937×10^{-5}
C_2H_2	0.6010×10^{-1}	0.7796×10^{-1}
C_2H_4	0.1526×10^{-5}	0.2567×10^{-5}
C_2H_6	0.7115×10^{-11}	0.1553×10^{-10}
C_6H_6	0.4456×10^{-21}	0.9725×10^{-21}
N_2	0.3377×10^{-2}	0.8633×10^{-2}
NH_3	0.9244×10^{-7}	0.1386×10^{-6}
HCN	0.2175×10^{-1}	0.2514×10^{-1}
H_2O	0.2560×10^{-6}	0.3611×10^{-6}
OH	0.8525×10^{-7}	0.1056×10^{-6}
CO_2	0.1467×10^{-7}	0.1735×10^{-7}
CO	0.1511	0.1643
CN	0.7421×10^{-2}	0.7533×10^{-2}
C_2H	0.7364×10^{-1}	0.
C_3H	0.5525×10^{-1}	0.
C_4H	0.3552×10^{-1}	0.
C_3	0.3938×10^{-2}	0.
C	0.2562	0.7603

It is also important to note that the speed of convergence can be drastically affected by whether or not trace species are eliminated during the iterative procedure to minimize the free energy. For the example in Table 4-2 if all of the species with mass fraction less thatn 10^{-5} are eliminated the number of iterations needed to converge to the minimum were seven, compared to twenty-one when the twenty-one species were considered.

It is possible to eliminate trace species during the convergence scheme, and when convergence has been achieved, recompute the value of trace species. This can be calculated by using the following equation:

$$x_i = \bar{x} \exp\left(-c_i + \sum_{j=1}^{m} a_{ij}\pi_j\right) \quad i = 1 \ldots n \quad (4\text{-}46)$$

Equation (4-46) is obtained by differentiating Equation (4-24) with respect to x_i and replacing Q(X), which is the quadratic approximation of the free energy function, with the exact function F(X). Note that the total number of moles $\bar{x}$ and the Lagrange multipliers π_j are constants since trace species have no effect on these values. Hence, the only necessary thing to compute x_i is to compute c_i from Equation (4-12).

Solid or Condensed Phase Species

It has been our experience that apart from control of the minimum size of the value of the convergence parameter λ, there has been no numerical difficulties encountered in determining equilibrium compositions in gaseous systems when trace species are eliminated during the iterative procedure. As has been previously stated, these trace species are reintroduced at the end of the iteration and their numerical values are recomputed by the use of Equation 4-46. Straight forward application of the iterative equations in Table 4-1 results in a rapid convergence to the minimum. In principle the same applies to systems with pure condensed species. However, difficulties are known to occur in these computations, and care should be exercised to circumvent them as will be discussed.

When formulating the chemical equilibrium problem for a particular chemical system, one assumes a number of chemical species that might be present at equilibrium. Some of these species will turn out to be present in trace quantities. Equation (4-46) is used to compute the numerical values of the moles of each of these trace species. Unfortunately, Equation (4-46) is not applicable to other than gaseous species.

Consequently, this procedure cannot be used for solid or condensed species. There is, however, a procedure and certain rules derived from thermodynamics that need to be followed rigorously for the elimination or addition of condensed species. These procedures are explained below.

When to Eliminate a Solid Species. There can be times during the convergence scheme when the moles of a solid or a condensed phase species becomes very small or negative. When this occurs the value of the convergence parameter λ, needs to be reduced. If this condition persists the value of λ can become zero. When this occurs the iterative procedure might not converge. It then becomes necessary to eliminate this condensed specie to assure convergence.

When to Add a Solid Specie. The complimentary problem of adding a condensed specie must be approached from a different viewpoint (4). Consider the adjoint Equation (4-24). This is the expression for the total free energy function to be minimized. Since Q(X) = F(X) at the minimum Equation (4-24) becomes:

$$G(X) = F(X) + \sum_{j=1}^{m} \pi_j \left(b_j - \sum_{i=1}^{n} a_{ij}x_i - \sum_{i=n+1}^{l} a_{ij}x_i\right) \quad (4\text{-}47)$$

when the material balance constraint is satisfied:

$$G(X) = F(X) \tag{4-48}$$

Suppose that for a given set of mole numbers, $X' = (x_1', x_2' \ldots x_1')$, $F(X)$ is a minimum. Then:

$$\left.\frac{\partial G}{\partial x_i}\right|_{X=x'} = 0 \qquad i = 1 \ldots n \tag{4-49}$$

$$\left.\frac{\partial G}{\partial x_i}\right|_{X=x'} = 0 \qquad i = n+1 \ldots 1 \tag{4-50}$$

Now consider adding a condensed specie to a system where this specie is already present in the gas phase. Denote this as the q' condensed specie and x_q' as the number of moles of the specie. The change in free energy due to the addition of this specie to the system can be obtained using a Taylor's series expansion, and is:

$$\Delta G = \frac{\partial G}{\partial x_q'} \Delta_q' + \sum_{i=1}^{n} \frac{\partial G}{\partial x_i'} \Delta_i' + \sum_{i=n+1}^{1} \frac{\partial G}{\partial x_i'} \Delta_i' \tag{4-51}$$

where

$$\Delta_i' = x_i - x_i' \tag{4-52}$$

Combining Equations (4-49), (4-50), (4-51), gives:

$$\Delta G = \frac{\partial G}{\partial x'_q} \Delta'_q \qquad (4\text{-}53)$$

For the free energy of the mixture to decrease, $\partial G/\partial x'_q$ must be negative. To minimize the free energy, the partial derivatives of the free energy function with respect to mole numbers are set equal to zero. For the condensed specie this gives:

$$\frac{\partial G}{\partial x_i} = [\overline{F}^o_T/RT]_i - \sum_{j=1}^{m} \pi_j \, a_{ij} = 0 \qquad (4\text{-}54)$$

Therefore, if the added condensed specie is to decrease, the free energy must have a value such that:

$$\sum_{j=1}^{m} \pi_j \, a_{ij} > (\overline{F}^o_T/RT)_i \qquad (4\text{-}55)$$

If the above is true for an added condensed specie, then it should be considered in the chemical system as the free energy will be less with it included.

Comparison of Equilibrium Composition Calculations With Published Data and Computations

In this section comparisons of published results with the results of the chemical equilibrium analysis

program are presented. Comparisons are made for five chemical systems. These are CO, CO_2, O and O_2 system; the ammonia equilibrium, rocket fuel reaction product system, the methane-water system and the hydrazine oxygen reaction products.

CO_2, CO, O and O_2 System. A comparison of the calculated values of the chemical equilibrium analysis program with results published by Kondratev (56) for a CO, CO_2, O and O_2 is shown in Figure 4-1. The continuous line represents the equilibrium composition as calculated by the equilibrium program. The dotted lines represent the values given by Kondratev (56). The agreement is excellent. The slight difference is due, probably, to the fact that different sources of thermodynamic data were used.

The Ammonia Equilibrium. A comparison is given of the equilibrium composition of the N_2, H_2 and NH_3 system as calculated by the equilibrium analysis program and the data presented by Dodge and Larson (57). The comparisons are presented for Tables 4-4, 4-5, 4-6 and 4-7 for pressures of 10, 30, 50 and 100 atmospheres, respectively. The data presented in these tables is the actual experimental values of the equilibrium composition of ammonia as measured by several individuals and presented by Dodge and Larson (57). These results

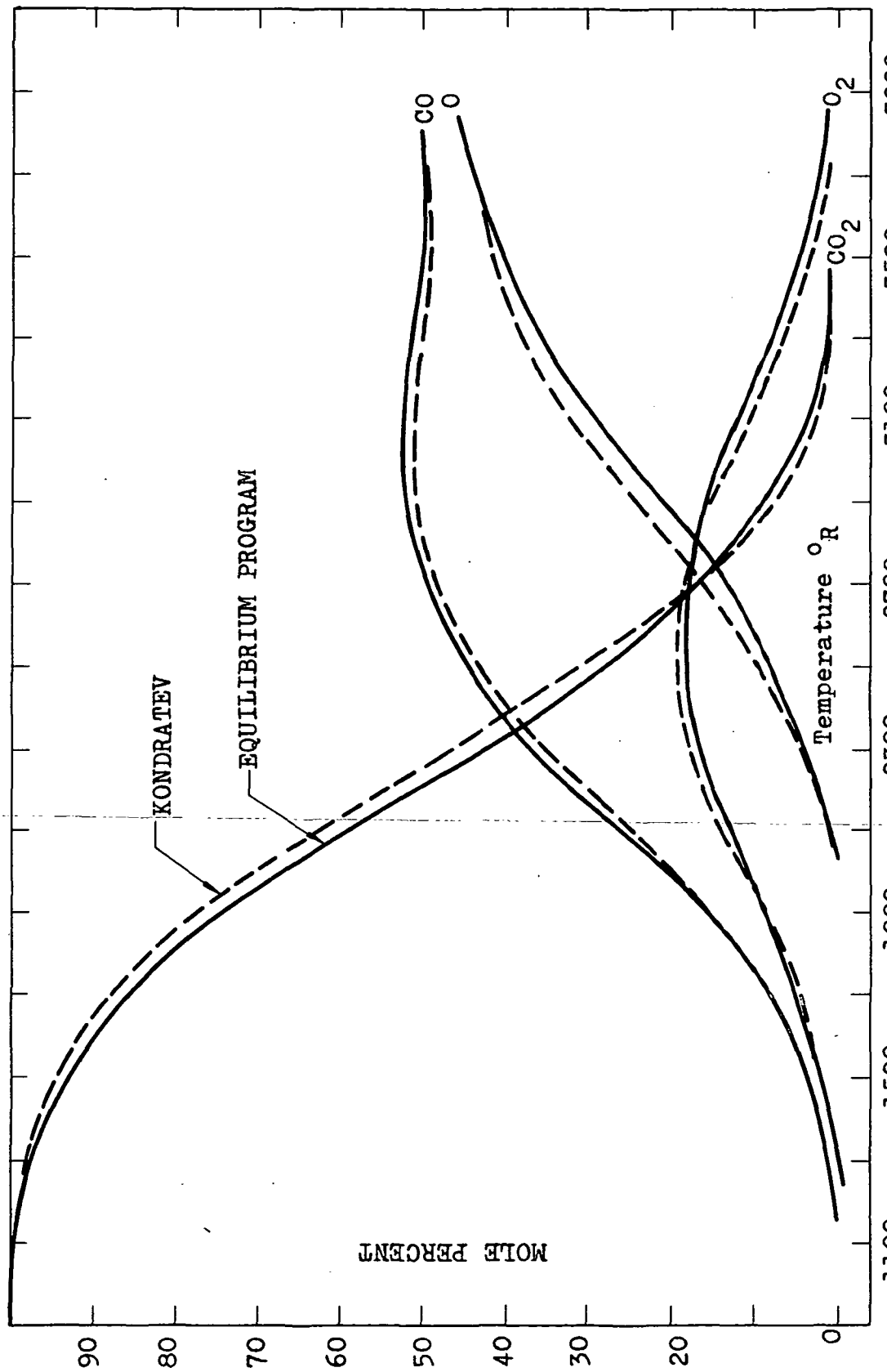

Figure 4-1. A Comparison of a Calculated Values of the Equilibrium Concentration Predicted by the Free Energy Minimization With Those of Kondratev (56).

TABLE 4-4. Equilibrium Composition (Mole Percent) of Ammonia at 10 Atmospheres.

Temperature (^{o}C)	Dodge	F.N.R.L.	Haber	Equilibrium Program
325	10.38			11.59
350	7.35	7.41	8.04	8.21
375	5.25			5.85
400	3.85	3.85	4.12	4.21
425	2.80			3.08
450	2.04	2.11	2.21	2.28
475	1.61			1.71
500	1.20	1.21	1.27	1.305

TABLE 4-5. Equilibrium Composition (Mole Percent) of Ammonia at 30 Atmospheres.

Temperature (°C)	Dodge	F.N.R.L.*	Haber	Nerst	Program
350	17.80	17.78	18.81	21.22	19.11
375	13.35				14.48
400	10.09	10.15	10.72	11.67	10.93
425	7.59				8.27
450	5.81	5.86	6.13	6.36	6.29
475	4.53				4.82
500	3.48	3.49	3.62	3.62	3.73

*Fixed Nitrogen Research Laboratory
United States Department of Agriculture

TABLE 4-6. Equilibrium Composition (Mole Percent) of Ammonia at 50 Atmospheres.

Temperature (^{o}C)	Dodge	F.N.R.I.	Haber	Equilibrium Program
350	25.11	25.23	26.03	26.37
375	19.44			20.73
400	15.11	15.27	15.86	16.15
425	11.71			12.52
450	9.17	9.15	9.50	9.72
475	7.13			7.57
500	5.58			5.92

TABLE 4-7. Equilibrium Composition (Mole Percent) of Ammonia at 100 Atmospheres.

Temperature (°C)	Dodge	F.N.R.I.	Haber	Equilibrium Program
350		37.35	37.35	37.69
375	30.95			31.19
400	24.91	25.12	25.13	25.48
425	20.23			20.62
450	16.35	16.43	16.26	16.60
475	12.98			13.31
500	10.40	10.61	10.43	10.69

show that the chemical equilibrium analysis program can predict the chemical equilibrium composition for systems in equilibrium. It is suspected that part of the difference between the actual and calculated values are due to non-idealities and to the experimental error of the measurement. In general the results agree within 5%.

Rocket Fuel Reaction Products. In Table 4-8 a comparison of the equilibrium composition of unsymetrical dimethyl hydrazine (UDNH), red fuming nitric acid propellant combination as calculated by the equilibrium analysis program and by Brandmeir and Harnett (32) is presented.

These authors calculated the equilibrium composition using free energy minimization. The comparison shows excellent agreement between the two programs. The temperature at which the equilibrium was calculated was 3000°K and the pressure was 10 atmospheres.

Methane Water Reaction. A comparison of results, with those of Oliver et al. (15), for the equilibrium reaction of five moles of Hydrogen and one mole of methane at 600°C and 1 atmosphere is presented in Table 4-9. Their results were obtained by the free energy minimization technique also. The

TABLE 4-8. Comparison of UDNH-RFNA Reaction Products at Equilibrium Predicted by Brandmair and Harnett and the Equilibrium Program at 3000°K and 10 Atmospheres.

	Composition (Mole Percent)	
Species	Brandmair and Harnett	Equilibrium Program
H_2	3.6569	3.6567
H_2O	40.7310	40.7273
OH	9.5222	9.5216
CO	7.3355	7.3350
CO_2	10.4574	10.4563
N_2	23.2108	23.2170
NO	0.9386	0.9387
N	2.08×10^{-3}	2.09×10^{-3}
H	.9554	.9553
O	.6136	.6136
O_2	2.578	2.578

TABLE 4-9. Equilibrium Composition for the Reaction of $5H_2O + CH_4$ at 600°C and one Atmosphere Pressure.

	Composition (Mole Percent)	
Species	Oliver *et al.*	Equilibrium Program
CH_4	1.16	1.17
H_2	43.36	43.35
H_2O	43.85	43.86
CO	3.15	3.14
CO_2	8.48	8.48

results show excellent agreement with chemical equilibrium composition calculated by the chemical equilibrium analysis program.

Hydrazine Oxygen Reaction. The equilibrium composition of the combustion of a stochiometric mixture of hydrazine and oxygen at 3500°K and 750 psia, as calculated by the equilibrium analysis program is presented in Table 4-10. These results are compared with those of White, et al. (3) and Napthali (58, 59). White et al. (3) showed that it took at least six iterations for the program to converge, our chemical equilibrium analysis program took three. The results with both authors shows excellent agreement.

The previous five comparisons of the chemical equilibrium analysis computations with the results of others have shown the integrity of the program. A slightly modified version of the chemical equilibrium analysis program is used as a subroutine in the ABLATIN1 and ABLATIN2 analysis programs to be discussed in Appendix A. The chemical equilibrium analysis program is discussed in detail in Appendix E.

Free Energy Minimization: Is it the Best Method?

Prior to 1958 all equilibrium calculations were performed using the equilibrium constant approach, the main proponent of which were Brinkley (9, 20) and Huff

TABLE 4-10. Equilibrium Composition of Products from the Combustion of a Stochiometric Mixture of Hydrazine and Oxygen at 3500°K and 750 psia.

Specie	Starting Point	White*	Equilibrium Program	Napthali**
H	.1	0.040668	0.0406415	0.04118
H_2	.35	0.147730	0.147700	0.14757
H_2O	.50	0.783153	0.783222	0.78358
N	.1	0.001414	0.01413	0.001410
N_2	.35	0.485247	0.485249	0.485210
NO	.1	0.027399	0.027395	0.027480
O	.1	0.017947	0.017935	0.017980
O_2	.1	0.037314	0.037303	0.037570
OH	.1	0.096872	0.096848	0.095820

*Reference (3)
**Reference (58, 59)

(17, 32, 23, 24). In that year, White, Johnson, and Dantzig (3) of the RAND Corporation proposed to calculate chemical equilibrium of reacting gases by minimizing the free energy. Their method sparked considerable interest and controversy. It caused users to be divided into two camps: the faithful equilibrium constant formulators and the free energy minimizers. The controversy flamed with claims and counter claims of assured convergence and of computational advantages offered by each method. As reported by Zeleznik and Gordon (11), "so heated became the controversy that when a panel discussion was arranged to discuss equilibrium computation in 1959, it was necessary to divide the panel into a free energy panel and an equilibrium constant panel."

In 1960 Zeleznik and Gordon (41) tried to settle the controversy by comparing the three general methods of Brinkley (9, 20), Huff (17, 22, 23, 24) and White with each other. They extended the form of these methods to permit condensed species as reaction products. An analytical proof was shown to indicate that the three methods could be placed in a form independent of the choice of components. Finally, they concluded that no one of the three methods offered "any significant computational advantages over the other two." However, in their most recent publications (11, 12), they seem

to reverse their standing by stating that free energy minimization does offer some computational advantages.

Free energy minimization has some distinct computational advantages in that the number of equations to be solved is equal to the number of element plus the number of solid species plus one. For a carbon hydrogen system with one solid species, the number of simultaneous equations to be solved are four regardless of the number of gas species. This advantage cannot be claimed by the equilibrium constant formulation method. In addition there is no need to specify an independent set of chemical reactions as is required by the equilibrium constant formulation. This would indeed be quite a task in setting up a problem for say a 100 species and 2 elements since a total of 98 independent chemical reactions must be postulated. For free energy minimization it is only necessary to estimate the number of species believed to be present at equilibrium and this greatly simplifies the laborious task of postulating a set of independent chemical reactions. Isomers are handled by free energy minimization as distinct chemical species while for the equilibrium constant formulation they require special treatment (59). Initial estimates which are required to be rather close for equilibrium constant formulation (4)

are not for free energy minimization. It has been found from experience that when postulating a chemical system it is best to have all of the guessed input compositions within 2 orders of magnitude of each other. This reduces the number of iterations required for a specified temperature and pressure.

All of the facts in this section tend to support the contention that as a general multipurpose scheme, for any number of species, free energy minimization is probably the best. This, of course, is not to say that existing programs implemented using the equilibrium constant approach are inferior. On the contrary, in the final analysis the success in implementing either technique is what determines its usefulness. For those that would prefer to have a "feeling" for what reactions are affecting equilibrium the most, the equilibrium constant formulation may be used. This kind of information cannot be obtained directly from free energy minimization since it does not use chemical reactions in its implementation.

When repetitive numbers of calculation are required, as in flow field calculation, free energy minimization might become time consuming and several specialized schemes (61, 62) have been developed to

take advantage of some special characteristic of the problem to reduce the time of solution. These schemes, of course, are quite restrictive for general applications; and they cannot be used for other than the solution to the particular problem for which they were developed. This is because any modification of the system, such as the inclusion of products not previously considered or the addition of a new element, would require a new analysis, algebraic manipulations and reprogramming.

Recently, four additional techniques for computing chemical equilibrium composition for gases, have been published in the literature (63, 64, 65, 66) and they are briefly discussed. One is by White (63) in which he develops a technique based on the contribution of each element to the total free energy of the molecule. In his new technique he makes claim that the method eliminates certain difficulties encountered by free energy minimization and in addition reduces the number of iterations required for convergence. The iterations are based not on the final value of the equilibrium composition of the chemical species, but on the final value of the Lagrange multipliers. There is, however, a drawback in that tables of the contribution, or partitioning of the free energy are necessary for this method, and these are not

yet available. Perhaps, as the author admits, not until these tables are readily available will there be much interest in this new method. The second technique is that of Lai, (64) which uses the mathematical duality between the minimum free energy and the mass conservation equations to compute chemical equilibrium. Another dual technique is that of Passy and Wilde (65) and it is based on the duality between geometric programming and the minimization of the Gibbs free energy function. Several questions were raised during Lai's (64) presentation of his paper about the validity of his convergence scheme, and this raises the possibility of divergence in cases more difficult than the one presented by the author.

The method of Passy and Wilde (65) is a completely new technique for solving single phase chemical equilibrium problems. The main advantage of transforming the problem to a posynomial minimization is a reduction in the number of variables to be solved. Moreover, the number of Lagrange multipliers is reduced to one which is interpreted physicially, as the total number of moles of the system at equilibrium. Since the method reduces the number of minimization variables, when implemented it will most probably reduce computing time. The method as derived is not applicable to polyphase

system and as such, its usefulness to this research where solid phases are considered is limited. The final and latest method in the literature is that of Meisnner et al. (66). In contrast with the three previous methods which fall into the category of minimization schemes, the method of Meisnner and co-workers (66) is a variation of the equilibrium constant formulation which they call the "reactor series method". The method proposes that for calculating equilibrium compositions for a system in which many reactions occur, the system should be reduced to a series of individual reactions occuring separately. The main advantage claimed by the authors is the simplicity of the calculation which is predicated on the fact that since only one reaction is treated at a time simple algebra is involved in every step. However, this method suffers from the main disadvantage of the equilibrium constant method, i.e., having to postulate a system of independent chemical reactions in comparison with free energy minimization where species believed to be present are the only things specified.

None of the four methods reviewed, except perhaps that of Passy and Wilde (65), which only applies to single phase system, offers any superior

advantage over the free energy minimization technique (3).

Summary

This chapter has presented a detailed derivation of the free energy minimization technique. Comparison with other well known methods were made to illustrate that free energy minimization was more suitable for a number of reasons. The principle one being that the only thing required to compute chemical equilibrium is to specify the number of species rather than the number of independent reactions as is required for other methods. Four recent techniques which appeared in the literature were briefly discussed and none seem to offer any particular advantage over free energy minimization as it has been applied to this research. In the next chapter a detailed presentation of the non-equilibrium flow analysis is given.

REFERENCES

1. del Valle, E. G., G. C. April and R. W. Pike, "Thermodynamic Equilibrium of a Reacting Gas Solid Mixture, I. Derivation of Equations and Convergence Procedure," NASA CR-79677 (Oct. 1, 1966).

2. del Valle, E. G., G. C. April and R. W. Pike, "Thermodynamic Equilibrium of a Reacting Gas Solid Mixture, II. Computer Implementation and Results," NASA CR-66309 (Feb. 1, 1967).

3. White, W. C., S. M. Johnson and G. B. Dantzig, "Chemical Equilibrium in Complex Mixtures": J. Chem. Phys., 28, No. 5, pp. 751-755 (1958). See also RAND Report P-1059 (Oct. 1957) by the same authors.

4. Kubert, B. R. and S. E. Stephanou, "Extension to Multiphase System of the Rand Method for Determining Equilibrium Composition;" In Kinetics Equilibrium and Performance of High Temperature Systems, G. S. Bahn and E. E. Zukoski, eds. Landon Butterworth, pp. 166-170 (1960).

5. Boynton, F. P., "Chemical Equilibrium in Multi-component Polyphase Systems," J. Chem. Phys., 32, pp. 1880-1881 (1960).

6. Boynton, F. P., "Computation of Equilibrium Composition and Properties in a Gas Obeying the Virial Equation of State": In, Kinetics Equilibria and Performance of High Temperature Systems, G. S. Bahn, ed., Gordon and Breach Science Publisher, New York, 1963.

7. Raju, B. N., Krishnaswami, C. S., "Chemical Equilibrium in Multiphase System", Indian J. Tech., 4, pp. 99-101 (1966).

8. Gordon, Sanford, Frank J. Zeleznik and Vearl N. Huff: "A General Method for Automatic Computation of Equilibrium Composition and Theoretical Rocket Performance of Propellants," NASA TN D-132, 1959.

9. Brinkley, Stuart R., Jr., "Calculation of Equilibrium Composition of Systems of Many Constituents," J. Chem. Phys., 15, (2), pp. 107-110, February, 1947.

10. Napthali, Leonard M., "Calculate Complex Chemical Equilibria," Ind. Eng. Chem., 53 (5), pp. 387-388 (1961).

11. Zeleznik, F. J. and S. Gordon, "Calculation of Complex Chemical Equilibrium," Ind. Eng. Chem., 60, pp. 27-57 (1967).

12. Zeleznik, F. J. and S. Gordon, "Calculation of Complex Chemical Equilibrium," Paper presented at American Chemical Society, Division of Industrial and Engineering Chemistry, Annual State of the Art Symposium on Applied Thermodynamics, 4th, Washington, D. C., June 12-14, 1967. A67-31315.

13. del Valle, E. G., R. W. Pike and G. C. April, "Modeling for a Set of Complex Chemical Reactions at High Temperature," Paper, Preprint 20F, 61st Annual Meeting of the American Institute of Chemical Engineering, Los Angeles (December 1-5, 1968).

14. Houghen, O. A., K. M. Watson, R. A. Ragatz, Chemical Process Principle, Part II, 2nd, p. 982, John Wiley and Sons, New York (1959).

15. Oliver, R. C., S. E. Stephanou and R. W. Vaier, "Calculating Free Energy Minimization," Chemical Engineering, p. 121, (Feb. 19, 1962).

16. Winkler, J., "New Methods for Determining the Dissociation of Combustion Gases in Rockets," Air Material Command, Wright-Patterson Air Force Base Translation F-TS-3523-RE (Nov. 1948).

17. Huff, V. N. and C. S. Calvert, "Charts for the Computation of Equilibrium Composition of Chemical Reactions in the Carbon-Hydrogen-Oxygen-Nitrogen System at Temperatures from 2000°K to 5000°K, NASA TN 1653 (July 1948).

18. Vichniewsky, R., E. Sale and J. Moradel, "Combustion Temperature and Gas Composition," Jet Propulsion, 25, 105 (1955).

19. McEwan and W. Skolnik, "An Analog Computer for Flame Gas Composition," Review of Scientific Instruments, 22, 125 (1951).

20. Brinkley, S. R., "Note on the Conditions of Equilibrium for Systems of Many Constituents," J. Chem. Phys., 15, 563 (1946).

21. Kandiner, H. J. and S. R. Brinkley, "Calculation of Complex Equilibrium Relation," Ind. Eng. Chem., 42, 850 (1950).

22. Huff, V. N. and S. Gordon, "Tables of Thermodynamic Functions for Analysis of Aircraft Propulsion System," NACA TN 2161 (1950).

23. Huff, V. N., and V. E. Morrel, "General Method for Computation of Equilibrium Composition and Temperature of Chemical Reactions," NACA TN 2113 (1950).

24. Huff, V. N., S. Gordon and V. E. Morrel, "General Method and Thermodynamic Tables for Computation of Equilibrium Composition and Temperatures of Chemical Reactions," NACA TN 1037 (1951).

25. Krieger, F. J. and W. B. White, "A Simplified Method for Computing Equilibrium Composition of Gaseous Systems," J. Chem. Phys., 16, 358 (1948).

26. Winternitz, P. F., "A Method for Calculating Simultaneous Homogeneous Gas Equilibria and Flame Temperature," Third Symposium of Combustion and Flame and Explosion Phenomena, Williams and Wilkins Company, Baltimore p. 79 (1949).

27. Villars, D. S., "Use of the 701 Computer for Complicated Thermodynamic Equilibria Calculation," Navy Ordinance Report 5326 (1956).

28. Villars, D. S., "Use of an IBM 704 Computer for Complicated Thermodynamic Equilibrium Calculations," Navy Ordinance Report 6382 (1958).

29. Villars, D. S., "A Method of Successive Approximation for Computing Combustion Equilibrium Calculation on a High Speed Computer," J. Phys. Chem., 63, 521 (1959).

30. Villars, D. S., "Computation of Complicated Combustion Equilibria on a High-Speed Digital Computer-In: Kinetics Equilibria and Performance on High Temperature System," G. S. Bahn and E. E. Zuboski, eds., London, Butterwood, p. 141 (1960).

31. Napthali, L. M., "Computing Complex Chemical Equilibria by Minimizing Free Energy," Ibid., p. 181.

32. Brandmaier, H. E. and J. J. Harnett, "The Computation of High Temperature Engine Performance," Ibid., p. 171.

33. Wilkins, L. R., "Note on the Linearization Method for Computing Chemical Equilibrium in Complex Systems," Ibid., p. 123.

34. Bahn, G. S., "Hand Calculation of Equilibrium Compositions as a Learned Habit, and Speed-Up Effected with the IBM 610 Computer," Ibid., p. 137.

35. Mentz, R. M., "Programme for Computing Equilibrium Temperature and Composition of Chemical Reactions," Ibid., p. 115.

36. McMahon, D. G. and R. Raback, "Machine Computation of Chemical Equilibria in Reacting Systems," Ibid., p. 105.

37. Hancock, J. H. and T. S. Motzkin, "Analysis of the Mathematical Model for Chemical Equilibrium," Ibid., p. 82.

38. Brinkley, S. R. and B. Lewis, "The Thermodynamic of Combustion Gases," Bureau of Mines Report 4806 (1952).

39. Brinkley, S. R., "Computational Methods in Combustion Calculations," High Speed Aerodynamic and Jet Propulsion, Vol. II. Combustion Process, p. 64. B. Lewis, ed. Princeton University Press, Princeton, N.J. (1956).

40. Goldwasser, S. R., "Calculating Equilibrium Gas Composition on a Digital Computer," Ind. Eng. Chem., 51, 595 (1959).

41. Zeleznik, F. J. and S. Gordon, "An Analytical Investigation of Three General Methods of Calculating Chemical Equilibrium Composition," NASA TN D-473 (1960).

42. Anthony R. G. and D. M. Himmelblau, "Calculation of Complex Chemical Equilibria by Search Techniques," J. Phys. Chem., 67, 1080 (1963).

43. Barnhard, P. and A. W. Hawkins, "Singularities Occuring in the Neutin-Raphson Solution of Chemical Equilibria," Kinetics, Equilibria and Performance of High Temperature Systems, G. S. Bahn, ed. p. 235, Gordon and Breach Publisher, New York, 1963.

44. Core, T. C., S. G. Saunders and P. S. McKittnick, "Versatile Specific Impulse Program for IBM 650 and 704 Computers," Ibid., p. 243.

45. Michels, H. H. and S. B. Schneideman, "Chemical Equilibrium in Real Gas Systems," Ibid., p. 205.

46. Fergenbutz, L. V., "A Method for Calculating Equilibrium Concentrations in Complex Mixture," General Dynamics/Convair Report ZPH-030 (April 30, 1959) N65703.

47. Smith, B. D., "Simplified Calculation of Chemical Equilibria in Hydrocarbon Systems Containing Isomers," A.I.Ch.E.J., 5, 26 (1959).

48. Erickson, W. D. and J. T. Kemper, "A Method for Computing Chemical Equilibrium Composition of Reacting Gas Mixture by Reduction to a Single Iteration Equation," NASA TN D-3488 (1963).

49. Smith, L., W. D. Erickson and N. R. Eastwood, "Equations for the Rapid Machine Computation of Equilibrium Composition of Air Derivatives for Low Field Calculation," NASA TN D-4103 (1967).

50. White, W. B., "Numerical Determination of Chemical Equilibrium and the Partitioning of the Free Energy," Jour. Chem. Phys., 46, 4171-4175 (1967).

51. Lai, C., "The Mathematical Duality in the Determination of Chemical Equilibrium Composition," Preprint 10E, Sixty Second National Meeting, A.I.Ch.E., Salt Lake City, Utah (May 21-24, 1967).

52. Passy, U. and D. J. Wilde, "A Geometric Programming Algorithm for Solving Chemical Equilibrium Problems," SIAM Journal, 16, 363-36 (1968).

53. Vale, H. J., "A Generalized Major Product Solution Method for Thermochemical Problems," In: Kinetics, Equilibria, and Performance of High Temperature Systems, G. S. Bahn, ed., p. 235, Gordon and Breach, New York, 1963.

54. Dodge, B. F., "Chemical Engineering Thermodynamics," p. 526, McGraw Hill, New York (1944).

55. Kondrat'ev, V. N., Chemical Kinetics of Gas Reactions, Pergammon Press, New York (1964).

56. Dodge, R. L. and R. T. Larson, "The Ammonia Equilibrium," Amer. Chem. Soc. Journ., 45, 2918-2930, (1923).

57. Napthali, L. M., "Complex Chemical Equilibria by Minimizing the Free Energy," Jour. Chem. Phys., 31, 263-264 (1959).

58. Napthali, L. M., "Complex Chemical Equilibria by Minimizing the Free Energy," Propulsion Research Laboratory, Department of Mechanical Engineering, Polytechnic Institute of Brooklyn, AFOSR DOC. No. TN-60-228, (January 1960).

59. Duff, R. E. and S. H. Bauer, "Equilibrium Composition of the C/H System of Elevated Temperatures," J. Chem. Phys., 36, p. 1754-1767 (1962).

60. Duff, R. E. and S. H. Bauer, "Equilibrium Composition of the C/H Systems at Elevated Temperatures," Los Alamos Scientific Laboratory Report LA-2556, September 18, 1961.

61. Smith, L. G., W. D. Erickson, and M. R. Eastwood, "Equations for the Rapid Machine Computation of Equilibrium Composition of Air and Derivatives for Flow-Field Calculations," NASA TN D-4103 (1967).

62. Erickson, W. D. and J. T. Kamper, "A Method for Computing Chemical Equilibrium Composition of Reacting-Gas Mixtures by Reduction to a Single Iteration Equation," NASA TN D-3488 (1966).

63. White, W. B., "Numerical Determination of Chemical Equilibrium and the Partitioning of the Free Energy," J. Chem. Phys., 46, p. 4177-4175 (1967).

64. Lai, C., "The Mathematical Duality in the Determination of Chemical Equilibrium Composition," 10E, 62nd National Meeting, A.I.Ch.E., Salt Lake City, Utah (May 21-24, 1967).

65. Passy, U., and D. J. Wilde, "A Geometric Program Algorithm for Solving Chemical Equilibrium Problems," SIAM J. Appl. Math., 16, pp. 363-373 (1968).

66. Meisnner, H. P., C. L. Krisik, and W. H. Dalzell, "Equilibrium Compositions with Multiple Reactions," IEC Fundamentals, 8, 659-665 (1969).

CHAPTER V

NON-EQUILIBRIUM FLOW ANALYSIS

Introduction

As mentioned in Chapter III, there are two limiting cases currently used to simplify the analysis of the flow of pyrolysis gases through the decomposition zone and char zone. These are to consider the flow frozen or in thermodynamic equilibrium. Frozen flow tends to under predict the energy absorbed in the decomposition and char zones since it does not account for the energy absorbed by the endothermic reactions. Equilibrium on the other hand, tends to over predict the total energy absorbed since it assumes that all the reactions proceed to their maximum extent. In order to obtain a more realistic analysis, a third method was also studied in this research whereby the reaction rates of the chemical species are governed by finite reaction rates. This of necessity requires the determination of all important chemical reactions and the analysis of the appropriate kinetic data corresponding to these reactions. This method of analysis, therefore, requires the laborious task of collecting, cataloguing and evaluating reaction kinetic data as it appears in the literature.

A procedure was developed to help simplify, but not totally eliminate, the difficulty encountered in evaluating kinetic data for the reactions, and to help narrow down the choice of selecting information from sources which sometimes do not agree among themselves. This procedure is called the isothermal analysis technique, and it is explained in a latter part of the chapter. In addition to the painstaking data handling and analyzing procedure there is the added task of numerically solving the equations. The non-equilibrium flow analysis is an order of magnitude more complex than the chemical equilibrium analysis of Chapter IV. The latter involves the solution of a set of algebraic equations with the energy equation; while the non-equilibrium flow analysis requires the solution of a set of non-linear ordinary differential equations (species continuity) with the energy equation. The numerical solution of these equations can become stiff (10) as will be explained subsequently.

Mathematical Formulation

The phenomenological equations that permit the calculation of the reaction rates for an arbitrary number of simultaneous chemical reactions involving an arbitrary number of chemical species is presented in this section.

A chemical reaction can be written in general as:

$$\sum_{j=1}^{l} r_{ij} A_j \underset{k_{r_i}}{\overset{k_{f_i}}{\rightleftharpoons}} \sum_{j=1}^{l} p_{ij} A_j \quad i = 1....L \tag{5-1}$$

For this ith chemical reaction the r_{ij} and p_{ij} represent the stochiometric coefficient of the reactants and products respectively. A_j represent the chemical species j. The forward and reverse reaction rate constants are k_{f_i} and k_{r_i}, respectively. Assuming that there are a total of l chemically reacting species whose composition can be determined by L chemical reactions, the rate of reaction of the j species, R_j, can be described by the following phenomenological equation:

$$R_j = \sum_{i=1}^{L} (p_{ij} - r_{ij}) \left\{ k_{f_i} \prod_{k=1}^{l} C_K^{r'_{ij}} - k_{r_i} \prod_{k=1}^{l} C_K^{p'_{ij}} \right\} \tag{5-2}$$

where C_K is the concentration of component K, k_{f_i} and k_{r_i} are the forward and reverse reaction rate constants, and r_{ij} and p_{ij} are the power on the concentration of the reactants and products respectively. r'_{ij} and p'_{ij} are equal to their corresponding stochiometric coefficients for elementary reactions only.

Equation (5-2) is a convenient and general formulation

for expressing the reaction rate of the jth species in L simultaneous chemical reactions. This form of the rate equation for species i is readily used in the computer implemented numerical solutions of the non-equilibrium flow analysis. The stochiometric coefficients stored in matrix form, where the species are identified by their row location and the reaction by their column location. Since there is no algorithim to relate the rows and columns for use in a generalized, all purpose input subroutine, i. e., the matrix of coefficients is a sparce matrix. The forward and reverse reaction rate constants are conveniently expressed in the following functional form:

$$k_i = A_i \, T^{-S_i} \, \exp(-E_i/RT) \quad i=1...L \qquad (5\text{-}3)$$

when $S_i=0$ Equation (5-3) reduces to the well known Arrhenius expression. A_i is the frequency factor and E_i is the activation energy.

Equations (5-2) and (5-3) are simple to program. However, the selection and analysis of the data for the important chemical reactions and the subsequent numerical problems that are encountered in describing chemically reacting flow, makes this analysis more difficult than the equilibrium case. The selection of the chemical reactions and the numerical problems encountered in their

solutions are explained in the next two subsequent sections.

Criteria for Reaction Selection

When developing a kinetics analysis for a chemically reacting flow system one must first determine what are all the possible chemical reactions. That is, one must perform an exhaustive analysis of all possible chemical reaction combinations and select from these, as a first approximation, those reactions which are thermodynamically feasible. To determine all the possible chemical reactions, three main sources were used (2, 3, 4). The work by Hockstein (2) covers over 20,000 possible reactions, not all applicable to this research. However, it has an extensive list of reactions for the carbon-hydrogen and carbon-oxygen systems. Pike (4) also covered most of the important hydrocarbon reactions which were of particular interest to this research. Moreover, Bahn (3) recently listed all of the possible reactions in the H-O-N system.

The first step in selecting the appropriate reactions was to eliminate those reactions which had reactants and products which could not be formed by any combination from the species present in the pyrolysis gases. A detailed explanation on how these compositions were obtained is given in Appendix F.

The next step was to determine those reactions from the remaining set which were thermodynamically feasible. Those that were feasible, were further analyzed using the isothermal analysis technique which is explained later in this section.

Composition of Pyrolysis Products: It has been mentioned that the composition of the pyrolysis gases has an important effect in the reaction selection process. It eliminates from consideration those reactions whose reactants could not be formed by any combination of the pyrolysis products. Thus, it is most important to estimate the composition of the pyrolysis gases with as much certainty as possible. Note that the composition of pyrolysis gases only affects the non-equilibrium analysis since equilibrium only requires the elemental composition to be known, and these are known from the chemical formulae of the components of the ablative composite and their compositions.

First attempts to study the non-equilibrium flow of pyrolysis products relied on the composition obtained from two sources. One being the composition obtained assuming chemical equilibrium (5) and the other by the analysis of the degradation products of low density nylon phenolic

resin by pyrolysis gas chromatography (6, 7). As noted in Appendix F, the unavailability of accurate analytical procedures and thermophysical properties for the high molecular weight pyrolysis products (i. e., phenol, cresol, toluene, etc.) left a region of definite uncertainty as to the composition of pyrolysis products. As a result, the major components of the degradation of the pyrolysis products were identified as methane, hydrogen, carbon dioxide, carbon monoxide and nitrogen by many (8, 9), with unknown quantities of water and high molecular weight residue completing the analysis.

Subsequent research by Sykes (10) confirmed the presence of phenol-based materials as primary constituents in the high molecular weight residues. Table 5-1 lists the species and the estimate of the composition of the pyrolysis products resulting from the degradation of a 40 percent (by weight) nylon, 60 percent phenolic resin ablative composite. How these estimates were arrived at is presented in Appendix F.

Equilibrium Conversion of Reactions: The second step in the development of a realistic kinetic analysis is to determine from the list of possible reactions which are thermodynamically unfavorable. By computing the equilibrium conversion of the reactions over the temperature range of

TABLE 5-1 Estimate of the Representative Composition of the Pyrolysis Products for a 40 percent Nylon, 60 percent by Weight Phenolic Resin Ablative Composite.

Species	Mass Percent	Mole Percent
H_2	2.57	20.92
CH_4	3.86	3.90
C_2H_2	3.88	2.41
C_2H_4	3.88	2.24
C_2H_6	0.64	.35
C_6H_6	2.57	.53
C_6H_6OH	23.10	3.97
CO	4.65	2.40
CO_2	4.60	1.69
H_2O	7.29	6.45
N_2	3.95	2.20
C(solid)	39.01	52.94

Element	Elemental Composition (Mass Percent)
C	73.80
H	7.36
O	3.95
N	14.89
Total	100.00

interest (500°F - 5500°F) one could examine the behavior of the equilibrium conversion of each reaction with temperature. The rule of thumb used was to eliminate from further consideration those reactions which had an equilibrium conversion of 5% or less at 5500°F. This is justifiable since kinetically their conversion would have been much less. We are assuming, of course, that the equilibrium conversion is determined in the endothermic direction. In Appendix H, the equilibrium conversion with respect to temperature for 99 possible chemical reactions is presented. These reactions were obtained from possible combinations of the pyrolysis products as presented in Table 5-1. It should be noted that many of the reactions considered, although thermodynamically feasible, were eliminated, since either one of the reacting species did not exist as a pyrolysis product, or could not be formed by any combination of important reactions. One example of this is the dissociation of N_2O as given by reaction 7 in Table H-3. As shown in Table 5-1, there is no N_2O present as a product of pyrolysis degradation, and practically none can be formed by the oxidation of nitrogen as indicated by the equilibrium conversion of reaction 17 of Table H-3. Therefore, there was no need to consider the dissociation of N_2O in the kinetic analysis, and this sort of reasoning was used to eliminate other

reactions.

Isothermal Analysis Technique: In Tables H-1 through H-7 a list of possible chemical reactions is presented along with the equilibrium conversion of these reactions. In these tables it is shown that many of the possible reactions do not have appreciable conversions, even at the higher temperatures and could be, therefore, eliminated from further consideration. In many instances as previously mentioned, reactions which were thermodynamically favorable were eliminated because their reactants did not exist, or could not be formed as products from the pyrolysis reactions. This point was illustrated with the N_2O dissociation reaction. However, there was a remaining group of reactions (too many to have been considered in the analysis) that could not be eliminated from consideration by any of the two previously mentioned procedures. Therefore, a criteria was developed to determine the kinetic importance of the remaining reactions in the temperature range from approximately $500^{o}F$ to $5500^{o}F$. By analyzing the conversion of the flow of an equal molal mixture of the reactants, one was able to infer the importance of such a reaction. The mass flux used was 0.01 lbs/ft^2-sec. and a char thickness of 0.25 inches with a porosity of 0.8.

In Figure 5-1 the conversions are presented for two reactions. These are the thermal decomposition of ethylene

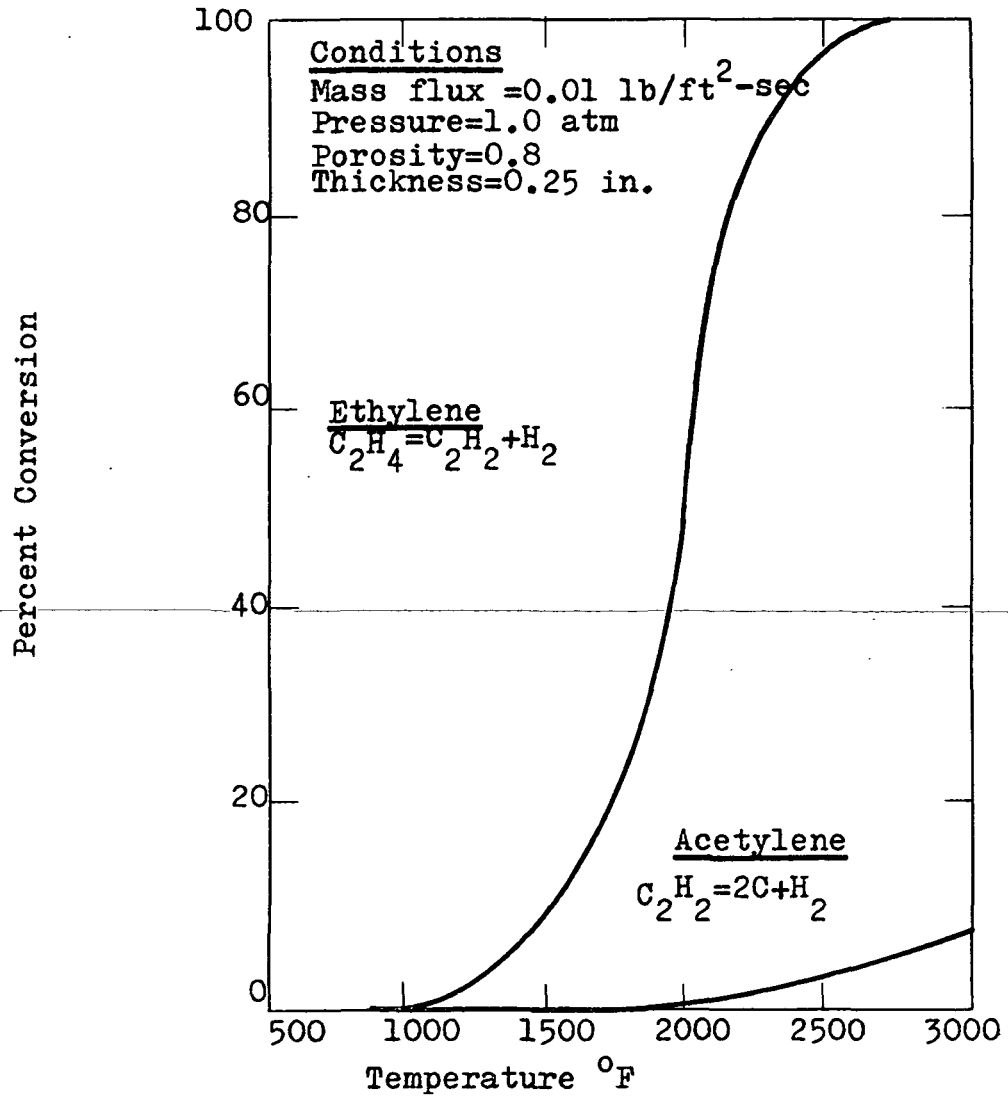

Figure 5-1. Conversion of Pure Ethylene and Pure Acetylene at Isothermal Conditions (500°F - 3000°F).

and acetylene species. It can be concluded by examining this figure that there could be no conversion of ethylene within the char for temperatures less than 1000°F and no conversion of acetylene for temperatures less than 2000°F. However, the thermal cracking of ethylene would be of importance for temperatures above 1000°F and for acetylene above 2000°F. In most instances the other reactions examined remained frozen below 1200 to 1500°F. But usually once the reaction started it would react very fast. This behavior, which is typical of reactions with high activation energies (>50 Kcal/mole) and high frequency factors ($>10^{15}$), was observed in the analysis. This very fast take-off of many of the reactions considered in the kinetic analysis was the cause of most of the numerical problems encountered in the integration of the equations of change. This behavior manifested itself in a condition known as stiffness, and more is said about this in a latter section.

To make the discussion quantitative, the conversion of a reactant is defined as the ratio of the amount consumed by reaction to the amount initially present. To determine the conversion of a chemical reaction a material balance is made on component j flowing through a volumetric section of the char having a cross-sectional area,

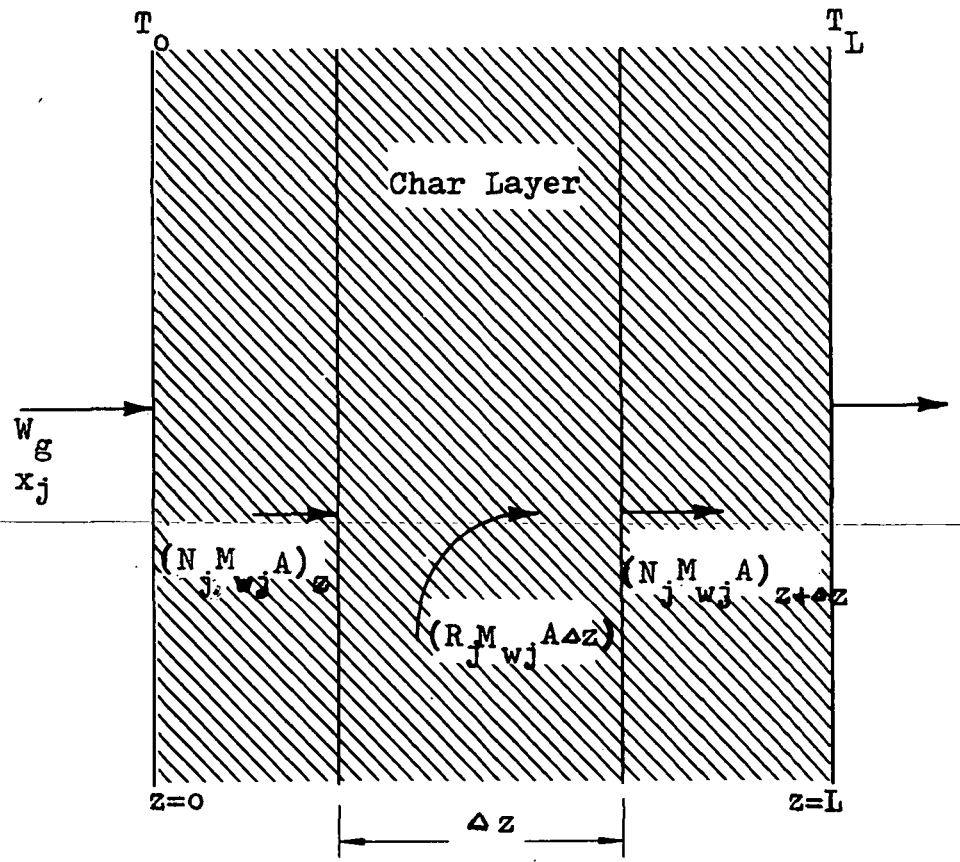

Figure 5-2. Schematic Diagram of the Char Layer.

A, and a width Δz as shown in Figure 5-2. If N_j is the molal flux of component j at z, the material balance on component j for steady flow in the z direction is:

$$(N_j M_{wj} A)_z + (R_j M_{wj} A).\Delta z - (N_j M_{wj} A)_{z+\Delta z} = 0 \qquad (5\text{-}4)$$

dividing the above by $M_{wj}A$ results in the following equation:

$$(N_j)_{z+\Delta z} = (N_j)_z - R_j \Delta z \qquad (5\text{-}5)$$

The above equation expresses the change in molal flux of each species as it reacts through the isothermal reactor. This equation is solved by a simple finite difference scheme from which the conversion X_j is calculated as follows:

$$X_j = (N_{jo} - N_j)/N_{jo} \qquad (5\text{-}6)$$

where N_{jo} is the molal flux of component j entering the char zone. By using this scheme the set of important chemical reactions was obtained and they are listed in Table 5-2. The computer program implemented solution for the finite difference Equation is listed in Appendix

TABLE 5-2 Chemical Reactions of Importance Considered in the Non-Equilibrium Flow Analysis

1.	$CH_4 = CH_2 + H_2$
2.	$CH_4 = CH_3 + H$
3.	$2CH_3 = C_2H_6$
4.	$C_2H_6 = C_2H_4 + H_2$
5.	$C_2H_4 = C_2H_2 + H_2$
6.	$C_2H_2 = 2C + H_2$
7.	$C_2H_2 = C_2H + H$
8.	$C_{(s)} + H_2O = CO + H_2$
9.	$C_{(s)} + CO_2 = 2CO$
10.	$H_2 + M = 2H + M$
11.	$H_2O + M = H + OH + M$
12.	$H + CO_2 = CO + OH$
13.	$CO_2 = CO + O$
14.	$C_6H_6O + H_2 = H_2O + C_6H_6$
15.	$C_6H_6 = 3C_2H_2$

D. The chemical reactions selected to simulate the chemical behavior of the pyrolysis gases are presented in Table 5-2.

Selecting the Right Data

The procedure developed to analyze and screen the many possible chemical reactions which occur in the C-H-O-N as explained in the previous section, was helpful in selecting a set of reactions which would most closely represent the actual chemical behavior of the pyrolysis gases. We recall that this selection is based on the use of the isothermal analysis technique. This technique computed the isothermal rate of conversion of a reaction over a temperature range. The degree of conversion over this range allowed us to form a judgement as to the importance of a given reaction. If a reaction was judged to be important (conversion $>$ 5 percent) it was included in the analysis, otherwise it was eliminated. Once the reactions were selected, one additional problem remained. This was the selection of data from a number of sources which qualitatively predicted the right trend in the reaction but which predicted quite different conversions. In other words, the problem was what to do in cases where two sources of data existed for a given reaction, which predict

different conversions at given isothermal conditions. The approach to this problem is explained below.

Comparison of Isothermal Conversion With Equilibrium Conversion

The comparison of the isothermal conversion with the equilibrium conversion over the temperature range of 500°F to 5500°F eliminated a great deal of the data selection problem. In most cases, the comparison showed that only one of the data sources would remain within the equilibrium constraints for a given reaction. Therefore, the choice of which source of data to use was obvious in these cases. However, there were instances in which the reaction rate data predicted concentrations in violation of known thermodynamic equilibrium constraints. This is attributed to the fact that in most cases the kinetic data was being extrapolated beyond the temperature range of applicability.

Rather than to eliminate these reactions it was decided to force them to be within the equilibrium constraints. This was achieved by using a reverse reaction rate constant calculated from the well known equation which relates the reverse constant with the equilibrium constant and the forward reaction constant. In doing so, a set of reactions that met equilibrium constraints was obatined. Again more than one source of data existed for each one of these reactions.

Fortunately, of the 15 reactions that were selected to simulate the kinetics, only four fell in this category, and are shown in Table 5-3. Therefore, a parametric study was conducted to evaluate the effect that each of these four reactions had on the kinetics analysis when a different source of data was used. The results showed less than one percent variations between the predicted values of the energy absorbed for each reaction. These small variations are attributed partly to the use of a reverse reaction rate constant (consistent with equilibrium) which tended to dampen out the differences in the values of the forward reaction rate constants. An explanation on how the parametric studies were conducted is given in the following chapter.

Discussion of the Kinetic Data for the Important Chemical Reactions in the Char Zone

Table 5-4 presents the list of the 15 reactions used in the non-equilibrium flow analysis. It also presents the kinetic data and literature sources of these reactions. The source of the preferred value is underlined.

Methane Decomposition: Reactions 5-1 and 5-2 were used to describe the decomposition of methane. Reaction 5-1 decomposes to CH_2 and H_2. Data for this reaction were

TABLE 5-3 Reactions for which more than one set of kinetic data was available after preliminary screening.

$CH_4 = CH_2 + H_2$
$C_2H_6 = C_2H_4 + H_2$
$C_2H_4 = C_2H_2 + H_2$
$C_2H_2 = 2C + H_2$

TABLE 5-4 Important Reactions and Associated Kinetic Data for the Pyrolysis Products of Nylon Phenolic Composites Between 500-6000°F.

General Form of the Reaction: $aA+bB+....+=rR+sS+....+$

General Rate Constant Equation: $k=k^{o}T^{-S}\ EXP(-E/RT)$

Reaction Number	Reaction	Rate Law	Activation Energy E,(KCAL/gm-mole)	Frequency Factor	S	References
5-1	$CH_4=CH_2+H_2$	k_fA	91.	$4.5x10^{13}$	0	37, 36
5-2	$CH_4=CH_3=H$	k_fA	103.	$1.x10^{15}$	0	38,36,40,41,42,43
5-3	$2CH_3=C_2H_6$	k_fA^2	28.2	$1.5x10^{10}$	0	44
5-4	$C_2H_6=C_2H_4+H_2$	k_fA	69.0	$9x10^{13}$	0	41,45,46,47,48
5-5	$C_2H_4=C_2H_2+H_2$	k_fA	72.0	$1.1x10^{13}$	0	41,45,46,49,50,51,52
5-6	$C_2H_2=2C+H_2$	k_fA	30.0	$1.7x10^{6}$	0	41,35,46,49,50,51,52
5-7	$C_2H_2=C_2H+H$	k_fA	35.5	$4.5x10^{11}$	0	54
5-8	$C+H_2O=CO+H_2$	k_fA	71.9	$2.3x10^{11}$	-0.5	61,55,56,57,58,59,60
5-9	$C+CO_2=2CO$	k_fA	85.0	$1.5x10^{10}$	0	62,63,64,65,66,67,68,69
5-10	$H_2+M=2H+M$	k_fAB	103.2	$3.6x10^{18}$	0.82	74,73,75,76
5-11	$H_2O+M=OH+H+M$	k_fAB	118	$1.7x10^{22}$	1.31	73,74,67
5-12	$CO_2=CO+O$	k_fA	71.9	$2.3x10^{11}$	-0.5	67,77,74,78,79
5-13	$H+CO_2=CO+OH$	k_fAB	33.	$1.3x10^{15}$	0	78
5-14	$C_6H_6O+H_2=H_2O+C_6H_6$	k_fAB	45.0	$2.x10^{13}$	0	71,72
5-15	$C_6H_6=3C_2H_2$	k_fA	52.0	$1.4x10^{9}$	0	39

reported by Palmer and Hirt (36) and Kozlov and Knorre (37). An activation energy of 91 Kcal/mole and a frequency factor of 4.5×10^{13} sec^{-1} were reported by Palmer and Hirt (36). Kozlov and Knorre (37) reported an activation energy of 101 Kcal/mole and a frequency factor of 1.26×10^{14} sec^{-1}. The data from both of these sources were used in the prediction of the total energy absorbed. It was observed that there was a negligible difference (less than one half of one percent) between the predicted values of the energy absorbed using the data of Palmer and Hirt (36) and that of Kozlov and Knorre (37). As a matter of interest to the reader, the calculated values reported in the latter part of this chapter for the total energy absorbed were those using the data of Kozlov and Knorre (37). The reverse reaction rate constants were not reported in the literature, however, they were easily computed knowing the forward reaction rate constant and the equilibrium constant. The equilibrium constant was calculated as a function of temperature using a modified version of the equilibrium analysis program described in Chapter IV. These values were fitted using an expression of the form $e^{(A+B/T)}$. The values for the constants A and B are given in Table 5-5 for the 15 chemical reactions used in the kinetic model.

A second competing reaction was used to describe the

TABLE 5-5 Constants for the Equilibrium Constant Fit of the Important Chemical Reactions.

General Form of Backward Constant: $K_b = EXP(A+B/T)$
General Form of the Reaction: $aA+bB+\ldots=rR+sS$

Reaction Number	Reaction	Rate Law	Constants $Ax10^{-2}$	$-Bx10^{-5}$
5-1	$CH_4=CH_2+H_2$	K_bRS	.1664396	.436510
5-2	$CH_4=CH_3+H$	K_bRS	.1725282	.5315890
5-3	$2CH_3=C_2H_6$	K_bR	.2030536	.4381153
5-4	$C_2H_6=C_2H_4+H_2$	K_bRS	.1604147	.1715366
5-5	$C_2H_4=C_2H_2+H_2$	K_bRS	.1538761	.2100359
5-6	$C_2H_2=2C+H_2$	K_bR	-.0597961	-.2595788
5-7	$C_2H_2=C_2H+H$	K_bRS	-.1603705	-.5805091
5-8	$C+H_2O=CO+H_2$	K_bRS	.1717659	.1626795
5-9	$C+CO_2=2CO$	K_bR	.2068289	.2015984
5-10	$H_2+M=2H+M$	K_bR^2	.1465827	.5507806
5-11	$H_2O+M=OH+H+M$	K_bRS	-.1615115	-.6283391
5-12	$CO_2=CO+O$	K_bRS	.1787079	.6348669
5-13	$H+CO_2=CO+OH$	K_bRS	.0446038	.1056866
5-14	$C_6H_6O+H_2=H_2O+C_6H_6$	K_bRS	-.0542079	-.0946318
5-15	$C_6H_6=3C_2H_2$	K_bR^3	.3830254	.6562869

decomposition of methane. This is reaction 5-3 which shows the decomposition of methane to methyl radical (CH_3) and hydrogen radical (H). For this reaction the data published by Palmer and Hirt (38) was used. The activation energy reported was 103 Kcal/mole with a frequency factor of 1.0×10^{15} sec^{-1}. This data was reported by Pike (39) as preferred in his critical evaluation of rate data for reactions in the C-H-O-N system. The range of activation energies in the literature varied from a low value of 73 Kcal/mole to a high of 103 Kcal/mole (36, 38,40,41,42,43). Frequency factor variations between 4.5×10^{13} to 1.0×10^{15} sec^{-1} were also reported.

Formation of Ethane: Reaction 5-3 was used to represent the formation of ethane from two methyl radicals. These radicals are formed in the decomposition of methane. The activation energy used was 28.2 Kcal/(gm.mole-sec). There was only one source of data known to this author for this reaction and it is reported by Steacie (44).

Decomposition of Ethane: Reaction 5-4 was used to describe the decomposition of ethane. In this reaction ethane decomposes to ethylene and hydrogen. Data for this reaction have been reported by a number of authors. These include Gulyaev and Polack (45), Kozlov and Knorre, Shah

(46), Bartlett and Bliss (47) and Steacie and Shane (48). An activation energy of 69 Kcal/gm.mole and a frequency factor of $9x10^{13}$ sec^{-1} were reported by Gulyaev and Polack (45). Kozlov and Knorre (41) reported an activation energy also of 69.0 and a frequency factor of $1x10^{14}$ sec^{-1}. This is very close to the data by Gulyaev and Polack (45) which reported a frequency factor of $0.9x10^{14}$ sec^{-1} and an activation energy of 69.0 Kcal/gm.mole. An activation energy of 64.1 Kcal/gm.mole and a frequency factor of $3.14x10^{13}$ sec^{-1} were reported by Bartlett and Bliss (47) which is also close to the data of Kozlov et.al. (41) and Gulyaev et.al. (45). Shah (46) reported an activation energy of 83 Kcal/gm.mole and a frequency factor of $6.04x10^{16}$ sec^{-1}. Both the activation energy and the frequency factor of Shah are way out of line to those of the three previously mentioned sources. For this reason the data of Shah was not used.

The range of activation energies and frequency factors reported (41,45,46,47,48) were 64 to 82 Kcal/gm.mole and $3.14x10^{13}$ to $6.04x10^{16}$ respectively.

The calculations of the total energy absorbed reported in the latter part of this chapter were based on the data of Kozlov and Knorre (41) for ethane decomposition.

Decomposition of Ethylene: The thermal degradation of ethylene to acetylene and hydrogen is given by reaction (5-5). Data for this reaction has been reported by Kozlov and Knorre (41), Gulyaev and Polack (45) and Shah (46). The activation energy and frequency factors reported by Kozlov and Knorre (41) and Gulyaev and Polack (45) were identical. Both reported an activation energy of 40.0 Kcal/gm.mole. However, Kozlov and Knorre (41) gave a temperature range of 1300-2000°K where the data would be applicable, while Gulyaev and Polack (45) gave a temperature range of 1600-3700°K. The range of activation energies and frequency factors reported (41,45,46) were 40.0 to 76.0 Kcal/gm.mole and 2.57×10^{8} to 1.8×10^{13} sec^{-1}, respectively.

A value of 40. Kcal/gm.mole and a frequency factor of 2.57×10^{8} sec^{-1} were used in the kinetic analysis.

Acetylene Decomposition: The thermal decomposition of acetylene to carbon and hydrogen is given by reaction (5-6). The number of data sources for this reaction was greater than average. One would think that a reaction so well studied, and of such commercial importance would show good agreement among the sources. Unfortunately, the opposite was the case. The greatest discrepancy in the calculated values of the energy absorbed were observed when

using different sources of data for this reaction. The difference amounted to about four percent.

Data for this reaction were reported by Kozlov and Knorre (41), Gulyaev and Polack (45), Shah (46), Happel and Kramer (49), Aten and Greene (50), Leroux and Mathieu (51), and Chase and Weingberg (52). Both Kozlov et.al. (41) and Gulyaev et.al. (45) reported a frequency factor of 1.7×10^6 and an activation energy of 30.0 Kcal/gm.mole. Kozlov et.al. (41) gave 2000°K as the temperature at which these data were applicable. Gulyaev et.al. gave a much wider temperature range of 1600°K to 3700°K.

Shah (46) reports an activation energy of 62 Kcal/gm.mole, twice that of the two previous authors, and a frequency factor of 9.7×10^{10} which is 50,000 times greater. Because of the higher activation energy and larger frequency factor, the data of Shah (46) would predict acetylene decomposition over a smaller range than the data of Kozlov (41) and Gulyaev (45). The data of Shah for ethane and ethylene decomposition also poses these characteristics.

The frequency factor of Happel and Kramer (49), 5.1×10^{10}, is of the same order of magnitude as that reported by Shah (46). However, the activation energy is approximately three and a half times smaller.

Aten and Greene (50) report an activation energy of

of 14.5 Kcal/gm.mole, slightly lower than Happel and Kramer (49), but half that of Kozlov (41) and Gulyaev (45). A frequency factor of 4.0×10^7 was given, which is twenty-three times greater than Kozlov and Gulyaev but 3000 times smaller than the one reported by Happel and Kramer (49). It is also about 2500 times smaller than the data of Shah (46). The temperature range for which the data is recommended is 900-1700°K. A much smaller temperature level than the 1600-3700°K range recommended by Gulyaev (45).

Leroux and Mathieu (51) report a frequency factor of 1.0×10^3 and an activation energy of 12.5 Kcal/gm.mole. These values are completely out of line with those reported in the literature by other authors. The temperature range for which these values are recommended are 298-398°K. Obviously, too low for the temperature range of interest in this research. The values of Leroux and Mathieu were never considered and they were not used in the study of the effects of kinetic data on the predicted values of the energy absorbed. The basis for this decision is obvious.

The data of Kozlov and Knorre (41) and Gulyaev and Polack (45) were used for reaction (5-6).

Reaction (5-7) was also used to describe the thermal decomposition of acetylene. The data of Eschenroeder and Lordi (54) was used to simulate this reaction. They reported

an activation energy of 35.5 Kcal/gm.mole and a frequency factor of 4.5×10^{11}. This was the only single reference found for this reaction.

Carbon-Steam Reaction: The reaction of carbon with steam to produce carbon monoxide and hydrogen is given by Equation (5-8). This reaction has been extensively studied and the amount of data available is copious (55, 56,57,58,59,60,61). The reaction has been established to be first order and activation energies of 26-90 Kcal/gm.mole have been reported. Most of this data in the literature is geared towards industrial applications and therefore the form in which the data was presented was not easily applicable to a generalized reaction kinetics routine. Fortunately, the data of Walker et.al.(61) for the graphite steam reaction was presented in Arrhenius forms, which conforms to the type of expression used in the kinetics subroutine. Walker et.al.(61) report an activation energy of 71.9 Kcal/gm.mole, and a frequency factor of 2.3×10^{11} sec^{-1}. The activation energy is close to the value of 70 Kcal/gm.mole reported by Pike (4) in his literature evaluation.

Carbon-Carbon Dioxide Reaction: This reaction has also

been thoroughly studied in the literature because of important industrial applications. Data for this reaction has been reported by Wu (64), Gadsby et.al. (65), Lewis and co-workers (66), Harper (67), Austin and Walker (68), and Glovina (69). The form of the reaction rate for the data of references (28-31) is:

$$r_{co_2} = \frac{k_1 P_{co_2}}{(1 + k_2 P_{co} + k_3 P_{co_2})} \qquad (5\text{-}7)$$

where k_1, k_2 and k_3 are constant and P_{CO_2} and P_{CO} are the partial pressure of CO_2 and CO respectively. The previous form of the equation was not used. Instead the form used was $k_1(A)$ where (A) represents the concentration of CO_2. In other words, the reaction was assumed to be first order with the concentration of CO_2. This approach was taken due to a suggestion by Swann (70) in which he pointed out that the CO_2 data available in the literature was for partial pressures of CO_2 much lower than the ones that would be encountered in re-entry simulation. Therefore, the literature data would not be any more accurate than the first order approximation. This approach was used by April (71) and Pike et.al. (72). They reported an activation energy of 50 Kcal/gm.mole, and a frequency factor of 1.0×10^6.

However, the activation energy used in our research was 35 Kcal/gm.mole and a frequency factor of 1.0×10^{11}. This is the data reported by Walker (62).

Hydrogen Dissociation: The hydrogen dissociation reaction, Equation (5-10), is another reaction that has been thoroughly studied in the literature. Ellis et.al. (73), Kaskan and co-workers (74), Fenimore (75), and Gardiner and Kistiakowsky (76) among others, have reported values for the activation energy and frequency factor of hydrogen dissociation reaction. The data of Kaskan and co-workers (74) was used in the kinetic analysis. They reported an activation energy of 103.2 Kcal/gm.mole and a frequency factor of 3.6×10^{18}. Similar values were also reported by Bartlett and Bliss (45) in their studies of methane decomposition.

It was observed in the kinetic analysis that no appreciable dissociation of hydrogen occurs below 2500°F which is in line with the high activation energy reported in the literature. This is also consistent with thermodynamic equilibrium calculations obtained with the chemical equilibrium program. This reaction was not used by April et.al. (71, 72) since their analysis was restricted to a maximum temperature of 3000°F, and is in line with our findings that reactions do not appreciably occur below

temperatures of 2500°F.

Water Dissociation: The thermal dissociation of water to hydrogen and hydroxyl radical is given by reaction (5-11). Harper (67), Ellis et.al.(73) and Kaskan (74) report values for the activation energy and frequency factor of water dissociation. Harper reports an activation energy of 7.7 Kcal/gm.mole and a frequency factor of $2.5 \times 10^{12} cm^3$/mole-sec. This is in marked contrast with higher values reported by Ellis et.al.(73) and Kaskan (74). The values used in the kinetic analysis were those reported by Ellis et.al.(73) and are 103.1 and 3.6×10^{18} for the activation energy and the frequency factor respectively.

Carbon Dioxide Dissociation: The carbon dioxide dissociation is given by reaction (5-12). Data for this reaction has been reported by Harper (67), Jensen and Kurzuis (78), Mahan and Solo (79), Davies (77), and in the literature review of Kaskan and Browne (74). Pike (4) in his literature review recommends the values reported by Davies. These are an activation energy of 74.4 and a frequency factor of 2.44×10^{11}. The values used in the kinetic analysis were reported by Harper (67) and are: 71.9 Kcal/gm.mole for the activation energy and 2.3×10^{11} for the frequency factor. Uncertainties in the value of the kinetic data for carbon

dioxide dissociation could not have had a very large impact in the predicted value of the energy absorbed since the initial mole fraction of CO_2 is of the order of 10^{-2}.

Carbon Dioxide-Hydrogen Reaction: The carbon dioxide hydrogen reaction which results in the production of carbon monoxide and hydroxyl radicals, is given by reaction 5-13. This reaction is important only at higher temperatures (>3000^{o}F) where the concentration of the active species (hydrogen and OH radicals) are significant. An activation energy of 33 Kcal/gm.mole and a frequency factor of 1.3 x 10^{15} reported by Fristrom (78) were used in the kinetic analysis. This reaction was added to the kinetic analysis for the sake of completeness. Its contribution to other energy absorbing reactions is insignificant.

Phenol Hydrogenation: The phenol hydrogenation reaction to water and benzene is given by reaction (5-14). This reaction was included in the analysis based on the experimental studies of April (71,72). Phenol reactions have been studied by many investigators (81, 82, 83, 84, 85). However, no kinetic data has been reported for this reaction. April (71) calculated a frequency factor of $2x10^{13}$ cm^3 $mole^{-1}$ sec^{-1} based on kinetic theory. He recommended an activation energy of 45 Kcal/gm.mole based on his comparisons with heats of reactions of phenol related components, such as ethyl benzene (48.9 Kcal/gm.mole). O-Xylene (47.3 Kcal/gm.mole), mesitylene

(47.6 Kcal/gm.mole) and hydrindol (45.8 Kcal/gm.mole).

Benzene Decomposition: The decomposition of benzene is given by reaction (5-15). The data for this reaction was reported by Pike (4). An activation energy of 52 Kcal/gm-mole and a frequency factor of 1.4×10^9 sec^{-1} was used.

Decomposition Kinetics of Ablative Composites

In the earlier part of this chapter we discussed the kinetic of the pyrolysis gases in the char zone. In this section we will briefly explain the technique and the data used to describe the kinetics of the degradation of the polymer composite.

The analysis of decomposition in depth requires that the rate of mass loss, or rate of temperature change with density be known. Data for the densities of virgin and degrading composites as a function of temperature have been reported by Sykes and Nelson (86) and Madorski (87).

The data of Sykes and Nelson (86) is particularly useful since it is for phenolic-nylon resins; The data was obtained using thermogravimetric analysis techniques. In Chapter II, the importance of using a kinetic equation of the Arrhenius type to correlate the experimental mass loss rate data for polymers was discussed. It was indicated in this chapter that the mass loss of material was affected by the heating rate, and that this effect was a source of difficulty for earlier researchers modeling the decomposition process.

Sykes and Nelson (86) used a pseudo-order kinetic expression of the Arrhenius type to eliminate this influence. The equation is:

$$\frac{d\rho_i}{dt} = \rho_{i,o}\{(\rho_i-\rho_{c,i})/\rho_{i,o}\}^{n_i} A_i \exp(-E_i/RT) \qquad (5\text{-}8)$$

Equation (5-8) expresses the rate of change of density of a polymer with temperature. $\rho_{i,o}$ is the initial or virgin density. ρ_i is the density of the material at temperature T, ρ_c the residual or char density, and A_i and E_i are the well known frequency factor and activation energy parameters.

In the present mathematical analysis it has been assumed that when an ablative composite degrades, it degrades independently of the other components; that is, no interaction is assumed to occur among the composites. There is no known experimental data that takes into account these interactive effects. Therefore, of necessity, this simplifying assumption has been made. This is mathematically expressed as:

$$\frac{d\rho}{dt} = v\,\frac{d\rho}{dz} \qquad (5\text{-}9)$$

and for quasi-steady flow the time dependent term can be modified by:

$$\frac{d\rho}{dt} = v\,\frac{d\rho}{dz} \qquad (5\text{-}10)$$

Thus, knowing the kinetic parameters for the various components in a blend of virgin material, specifying the surface recession velocity, and the temperature history from the energy equation, the variation in density of the virgin materials can be predicted by the use of Equations (5-8), (5-9) and (5-10).

Differential Thermal Analysis: The DTA thermograms of nylon, phenolic and phenolic microballoons which compare the phenolic-nylon composite as obtained by Sykes and Nelson are shown in Figure 5-3. The results shown were obtained by heating the material at 10°C/min in a helium atmosphere to the temperature shown. The reactions which occurred upon heating are either endothermal or exothermal, with the endothermal reactions extending downward from the base line $\Delta T=0$.

As shown in Figure 5-3 the thermogram of nylon undergoes two endothermic processes, one with the peak at 260°C and the second at approximately 417°C. As explained by Sykes and Nelson (86), the first endotherm is associated with the melting of the Crystalline portion of the polymer (heat of fussion = 73.6 KJ/Kg of original material) while the second corresponds to decomposition. The decomposition, which occurs between 350°C and 500°C, absorbs 630 KJ/Kg of original material. According to Sykes and Nelson (86) "the apparent exothermal portion of the thermogram after 470°C results from the change in the total heat capacity accompanying decomposi-

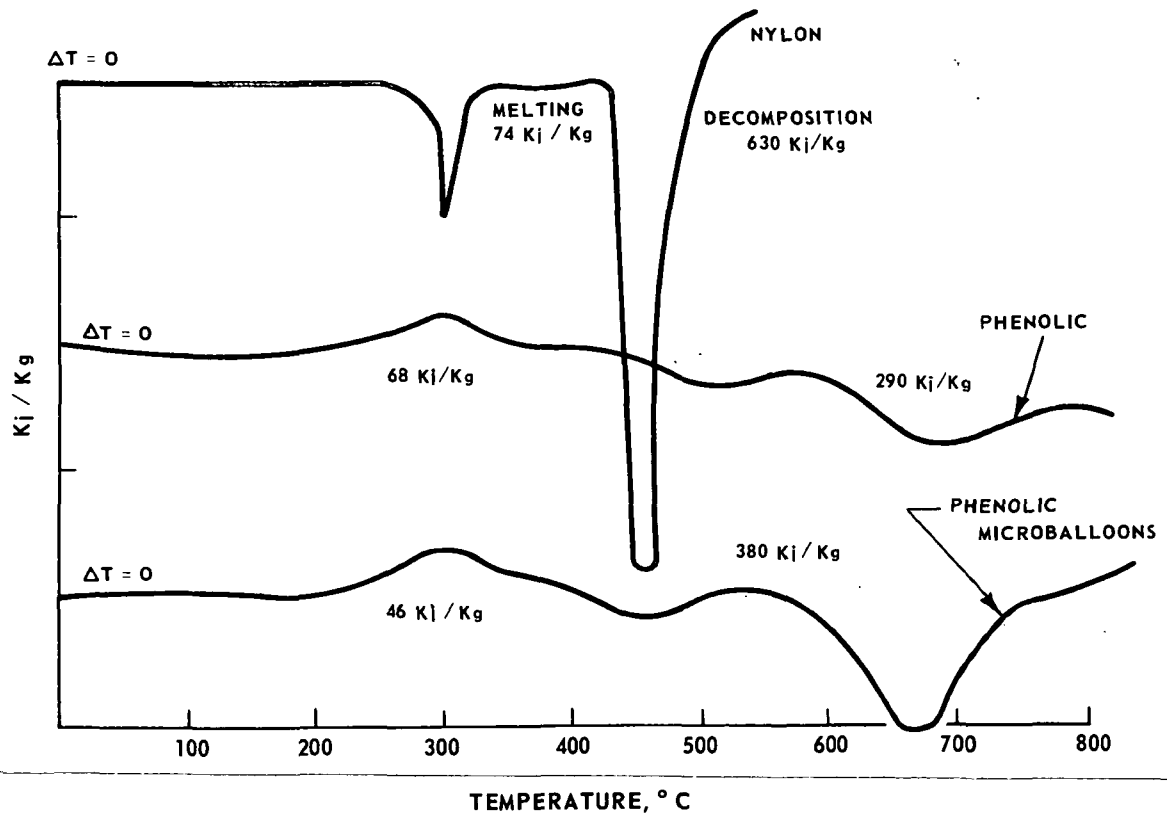

Figure 5-3. Differential Thermal Analysis Thermogram of Nylon, Phenolic and Phenolic Microballoons as Reported by Sykes and Nelson (86).

tion".

The center thermogram of Figure 5-3 is for phenolic which is used as the binder in the phenolic-nylon composite. The thermogram shows an exothermal reaction at 265°C followed by two overlapping endothermal decomposition reactions at 450°C and 625°C. The exothermal reaction evolves 68 KJ/Kg, and the pyrolysis reactions between 350°C and 850°C absorbed 293 KJ/Kg.

The thermogram for the phenolic microballoons, which is shown in the lower portion of Figure 5-3, is composed of small hollow micro-spheres of phenolic. The decomposition of this material is very similar to the phenolic binder. The exothermal reaction occurs approximately at 270°C and evolves about 47 KJ/Kg while the two overlapping endothermal reactions between 350°C and 850°C absorb 377 KJ/Kg.

Thermogravimetric Analysis: In conjunction with their DTA work, Sykes and Nelson (86) report the results of the thermogravimetric analysis (TGA) of the three separate constituents. Figure 5-4 shows the TGA plot of the residual mass fraction as a function of temperature.

The TGA data of Sykes and Nelson (86) shows one sharp mass loss between 350°C and 500°C for nylon. Almost all of the nylon is converted to gaseous product through this temperature range with less than ten percent remaining at 500°C.

The TGA thermogram of phenolic and phenolic microballoons also shown in Figure 5-4, shows the mass loss rate

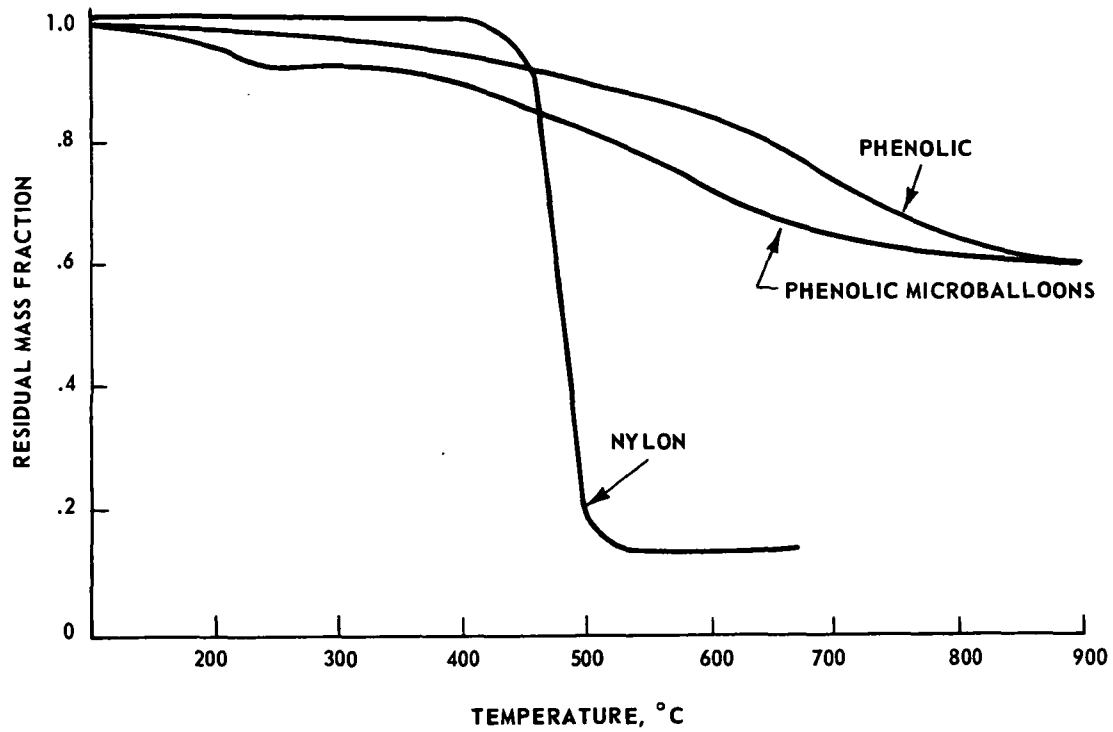

Figure 5-4. Thermogravimetric Analysis Thermogram of Nylon, Phenolic and Phenolic Microballoons as Reported by Sykes and Nelson (86).

to continue through 850°C. Sykes and Nelson (86) determined that the residue of both phenolic materials was 54 percent of their original mass.

The results of analysis of the three materials used in the composite phenolic-nylon material were very conveniently summarized by Sykes and Nelson (86) in a form which could be conveniently used by Equation (5-8). Table 5-6 shows their summary.

The data shown in Table 5-6 was used in this research to compute the mass loss rate of the phenolic-nylon resin.

Silicone Elastomers: The decomposition of silicone elastomers was computed using the same procedure as for phenolic-nylon: i.e., using Equation (5-8) to compute the degradation process.

At the time these computations were performed, Sykes had not published his results and the numbers presented in Table 5-7 were obtained by private communication with him (88).

As shown in Table 5-7, a single reaction was used to describe the decomposition of this elastomer.

The advantage of using Equation (5-8) as a general equation is that it will allow future use of the program for other ablative composites as their kinetic constants become available.

The data shown in Tables 5-6 and 5-7 were used in this research to compute the degradation rate of the two compo-

TABLE 5-6: Kinetic Parameters for the Degradation of Nylon, Phenolic and Phenolic Microballoons as Reported by Sykes and Nelson (86).

Material	Reactions	Activation Energy KJ/mole	Frequency Factor sec^{-1}	Reaction Order	Density (lbs/ft^3) Initial	Residual
Nylon	1	232	8.3×10^{14}	1.0	68.6	5.15
Phenolic Resin	3	114	5.1×10^{8}	3.0	80.0	43.28
		100	2.5×10^{5}	1.3		
		140	2.0×10^{7}	3.1		
Phenolic Microballoons	3	70	2.0×10^{5}	2.0	17.8	9.65
		122	9.7×10^{6}	2.0		
		172	1.3×10^{10}	3.0		

TABLE 5-7 Kinetic Parameters for the Degradation of Silicone Elastomers (88)

Material	Reactions	Activation Energy KJ/mole	Frequency Factor sec^{-1}	Reaction Order	Density (lbs/ft^3) Initial	Residual
Silicone Elastomers	1	181	5.37×10^{10}	1	62.08	2.48

sites. The decomposition rate computed from these data coupled to the char kinetic analysis (for the phenolic composite only) and the equilibrium analysis (for both composites) constituted the novel approach in this research. The results of this approach are presented in the next chapter.

Numerical Difficulties Encountered When Integrating The Chemical Kinetics Equations

Numerical difficulties were encountered when the energy and species continuity equations for finite rate chemistry were simultaneously solved using a fourth order Runge-Kutta. The step size of the Runge-Kutta analysis was determined by the kinetics of the reacting flow. To preserve stability it was necessary, in many instances, to maintain a small step size, as small as 10^{-8} feet, in regions where the flow was undergoing very rapid chemical changes. This condition created by the very rapid chemical reactions caused the integration to proceed very slowly. This numerical condition is known as stiffness (1, 10-15). It occurs in many physical systems which give rise to ordinary differential equations. It occurs when the simultaneous relaxation of different components vary at greatly different time rates. Mathematically it is observed when the eigenvalues of the differential equations are widely separated (13-15). A parasitic eigenvalue is one that is associated with the extraneous solution of the difference equation used to approximate the differential equation. This extraneous solution grows with

time, and will eventually dominate the numerical solution if it is not suppressed. The larger the parasitic eigenvalue, the more difficult is the suppression of the spurious solution. When the solution to the differential equation does not contain an exponential function the positive eigenvalue is called parasitic saddle and the negative, parasitic stiff. The integration interval is, thus, determined by the fastest rate, and the region of integration is determined by the slowest rate (11).

Physical Concept of Stiffness: The physical interpretation of stiffness in a non-equilibrium reacting flow system is that the species are created and destroyed in a time scale that is orders of magnitude smaller than the time scale of the fluid particles. When the ratio of flow time to reaction time increases as the reaction is moving towards equilibrium, the parasitic eigenvalues increase, causing the equations to become stiff (21).

Mathematical Concept of Stiffness (20): Consider A to be a nonsingular m x m matrix with eigenvalue λ_i i=1...m. Let $R_e\lambda_i > 0$, i=1...m. If max $(R_e\lambda_i)/\min(R_e\lambda_i)$ is a large number then the linear system of differential equations:

$$\dot{x} = Ax \qquad (5\text{-}11)$$

is said to be stiff. For nonlinear system a similar argument applies.

Most standard methods of numerical integration are not effective for stiff systems. Their deficiency lies in their inability to approximate the true value of the stiff component. When this is achieved (as for example in the Pade approximation used by Magnus and Schectner (34)),the numerical difficulty is bypassed. For most standard methods, as is the case with the Runge-Kutta, the numerical integration is not effective for stiff systems. They require a stability condition of the form:

$$\max \ |h.\lambda_i| < \text{const} \qquad (5\text{-}12)$$

which makes h smaller as λ_i increases. When the eigenvalues of A have negative real parts, the condition 5.8 prevails for the duration of a calculation, even though the solution has essentially no dependence on theλ_i (for which $|R_e \ \lambda_i|$ is large), except for a small initial interval.

To circumvent the restriction 5.8 for stiff system, different integration schemes have recently been published in the literature (1, 11, 12, 13, 14,,15, 17, 18, 19, 20, 21, 22, 23, 24, 25, 26, 31, 32, 33, 34, 35). Numerical experiments with these schemes have shown them to be more effective, the stiffer the system (30). We shall examine some of them in the following paragraphs.

Numerical Methods for Integrating Coupled Differential Equations With Varying Time Constants

In problems of high temperature flows, the chemical rate equations sometimes involve both fast and slow reactions in some regions of integration. Integrating the chemical kinetic equations has been a major source of difficulty because the very fast reactions determine the integration interval causing the step size to become very small, and thus, increasing considerably computing time. Three procedures to integrate these equations have been used to solve this type of problem. These are the explicit series solutions (11, 12, 13, 14, 16, 19, 21, 24, 27, 28, 29), the implicit series solution (1, 10, 13, 14, 15, 17, 18, 19, 21, 22, 23, 25, 26, 30), and Moretti's (31) linearization scheme which is also known as the subdomain method, or the method of rational approximation (19). One example of an explicit series solution is the Runge-Kutta analysis which has a small truncation error. As with all explicit techniques, this method has the advantage of being simple and straightforward. It requires only first derivatives and knowledge of the value of the independent variable at the previous step. It is a marching procedure which gives the value of the independent variable as the integration proceeds. The implicit methods, on the other hand, are much more complicated to program since they require iterative solutions, and in most cases, they also require higher order derivatives, as in the method of Lomax (14). However, they have

the major advantage of requiring a larger step size to maintain stability, Near equilibrium when the step size is reduced, the implicit methods lose their value in speed and computation. Recently Liu (21) investigated both implicit and explicit methods of solution for solving non-equilibrium boundary layer problems. He claimed that the Runge-Kutta method was as good as any to obtain converged solutions. However, computer time was slightly higher than the other implicit techniques he investigated. The limit of the step size in the implicit method is dependent upon the magnitude of error introduced by truncation of the series used to approximate the solution and not on stability consideration (19).

The third method of solution, rational approximation, was proposed by Moretti (31). In it Moretti linearized the rate term in the species continuity equation. Moretti's method presents the advantage of a smaller step size. However, it is more complicated to program than the Runge-Kutta analysis.

In conclusion, then, explicit techniques as the Runge-Kutta analysis are easier to program than the implicit techniques. However, they suffer from the disadvantage of requiring a smaller step size than implicit techniques. They also fail when near equilibrium conditions exist; the implicit techniques do permit small advances toward equilibrium "but at a price of excessive labor and computing time" (21).

Justification for Selecting the Fourth Order Runge-Kutta Analysis

In the previous section several of the most important techniques for integrating stiff equations were mentioned. In this examination, it was indicated that implicit techniques were unconditionally stable, while explicit techniques were conditionally stable and required a small value of h to keep them within the stability region. Even with this drawback, the fourth order Runge-Kutta was chosen as the integration scheme for this research. For our problem the case of programming far outweighted the computational speed of a more difficult technique to implement numerically. Besides, the implicit technique for one dimensional flow would have been attractive if the integration had to be performed over a distance of several feet, but not over a distance of 1/4 inch as in this research. Moreover, Lomax (14) in his review of integration schemes for integrating stiff equations stated that "if nothing special is known a priori about the differential equation, the standard fourth order Runge-Kutta is probably the best. It is self-starting, has low computing storage capabilities, is easy to program, has good accuracy $0(h^5)$, and...is more stable than any of the standard predictor corrector process". It is interesting to note also, that Liu (21) used a fourth order Runge-Kutta to solve the boundary layer equations after a detailed study of different integration schemes which were developed to handle stiff equations.

Selecting a Runge-Kutta Step Size to Maintain Stability

Kliegel and Tyson (18) have shown a method for computing a step size h that would maintain the numerical integration for the Runge-Kutta technique to be stable. This technique consisted in defining a fluid mechanic characteristic time, T_f , and a chemical relaxation time, T_c , respectively as:

$$T_f = \frac{L}{u} \tag{5-9}$$

and

$$T_c = \frac{C_i - C_i^*}{dC_i/dt} \tag{5-10}$$

where L is a length and u a velocity, C_i is the actual concentration of species i, and C_i^* is the concentration if the system were at equilibrium, and dC_i/dt is the rate of reaction of said species. To maintain stability it was required that:

$$\frac{Tf\ h}{T_c} < 5.6 \tag{5-11}$$

This is a simple and straightforward method for checking stability. However, it was estimated that to compute at every step the equilibrium composition of all the species for our system would more than offset any gain of

computing an optimum step size. Hence, a more rapid method of solving for a stable step size was required even if it did not provide the optimum solution of the step size.

Two empirical techniques were developed to compute a step size that would give a stable solution. One was to keep a double material balance, one on the gas species and one on the solid species. As long as these material balances checked to four significant figures, the solution was observed to be stable. This technique was rather successful as long as all species were present in larger than trace amounts, or when reaction rates would not abruptly change. Unfortunately, this technique did not work well for very small mass fluxes (0.005).

The other technique developed was as follows: Consider N_i, the mass flux of species i and ΔN_i, the change in mass flux of i due to a chemical reaction. If,

$$\frac{\Delta N_i}{N_i} < 0.1 \qquad (5\text{-}12)$$

the solution was observed to be stable.

This empirical criteria of Equation (5-12) works as long as the kinetics are controlling the step size. However it does not work at lower temperatures (1500^{o}F) where the fluid mechanics step is the controlling element in the solution. This problem was circumvented by specifying a maximum step size that maintained stability when the reac-

tions were very slow. The computer running time was on the average, 15 minutes on an IBM 360 Model 65.

Summary

The development of the non-equilibrium flow analysis has been presented. The success of this analysis lies in part in selecting the important chemical reactions in the temperature range of interest, which in this research is 500°F to 5500°F. To select these chemical reactions a three step procedure was outlined. First, the composition of the pyrolysis gases had to be established as accurately as possible. This was necessary to determine all possible chemical reaction combinations based on the original pyrolysis products. Once these reactions were compiled, a thermodynamic equilibrium study was performed by computing the extent of each reaction by the free energy minimization technique. This second step helped to determine those reactions which were not thermodynamically feasible in the temperature range 500 to 5500°F. The final step was to analyze the kinetic data for each of the chemical reactions left. This was done by computing the conversion of an equimolal mixture of reactants flowing isothermally through 0.25 inch reactor.

The second part of this chapter dealt with the numerical implementation to describe the rate of finite reaction process. It was shown that the rate of reaction of a specie could be represented by a simple phenomenological

expression of the form of Equation (5-2). The implementation of this equation for computer use is simple, however, its solution was the cause of many numerical problems. It was seen that these numerical problems, associated with reacting flow, have been attributed by many as a mathematical phenomena known as stiffness (1, 10-23, 31). Three numerical methods currently in use to integrate the coupled energy and chemical kinetic (continuity) equations were briefly described. These were the Runge-Kutta, implicit procedures, and the subdomain method, or method of rational approximation.

In the next chapter the results of the solution of the equations of change for decomposition in depth will be presented.

REFERENCES

1. Magnus, D. E., and H. S. Schechter, "Analysis of Error Growth and Stability for the Numerical Integration of the Equations of Chemical Kinetics", NASA-CR-66971, GASL TR-607 (June 1966).

2. Hockstein, A. R., ed. Bibliography of Chemical Kinetics and Collisions Processes (IFI/Plenum, New York, 1969).

3. Bahn, G. S., Reaction Rate Compilation for the H-O-N System, Gordon and Breach Science Publishers, New York (1968).

4. Pike, R. W.,"Evaluation of the Literature for Chemical Reactions and Reaction Rates for the Decomposition Products from Charring Ablator", LWP-181, NASA (Jan. 21, 1966).

5. del Valle, E. G., R. W. Pike and G. C. April, "Transport Phenomena in the Char Zone During Ablation. II. Equilibrium Composition of the Degradation Products of Ablation", Paper 13e, 63rd National Meeting of the A. I. Ch. E., Salt Lake City, Utah (May 1967).

6. Nelson, J. B., "Determination of Kinetic Parameter of Six Ablation Polymers by Thermogravimetric Analysis" NASA TN D-3919 (1967).

7. Sykes, George F., Jr., "Decomposition Characteristics of a Char-Forming Phenolic Polymer Used for Ablative Composite", NASA TN D-3810 (1967).

8. Scala, S. M. and L. M. Gilbert, "Thermal Degradation of Char-Forming Plastic During Hypersonic Flight", ARS J., 32, 917-924 (1962).

9. Kratsch, K. M., L. F. Hearne, and H. R. McChesney, "Thermal Performance of Heat Shield Composite During Planetary Entry", AIAA-NASA National Meeting, Palo Alto, California (September 30-October 1, 1968).

10. Curtis, C. F., and J. O. Hirschfelder, "Integration of Stiff Equations". Proc. Nat. Acad. Scie., 38, 235-243, (1952).

11. Treanor, C. E., "A Method for the Numerical Integration

of Coupled First-Order Differential Equation With Greatly Different Time Constants", Math. of Comp., 20, 639-645 (1966).

12. Clansen, R. J., "The Numerical Integration of Kinetic Equations for Chemical Systems Having Both Slow and Fast Reactions", RAND Corporation Report P-3547, Santa Monica, California (September 1967).

13. Lomax, Harvard, and H. E. Bailey, "A Critical Analysis of Various Numerical Integration Methods for Computing the Flow of a Gas in Chemical Non-Equilibrium", NASA TN D-4109 (1967).

14. Lomax, Harvard, "Stable Implicit and Explicit Numerical Methods for Integrating Quasi-Linear Differential Equations with Parasitic and Parasitic Saddle Eigen Values", NASA TN D-4703 (1968).

15. Lomax, Harvard, H. E. Bailey, and F. B. Fuller, "On Some Numerical Difficulties in Integrating the Equations for One-Dimensional Non-Equilibrium Flow", NASA TN D-5176 (1969).

16. Kaye, Harvey, "Numerical Solutions of Near Equilibrium Boundary Layers", AIAA J., 7, 172-173 (1969).

17. Gurney, J. P., R. A. Napier, and I. N. Momtchiloff, "Integration of Near Equilibrium Flows in Propulsive Nozzles", Chemical Engineering Progress Symposium Series, 62, 142-149 (1966).

18. Kliegel, J. R., and T. J. Tyson, "Discussion of Chemical Kinetic Integration Techniques", Paper No. WSS/CI 68-45, October 28, 1968.

19. Audch, J. B., "Numerical Method of Solution of Chemical Kinetics Equations", Heat Technology Laboratory Report, HTL-TR-40, NASA CR-89657 (September 1967).

20. Seinfold, J. H., Leon Lapidus, and Myungkyu Hwang, "Review of Numerical Integration Techniques for Stiff Ordinary Differential Equations", Ind Eng. Chem. Fundam. 9, 266-275 (1970).

21. Liu, Tsong-mou, "Hydrogen Injected into Air at an Axisymmetric Stagnation Point", Ph.D. Dissertation, University of California at San Diego (1970).

22. Fowler, M. E., and R. M. Warten, "A Numerical Integration Technique for Ordinary Differential Equations with Widely Separated Eigenvalues", IBM Journal of Research and Development, 11, 537-543 (1967).

23. Rosenbrock, H. H., Some General Implicit Processes for the Numerical Solution of Differential Equations, Computer Journal, 5, 329-330 (1963).

24. Lawson, J. D., "Generalized Runge-Kutta Processes for Stable System with Large Lipschutz Constants", SIAM J. Numer. Anal., 4, 372-381 (1967).

25. Sandberg, I. W., and H. Schuman, "Numerical Integration of Stiff Nonlinear Differential Equations", Bell System Technical Journal, 511-527 (April 1968).

26. Liniger, W. and R. A. Willoughby, "Efficient Integration Methods for Stiff Systems of Ordinary Differential Equations", SIAM J. Numer. Anal., 1, 47-66 (1970).

27. Brown, R. R., J. D. Riley and M. M. Bennett, "Stability Properties of Adams-Moulton Type Methods", Mathematics of Computation, 19, 90-96 (1965).

28. Krogh, F. T., "Predictor-Gorrector Methods of High-Order with Improved Stability Considerations", Journal of the Association for Computing Machinery, 13, 374-385 (1966).

29. Crane, R. L. and R. W. Klopfenstein, "A Predictor-Corrector Algorith with an Increased Range of Absolute Stability", Journal of the Association for Computing Machinery, 13, 374-386 (1966).

30. Miranker, W. L., "Difference Schemes for the Integration of Stiff Systems of Ordinary Differential Equations", IBM Research Report RC-1977, Yorktown Heights, New York, January 8, 1968.

31. Moretti, G., "A New Technique for the Numerical Analysis of Non-Equilibrium Flows", AIAA. J., 3, 233-229 (1965).

32. Moretti, G. and M. Abbett, "Non-Equilibrium Effects for Quasi-Equilibrium Flows in Nozzles", AIAA Paper 66-636, Propulsion Joint Specialist Conference, Colorado Springs, Colorado (June 13-17, 1966).

33. De Groat, J. J. and M. J. Abbett, "A Computation of One-Dimensional Combustion of Methane", AIAA J., 3, 381-387 (1965).

34. Magnus, D. E., and H. S. Schechter, "Analysis and Application of the Pade Approximation for the Integration of Chemical Kinetic Equations", GASL TR-642, General Applied Science Laboratories, Inc., Westbury, L.I., New York (March 1967).

35. Distefano, G. P., "Stability of Numerical Integration Techniques", AIChE J., 14, 946-955 (1968).

36. Palmer, H. B., and T. J. Hirt, "The Activation Energy for the Pyrolysis of Methane", J. Phys. Chem., 67, 709 (1963).

37. Kozlov, G. I., and V. G. Knorre, "Kinetics of Thermal Decomposition of Methane by the Single-pulse Shock-tube Method", Russian Journal of Physical Chemistry, 37, 1128 (1963).

38. Palmer, H. B., and J. T. Hirt, "Kinetics of Decomposition of Pyrolytic Carbon Films from Methane and Carbon Suboxide. Carbon, 1, 65 (1963).

39. Pike, R. W., "Evaluation of the Literature for Chemical Reactions and the Reaction Rates for the Decomposition Products from Charring Ablators", NASA LWP-181, Jan. 21, 1966.

40. Bradley, J. M., Shock Waves in Chemistry and Physics. John Wyley, Inc., New York (1962).

41. Kozlov, G. I., and V. G. Knorre, "Single Pulse Shock-tube Studies on Kinetics of Thermal Decomposition of Methane", Combustion and Flame, 6, 253 (1962).

42. Thon, N., ed., Table of Chemical Kinetics Homogenous Reactions N.B.S. Circular 510 (September 1958), Supplement 1 (November 1965); N.B.S. Monograph 34, Volume 1 (September 1961), Volume 2 (July 1964).

43. Palmer, H. B., and J. T. Hirt, "Thermal Decomposition Kinetics of Carbon Suboxide", J. Am. Chem. Soc., 84, 113 (1962).

44. Steacie, E. W. R., "Atomic and Free Radical Reactions", 2nd ed., Vol. 1, p. 141, Reinhold Publishing Co., New York (1954).

45. Gulyaiev, G. V., and L. S. Polak, "The Kinetics of the Thermal Decomposition of Methane", Translation from Kinetika i Kataliz, 6, 399 (1965).

46. Shah, M. J., "Computer Control of Ethylene Production", Ind. Eng. Chem., 59, 70 (May 1967).

47. Bartlit, J. R., and H. Bliss, "Kinetics of Ethane Pyrolysis, AIChE J. 11, 562 (1965).

48. Quinn, C. P., "The Thermal Dissociation and Pyrolysis of Ethane", Proc. Roy. Soc. 275, 1361 (1963).

49. Happel, J. and L. Kramer, "Acetylene and Hydrogen from the Pyrolysis of Methane", Ind. Eng. Chem.59, (1), 39, (1967).

50. Aten, C. F., and E. F. Greene, "The Rate of Formation of Carbon from the Pyrolysis of Acetylene in Shock Waves", Discussions of the Faraday Society, (22), 162 (1956).

51. Leroux, P. J. and P. M. Mathieu, "Kinetics of the Pyrolysis of Methane to Acetylene", Chem. Engr. Prog. 57, (11), 54, (1961).

52. Chase, J. D. and F. J. Weinberg, "The Acetylene Decomposition of Reaction Mechanism from Global Flame Kinetics", Proc. Roy. Soc. A., 275, 411 (1963).

53. Gaydon, A. G. and Wolfhard,H. G., Flames, Their Structure, Radiation and Temperature, p. 202, Chapman and Hall, London (1960).

54. Eschenroeder, A. Q., and J. A. Lordi, "Catalysis of Recombination in Non-Equilibrium Nozzle", J. Phys. Chem. 66, 721 (1962).

55. Scott, G. S., "Mechanism of the Steam-Carbon Reaction", Ind. Eng. Chem., 33, 1279 (1941).

56. Lewis, W. K., E. R. Gilliland and H. Hipkine, "Carbon-Steam Reaction at Low Temperatures", Ind. Eng. Chem., 45, 1967 (1953).

57. Mayers, M. A., "The Rate of Oxidation of Graphite by Steam ", J. Am. Chem. Soc., 56, 1879 (1934).

58. Benford, J. S., Jr., and H. Eyring, "Kinetics of the Steam Carbon Reaction", J. Phys. Chem., 60, 486, (1956).

59. Warner B. R., "Mechanism of the Steam-Carbon Reaction", J. Am. Chem. Soc., 65, 1447 (1943).

60. Johnstone, H. F., C. Y. Chen, and D. S. Scott, "Kinetics of the Steam-Carbon Reaction in Porous Graphite Tubes", Ind. Eng. Chem., 4, 1564 (1952).

61. Walker, P. L., Jr., F. Ruskino Jr., and L. G. Austin, "Gas Reactions of Carbon". Advances in Catalysis, 11, Academic Press, Inc., New York (1959).

62. Walker, P. L., Jr., "Chemistry and Physics of Carbon," Vol. 4, p. 287-383, Marcel Decker, Inc, New York (1965).

63. Thiele, E. W. and R. T. Haslam, "Mechanism of the Steam Carbon Reactions", Ind. Eng. Chem., 19, 882 (1927).

64. Wu, P. C., "Effect of Carbon Monoxide in Causing Non-Uniform Gasification of Graphite by Carbon Dioxide", D. Sc. Thesis, M.I.T., Cambridge, Mass. (1949).

65. Gadsby, J., F. J. Long, P. Sleightholm, and K. W. Sykes, "Effect of Carbon Monoxide in Causing Non-Uniform Gasification of Graphite by Carbon Dioxide", Proc. Roy. Soc. A., 193, 357 (1948).

66. Lewis, W. K., E. R. Gilliland, and G. T. McBride, Jr., "Effect of Carbon Monoxide in Causing Non-Uniform Gasification of Graphite by Carbon Dioxide", Ind. Eng. Chem., 41, 1213 (1949).

67. Harper, J. W., "Chemical Reaction and Rate Data", Boeing Contract Nas8-5608, Schedule II, Part I, Task 4.3.7., 5-9811-4-143, Nov. 1, 1965.

68. Austin, L. G. and P. L. Walker, Jr., "Effect of Carbon Monoxide in Causing Non-Uniform Gasification of Graphite by Carbon Dioxide". AIChE J., 9, 303 (1963).

69. Glovina, E. S. and Khaustovich, G. P., "The Interaction of Carbon with Carbon Dioxide and Oxygen at Temperatures up to 3000°K. Eighth Int. Symp. on Combustion, William and Wilkins Co., Baltimore (1962).

70. Swann, R. T., Private Communication to R. W. Pike, March 14, 1968.

71. April, G. C., Evaluation of the Energy Transfer in the Char Zone During Ablation, Ph. D. Thesis, Louisiana State University, Baton Rouge, (1969).

72. Pike, R. W., G. C. April and E. G. del Valle, "Evaluation of the Energy Transfer in the Char Zone During Ablation", Part I; Theoretical and Experimental Results for Heat Shield Surface Temperature up to 3000°F," May 1, 1969.

73. Ellis, G. E. and H. B. Knell, "Literature Survey of the Kinetics of the H-O-N System". Contract AF33(657)-8491 (Nov. 1962).

74. Kaskan, N. E. and W. G. Browne, "Kinetics of the H_2CO/O_2 System". General Electric, Contract AF04(694)-222 (July 1964).

75. Fenimore, C. P., Chemistry in Premixed Flames, McMillian Co., New York, (1964).

76. Gardiner, W. C. and G. B. Kistiakowsky, "Thermal Dissociation Rate of Hydrogen", J. Chem. Phys., 35, 1765, (1961).

77. Davies, W. O., "Carbon Dioxide Dissociation at 3500-6000°K", J. Chem. Phys., 41, 1846 (1964).

78. Jensen, D. E., and S. C. Kurzuis, "Rate Constants for Calculations on Nozzle and Rocket Exhaust Flow Fields", Aero. Chem. Research Labs, Report No. TP-149, NASA Contract NAS8 (1966).

79. Mahan, B. H. and R. B. Solo, "Carbon Monoxide-Oxygen Atom Reaction", J. Chem. Phys., 37, (11) (December 1962).

80. Fristrom, R. M., "Radical Concentration and Reactions in a Methane-Oxygen Flame", 9th Symposium on Combustion at Cornell University, Ithaca, New York, Combustion Institute, Paper No. 20 (1963).

81. Carletton, Ellis, Hydrogenation of Organic Substances, 3rd ed., D. Van Nostrand Co., Inc. New York (1930).

82. Augustine, R. L., Catalytic Hydrogenation, Marcel Dekker, Inc., New York (1965).

83. Sabatier, E. N., J. H. Reid, Catalysis in Organic Chemistry, D. Van Nostrand Co., Inc., New York 216 (1922).

84. Diwoky, F. F. and Homer Adkins, "Competitive Hydrogenation", Jour. Am. Chem. Soc., 53, 1868 (1931).

85. Adkins, Homer, J. I. Cramer, "The Use of Nickel as a Catalyst for Hydrogenation", Jour. Am. Chem. Soc., 52, 4349 (1930).

86. Sykes, G. F. and J. B. Nelson, "Thermo Analysis of Ablation Materials", Preprint 7B, 61st National Meeting of the AIChE, Houston, Texas (Feb. 19-23, 1967) NASA Accession Number (N68-25277).

87. Madorski, S. L., Thermal Degradation of Polymers, Interscience Publisher, New York (1964).

88. Sykes, G. F., Private Communication (July, 1969).

CHAPTER VI

ANALYSIS OF THE IN-DEPTH RESPONSE OF ABLATIVE COMPOSITES

The ablation phenomena of heat shield materials during reentry is comprised of a large number of complex chemical, thermal and physical processes. Three analyses were developed to predict heat shield performance, i.e., the total energy absorbed by an ablator. These analyses differ in the method of calculating the chemical generation term. When the chemical generation term is zero, the analysis is called frozen; when calculated from equilibrium thermodynamic considerations it is called equilibrium; when calculated using reaction rate information it is called non-equilibrium or kinetics analysis. These analyses have been described in previous chapters.

The analyses developed in this research are to describe the energy absorbed in both the decomposition and char zone of char forming ablators. The first two analyses, frozen and equilibrium, were used to compute the lower and upper bounds of the energy absorbed by a nylon-phenolic resin composite and a silicon elastomer composite. The non-equilibrium flow analysis was used to compute the energy absorbed in the decomposition zone and in the char zone of a nylon-phenolic resin composite only. This latter analysis was not

extended to the silicon elastomers for two reasons: One was the lack of good kinetic data on the silicon-carbon reactions and the other was the absence of reliable data on the components and composition resulting from the degradation of these polymers. Accurate information on the species resulting from the degradation of the polymers is essential to develop an accurate and realistic kinetics analysis. That is, to postulate all the important chemical reactions requires an intimate knowledge of the species that form during polymer degradation. This information was not available for the development of a silicone elastomer kinetics model.

Results of the energy absorbed as predicted by the three analyses are presented in this chapter. Of the three analyses, equilibrium and non-equilibrium analyses are very close to each other in the prediction of the total energy absorbed, while frozen predicts a total energy absorbed which is approximately a factor of 10 lower than the other two analyses.

Energy Absorption in an Ablator

We have discussed in previous chapters the foundation for the development of the three methods of analyses used in this research which are frozen, equilibrium and non-equilibrium. In this chapter, we are going to compare the results of the three analyses. We shall begin by explaining the principal energy absorbing mechanism in an ablator, both in the virgin plastic and in the char, and, to what extent

the three methods of analysis possess or lack these energy absorbing mechanisms. In addition, we will give an approximate temperature range at which these energy absorbing mechanisms become important contributing factors to the total energy absorbed in the ablator.

Energy Absorbing Mechanisms in the Virgin Plastic

In Chapter V we presented the data for the decomposition of phenolic-nylon by Sykes and Nelson (3). In Figure 5-3 we showed the thermogram of nylon-phenolic and phenolic microballoon decomposition with the total energy absorbed for each of these ablator components. Using Sykes et. al. (3) data, we calculated, for example, that at a surface recession velocity of 0.02 ft/sec, the gas mass flux generated by the decomposition of the virgin plastic for the non-equilibrium case is 0.4231 lb/ft^2-sec. From this data we also calculated the total heat absorbed by the decomposition process itself and found it to be approximately 91 BTU/ft^2-sec at the above mentioned surface recession velocity. The total energy absorbed in the virgin plastic, however, was approximately 99 BTU/ft^2-sec. The difference of 8 BTU/ft^2-sec is the heat absorbed by the sensible enthalpy of the plastic, and of the sensible enthalpy of the gas generated by the plastic decomposition.

In conclusion, we can say that the predominant energy absorbing mechanism in the plastic zone is that due to the heat absorbed by the decomposition process of the plastic

composites, and less than 10 percent to the sensible enthalpy gain of the plastic and the gas. In our analysis we did not segregate the decomposition process into a melting step and the actual decomposition or breakdown of the polymer. Rather, we lumped both together. However, by analyzing the data in Figure 5-3 we can see that, as expected, most of the heat absorbed is due to the breakdown of the polymer and 10-12 percent only is due to melting of the polymer.

Energy Absorbing Mechanisms in the Char

The energy absorbing mechanisms in the char are basically three. One is due to sensible enthalpy gain, the other is due to chemical reactions, and the third one is due to sublimation. In the case of the virgin plastic the energy absorbing mechanisms were independent of whether the analyses used were frozen, equilibrium or non-equilibrium since the treatment of the virgin plastic is independent of the method of analyses in the char zone. However, in the char zone for example, chemical reactions are a function of which method of analysis we used. Therefore, identification of the temperature range at which each mechanism becomes important is much more difficult.

First Energy Absorbing Mechanism: Of the three energy absorbing mechanisms, two are related to chemical or phase changes. The energy absorbing mechanism in the frozen flow

case is that associated with the heat absorbed by the gas (transpiration cooling) in conjunction with the heat absorbed by the solid carbon matrix (the char). Figure 6-1 shows a plot of the total energy absorbed as calculated by frozen, equilibrium and non-equilibrium case. As we can see from this plot, the total amount of energy absorbed by the frozen flow (transpiration cooling and sensible enthalpy gain of the char) is 1500 BTU/ft^2-sec, while for non-equilibrium and equilibrium, the energy absorbed is 18300 and 19300 BTU/ft^2-sec, respectively. We can see from this plot that transpiration cooling plays a very small part in the total amount of energy absorbed in the char. Examination of the data of Figure 6-1 shows that sensible enthalpy gain of the gas and the solid matrix is an order of magnitude lower than that absorbed by chemical reactions.

Second Energy Absorbing Mechanism: The second energy absorbing mechanism is that due to the heat absorbed by chemical reactions. This is best illustrated by comparing the difference in energy absorbed between equilibrium and frozen analyses. Figure 6-2 illustrates this difference. This large difference is due to the highly endothermic chemical reactions that take place in the char zone. If this were not the case, the difference would not be that pronounced. Equilibrium analysis, however, is an ideal model of the reactions, and comparison of frozen and equilibrium analyses throws little light as to when reactions, in practice, become

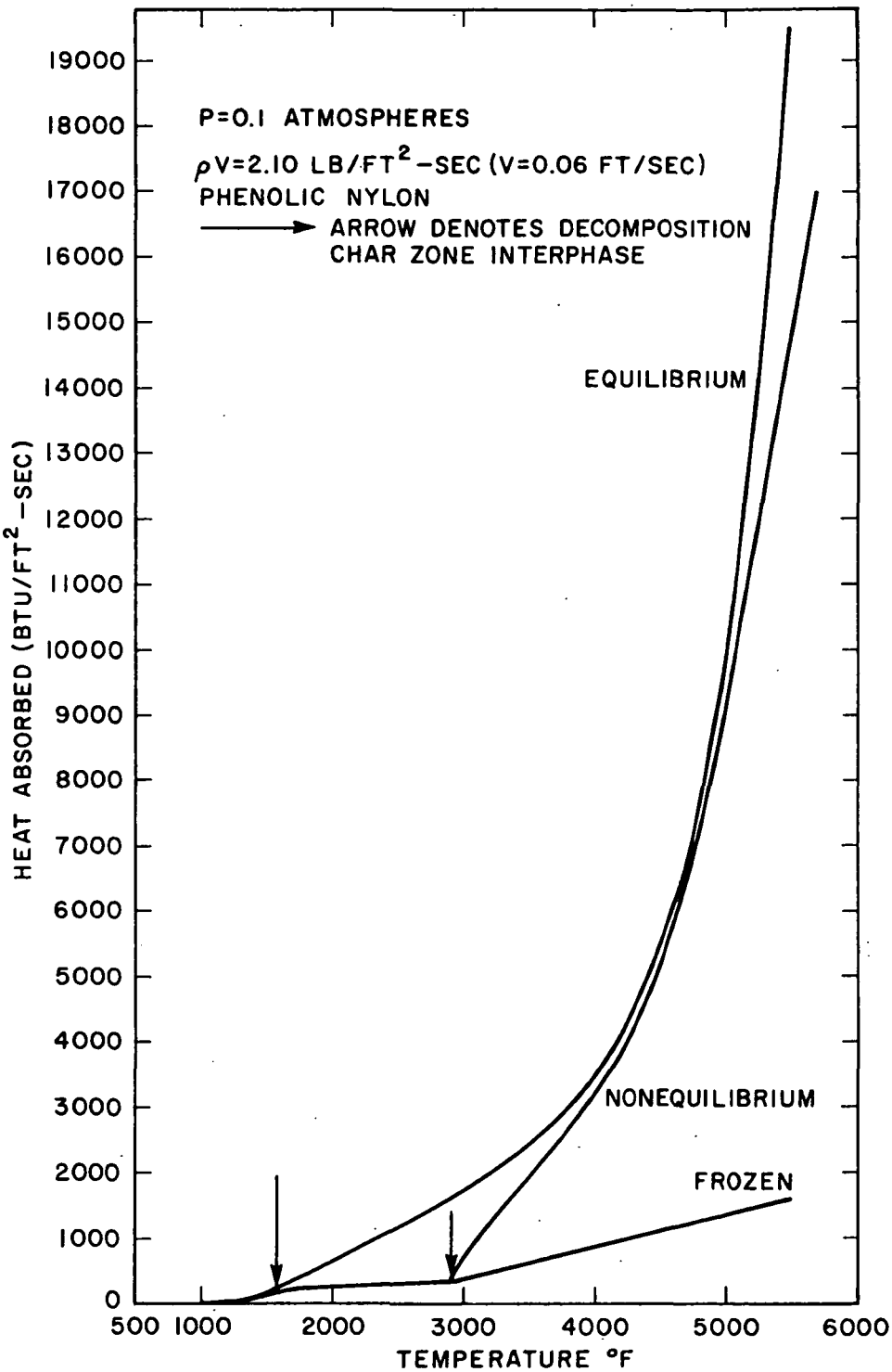

Figure 6-1. A Comparison of the Rate of Heat Absorbed Frozen, Non-equilibrium and Equilibrium Analyses at a Pressure of 0.1 Atm. and a Total Mass Flux of 2.1 lb/ft^2-sec., (v=0.06 ft/sec).

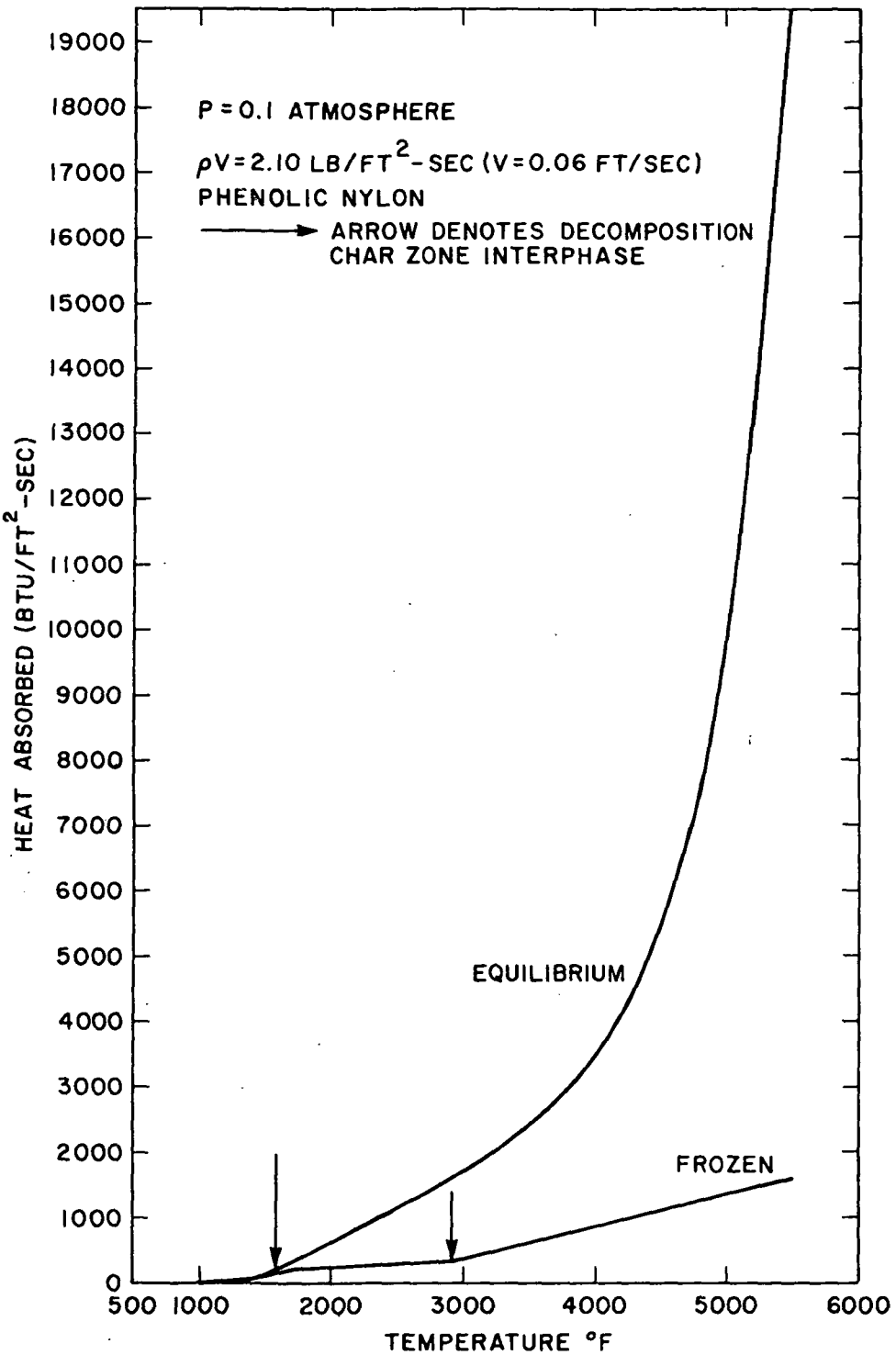

Figure 6-2. A Comparison of the Rate of Heat Absorbed Between Frozen and Equilibrium as a Function of Ablator Temperature at 0.1 atmosphere and a Total Mass Flux of 2.10 lb/ft^2-sec. (v=0.06 ft/sec).

important energy absorbing mechanisms. However, a comparison of frozen and non-equilibrium analyses or kinetic analysis should show the difference. For example, Figure 6-3 compares the total energy absorbed between frozen and non-equilibrium at a total mass flux of 2.10 lb/ft^2-sec. Figure 6-4 compares the two analyses also, but at a mass flux of 0.7 lb/ft^2-sec. At the higher mass flux of 2.10, the decomposition/char zone temperature interface is approximately 2900° F, where the gases start reacting quickly as is evident by the sharp difference in slope. At the lower mass flux of 0.7 where the decomposition/char zone temperature interface is lower ($\sim$2250°F), the gases also start reacting quickly. The studies of April and Pike et. al. (2) also showed that reactions become important energy absorbing mechanisms at temperatures above 2000°F. To illustrate this point we show Figures 6-5, 6-6, 6-7 and 6-8. Figure 6-5 compares the temperature profiles for equilibrium,non-equilibrium and frozen flow at an assumed front surface temperature of 1500° F and an imposed mass flux of 0.05 lb/ft^2-sec at the back surface of the char. This figure shows that both the frozen and non-equilibrium curves, for all practical purposes, are indistinguishable. This is because at the low temperatures of 1500°F the gases remain essentially frozen as the temperature is not high enough for chemical reactions to begin. Figure 6-6, on the other hand, shows that for an assumed front surface temperature of 2000°F the non-equilibrium and frozen flow analyses differ. Figures 6-7 and 6-8 which are

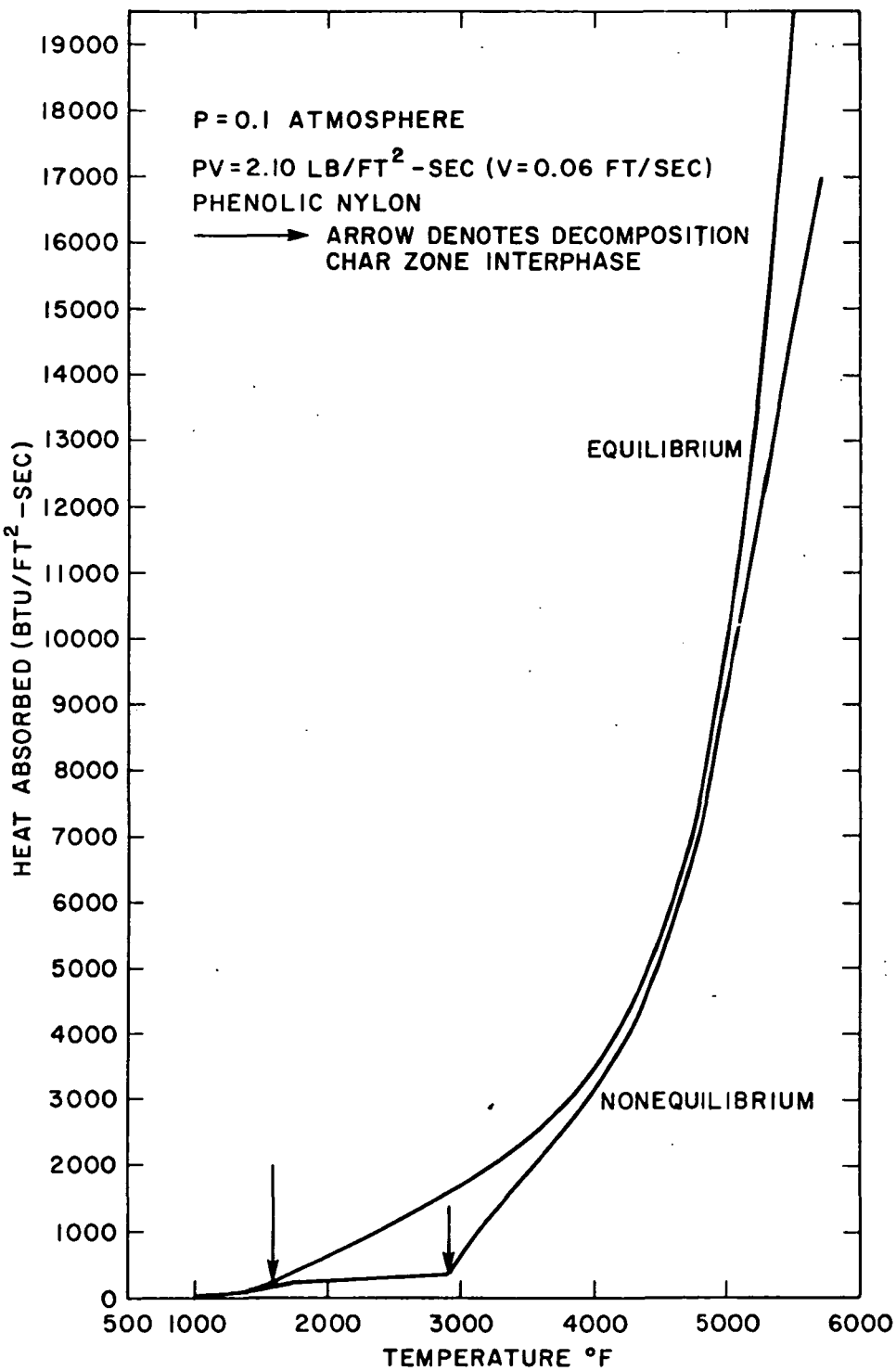

Figure 6-3. A Comparison of the Rate of Heat Absorbed Between Frozen and Non-equilibrium at a Pressure of 0.1 Atmospheres and a Total Mass Flux of 2.10 lb/ft^2-sec. (v=0.06 ft/sec).

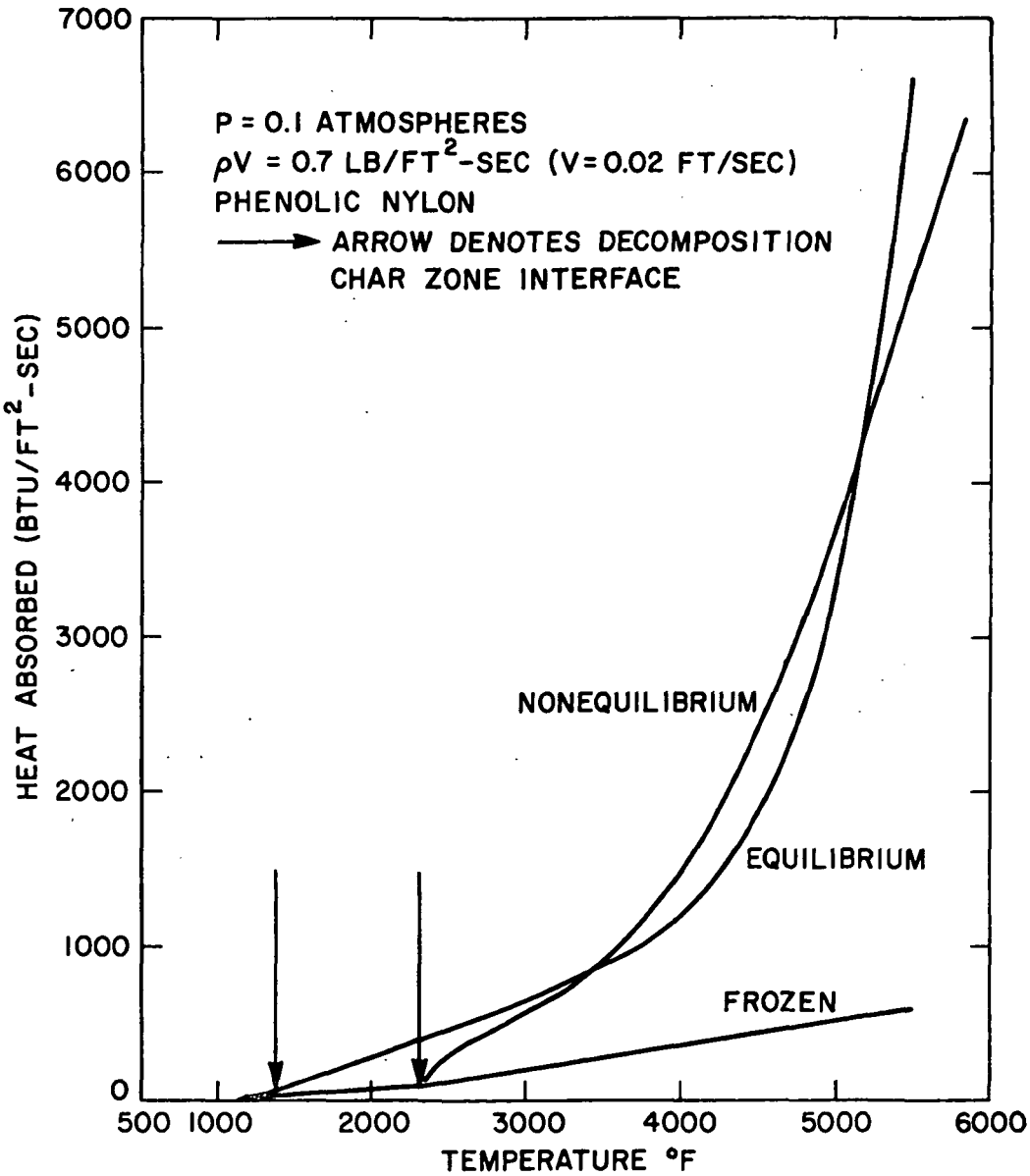

Figure 6-4. A Comparison of the Rate of Heat Absorbed for Frozen, Equilibrium and Non-equilibrium Analyses at a Pressure of 0.1 Atmospheres and a Total Mass Flux of 0.7 lb/ft^2-sec. (v=0.02 ft/sec).

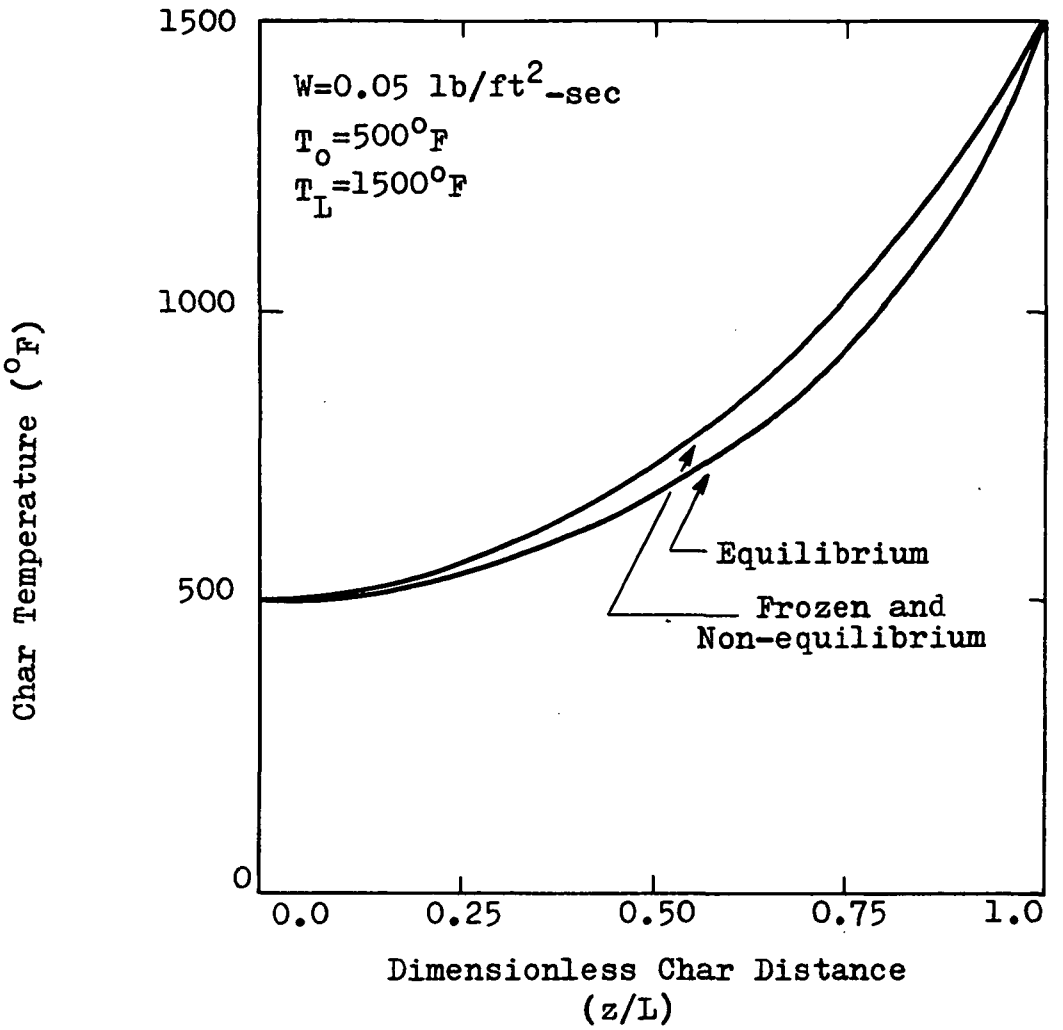

Figure 6-5. Temperature Profile for the Frozen, Equilibrium, and Non-equilibrium Flow of Pyrolysis Gases Through the Char Zone of a Nylon-Phenolic Resin Ablator at a Front Surface Temperature of 1500°F as Reported by April (1) and Pike et. al. (2).

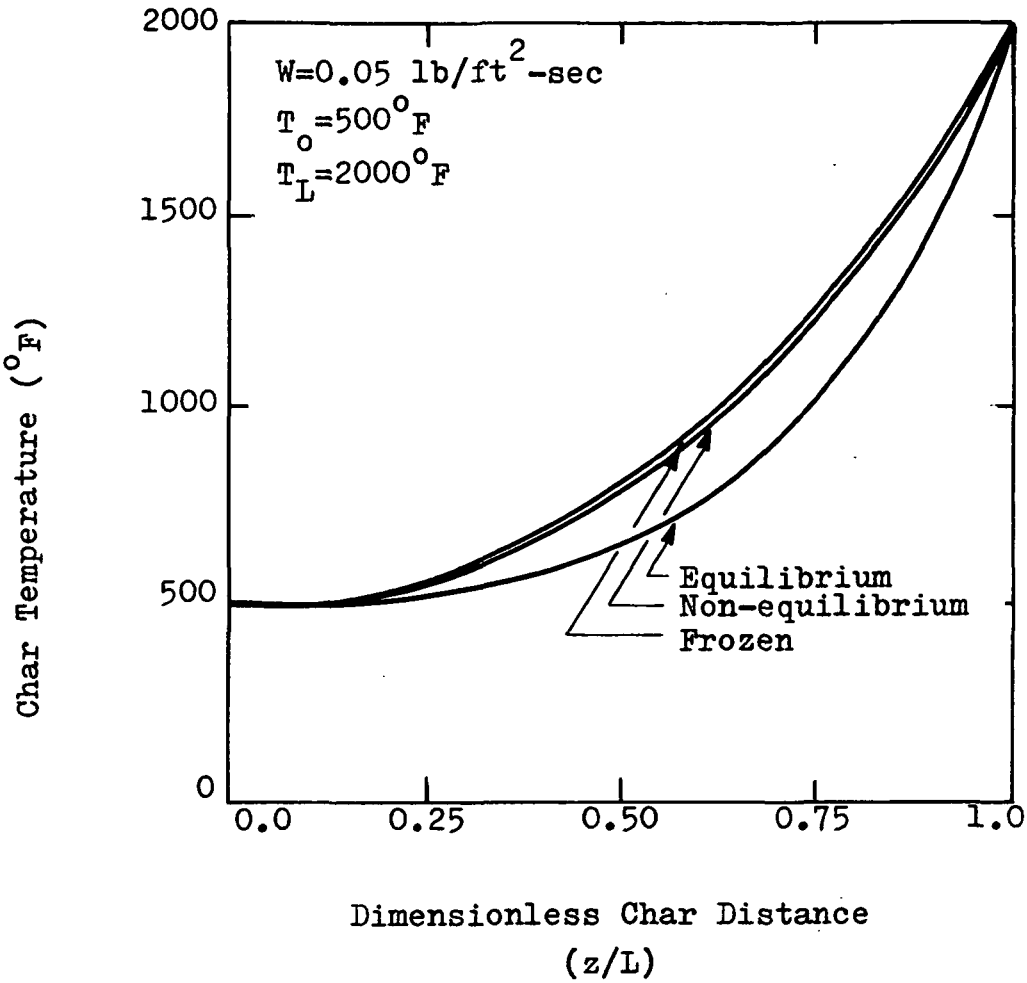

Figure 6-6. Temperature Profile for the Frozen, Equilibrium, and Non-equilibrium Flow of Pyrolysis Gases Through the Char Zone of a Nylon-Phenolic Resin Ablator at a Front Surface Temperature of 2000°F as Reported by April (1) and Pike et. al. (2).

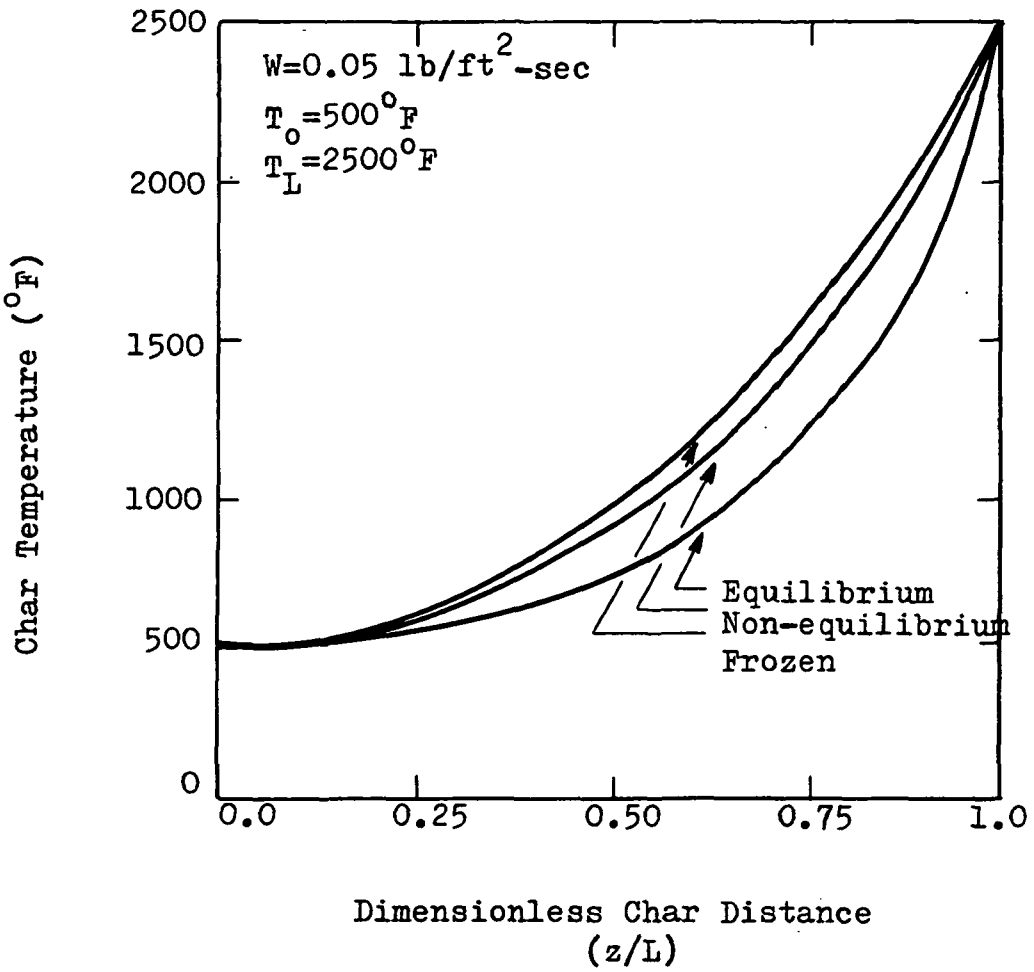

Figure 6-7. Temperature Profile for the Frozen, Equilibrium, and Non-equilibrium Flow of Pyrolysis Gases Through the Char Zone of a Nylon-Phenolic Resin Ablator At a Front Surface Temperature of 2500°F as Reported by April (1) and Pike et. al. (2).

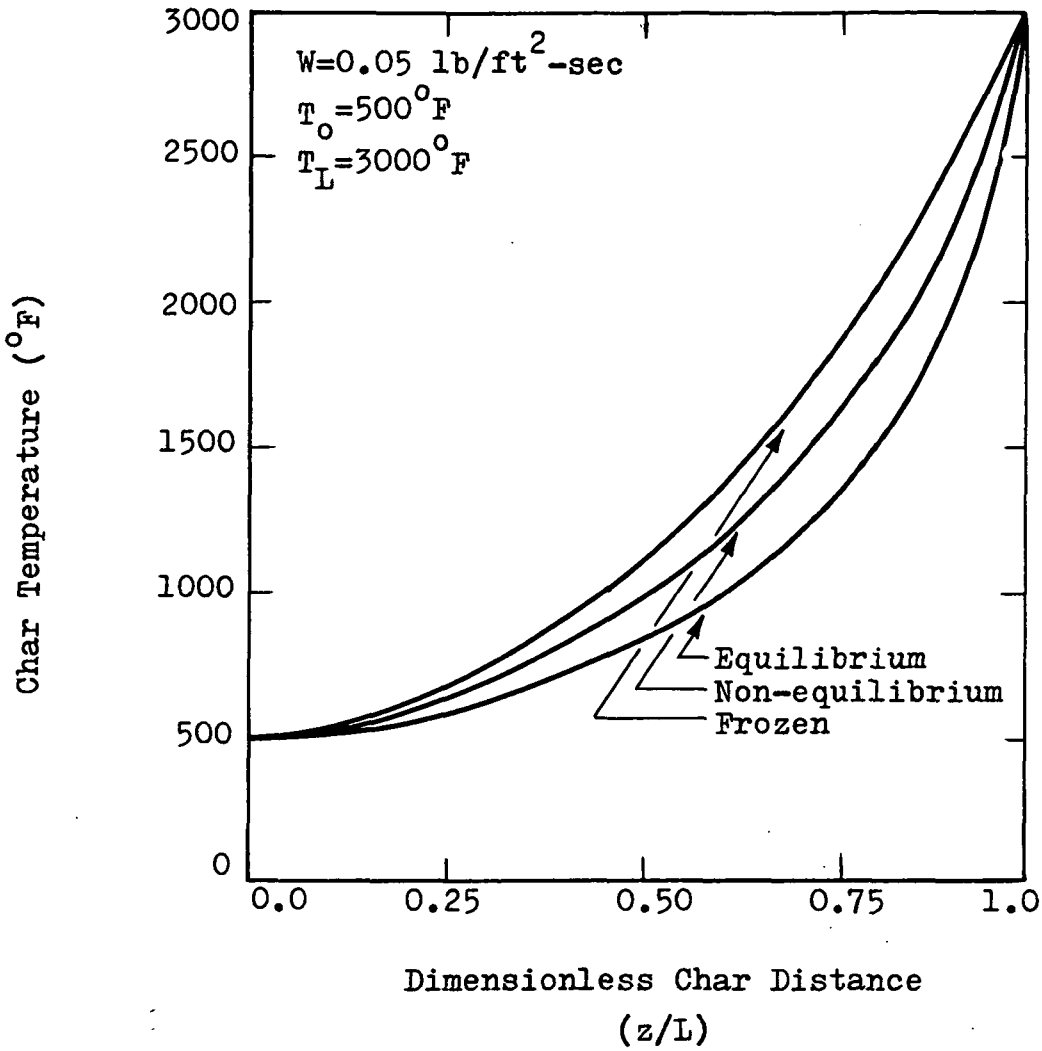

Figure 6-8. Temperature Profile for the Frozen, Equilibrium, and Non-equilibrium Flow of Pyrolysis Gases Through the Char Zone of a Nylon-Phenolic Resin Ablator at a Front Surface Temperature of 3000°F as Reported by April (1) and Pike et. al. (2).

plots for 2500 and 3000°F front surface temperature, respectively, further illustrate this point. Therefore, we can state that kinetic reactions become important energy absorbing mechanisms above 2000°F.

Third Energy Absorbing Mechanisms: In Figure 6-9 a comparison of the total energy absorbed versus temperature for equilibrium and non-equilibrium with the behavior of the carbon/gas ratio superimposed, is shown. As shown in this figure, the carbon/gas ratio for both analyses remain practically constant up to a temperature of 4800°F. At this temperature the ratios begin to decrease, but with equilibrium decreasing at a faster rate. The reduction in carbon/gas ratio is due in part to a mechanism known as sublimation, where the solid carbon becomes a gas. It is this mechanism (i.e., sublimation) which accounts for the divergence of the two analyses at the higher energy spectrum.

In conclusion, we have shown that there are three principal energy absorbing mechanisms in the char: transpiration cooling which is practically independent of temperature, except for the temperature effect on heat capacity; a reaction kinetic regime which begins at temperatures above 2000°F; and a sublimation region which begins at temperatures of about 4800°F and above.

A Comparison of the Decomposition/Char Zone Boundary Conditions Between Equilibrium and Non-Equilibrium Analyses.

As we saw in Figure 6-1, the decomposition-char zone

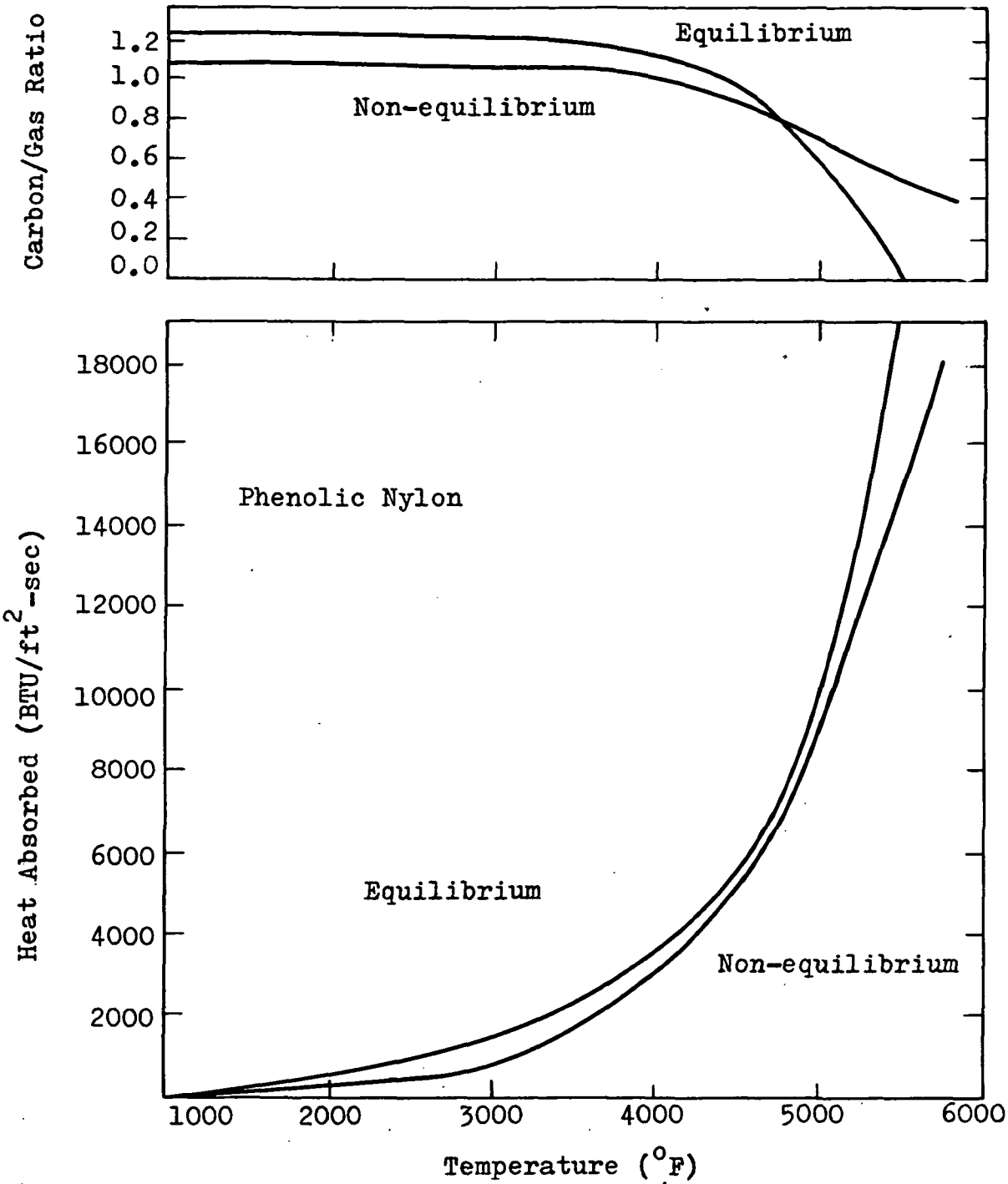

Figure 6-9. A Comparison of Carbon/Gas Ratio for the Equilibrium and Non-equilibrium Analyses Illustrates the Effect of the Divergence on the Two Curves Above 4800^{o}F.

interface temperatures are different. For non-equilibrium this temperature is determined when the density of the degrading plastic is equal to the density of the char. For phenolic-nylon the density of the virgin, undegraded polymer is approximately 35 lb/ft^3. As the polymer is heated the virgin plastic begins to degrade and looses mass (as a gas) but not volume. Therefore, the density of the polymer begins to decrease as we integrate forward towards the char front.

There is a point at which the polymer density becomes equal to the char density, and we call this the decomposition/char zone interface. For phenolic-nylon this char density has been experimentally determined to be 13 lb/ft^3. Therefore when the polymer density reaches 13 lb/ft^3, the program enters the char zone and activates the kinetic model.

In the case of the equilibrium analysis we cannot use the density of 13 lb/ft^3 as the criteria for defining the decomposition/char zone interface. If we were to use this criteria we would find a discontinuity at the boundary between the two regions. This discontinuity would be in the mass flux of the gas predicted by the polymer decomposition kinetics and that predicted by the equilibrium analysis. To avoid this discontinuity we define the interface at that point where the mass flux from the decomposition of the polymer equals that required by chemical equilibrium. Since the equilibrium composition of a mixture is only a function

of temperature, pressure and elemental composition, we can determine a priori, for phenolic-nylon, what the equilibrium mass flux has to be as a function of temperature for every surface recession velocity. Having done this, the computer program checks at every integration step whether or not the mass flux generated by polymer degradation is equal to that required by equilibrium considerations. When these conditions are met for equilibrium analysis, we define this as the decomposition/char zone interface. When the integration procedure enters the char, the gases are assumed to be in chemical equilibrium and the program continues to integrate the equations of change under this assumption.

It is interesting to note at this point that because equilibrium tends to overpredict the carbon/gas ratio as compared to actual experiments, the mass flux of gas formed by the degradation of the polymer required to match equilibrium conditions, is small. Therefore, as shown in Table 6-1 (P=0.1 atm.) we see that at the end of the decomposition zone or beginning of the char zone, the gas mass flux for equilibrium is smaller than for non-equilibrium. As we see the gas mass flux for non-equilibrium is approximately 61.6 percent greater than for equilibrium for a total mass flux ρv, of 0.7 lb/ft^2-sec., (or a surface recession velocity, v, of 0.02 ft/sec). At a total mass flux of 2.10 (v=0.06 ft/sec) the gas mass flux for non-equilibrium is 61.4 percent greater. Table 6-2 is similar to 6-1 but the conditions are those for a pressure of 1 atmosphere. At a

TABLE 6-1 : Comparison of Equilibrium and Non-Equilibrium Analysis Gas Mass Flux at the Back Surface of the Char, at Various Surface Recession Velocities* and at a Pressure of 0.1 atmosphere.

Surface Recession Velocities (ft/sec)	Equilibrium Analysis (lb/ft^2-sec)	Non-Equilibrium Analysis (lb/ft^2-sec)
0.02	0.2613	0.4231
0.03	0.3922	0.6348
0.04	0.5243	0.3463
0.05	0.6537	1.058
0.06	0.7865	1.2694

* Total Mass Flux is defined as the product of the initial density of the virgin polymer times the surface recession velocity. Since the density of the virgin polymer is approximately 35 lb/ft^3, the total mass flux at a surface recession velocity of 0.02 ft/sec is 0.7 lb/ft^2-sec.

TABLE 6-2: Comparison of Equilibrium and Non-equilibrium Analysis Gas Mass Fluxes at the Back Surface of the Char Zone, at Various Surface Recession Velocities and a Pressure of 1.0 atmosphere.

Surface Recession Velocity (ft/sec)	Equilibrium Analysis (lb/ft^2-sec)	NonEquilibrium Analysis (lb/ft^2-sec)
0.02	0.2592	0.4231
0.03	0.3911	0.6343
0.04	0.5248	0.8463
0.05	0.6552	1.658
0.06	0.7831	1.2694

surface recession velocity of 0.02 ft/sec non-equilibrium gas mass flux is 63.2 percent greater than for equilibrium. Therefore, the gas mass flux at the back surface of the char is always greater for non-equilibrium than it is for equilibrium. It is important that we keep in mind this fact, because it bears heavily on explaining the behavior of the equilibrium and non-equilibrium heat curves plots shown in this chapter.

Table 6-3 and 6-4 show the decomposition/char zone temperature interface at various surface recession velocities for 0.1 and 1.0 atmospheres respectively. We see in both of these tables that the temperature of the interface is lower for equilibrium than for non-equilibrium. This is expected since as we explained before, the extent of polymer degradation required to meet the gas mass flux at the equilibrium boundary conditions is less than for non-equilibrium. For example, at a surface recession velocity of 0.02 ft/sec. the temperature required to meet the equilibrium boundary conditions is 1386.9^{o}F as is shown in Table 6-3. This is 929^{o}F less than for non-equilibrium. In comparing the two tables we can also notice that the temperature at the interface is not affected by pressure. This is expected because the depolymerization kinetics are not a function of pressure, and as we said before, the plastic will keep degrading until it reaches a density of 13 lb/ft^{3}, which is the density of the char. On the other hand, pressure slightly affects the interface temperature in all the cases examined for equili-

TABLE 6-3: Comparison of Equilibrium and Non-Equilibrium Analysis Temperatures at the Back Surface of the Char Zone, at Various Surface Recession Velocities and a Pressure of 0.1 atmosphere.

Surface Recession Velicities (ft/sec)	Equilibrium Analysis (^{o}F)	Non-Equilibrium Analysis (^{o}F)
0.02	1386.9	2315.9
0.03	1450.7	2514.6
0.04	1499.9	2664.5
0.05	1537.2	2789.1
0.06	1570.9	2894.7

TABLE 6-4: Comparison of Equilibrium and Non-Equilibrium Analysis Temperatures at the Back Surface of the Char Zone, at Various Surface Recession Velocities and a Pressure of 1.0 atmosphere.

Surface Recession Velocities (ft/sec)	Equilibrium Analysis (^{o}F)	Non-Equilibrium Analysis (^{o}F)
0.02	1384.2	2315.9
0.03	1449.8	2514.6
0.04	1499.9	2664.5
0.05	1538.1	2789.1
0.06	1571.8	2894.7

brium; the difference varying from a high of 2.7°F at v=0.02 ft/sec to a low of 0.09°F at v=0.06 ft/sec (see Tables 6-3 and 6-4). It should also be noted that the interface temperature monotonically increases with surface recession velocity for both equilibrium and non-equilibrium. This should be expected since the higher the surface recession velocity (or the total mass flux), that is, the more severe the conditions that we are trying to simulate are, then the steeper the temperature profile should be inside the ablator.

Table 6-5 and 6-6 show the chemical composition of the gases at the char back end for 0.1 and 1 atmospheres respectively. Each shows in addition one species composition at two surface recession velocities. As we can see in Table 6-5, the species composition for equilibrium varies depending on whether the surface recession velocity v, is 0.02 or 0.06 ft/sec. This is not because the compositions are a direct function of surface recession velocity, but because the compositions are a function of back surface temperature, which in turn is a function of surface recession velocity. (See Tables 6-3 and 6-4 which show how surface recession velocities affect decomposition/char zone temperature interface). As we examine Table 6-5 and 6-6, we can notice that the equilibrium compositions are slightly different at the two surface recession velocities, but yet do not vary for non-equilibrium. The same is true when we compare them at both 0.1 and 1.0 atmospheres respectively. Unfortunately, this should not be so, but as we have said

TABLE 6-5: A Comparison of Species Composition at the Back Surface of the Char for Equilibrium and Non-Equilibrium Analyses at a Surface Recession Velocity of 0.02 and 0.06 ft/sec and a Pressure of 0.1 Atmosphere.

	Equilibrium (mole fraction)		Non-Equilibrium (mole fraction)	
	FT/SEC: v=0.02	v=0.06	FT/SEC: v=0.02	v=0.06
CH_2	-	-	-	-
CH_3	-	-	-	-
CH_4	0.0041	0.0008	0.0804	0.0804
C_2H	-	-	-	-
C_3H	-	-	-	-
C_4H	-	-	-	-
C_2H_2	-	-	0.0480	0.0480
C_2H_4	-	-	0.0450	0.0450
C_2H_6	-	-	0.0070	0.0070
C_6H_6	-	-	0.0107	0.0107
C_6H_6O	-	-	0.0794	0.0794
CN	-	-	-	-
CO	0.2105	0.2153	0.0480	0.0480
CO_2	0.0015	0.0001	0.0338	0.0338
H	-	-	-	-
H_2	0.7379	0.7419	0.4891	0.4891
H_2O	0.0041	0.0003	0.1014	0.1014
OH	-	-	-	-
M_2	0.0419	0.0416	0.0572	0.0572
MH_3	-	-	-	-
HCN	-	-	-	-
O	-	-	-	-
C_3	-	-	-	-
$C_{(s)}$*	1.227	1.215	1.062	1.062

*The symbol $C_{(s)}$ represents the moles of carbon per mole of gas.

TABLE 6-6: A Comparison of Species Composition at the Back Surface of the Char for Equilibrium and Non-Equilibrium Analyses at a Surface Recession Velocity of 0.02 and 0.06 ft/sec and a Pressure of 1.0 Atmosphere.

	Equilibrium (mole fraction)		Non-Equilibrium (mole fraction)	
	FT/SEC:		FT/SEC:	
	v=0.02	v=0.06	v=0.02	v=0.06
CH_2	-	-	-	-
CH_3	-	-	-	-
CH_4	0.0366	0.0151	0.0804	0.0804
C_2H	-	-	-	-
C_3H	-	-	-	-
C_4H	-	-	-	-
C_2H_2	-	-	0.0480	0.0480
C_2H_4	-	-	0.0450	0.0450
C_2H_6	-	-	0.0070	0.0070
C_6H_6	-	-	0.0107	0.0107
C_6H_6O	-	-	0.0794	0.0794
CN	-	-	-	-
CO	0.1775	0.2071	0.0480	0.0480
CO_2	0.0110	0.0025	0.0338	0.0338
H	-	-	-	-
H_2	0.6964	0.7234	0.4891	0.4891
H_2O	0.0335	0.0094	0.1014	0.1014
OH	-	-	-	-
N_2	0.0449	0.0425	0.0572	0.0572
NH_3	0.0001	-	-	-
HCN	-	-	-	-
O	-	-	-	-
C_3	-	-	-	-
$C_{(s)}$*	1.320	1.24	1.062	1.062

* The symbol $C_{(s)}$ represents the moles of carbon per mole of gas.

before, there is no known method available to predict non-equilibrium composition of degrading gases directly from the polymer degradation. Therefore, as a compromise we had to use available experimental data and come up with the best estimate of the species composition at the back surface of the char zone. Therefore, for all non-equilibrium cases run, varying the surface recession velocity and the pressure, we used the same chemical composition.

A Comparison of the Total Energy Absorbed for Equilibrium, Non-Equilibrium and Frozen Flow Analysis for Phenolic-Nylon

In developing the three methods of analysis, frozen, equilibrium and non-equilibrium, the purpose of this research was to determine the effects that each method of analysis had on the predicted value of the total energy absorbed in an ablator. Before we get into the details of analyzing the cases examined in this research, it is worthwhile to briefly summarize how the approach of our analysis evolved and how it differs from the initial research of April (1) and Pike et. al. (2). The initial research that was done involved looking at the char zone only. In this initial stage of development a mass flux was assumed at the back surface of the char, and in addition a front surface temperature of the char was assumed as a parameter (see Figures 6-5 through 6-8). The back surface of the char was always assumed to be at 500°F. Therefore, in comparing frozen, equilibrium and non-equilibrium calculations, the boundary conditions at the back end of the char were always the same in terms of

temperature and mass flow.

In this research we went a step further and coupled the plastic zone to the decomposition zone. The result of this coupling makes the analysis of the heat curves more complex. Basically, because this coupling, as we have seen in Tables 6-1 through 6-6, has resulted in boundary conditions which are not the same for equilibrium and non-equilibrium both in terms of temperature and mass flux. As a result when we look at the total energy absorbed we have to take these differences into consideration in analyzing the values of the total energy absorbed.

In Figures 6-10 through 6-16 we present the comparison of the total energy absorbed for the three methods of analysis at two pressure levels. As we examine these curves we notice that the non-equilibrium curves cross the equilibrium curves for all cases examined, except one. The reason for this crossover is obvious when we look at the gas mass flux at the back surface of the char. As we have already shown, the gas mass flux for non-equilibrium is about 60 percent greater than for equilibrium. The crossover occurs because at temperatures above 2000^{o}F the total rate of heat absorbed by the non-equilibrium gases is initially greater than for equilibrium. This is not because the non-equilibrium analysis chemical reactions are more endothermic than those for chemical equilibrium, but because the higher gas mass flux of the non-equilibrium analysis coupled with the heat absorbed by the kinetic reactions is sufficient to overcome the

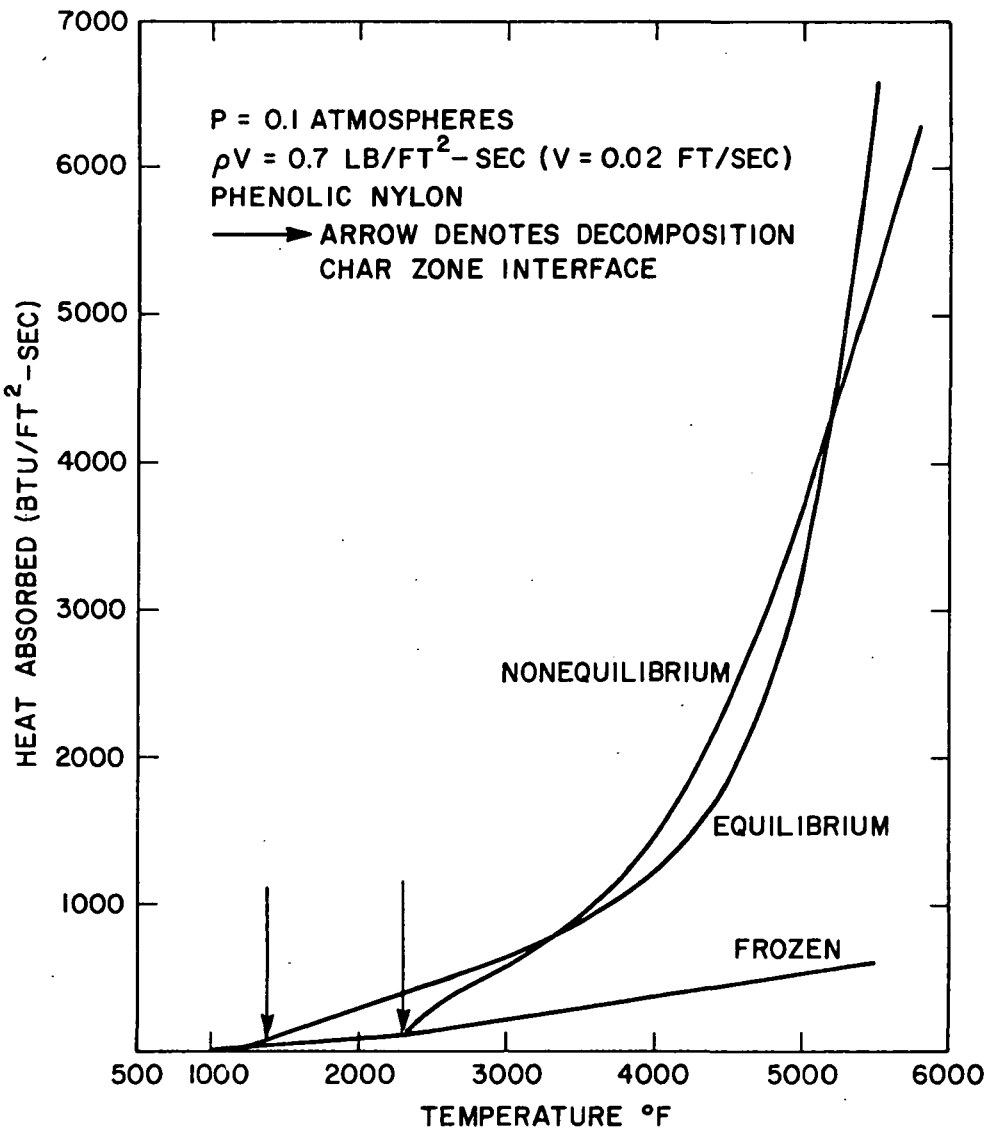

Figure 6-10. A Comparison of the Rate of Heat Absorbed for Frozen, Equilibrium and Non-equilibrium Analyses at a Pressure of 0.1 atm and a Mass Flux of 0.7 lb/ft^2-sec (v=0.02 ft/sec).

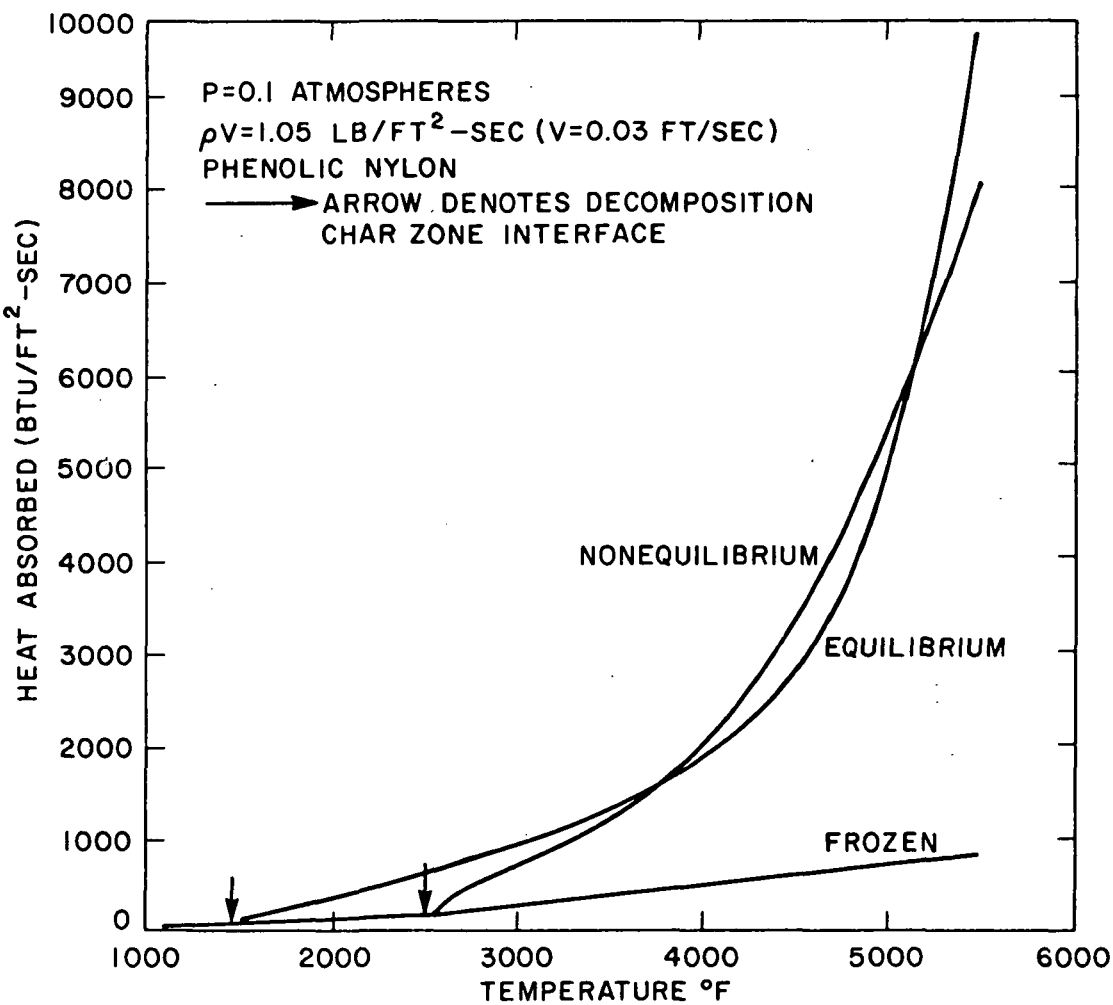

Figure 6-11. A Comparison of the Rate of Heat Absorbed for Frozen, Equilibrium and Non-equilibrium Analyses at a Pressure of 0.1 atm and a Total Mass Flux of 1.05 lb/ft^2/sec).

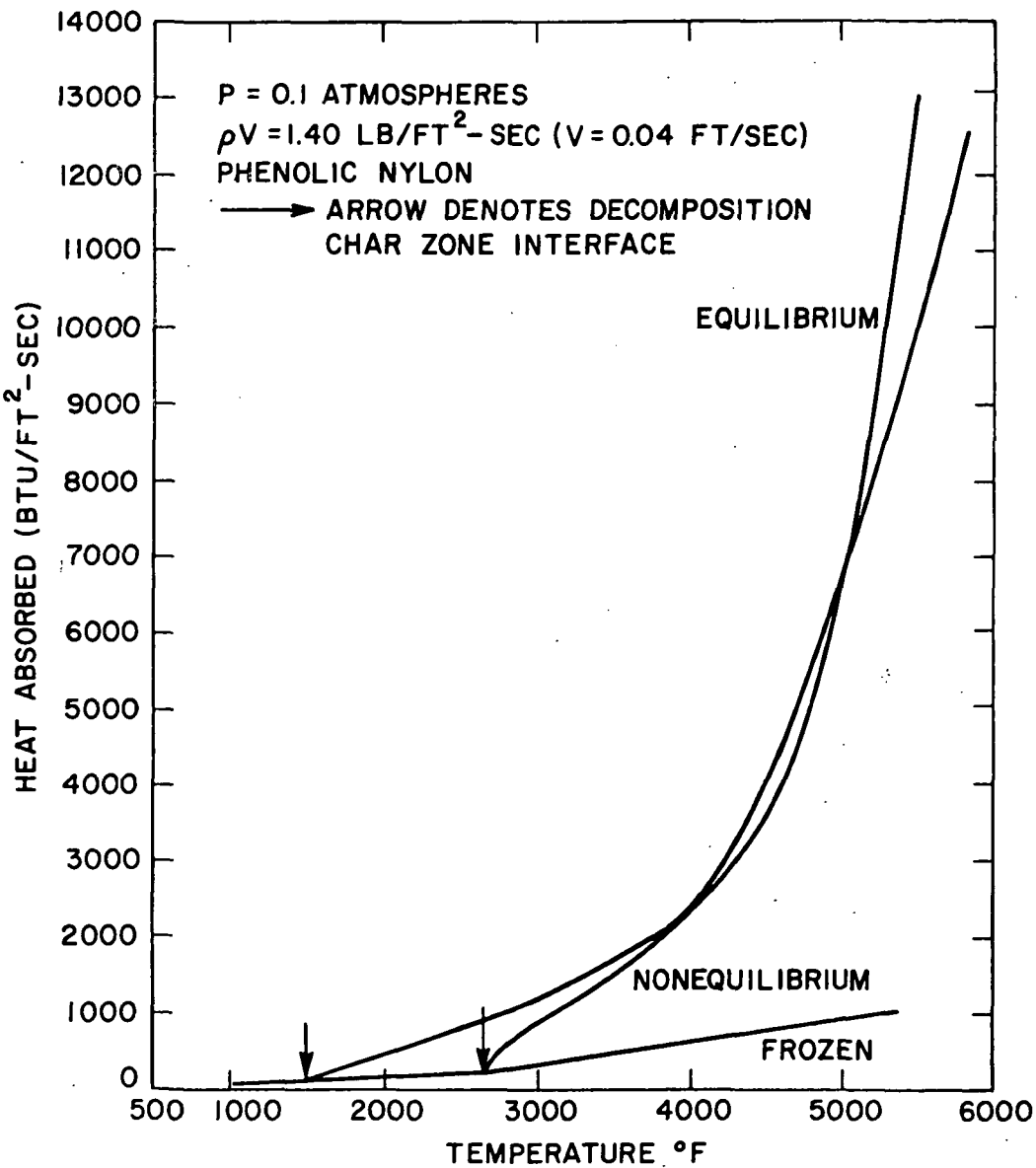

Figure 6-12. A Comparison of the Rate of Heat Absorbed for Frozen, Equilibrium and Non-equilibrium Analyses at a Pressure of 0.1 atm and a Total Mass Flux of 1.40 lb/ft^2-sec, (v=0.04 ft/sec).

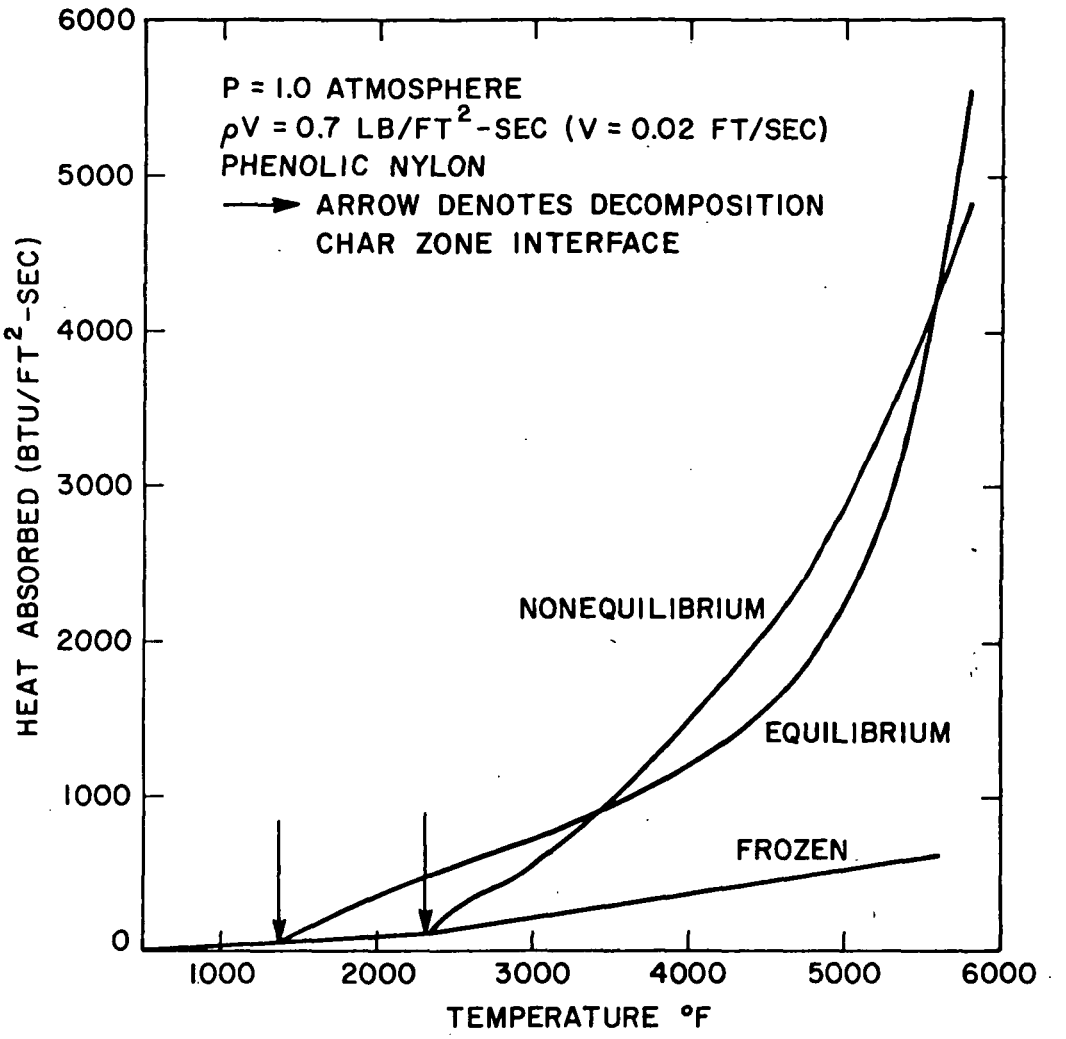

Figure 6-13. A Comparison of the Rate of Heat Absorbed for Frozen, Equilibrium and Non-equilibrium Analyses at a Pressure of 1.0 atm and a Total Mass Flux of 0.7 lb/ft^2-sec, (v=0.02 ft/sec).

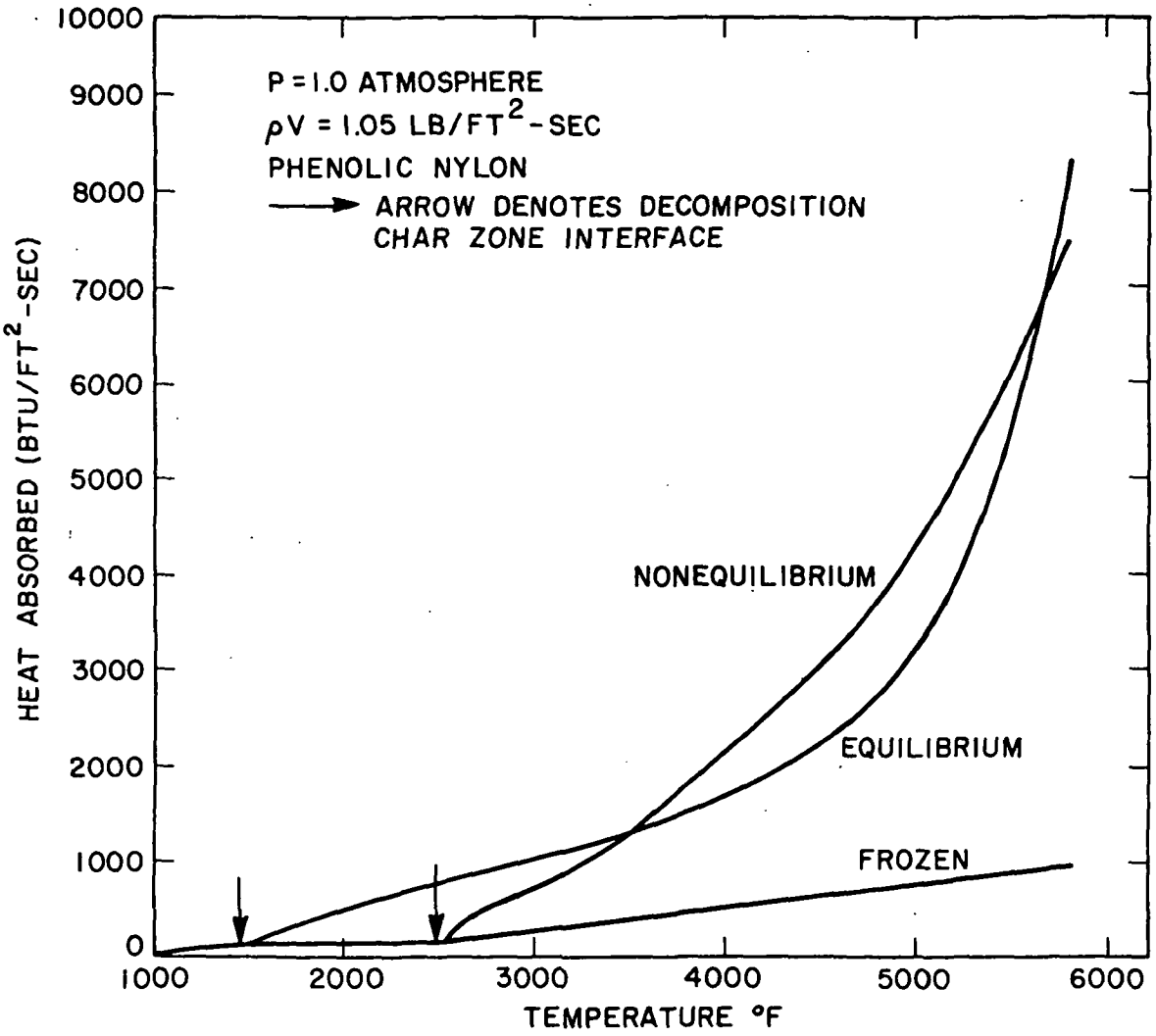

Figure 6-14. A Comparison of the Rate of Heat Absorbed for Frozen, Equilibrium and Non-Equilibrium Analyses at a Pressure of 1.0 atm and a Total Mass Flux of 1.05 lb/ft^2-sec, (v=0.03 ft/sec).

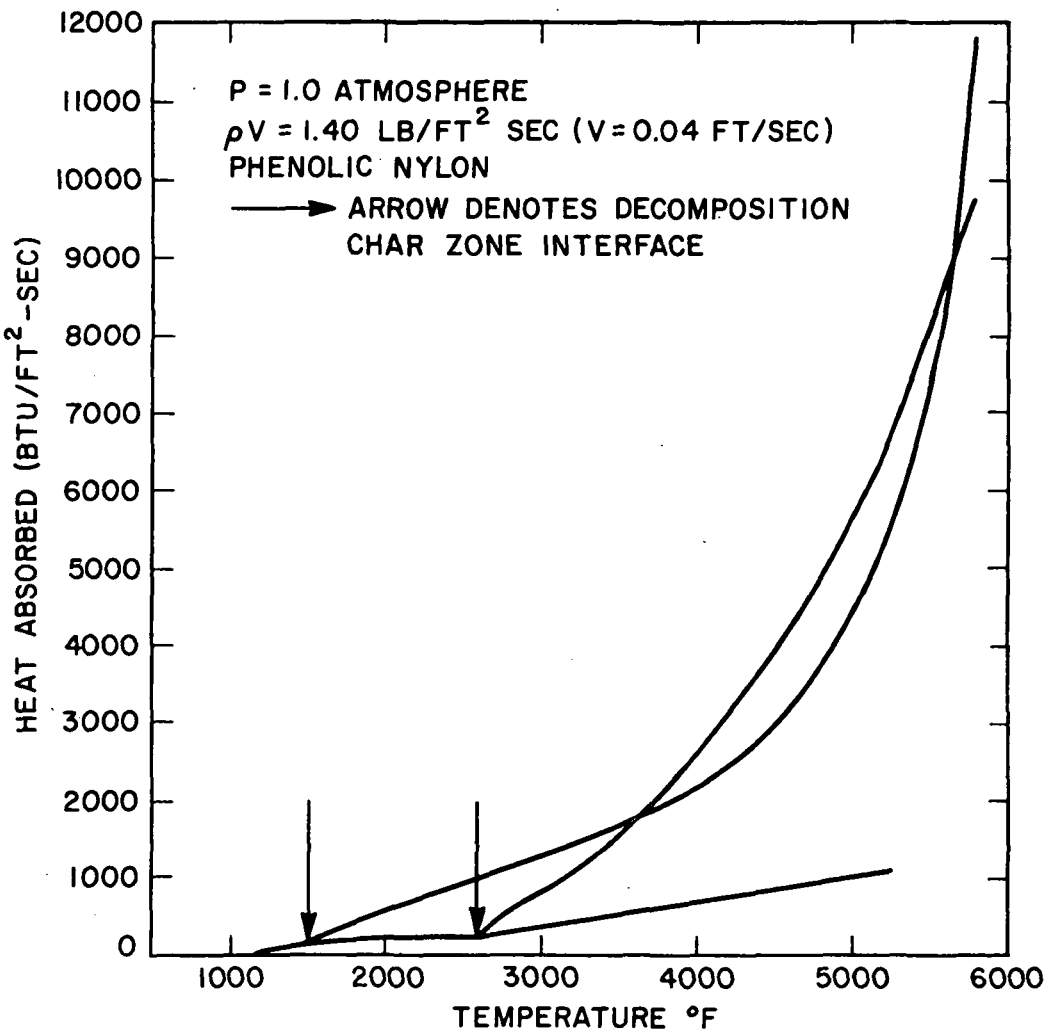

Figure 6-15. A Comparison of the Rate of Heat Absorbed for Frozen, Equilibrium and Non-equilibrium Analyses at a Pressure of 1.0 atm and a Total Mass Flux of 1.4 lb/ft^2-sec, (v=0.04 ft/sec).

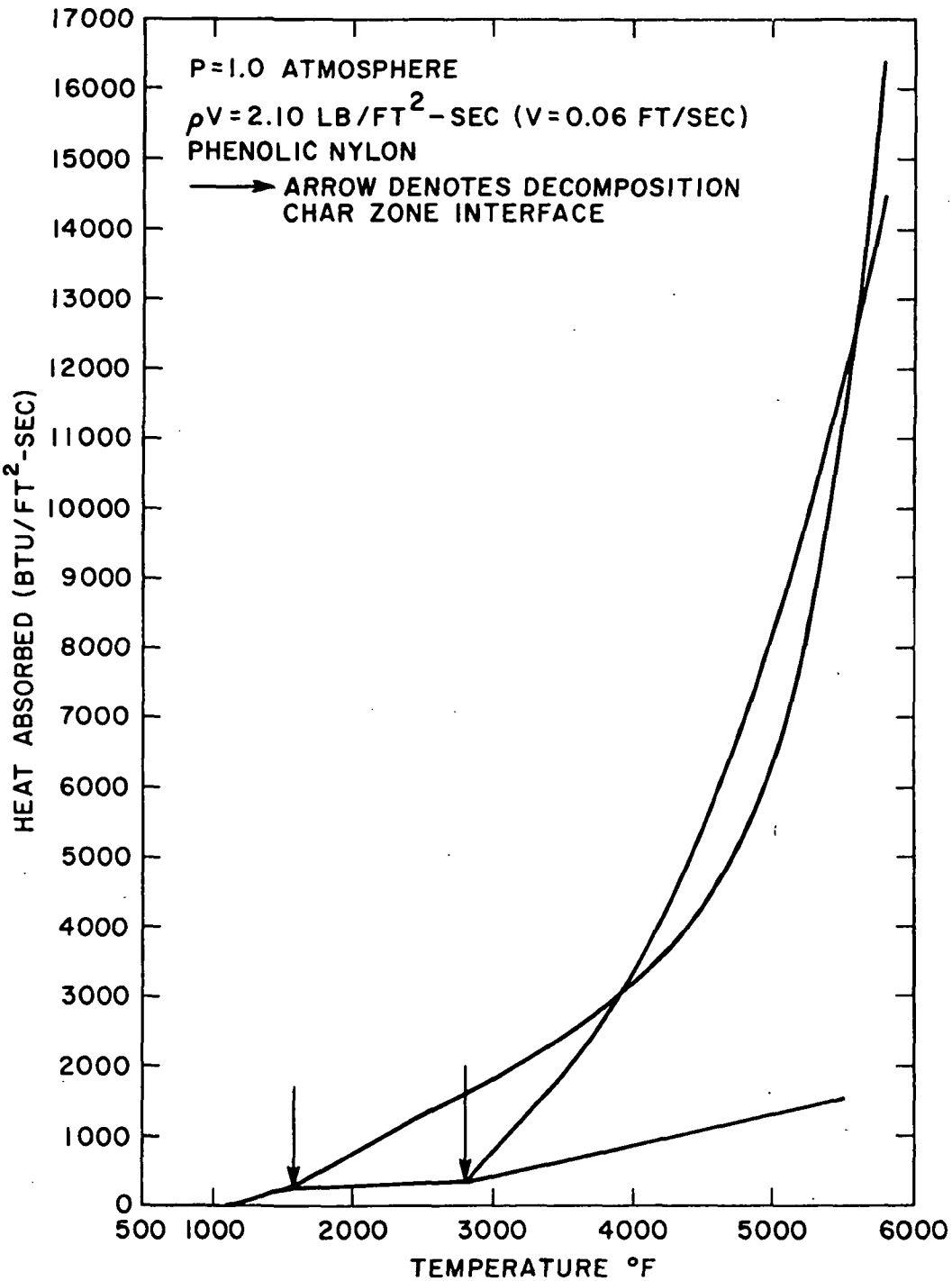

Figure 6-16. A Comparison of the Rate of Heat Absorbed for Frozen, Equilibrium and Non-equilibrium Analyses at a Pressure of 1.0 atm and a Total Mass Flux of 2.1 lb/ft^2-sec, (v=0.06 ft/sec).

much lower mass flux rate of chemical equilibrium. As the temperature increases, however, the carbon in the chemical equilibrium model begins to react into the gas phase, increasing the equilibrium gas mass flux. As this same mass flux increases, the equilibrium heat absorbed finally overtakes the non-equilibrium curve and surpasses it.

A Comparison of the Total Heat Absorbed for Frozen, Equilibrium and Non-Equilibrium at 0.1 Atmosphere

The results for frozen, equilibrium and non-equilibrium analyses have been calculated at various surface recession velocities and at two pressure levels. In this section we will discuss the results at 0.1 atmosphere.

Figure 6-10 shows a plot of the total energy absorbed as calculated by the three methods of analysis at a surface recession velocity, v, of 0.02 ft/sec. This velocity corresponds to a total mass flux of 0.7 lb/ft^2-sec. It should be noted again that the total mass flux is the product of the density of the virgin material (35 lb/ft^3 for phenolic-nylon) and the surface recession velocity. The arrows shown in this figure, and subsequent figures, denote the end of the decomposition zone or beginning of the char zone. The reader is referred to Table 6-3 for the exact temperatures of decomposition/char zone interface. Figures 6-11, 6-12 and 6-3 (which has been shown earlier) correspond to total mass fluxes, ρv, of 1.05(v=0.03 ft/sec), 1.40(v=0.04 ft/sec) and 2.10(v=0.06 ft/sec) lb/ft^2-sec. We should notice that all the equilibrium curves shown in these figures, end at a tem-

perature of 5500°F. This temperature was not selected arbitrarily, rather it is the temperature at which all the solid carbon, either by reacting with other gases or by sublimation, disappear. The disappearance of all the solid carbon obviously denotes the physical end of the char zone. Table 6-7 shows a summary of the equilibrium flow results. Table 6-8, however, compares non-equilibrium and equilibrium flow results for the various surface recession velocities already mentioned. The reader will notice that the case for v=0.01 ft/sec was not run for the non-equilibrium case. The reason for this was the excessive amount of computer time required to complete this case. We will expand on this at the end of the chapter.

For the cases where ρv=0.7, 1.05 and 1.40 lb/ft^2-sec, there is a crossover between the equilibrium and non-equilibrium curves. We have already explained the reason for this crossover. This crossover however, does not occur for the case where total mass flux is 2.10 lb/ft^2-sec (v=0.06 ft/sec). If we go back to Table 6-3 we will notice that as the surface recession velocity increases the difference between the equilibrium and non-equilibrium decomposition/char zone temperature interface also increases; being smallest at v=0.02 ft/sec, with a difference of 929°F, and largest at v=0.06 ft/sec, with a difference of 1324°F. This very large difference in temperature allows the equilibrium heat curve a head start. The non-equilibrium curve can never surpass it because by the time it approaches the equilibrium curve at about 4200°F, the

TABLE 6-7: Comparison of the Total Energy Absorbed at Various Surface Recession Velocities: Equilibrium Analysis (P=0.1 Atm; Nylon-Phenolic Composites).

	Heat Absorbed in BTU/ft^2-sec.					
T ($^\circ$F)	0.01 ft/sec	0.02 ft/sec	0.03 ft/sec	0.04 ft/sec	0.05 ft/sec	0.06 ft/sec
500	0.0	0.0	0.0	0.0	0.0	0.0
600	0.3	0.3	0.3	0.3	0.3	0.3
1000	3.7	3.9	4.0	4.1	4.1	4.1
1400	62	75.3	85.4	92.7	97.2	100.4
1800	133	218	291	353	409	458
2200	201	354	495	626	750	867
2600	272	496	707	909	1104	1292
3000	347	646	932	1209	1478	1510
3400	434	820	1194	1557	1915	2266
3800	552	1056	1548	2029	2505	2973
4200	739	1429	2107	2775	3437	4092
4600	1070	2091	3101	4101	5094	6080
5000	1707	3366	5014	6650	8281	9904
5200	2223	4397	6560	8712	10859	12997
5400	2918	5788	8647	11495	14336	17170
5500	3306	6581	9821	13104	16296	19555

TABLE 6-8: Comparison of the Total Energy Absorbed for Equilibrium and Non - Equilibrium at Various Surface Recession Velocities and a Pressure of 0.1 Atmosphere (Phenolic-Nylon).

	Heat Absorbed in BTU/ft^2-sec							
	v=0.02 ft/sec		v=0.03 ft/sec		v=0.04 ft/sec		v=0.06 ft/sec	
T($^\circ$F)	EQ	NON-EQ	EQ	NON-EQ	EQ	NON-EQ	EQ	NON-EQ
500	0.0	0.0	0.0	0.0	0.0	0.0	0.0	0.0
600	0.3	0.3	0.3	0.3	0.3	0.3	0.3	0.3
1000	3.9	3.9	4.0	4.0	4.1	4.1	4.1	4.1
1400	75.3	75.3	85.4	85.4	92.7	92.7	100.4	100.4
1800	218	90.8	291	132	353	172	458	250.5
2200	354	97.4	495	142	626	186	867	269
2600	496	468.4	707	331	909	196	1292	288
3000	646	588.1	932	724	1209	805	1510	758
3400	820	852.8	1194	1114	1557	1321	2266	1601
3800	1056	1229	1548	1635	2029	1983	2973	2543
4200	1429	1799	2107	2420	2775	2965	4092	3896
4600	2091	2610	3101	3616	4101	4481	6080	5987
5000	3366	3736	5014	5393	6650	6819	9904	9283
5200	4397	4356	6560	6402	8712	8197	12997	11310
5400	5788	5002	8647	7444	11495	9653	17170	13528
5500	6581	5332	9821	7967	13104	10387	19555	14682
5800		6374		9514		12535		18155

carbon in the chemical equilibrium model begins to react into the gas phase increasing both the gas flux and the rate of heat absorbed.

A Comparison of the Total Heat Absorbed for Frozen, Equilibrium and Non-Equilibrium Analyses at One Atmosphere

In the previous section we discussed the results of frozen, equilibrium and non-equilibrium analyses for a pressure of 0.1 atmosphere. In this section we will discuss similar results but for a pressure of 1 atmosphere.

Figure 6-13 shows a plot of the total heat absorbed by frozen, equilibrium and non-equilibrium for a surface recession velocity of 0.02 ft/sec(ρv=0.7 lb/ft^2-sec). The total amount of heat absorbed predicted by the equilibrium analysis is 5599 BTU/ft^2-sec, that for non-equilibrium is 4800 BTU/ft^2-sec and for frozen, 625 BTU/ft^2-sec. It should be noted that for 1.0 atmosphere the equilibrium analysis predicts a front surface temperature of 5800^{o}F. This is the temperature at which the solid carbon concentration approaches zero. This temperature is 300^{o}F higher than the case of 0.1 atmosphere. One would expect this because when the pressure increases by a factor of ten, the energy required for the carbon to enter the gas phase has to be greater. Putting it another way, the higher the pressure, the higher the front surface temperature required to get the carbon into the gas phase. This is because the higher pressure tends to keep the carbon in the solid phase. Figures 6-14, 6-15 and 6-16 show

plots as those shown in Figure 6-13, but these are for surface recession velocities of 0.03, 0.04 and 0.06 ft/sec respectively. We have summarized the results of the total energy absorbed by equilibrium in Table 6-9. In Table 6-10 we have summarized the results of the non-equilibrium analysis and compared it to those of equilibrium.

Effect of Surface Recession Velocity on Heat Absorbed on the Phenolic-Nylon Resin: Parameter Study

In Table 6-8, the tabulated results of the total energy absorbed at a number of surface recession velocities are shown for both the equilibrium and non-equilibrium analyses. The pressure at which these results are tabulated is 0.1 atmosphere. In Table 6-10 similar results are tabulated but for a pressure of 1 atmosphere.

First we shall analyze the results at a pressure of 0.1 for equilibrium. Figure 6-17 shows these results graphically. As expected, the higher the surface recession velocity, the larger the amount of heat absorbed. It should also be noted that the curves get closer to each other as the surface recession velocity increases.

If we take the energy absorbed at v=0.01 ft/sec as the equilibrium base case shown in Table 6-6, and compare it to the cases for v=0.02, 0.03, 0.04, 0.05 and 0.06 ft/sec, there is almost a one to one correspondence between the ratio of the velocities and that of the total energy absorbed. So for 2, 3, 4, 5 and 6 times the surface recession velocity of the base case, we find that the total energy absorbed is 1.99,

TABLE 6-9: Comparison of the Total Energy Absorbed at Various Surface Recession Velocities: Equilibrium Analysis (P=1. atm; Nylon-Phenolic Composites).

	Heat Absorbed in BTU/ft^2-sec.					
T(°F)	0.01 ft/sec	0.02 ft/sec	0.03 ft/sec	0.04 ft/sec	0.05 ft/sec	0.06 ft/sec
500	0.0	0.0	0.0	0.0	0.0	0.0
600	0.3	0.3	0.3	0.3	0.3	0.3
1000	3.7	3.9	4.0	4.1	4.1	4.1
1400	102	86	85	93	97	100
1800	214	310	380	436	487	530
2200	286	454	596	725	849	963
2600	357	596	809	1010	1203	1389
3000	430	742	1028	1300	1567	1826
3400	509	900	1264	1616	1961	2299
3800	601	1083	1540	1983	2421	2850
4200	720	1321	1897	2458	3014	3562
4600	893	1668	2417	3152	3881	4603
5000	1185	2252	3294	4321	5343	6356
5200	1417	2715	3988	5247	6499	7746
5400	1744	3369	4970	6555	8136	9708
5600	2209	4300	6366	8417	10463	12500
5800	2858	5599	8315	11016	13709	16397

TABLE 6-10 : Comparison of the Total Energy Absorbed for Equilibrium and Non-Equilibrium at Various Surface Recession Velocities and a Pressure of One Atmosphere (Phenolic-Nylon)

	Heat Absorbed in BTU/ft^2-sec.									
	v=0.02ft/sec		v=0.03ft/sec		v=0.04ft/sec		v=0.05ft/sec		v=0.06ft/sec	
T(°F)	EQ	NON-EQ	EQ	NON-EQ	EQ	NON-EQ	EQ	NON-EQ	EQ	NON-EQ
500	0	0	0	0	0	0	0	0	0	0
600	0.3	0.3	0.3	0.3	0.3	0.3	0.3	0.3	0.3	0.3
1000	3.9	3.9	4.0	4.0	4.1	4.1	4.1	4.1	4.1	4.1
1400	86	72	85	85	93	93	97	97	100	100
1800	310	91	380	132	436	172	487	211	530	250
2200	454	97	596	142	725	186	849	227	963	269
2600	596	334	809	378	1010	196	1203	243	1389	288
3000	742	549	1028	724	1300	312	1567	838	1826	304
3400	900	896	1264	1178	1616	1377	1961	1519	2299	1619
3800	1083	1320	1540	1799	1983	2149	2421	2429	2350	2660
4200	1321	1739	1897	2501	2458	3120	3014	3644	3562	4094
4600	1668	2238	2417	3294	3152	4230	3881	5088	4603	5872
5000	2252	2908	3294	4347	4321	5657	5343	6922	6356	8130
5200	2715	3310	3988	4988	5247	6026	6499	8022	7746	9462
5400	3369	3760	4970	5708	6555	7504	8136	9261	9708	10961
5600	4300	4257	6366	6501	8417	8586	10463	10635	12500	12625
5800	5599	4800	8315	7400	11016	9800	13709	12138	16397	14500

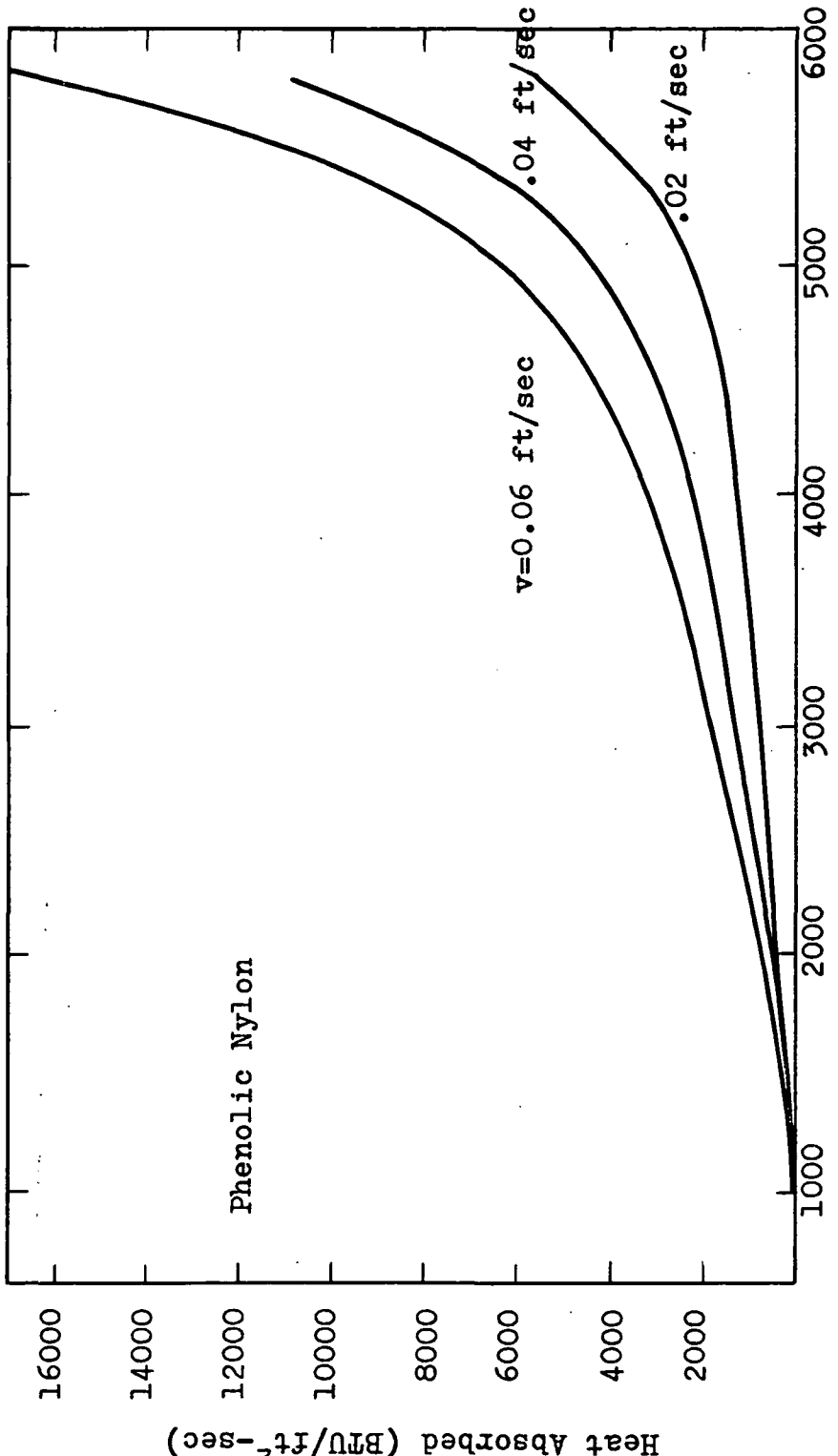

Figure 6-17. A Comparison of the Total Energy Absorbed at Various Surface Recession Velocities: Equilibrium Analysis (P=0.1 atm; Nylon-Phenolic Composites).

2.98, 3.97, 4.95 and 5.94 times that of the base case respectively. One would expect it to be exactly 2, 3, 4, etc., times the base, that is, if we were analyzing the char zone only. After all, equilibrium reactions are not a function of surface velocity, so doubling the mass through the char would exactly double the total amount of energy absorbed. However, the reason the ratios are not exactly the same can be found by looking at the decomposition/char zone interface temperature at each of these surface recession velocities (see Table 6-3). We see for example that at v=0.02 ft/sec the interface temperature is 1387^{o}F, at v=0.03 ft/sec it is 1451^{o}F, at v=0.04 ft/sec it is 1500^{o}F, and so on. Therefore, the lower the surface recession velocity, the lower the back surface temperature of the char and the sooner the equilibrium gases will begin to react in the char. We can see, for example, that at v=0.02 ft/sec the gases are in equilibrium at 1387^{o}F and begin to absorb heat at that temperature. At v=0.03 ft/sec, on the other hand, the gases will not reach equilibrium conditions until they reach a temperature of 1451^{o}F.

In Table 6-8, we show also the tabulated results of the total energy absorbed for non-equilibrium. In addition, the results are plotted in Figure 6-18.

The non-equilibrium case shows more vividly the effect that the surface recession velocities have on the temperature boundary conditions and therefore on the shape of the heat curve. It also shows that an increase in the surface reces-

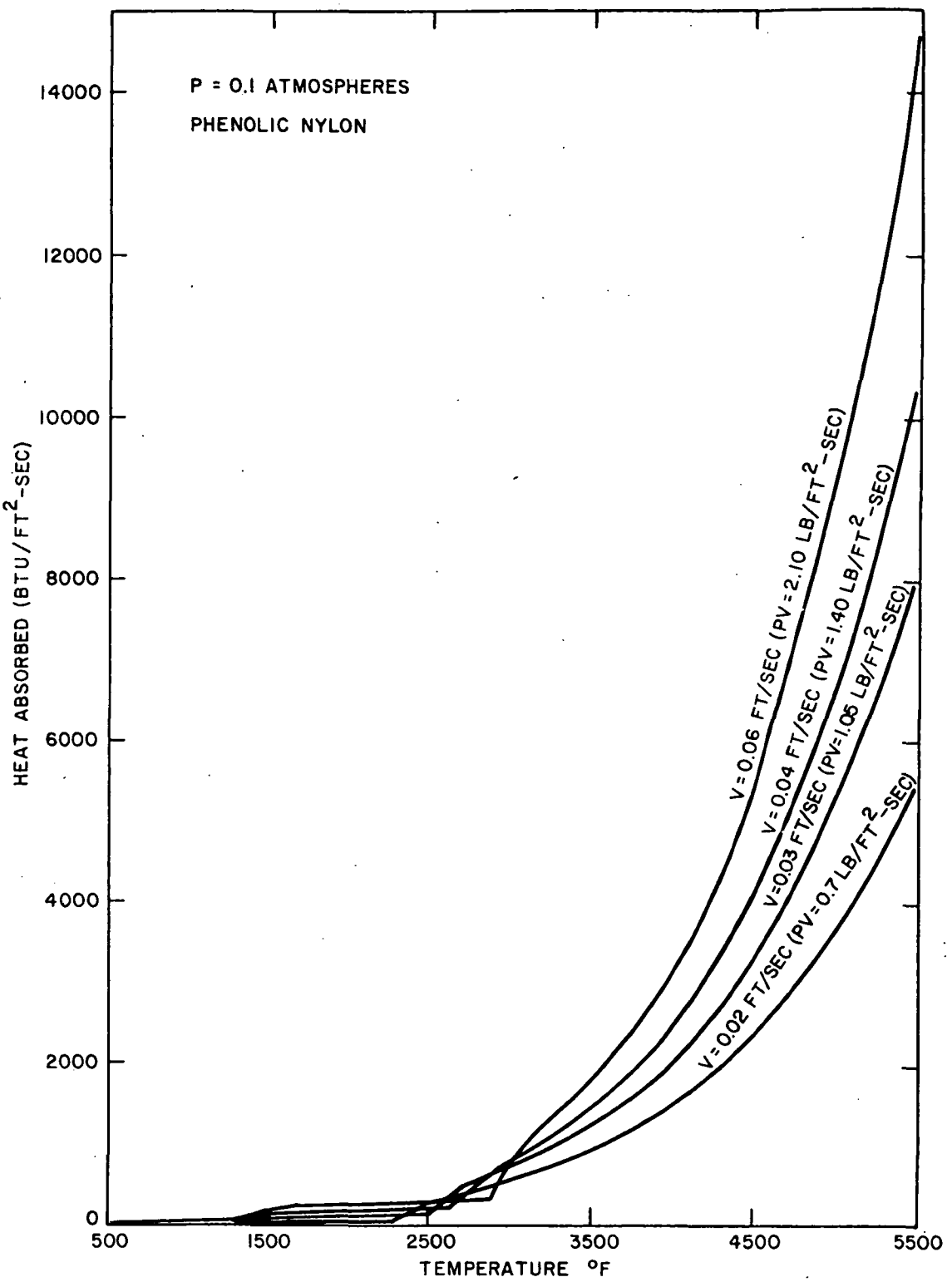

Figure 6-18. A Comparison of the Total Energy Absorbed at Various Surface Recession Velocities. Non-equilibrium Analysis (P=0.1 atm, Phenolic-Nylon Composites).

sion velocity results also in an increase in the temperature of the decomposition/char zone interface. This causes the heat curves to cross over one another close to the interface. For example, from Figure 6-18 we can see that the heat absorbed at a surface recession velocity of 0.02 ft/sec is greater than that of the other surface recession velocities plotted between the temperatures of 2500°F to 2600°F. We can also see, for example, that at a surface recession velocity of 0.03 ft/sec the accumulated heat absorbed is greater than that of 0.06 ft/sec, between the temperatures of 2600° F and 2900°F. The reason for this crossover is that at the lower mass velocities the gases begin to react earlier than at the higher mass flux.

If we compare the energy absorbed at v=0.02 ft/sec with that at 0.03 ft/sec we see that the total heat absorbed at 0.03 ft/sec is about 1.5 times that of 0.02 ft/sec. Since we do not have a case for v=0.01 ft/sec, for the reason that we have already mentioned, we will use v=0.02 ft/sec as the base case for comparison. As with equilibrium there is almost a one to one correspondence between an increase in surface recession velocity and total heat absorbed. We can see, therefore, that at 1.5, 2, and 3 times the surface recession velocity of 0.02 ft/sec, the total quantity of energy absorbed is 1.49, 1.97 and 2.84 for 0.03, 0.04 and 0.06 ft/sec respectively. In the equilibrium case we explained that the reason the correspondence of the ratios of energy absorbed were not exact integers of the surface recession

velocity (or for that matter the mass flux , ρv) was because of the differences encountered in the boundary conditions. For non-equilibrium we can also apply the same reasoning. However, it should be noted that for non-equilibrium it is not necessary to get a close one-to-one correspondence. Basically because one can argue that the higher the surface recession velocity, i.e., the higher the mass flux through the char, the lower the residence time in the char and hence, the lower the time for reaction. Apparently, the reduction in residence time experienced at 0.06 ft/sec, for example, has had a small effect on the extent of the kinetic reactions.

Effect of Pressure on Heat Absorbed by the Phenolic-Nylon Resin

A parameter study was conducted on pressure to analyze the effect on the total heat absorbed. The reason for this study is that the reentry pressure is not constant and varies with the trajectory of the vehicle. Two pressure levels were selected to bracket this effect: these pressures were 0.1 and 1.0 atmospheres respectively. The lower pressure level is the one encountered by the reentry vehicle at the higher altitudes while the 1.0 atmosphere level is the theoretical maximum and achieved only at the lower altitude in the trajectory.

A plot of pressure effect for a surface recession velocity of 0.06 ft/sec is shown in Figures 6-19 and 6-20. These plots are for the equilibrium and non-equilibrium analyses

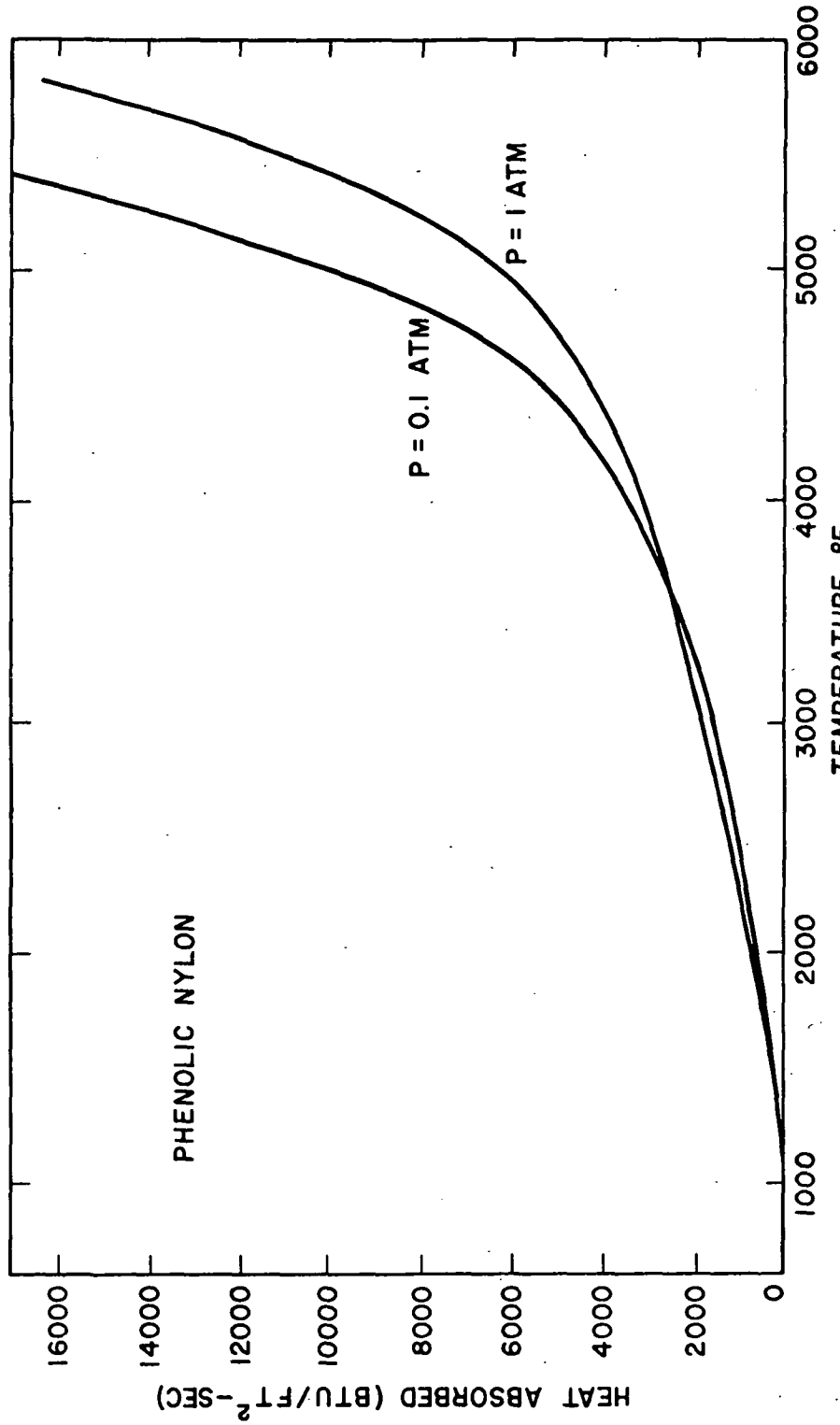

Figure 6-19. Effect of Pressure on the Total Heat Absorbed: Equilibrium Analysis (v=0.06 ft/sec).

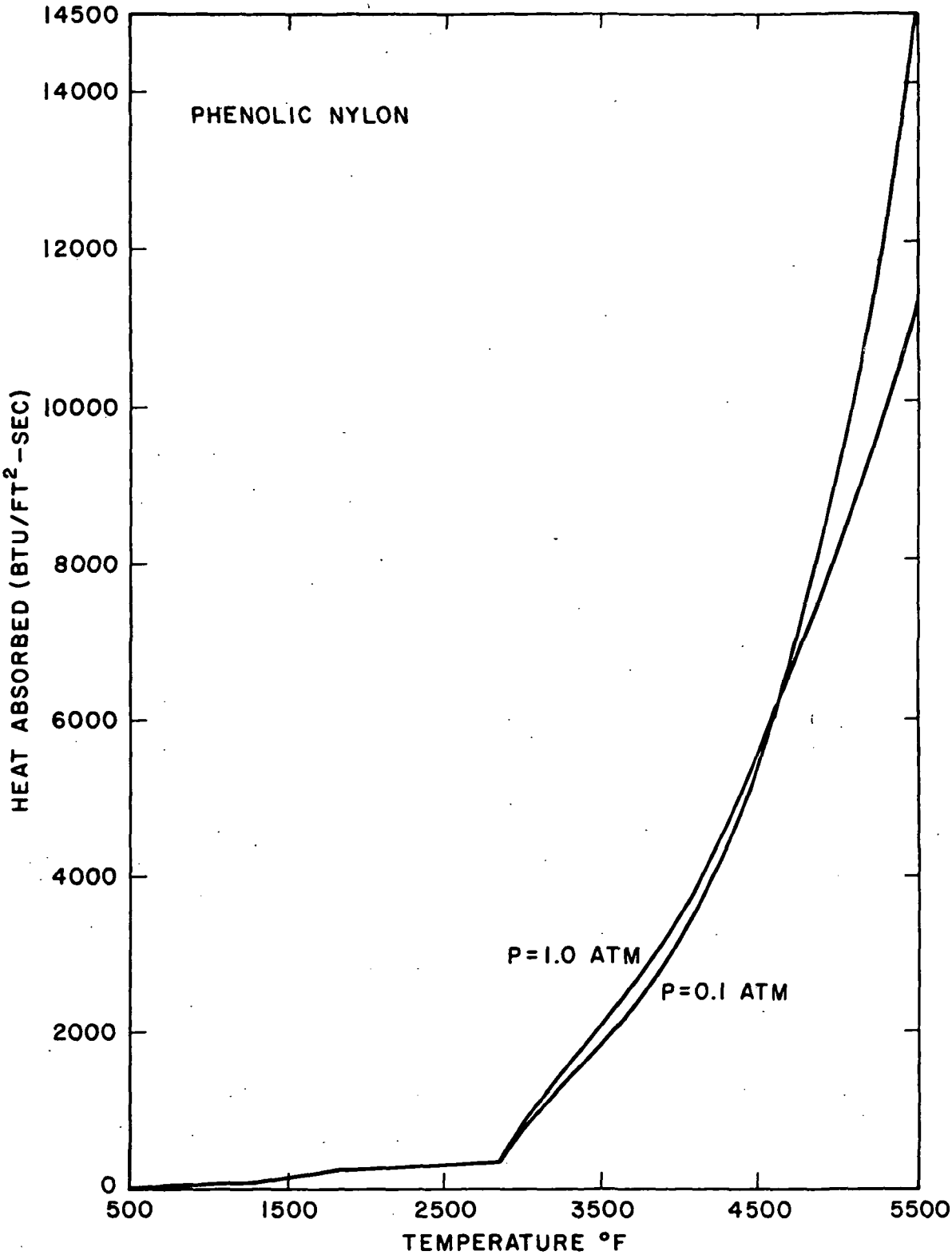

Figure 6-20. Effect of Pressure on the Total Heat Absorbed: Non-equilibrium Analysis (v=0.06 ft/sec).

respectively.

For the equilibrium case shown in Figure 6-19, the heat curve for 1.0 atmosphere remains above that for 0.1 atmosphere until it reaches a temperature of approximately 3600°F, and then it falls below the heat curve for 0.1 atmosphere. For the non-equilibrium case shown in Figure 6-20 a similar behavior is manifested by the 1.0 atmosphere heat curve; although, the 1.0 atmosphere curve falls below the 0.1 atmosphere at a temperature of about 4600°F. Before the crossover for both the equilibrium and non-equilibrium case, the effect of pressure is small.

Looking at Table 5-2, where the kinetic reactions are listed, one would expect that at P=0.1 atmosphere the heat curve would be higher since more of the kinetic reactions are favored by lower pressure than by higher pressure. There are some that are not affected at all. However, there are two reactions which are favored by higher pressure and these are the carbon-water and the carbon-carbon dioxide reactions. To be able to assess whether these reactions play an important part at temperatures lower than 4600°F we have to compare a plot of the species composition concentration at both pressures. In Figures 6-21 and 6-22 a concentration versus temperature plot is shown. In comparing the two plots we can see that the water concentration decreases more rapidly at 1.0 than at 0.1 atmosphere. In addition, it is also evident from the plot that the carbon-carbon dioxide reaction is taking place as is evident by the more rapid

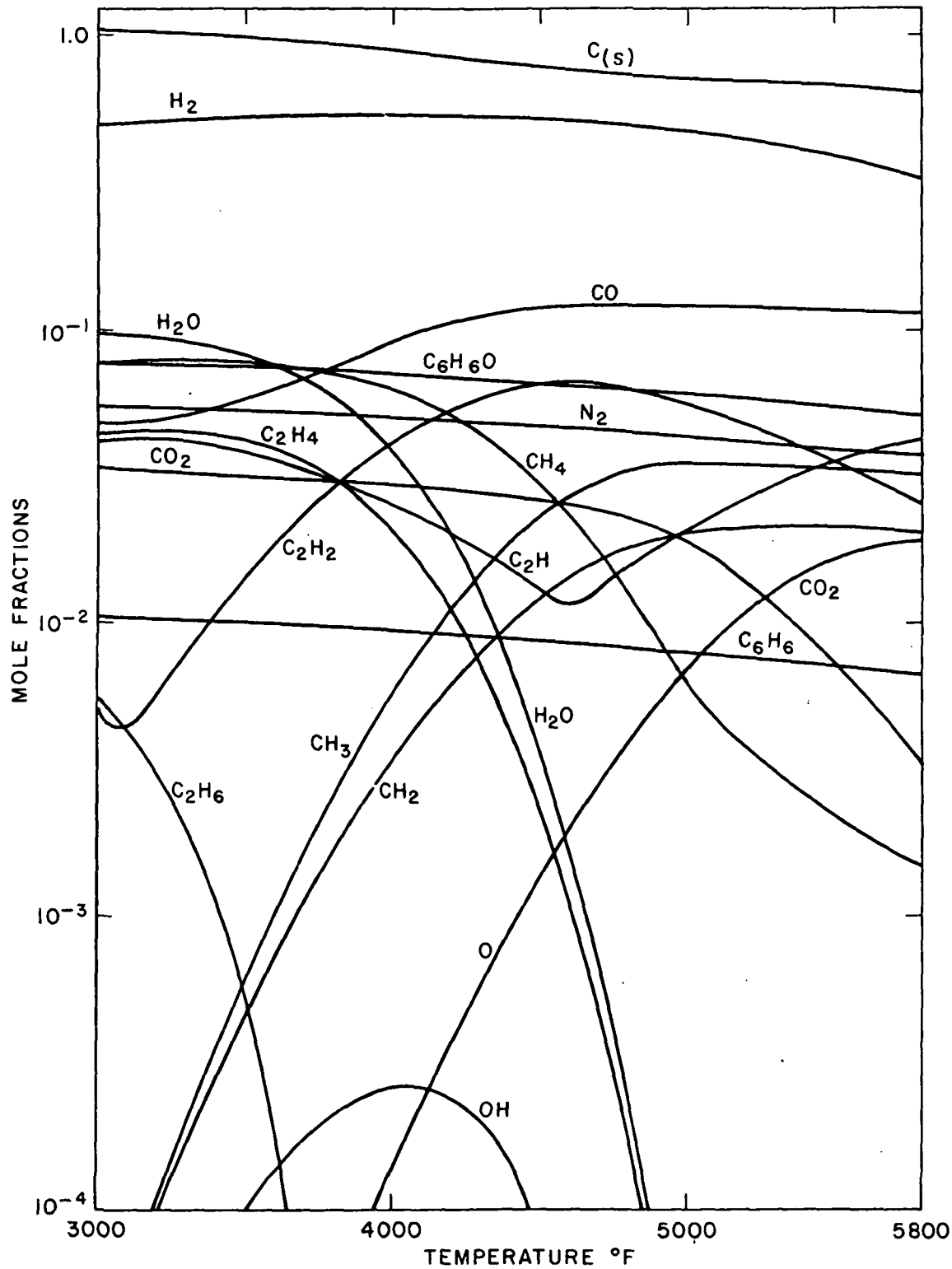

Figure 6-21. Chemical Composition of the Phenolic-Nylon Pyrolysis Gases as Predicted by the Non-equilibrium Analysis at a Pressure of 1.0 atm. and a Surface Recession Velocity of 0.06 ft/sec.

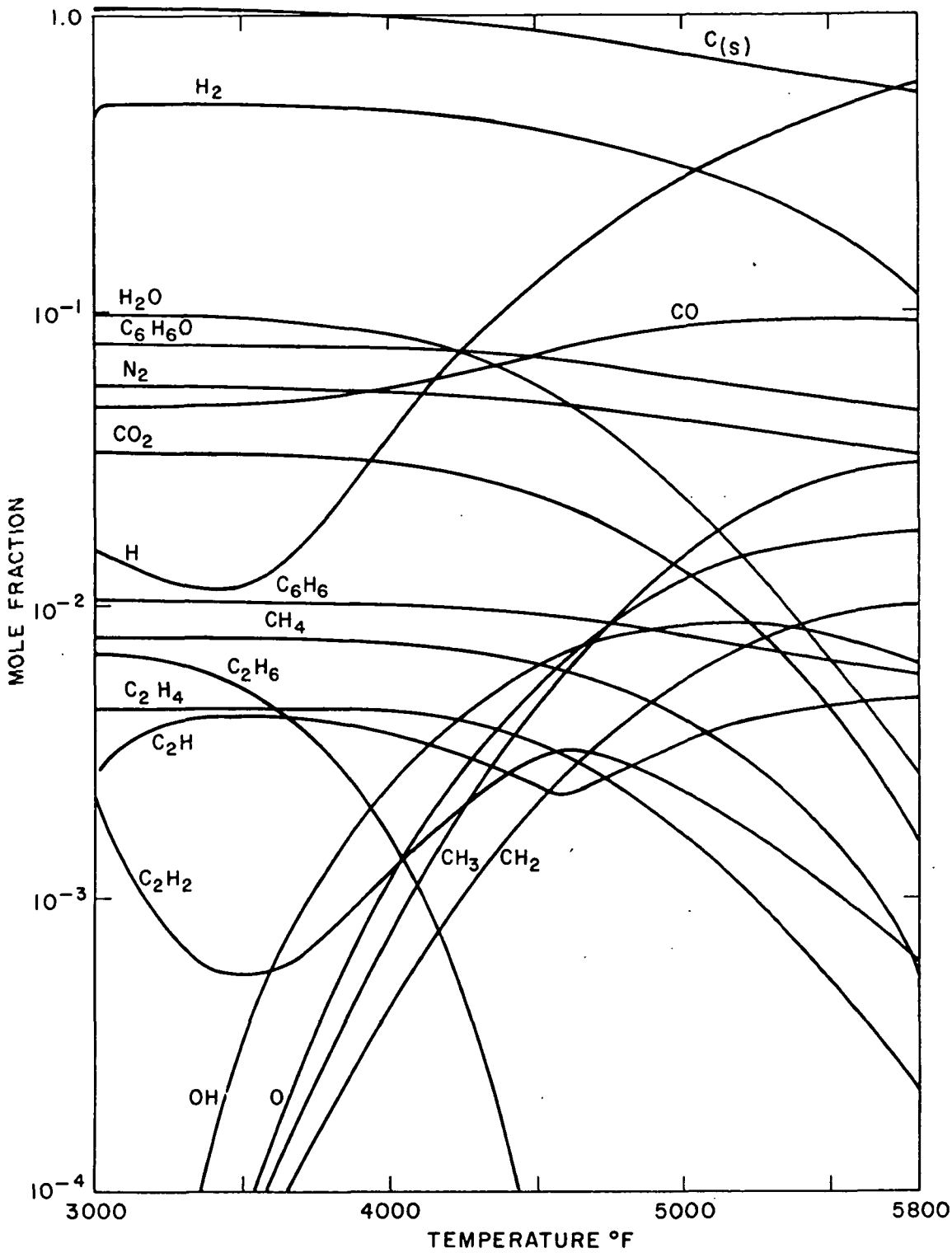

Figure 6-22. Chemical Composition of the Phenolic-Nylon Pyrolysis Gases as Predicted by the Non-equilibrium Analysis at a Pressure of 0.1 atm and a Surface Recession Velocity of 0.06 ft/sec.

increases in carbon monoxide concentration. We see a similar behavior for the water and carbon dioxide concentration in the equilibrium calculations as is evident from the plots of Figure 6-23 and 6-24. Figure 6-23 and 6-24 are plots of equilibrium concentration versus temperature at pressures of 1.0 and 0.1 atmospheres respectively. We want to caution the reader that the extrapolation of the non-equilibrium argument to the equilibrium domain might be erroneous. In the calculations of equilibrium composition we used the free energy minimization technique which does not require the postulation of a reaction mechanism, and, as in any chemical equilibrium process, it is independent of the path. Therefore, to associate any particular mechanism to such complicated process may be dangerous. For the equilibrium case it should be sufficient to say that because of the free energy of the complex mixture, the endothermicity of the gas at a 1.0 atmosphere is greater below a temperature of 3600^{o}F.

What Figures 6-19 and 6-20 illustrate is that unless the front surface temperature is above 4000^{o}F, the effect of pressure on total heat absorbed is essentially the same for 0.1 and 1.0 atmosphere.

Numerical Difficulties

As we have mentioned before, the numerical integration technique used to solve the equations of change for frozen, equilibrium and non-equilibrium analyses was a fourth order Runge-Kutta. With the equilibrium and frozen analyses we

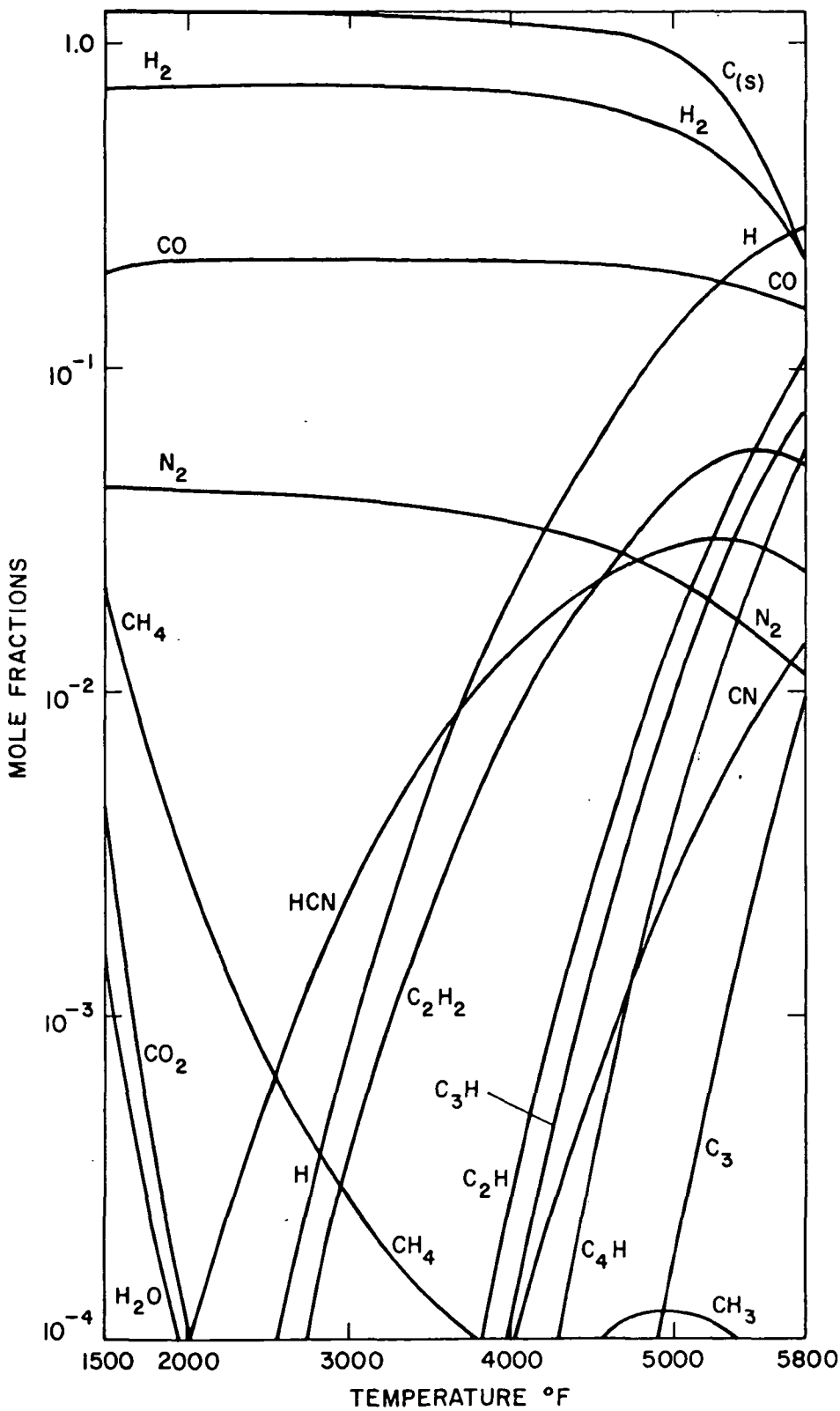

Figure 6-23. Equilibrium Composition of the Phenolic-Nylon Pyrolysis Gases in the Char at a Pressure of 1.0 Atmospheres.

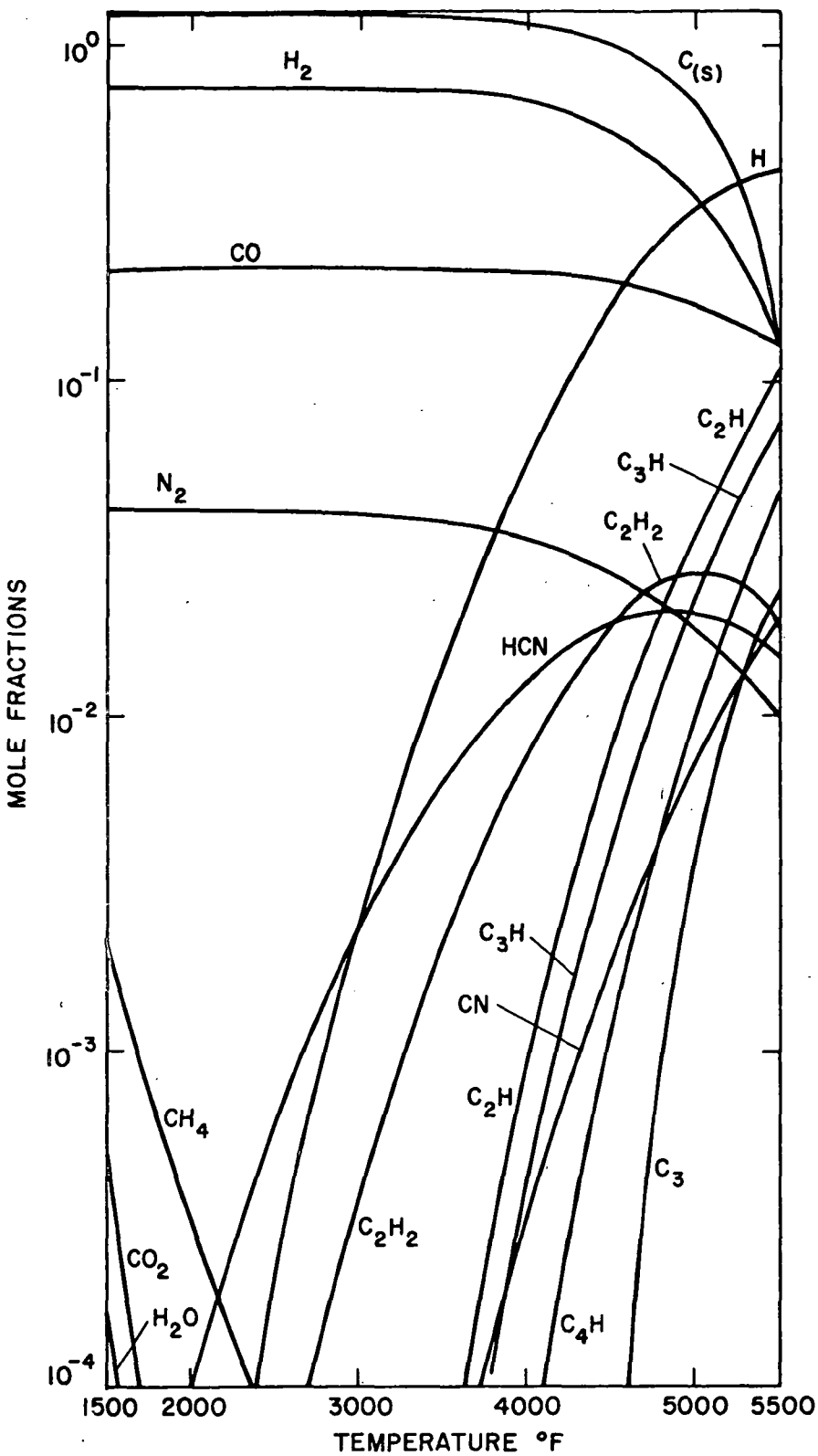

Figure 6-24. Equilibrium Composition of the Phenolic-Nylon Pyrolysis Gases in the Char, at a Pressure of 0.1 Atmospheres.

did not experience any particular difficulty. However, with the non-equilibrium analysis we did. Basically, the reason for our difficulties were the stiff system of equations encountered in the non-equilibrium analysis. Because of this stiff system the size of the integration step had to be very small to avoid a totally erroneous solution. As a result we used excessive amounts of computer time and had to limit the number of cases analyzed. In Figure 6-25 we show a plot of mass flux versus IBM/360 CPU time. As expected, at the higher mass flux the CPU time decreases in an exponential fashion. The reasons are basically two. One is that at the higher flow rates, the residence time is lower in the char. Secondly, as we showed earlier in the chapter, at the higher flow rates (mass flux) the temperature of the decomposition zone is higher and the thickness of the char is smaller. Therefore, the number of integration steps required to solve the equations of change are fewer, thus requiring a lesser amount of CPU time.

Effect of Chemical Reaction Rate Data on the Non-Equilibrium Flow Calculations

In order to study the sensitivity of the analysis to the chemistry model, a study was performed by taking each of the four reactions shown in Table 5-3 one at a time and using the reported sets of kinetic data discussed in Chapter V. The predicted values of the energy absorbed for each set of kinetic data was determined, and the conditions selected for the study were for a pressure of one atmosphere and a surface

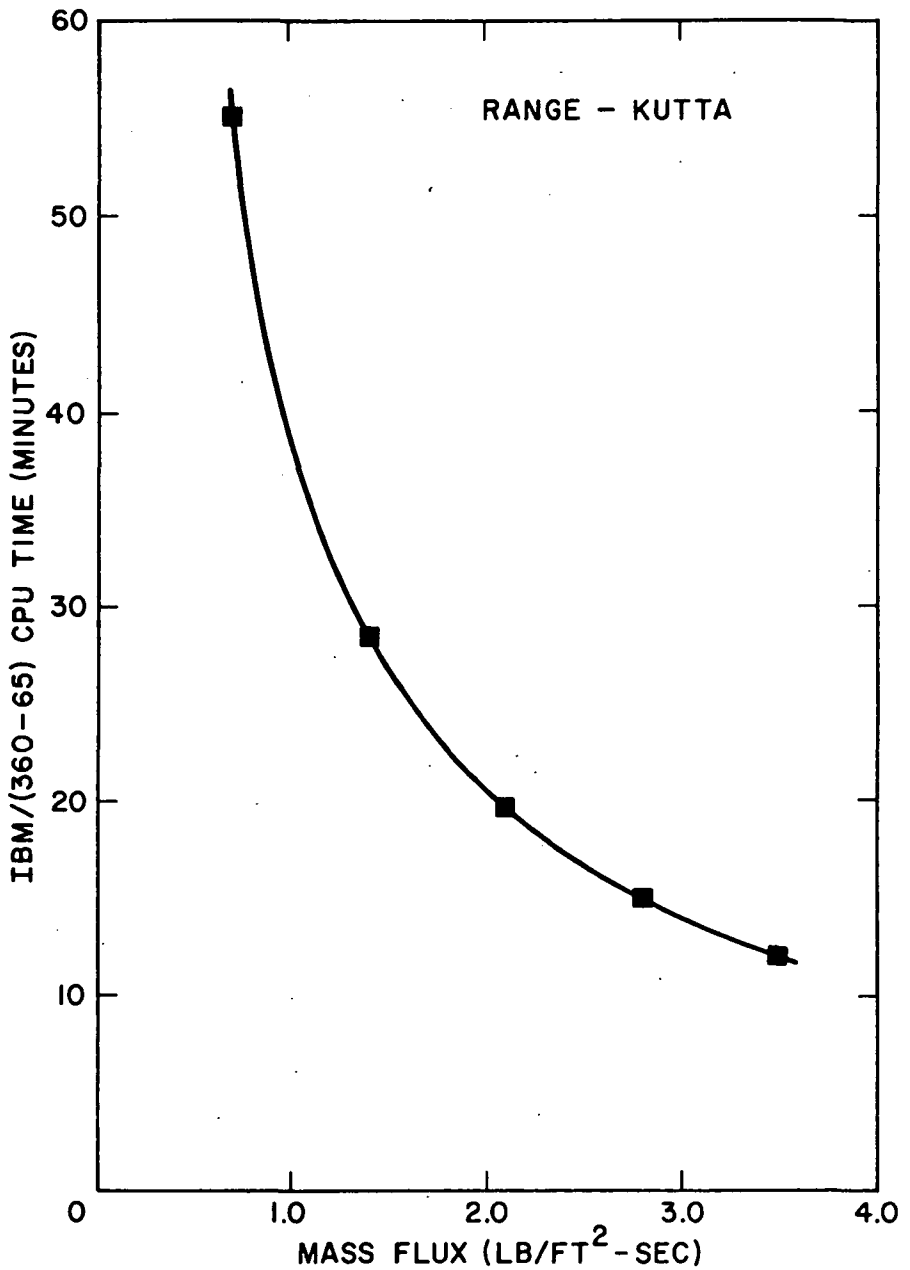

Figure 6-25. Runge-Kutta Solution Time of the Non-equilibrium Analysis versus Mass Flux.

recession velocity of 1×10^{-3} ft/sec. For all the reactions in Table 5-3, except for the acetylene reaction, the variations in the predicted values of the energy absorbed were less than one half of one percent. For the acetylene reaction the variation in energy absorbed was about 4 percent as discussed in Chapter V. These variations were not believed to be significant when one considers the wide discrepancy that exists in the kinetic data that is available in the literature. This close agreement is not fortuitous. But it is the product of a very critical study of the kinetic literature, of a very meticulous approach in selecting reactions, and a very close scrutiny of hundreds of test runs that were made over a period of two years. No doubt that some of the assumptions made had a lot of subjective intuition in them. But by and large the process of selecting the kinetics was made as scientifically objective as possible. Finally, it is very probable that even though the kinetic data for the four reactions in Table 5-3 appear different on paper, that is, each has a different activation energy and frequency factor, each is representative of what occurs within the temperature range for which the data are applicable. Therefore, the use of a reverse reaction rate constant tends to dampen the errors incurred in extrapolating the kinetic data beyond the limits set by the experimental measurements. This probably contributed to the very close agreement in answers obtained when using different sources of data contrary to the author's expectations.

Summary of the Results for Phenolic-Nylon

Up to this point we have analyzed the results of frozen, equilibrium and non-equilibrium analyses coupled to the virgin plastic zone. We have analyzed the energy absorbing mechanisms both in the virgin plastic zone and in the char zone.

In the virgin plastic zone we concluded that decomposition was the dominant energy absorbing mechanism. In the char zone we identified three principal energy absorbing mechanisms which were transpiration cooling, chemical reactions and sublimation. We established that chemical reactions become important energy absorbing mechanisms above 2000^{o}F, we pointed out that the carbon-gas and the sublimation reactions become important energy absorbing mechanisms at temperatures above 4600^{o}F - 4800^{o}F. We also compared the equilibrium and non-equilibrium analyses boundary conditions and noted how each varied with increasing surface recession velocity. We explained why the decomposition/char zone temperature and mass flow rates for equilibrium and non-equilibrium analyses were affected by both pressures and surface recession velocities and how these differences affected the shape of the heat curve for both analyses.

We compared the three analyses at a pressure of 0.1 and 1.0 atmospheres and at the same surface recession velocity. We studied the effect of both pressure and surface recession velocities on the total energy absorbed for both equilibrium and non-equilibrium.

We noticed that pressure had little effect on the total energy absorbed for equilibrium and non-equilibrium except at temperatures above 3600°F and 4600°F respectively. In analyzing the pressure effects we postulated that the carbon-carbon dioxide and the carbon-water reactions were probably the reason as to why the heat absorbed at 1.0 atmosphere was initially greater than at 0.1 atmosphere. We arrived at this conclusion by analyzing the plots of species composition versus temperature. Finally, we explained some of the numerical difficulties we encountered with the non-equilibrium analysis because of the stiff system of equations we were solving. We showed a plot of CPU time versus mass flux to illustrate this point.

In conclusion then we can say that frozen flow analysis is a very poor approximation to the total amount of energy absorbed in the ablator. However, equilibrium is a reasonable approximation to non-equilibrium even though it suffers from its inherent simplifying assumptions that the gases are always in equilibrium irrespective of the temperature.

Silicone Elastomers

To complete this research, a brief study was made of another ablative composite, the silicone elastomer. This composite was chosen because it has good ablative properties. Compared to the phenolic-nylon composite, the silicone elastomer is a much denser composite; 63 lb/ft^3 versus 35 lb/ft^3 for the phenolic-nylon. The char formed by the silicone

elastomers is also denser than for phenolic-nylon (29 versus 13). Per pound of material, the nylon absorbs 1.7 times more heat than the silicone elastomers. This is based on computations performed using equilibrium analysis.

As shown in Figure 6-26 the total heat absorbed in the ablator is greater at 0.1 atmosphere than at 1.0 atmosphere which is the behavior observed for the phenolic-nylon composite also. In addition, as shown in Figure 6-26, the comparison at a surface recession velocity of 0.034 ft/sec (ρv= 2.10 lb/ft^2-sec) for a pressure of 0.1 and 1.0 atmosphere shows that there is also a crossover of the two curves, with the 1.0 atmosphere heat curve being slightly higher than the non-equilibrium curve-up to a temperature of about 3100^{o}F. This crossover was also observed in the phenolic-nylon case both for the equilibrium and non-equilibrium analyses. Examination of Figures 6-27 and 6-28 shows that the carbon-water and carbon-carbon dioxide reactions are favored at P=1. atmosphere. This is evident by the rapid decrease of water concentration and the increase in CO concentration. It also appears that the silicone oxygen reaction is an important one since silicone oxide concentration also increases and it is favored at the higher pressure.

The results for silicone elastomers at two pressure levels and at three surface recession velocities are presented on Tables 6-11 and 6-12. As was the case with phenolic-nylon the front surface temperature at 0.1 atmosphere is lower than at 1. atmosphere. Also, as was the case with phenolic-nylon,

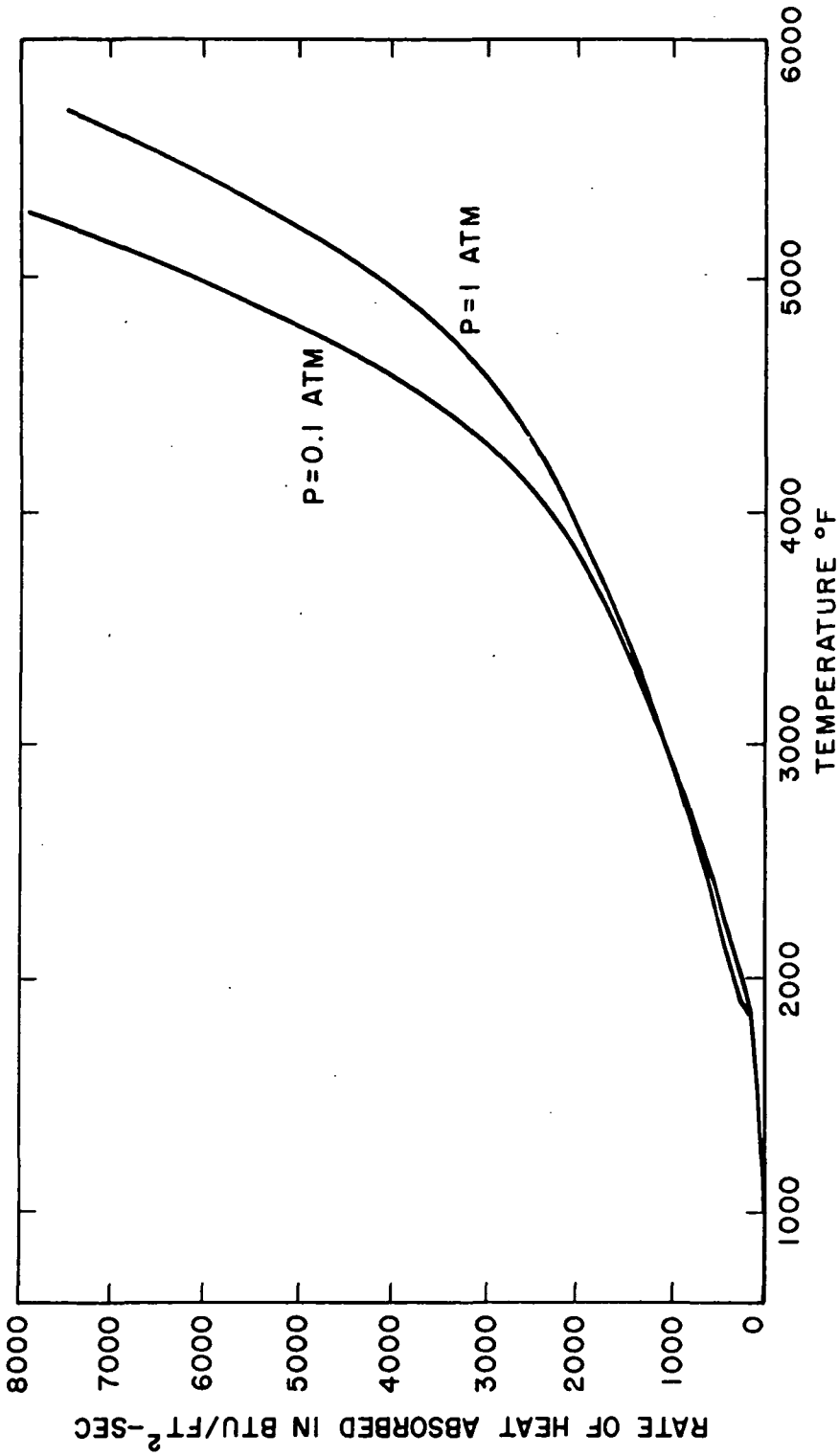

Figure 6-26. Effect of Pressure on the Total Heat Absorbed at a Surface Recession Velocity of v=0.034 ft/sec (Silicone Elastomers).

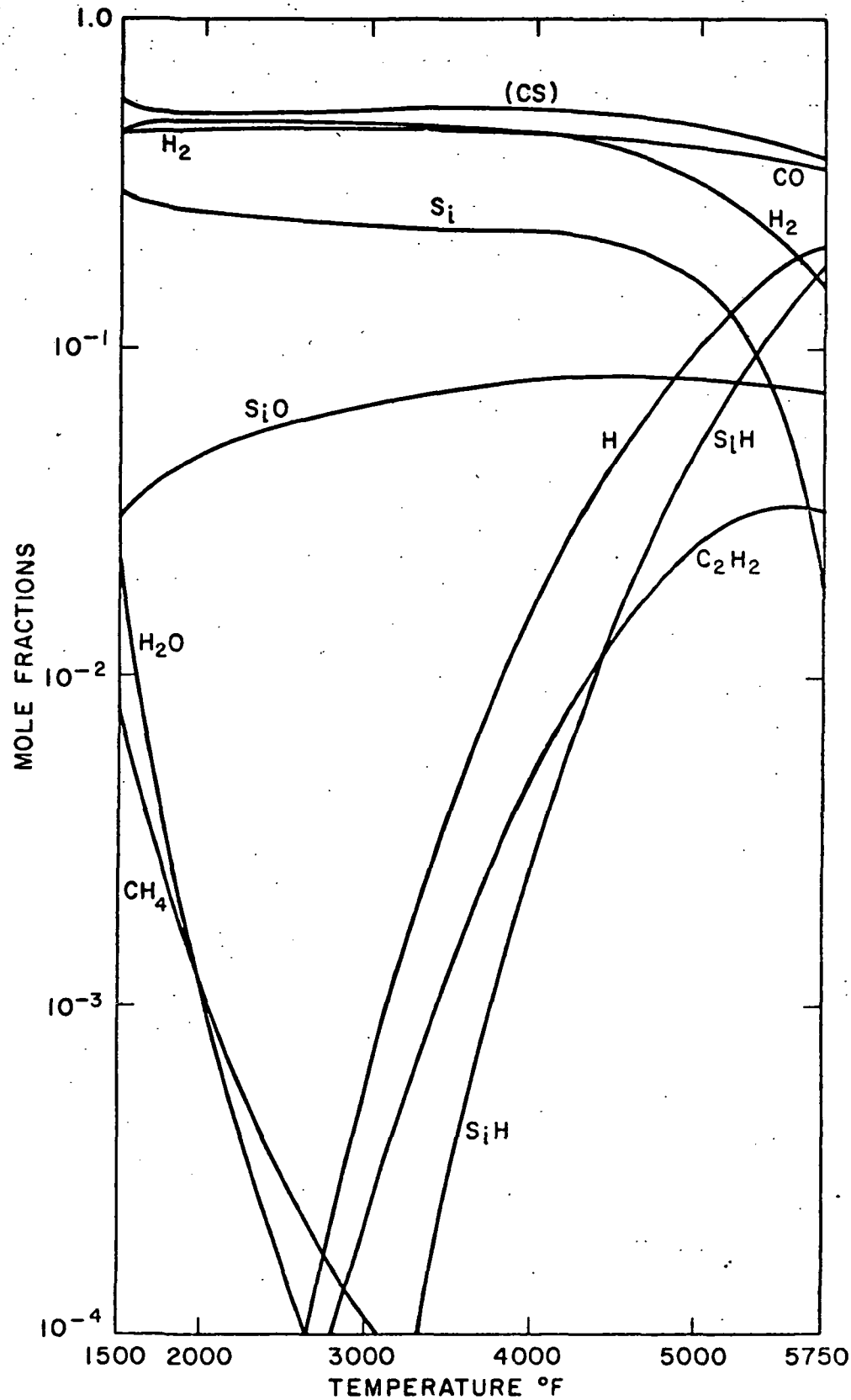

Figure 6-27. Equilibrium Composition of the Silicone Elastomer Pyrolysis Gases in the Char at a Pressure of 1.0 Atmospheres.

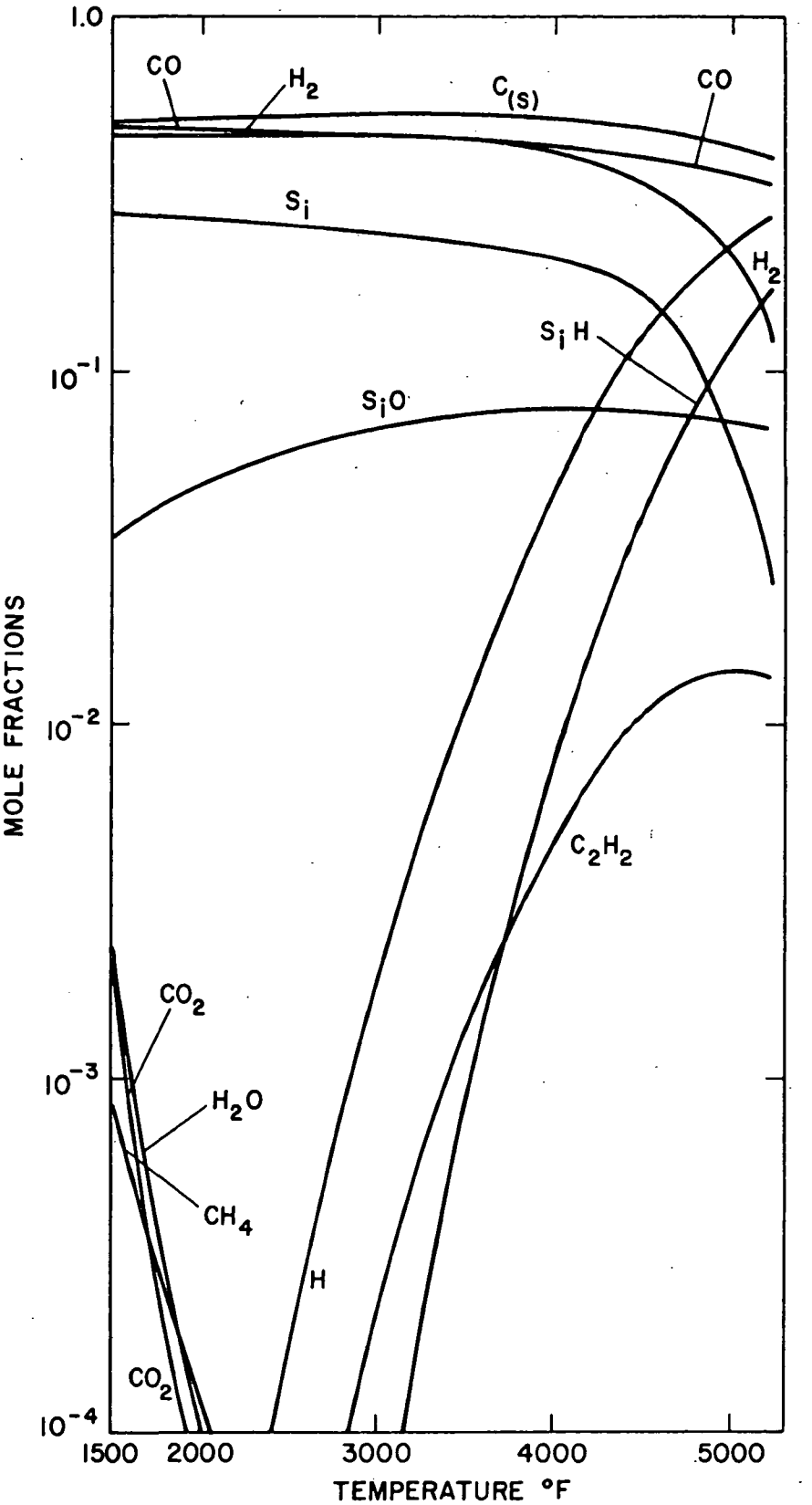

Figure 6-28. Equilibrium Composition of the Silicone Elastomer Pyrolysis Gases in the Char at a Pressure of 0.1 Atmospheres.

TABLE 6-11: Comparison of the Total Energy Absorbed at Three Surface Recession Velocities: Equilibrium Analysis (P=0.1 atm; Silicone Elastomer).

	Heat Absorbed in BTU/ft^2-sec.		
T (^{o}F)	v=0.011 ft/sec	v=0.028 ft/sec.	v=0.034 ft/sec.
500	0.	0.	0.
600	0.4	0.4	0.4
1000	1.1	1.1	1.1
1400	22.9	24.7	24.9
1800	122	172.2	174.1
2200	227	436	491
2600	333	699	807
3000	441	969	1133
3400	564	1277	1503
3800	729	1689	1998
4200	995	2351	2793
4600	1452	3493	4167
5000	2153	5241	6269
5200	2551	6236	7464

TABLE 6-12: Comparison of the Total Energy Absorbed at Three Surface Recession Velocities; Equilibrium Analysis (P=1. atm; Silicone Elastomers).

	Heat Absorbed in BTU/ft^2-sec.		
T ($^\circ$F)	v=0.011 ft/sec.	v=0.028 ft/sec.	v=0.034 ft/sec.
500	0.	0.	0.
600	0.4	0.4	0.4
1000	1.1	1.1	1.1
1400	22.9	24.7	24.9
1800	173	193	187
2200	286	475	527
2600	392	739	844
3000	498	1004	1163
3400	610	1283	1498
3800	736	1600	1878
4200	900	2008	2369
4600	1139	2604	3086
5000	1505	3518	4185
5400	2040	4845	5779
5700	2522	6055	7235

the total energy absorbed at 0.1 atmosphere is greater than at 1.0 atmosphere.

A non-equilibrium kinetic model for silicone elastomers was not developed. Characterization of this composite would have been more difficult than for phenolic-nylon. In addition, the lack of kinetic data for silicone reactions, and the solid state reaction of silicone with silicone oxides and carbides would have made the kinetic analysis unreliable. Furthermore, we already knew that the equilibrium and non-equilibrium analyses for the phenolic-nylon had shown very close agreement, and it was postulated that probably a similar behavior could be expected of the silicone elastomers.

Summary

This chapter has presented the results of the in-depth response of the two ablative composites, phenolic-nylon and silicone elastomers. The bulk of the effort was devoted to phenolic-nylon since it is the composite that has shown the better performance in high heating rate environments. For phenolic-nylon we analyzed, based on the data available, the important energy absorbing mechanisms both for the virgin plastic and for the char zone. We also compared the results of frozen-equilibrium and non-equilibrium graphically, at two pressure levels, and at two surface recession velocities.

The effects of pressure and of surface recession velocities on the total rate of heat absorbed were studied both

for the phenolic-nylon and silicone elastomer composites. One fact should be underlined, and that is that below 3000^{o} F, chemical reactions are not the most important energy absorbing mechanisms. This is the reason why April (1) concluded that equilibrium analysis was not representative of what occurred in an ablator with a front surface temperature of below 3000^{o}F. However, in our studies which have been carried out to temperatures equal to or greater than 5500^{o}F, equilibrium was found to be a reasonable approximation to characterize the ablative composites.

REFERENCES

1. April, G. C., Evaluation of the Energy Transfer in the Char Zone During Ablation, Ph.D. Thesis, Louisiana State University, Baton Rouge, La. (1969).

2. Pike, R. W., G. C. April and E. G. del Valle,"Evaluation of the Energy Transfer in the Char Zone During Ablation"; Part I; Theoretical and Experimental Results for Heat Shield Surface Temperature up to 3000°F, NASA CR 107533 (May 1, 1969).

3. Sykes, G. F. and J. B. Nelson, "Thermo Analysis of Ablative Materials", Preprint 78, 61st National Meeting of the AIChE, Houston, Texas (Feb. 19-23) (1967) NASA Accession Number (N68-25277).

CHAPTER VII

SUMMARY, CONCLUSIONS AND RECOMMENDATIONS

Summary

This research has delat with the analysis of the heat absorbed of phenolic-nylon and silicone elastomer ablative composites. The bulk of the research was concentrated on phenolic-nylon since it has shown the better performance in high heating rate environments. Frozen, equilibrium and non-equilibrium analysis calculations were performed for this composite. The equations of change applicable to each of these analyses were described in Chapter III and the extensive thermodynamic and physical property data required to solve these equations are reported in detail in the Appendices. In addition, a thorough analysis and screenings of hundreds of reactions were done to arrive at the most representative set of kinetic equations for the gases resulting from the decomposition of the phenolic-nylon resin composite. One special precaution taken in this research was to calculate the equilibrium constant for each of the kinetic equations selected to represent the reacting pyrolysis gases in the char. This was done because we wanted to assure ourselves that in extrapolating the kinetic data to temperatures above these for which the data were collected we did not violate any equilibrium consideration.

The basic characteristic of this research is

the coupling of the polymer type virgin plastic zone to the char zone analysis. This was performed by taking into account the decomposition of the plastic composites into gases, with their corresponding heat absorption and the transpiration cooling and chemical reaction effects that these gases have on the heat absorption in the char.

The silicone elastomer study was performed only using chemical equilibrium analysis because, as explained in the previous chapter, essentially no kinetic data existed for the possible silicone reactions. The equilibrium analysis of the silicone elastomers demonstrates the generality of the program. Therefore, given the necessary input information as explained in Appendices A and B, any char forming ablator can be analyzed using the program developed during this research.

Conclusions

Based on the results of this research, the following conclusions are drawn:

1. The reacting flow of pyrolysis products from a 40 percent nylon, 60 percent phenolic-resin composite is accurately described by a non-equilibrium model employing 15 reactions and 19 chemical species.
2. The total heat absorbed as predicted by the equilibrium and non-equilibrium analyses is a strong function of surface recession velocity

but a weak function of pressure, especially at temperatures below 3600°F for equilibrium and 4600°F for non-equilibrium.

3. Surface recession velocity (or total mass flux), which is a way of simulating a high heating environment, has a large effect in the decomposition/char zone temperature interface and in the total heat absorbed.

4. Differences in the conditions at the decomposition/char zone temperature interface between equilibrium and non-equilibrium are due to the manner in which the gas mass flux is matched for equilibrium.

5. The non-equilibrium analysis for a given surface recession velocity predicts, always, a higher mass flux at the decomposition/char zone interface because the plastic composite is allowed to degrade to the experimentally determined density of the char. This density is lower than that required to match the conditions for the equilibrium analysis; 13 versus $\sim$ 21-22 lbs/ft^3.

6. Because the decomposition/char zone temperature interface is always higher than 2000°F (for all cases analyzed), the gases that enter react very quickly. This is evident by the sharp slopes shown for non-equilibrium heat curves in Chapter

VI.

7. As a consequence of the sharp reaction rates observed in the non-equilibrium (or kinetic's) case, the need to reduce the Runge-Kutta step size was necessary to maintain the stability of the numerical solution. This resulted in excessive amounts of computer time which limited the number of cases analyzed. The lowest surface recession velocity analyzed was for $v=0.02$ ft/sec ($\rho v=0.35$ lb/ft^3-sec). No such restrictions were necessary for equilibrium or frozen.
8. The principal energy absorbing mechanism in the plastic region is the decomposition process.
9. In the char the three principal energy absorbing mechanisms are transpiration cooling, heat absorbed by the reacting gases, and that due to sublimation.
10. The equilibrium and non-equilibrium heat curves diverge at the higher temperature because of carbon sublimation.
11. The numerical difficulties experienced with the non-equilibrium analysis was due to a phenomenon called stiffness which is caused by very fast reactions. These fast reactions usually occur at temperatures above 3000°F.
12. The use of reverse reaction rate constants in the

non-equilibrium analysis prevented the violation of equilibrium constraints that might have occurred in extrapolating the kinetic data, beyond the limit set by the experimental measurements.

In-Depth Analysis of Silicone Elastomers: The mathematical formulation for the in-depth analysis of silicone elastomers was the same as for phenolic-nylon, with the exception that the degradation phenomena of the virgin or plastic zone was described by a single degradation reaction. The total heat absorbed by this composite was calculated using equilibrium analysis. Two pressure levels, and mass fluxes similar to those used for phenolic-nylon (0.7, 1.05, etc., lbs/ft^2-sec) were used. As we saw in Chapter VI the total amount of heat absorbed below 3000^oF showed the same insensitivity to pressure as phenolic-nylon. Similar to the case of phenolic-nylon, surface recession velocity has a marked effect in the total heat absorbed by the ablator.

In conclusion, silicone elastomers show the same qualitative trends observed in phenolic-nylon for the several parameter studies considered. However, phenolic-nylon is a more efficient ablator because per pound of material it absorbs more heat.

Recommendations

The following are general recommendations based on the

results of our research.

Thermodynamics: In the area of thermodynamics, the free energy and heat capacity data for over 90 components was compared (where this comparison was possible) using data from NASA (1), JANAF thermochemical tables (2), API Project 44 (3), and data reported by Los Alamos Scientific Laboratory (4). In most cases, the data for light gases was consistent. Where we had the choice, we selected the data from NASA because all of the components required to describe the equilibrium composition, except for phenol and benzene, which were not included in NASA's work, were in the form of an easily used polynomial ($a+bT+cT^2+...+eT^4$). On the other hand, API Project 44 (which presented the data in tabular form) and that of Los Alamos, required transformation and data fitting to conform to NASA's form. However, for such high molecular weight components as benzene and phenol we were forced to use non-NASA data (2). There were compounds such as toluene, 2, 4-xylenol that were reported by Sykes (5) which were not included in the thermodynamic analysis because of lack of thermodynamic data; although these higher molecular weight compounds are probably unimportant as far as the impact on the total energy absorbed. However, for the sake of thoroughness, if the data becomes available, they should be incorporated into the equilibrium analysis.

Kinetics: A great deal of time and effort was devoted to narrow down the possible chemical reactions. In some cases we were fortunate to find more than one reference to

the final set of reactions selected. (See Table 5-2). In such cases, we did conduct studies on the effect of kinetic data, but as shown in Table 5-3, there were only four reactions where this was possible. Therefore, a sensitivity study of the effect of activation energy and frequency factor changes on the total energy absorbed should be conducted, especially for the phenol and benzene reactions.

Decomposition Zone: The analysis of the decomposition zone could be improved and a more accurate fit of the thermogravimetric data can be made. The fit used was preliminary (5) and some of it reported by private communications with NASA (6). When the more accurate and final fit is available it should be used. These comments apply also to the silicone elastomers since the data used was based on some preliminary results.

Runge-Kutta: The method used to solve the equations of change was a standard fourth order Runge-Kutta. This method worked well for non-equilibrium analysis for temperatures below 3000^{o}F. However, above this temperature numerical difficulties were encountered because of the very rapid reactions which occurred; i.e., stiffness of the set of equations. To be able to get around this stiffness of the set of equations, it was necessary to reduce the step size by four orders of magnitude from that of the equilibrium analysis.

Therefore, in future studies of this kind, implicit techniques should be used to avoid the excessive use of com-

puter time and avoid the numerical difficulties encountered in this research.

Free Energy Minimization Formulation: In the carbon-hydrogen-oxygen-nitrogen system (that of the phenolic-nylon) the matrix of coefficient required to solve the equilibrium of an all gaseous mixture is always five (see Chapter IV for details). However, if solids are to be considered in the formulation, the rank of the matrix of coefficients is increased by one every time a solid is added to the formulation. For phenolic-nylon the rank of the matrix was increased by one since carbon was the only solid species considered. However, the rank of the matrix was increased by two for the silicone elastomers since both carbon and silicone were the solid species.

The formulation just described creates a problem in that when the concentration of the solid species decreases or vanishes (as when carbon begins to sublime and the solid carbon disappears), the matrix becomes singular. The singularity is due to the fact that all the coefficients of the row-column combination of the solid species approach zero. For the phenolic-nylon case, the computations were stopped when the concentration of carbon was less than 10^{-2} since it was considered that at this concentration no more char existed. This of course, did not result in any serious error.

However, in the silicone elastomer case the same criteria was used; i.e., when any of the solids reached a concentration of 10^{-2}, the temperature at which this occurred was

assumed to be the front end of the char. Unfortunately, some carbon still remained (about 1/2 mole of carbon per mole of gas) in the silicone analysis. Therefore, an automatic procedure should be implemented to reduce the rank of the matrix by one every time a solid reaches a very small concentration so as to avoid the problem encountered with the silicone case.

Sublimation: In future work, a sublimation model to account for the carbon solid to carbon gas phase change should be incorporated into the non-equilibrium analysis because, although small, there was a residual amount of solid carbon that remained at the front end of the char which should completely disappear.

REFERENCES

1. Mc Bride, B. J., S. Heimel, J. G., Ehbens, S. Gordon, "Thermodynamic Properties to 6000°K for 210 Substances Involving the First Eighteen Elements", NASA SP-3001, (1963).

2. Stull, D. R., JANAF Thermochemical Tables - Dow Chemical Co., Ed., August 1965. Issued by the Bureau of Standards as PB-168 370.

3. Rossini, F. D., K. S. Pitzer, R. M. Arnett and G. C. Pimengal, "Selected Values of Physical and Thermodynamic Properties of Hydrocarbons and Related Compounds". American Petroleum Institute Project 44, Carnegie Press, Pittsburg, Pa. (1953).

4. Duff, R. E., and S. H. Bauer, "The Equilibrium Composition of the C/H System at Elevated Temperatures", Los Alamos Scientific Laboratory Report LA-2556, TID-4500, Los Alamos, California (Sept. 18, 1961).

5. Sykes, G. F. and J. B. Nelson, "Thermoanalysis of Ablation Materials", Preprint 7B, 61st National Meeting of the AIChE, Houston, Texas (Feb. 19-23, 1967) - NASA Accession Number (N68-25277).

6. Sykes, G. F., Private Communication (July, 1969).

NOMENCLATURE

SYMBOL	DESCRIPTION	UNITS
A	area	L^2
A_i	frequency factor	
A_{ij}	identification of species in the jth chemical reaction.	dimensionless
a	ration of char density to virgin material density (see Equation (2-23).	dimensionless
a_{ij}	gram atoms of element j per mole of species i.	atoms/mole
B_i	Runge-Kutta parameters in the species continuity numerical solution method.	M/L^2t
b_j	moles of element j defined by Equation (4-1).	moles
b'_j	moles of element j in the gas phase (Equation (4-34).	moles
$C_{p,i}$	heat capacity of component i at constant pressure.	L^2/t^2T
$C_{p,g}$	average heat capacity of a gas mixture.	L^2/t^2T
C_k	concentration of component K.	moles/L^3
c	number of composites in the virgin material.	dimensionless
c_i	free energy function defined for species i defined by Equation (4-12).	dimensionless
E	energy of activation.	ML^2/mole-t^2

SYMBOL	DESCRIPTION	UNITS
E^*	non-dimensional energy of activation.	dimensionless
F	mathematical function defined by Equation (3-39).	T/L^2
	free energy function defined by Equation (4-15).	ML^2/t^2
$\bar{F}$	molar free energy.	ML^2/t^2
$\bar{F}^o$	molar free energy at standard state of 298°K and 1 atm.	ML^2/t^2
f	free energy function defined by Equation (4-11).	dimensionless
	any mathematical function.	dimensionless
$\bar{f}_i$	fugacity of species i.	M/Lt^2
$\bar{f}_i^o$	fugacity at standard state.	M/Lt^2
G	augmented function of the quadratic approximation to the free energy function defined by Equation (4-25).	ML^2/t^2
	mathematical function defined by Equation (3-38).	T/L
g	acceleration of gravity.	L/t^2
H	enthalpy.	ML^2/t^2
h	integration step size.	L
J	molar flux.	$moles/L^2t$
j	mass flux.	M/L^2t
k	thermal conductivity.	ML/t^3T
	reaction rate constant.	$t^{-1}(L^3/moles)^{n-1}$

SYMBOL	DESCRIPTION	UNITS
k_e	effective thermal conductivity.	ML/t^3T
L	ablator thickness.	L
	total number of chemical reactions.	dimensionless
l	total number of chemical species. (gases+solids).	dimensionless
M_w	molecular weight.	M/moles
m	total number of chemical elements.	dimensionless
N_j	molal flux of component j.	moles/L^2t
n	total number of gas species.	dimensionless
P	total pressure.	M/Lt^2
P_{ij}	stochiometric coefficient of product i in reaction j.	dimensionless
Q	volumetric flow rate.	L^3/t
	heat of pyrolysis.	M/Lt^3
	quadratic approximation to the free energy function defined by Equation (4-24).	ML^2/t^2
Q^*	non-dimensional heat of pyrolysis defined by Equation (2-40).	dimensionless
q	energy transfer by conduction, convection or radiation.	M/Lt^3

SYMBOL	DESCRIPTION	UNITS
	energy absorbed by the degradation of plastic composites, Equation (3-19).	M/Lt^3
R	ideal gas constant.	ML^2/t^2T-mole
	chemical reaction rate.	mole/L^3t
$\bar{R}$	effective chemical reaction rate for gas and solid species defined in Equation (3-22).	mole/L^3t
r_{ij}	stochiometric coefficient of reactant i in reaction j.	dimensionless
S	power on the temperature in the functional expression to calculate reaction rate constants in Equation (5-3)	dimensionless
	number of solid species.	dimensionless
T	temperature.	T
$\dot{T}$	temperature gradient.	T/L
T_f	characteristic time as defined by Equation (5-9).	t
T_c	relaxation time as defined by Equation (5-10).	t
t	time.	t
u	gas velocity.	L/T

SYMBOL	DESCRIPTION	UNITS
v	volume.	L^3
v	surface recession velocity.	L/t
W	total mass flux.	M/L^2t
W_p	mass flux based on the velocity in the pore's space.	M/L^2t
X_j	conversion of species j as defined by Equation (5-6).	dimensionless
x_i	calculated value of moles of species i in the free energy minimization calculations.	moles
$\bar{x}$	total moles of gaseous species.	moles
$\hat{x}$	distance defined by Equation (2-29).	L
Y_i	assumed value of moles of species i in the free energy minimization calculations.	mole
$\hat{Y}$	distance defined by Equation (2-6).	L
z	distance in the axial direction.	L

SYMBOL	DESCRIPTION	UNITS
$\bar{z}$	compressibility factor.	dimensionless
Greek:		
α	viscous coefficient in the modified Darcy's Law Equation.	L^{-2}
	constant defined by Equation (2-24)	dimensionless
	activity coefficient defined Equation (4-4).	dimensionless
β	inertial coefficient in the modified Darcy's Law Equation.	L^{-1}
	non-dimensional energy of activation defined by Equation (2-45).	dimensionless
γ	permiability of a porous medium.	L^2
	non-dimensional heat capacity defined by Equation (2-39).	dimensionless
δ	Kronocker Delta.	dimensionless
Δ	a difference between two parameters.	dimensionless
∇	del operator.	dimensionless
ε	porosity.	dimensionless
$\bar{\varepsilon}$	emissivity	dimensionless
η	dimensionless char distance.	dimensionless
θ	dimensionless temperature.	dimensionless
λ	eigen value.	dimensionless
μ	viscosity.	M/Lt
¶	Lagrange multiplier.	ML^2/t^2
ρ	density.	M/L^3

SYMBOL	DESCRIPTION	UNITS
$\bar{\sigma}$	Stefan-Boltzman constant.	M/t^3T^4
σ	collision diameter.	L
τ	shear stress.	M/Lt^2
Subscript:		
c	convection or conduction.	
e	effective.	
g	gas.	
L	front surface of char.	
o	initial condition.	
p	pressure.	
	pyrolysis.	
r	radiation.	
s	solid.	
T	temperature.	
Superscript:		
o	standard or reference state.	
.	derivative.	